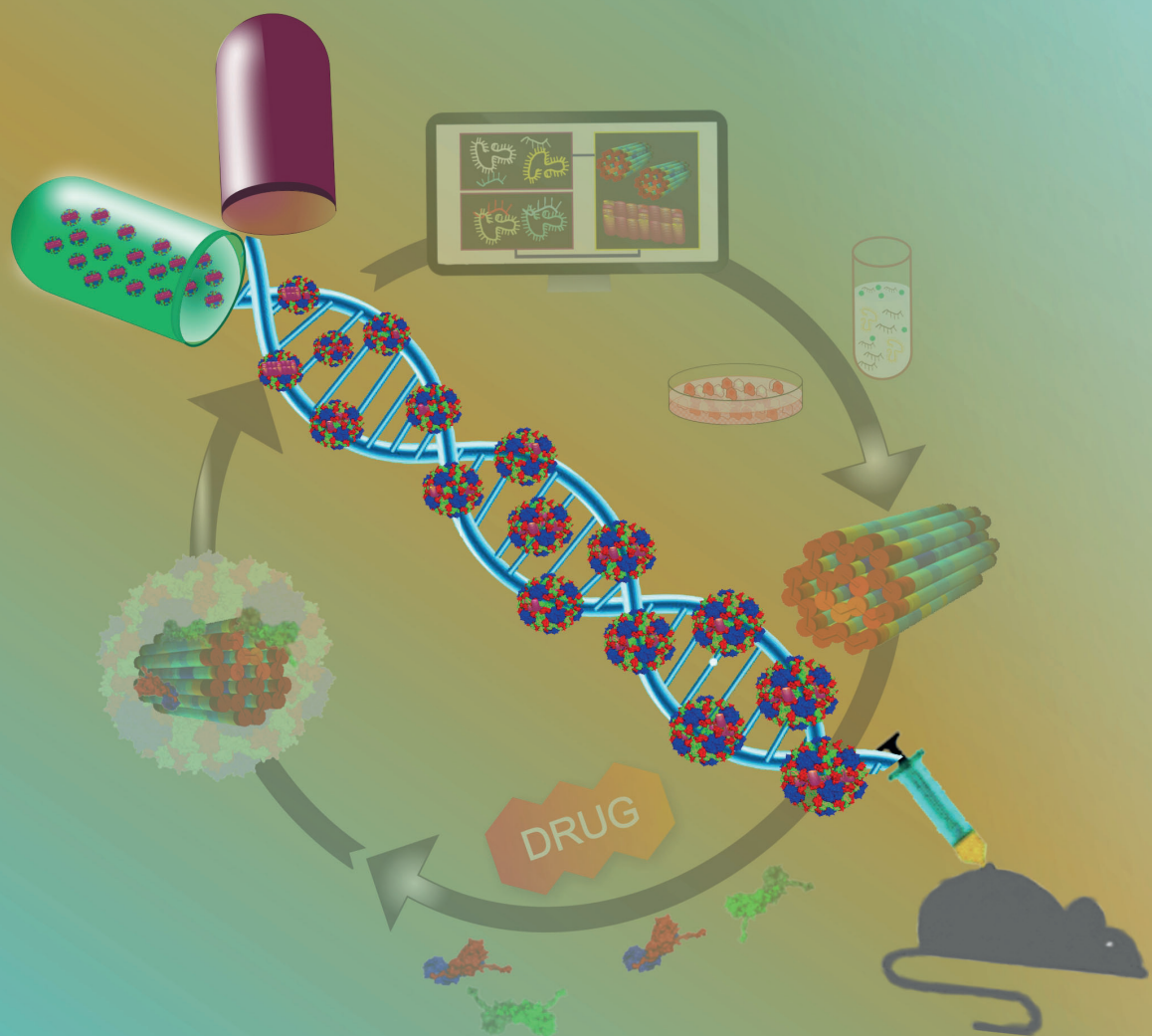


# Virus Coated DNA Nanostructures: A Biological Way for Drug Delivery



GAURAV SINGHAI

**VIRUS COATED DNA NANOSTRUCTURES: A  
BIOLOGICAL WAY FOR DRUG DELIVERY**

Gaurav Singhai



This dissertation has been approved by:

Supervisor

Prof. dr. ir. J.J.L.M. Cornelissen

Co-supervisor

Dr. I. Koeper

The research in this thesis was conducted under the *cotutelle doctoral program* between Department of Biomolecular Nanotechnology (BNT), The MESA+ Institute for Nanotechnology of the University of Twente and Flinders Centre for NanoScale Science & Technology, School of Science & Engineering of Flinders University, Australia.

UNIVERSITY OF TWENTE.

**MESA+**  
INSTITUTE FOR NANOTECHNOLOGY



**ISBN:** 978-90-365-5203-5

**DOI:** 10.3990/1.9789036552035

**Cover art:** Deepesh Gupta and Gaurav Singhai

**Printed by:** Ipskamp

Copyright © 2021 Gaurav Singhai, The Netherlands.

All rights reserved. No parts of this thesis may be reproduced, stored in a retrieval system or transmitted in any form or by any means without permission of the author.

VIRUS COATED DNA NANOSTRUCTURES:  
A BIOLOGICAL WAY FOR DRUG DELIVERY

DISSERTATION

to obtain  
the degree of doctor at the University of Twente,  
on the authority of the rector magnificus,  
prof. dr. ir. A. Veldkamp,  
on account of the decision of the Doctorate Board  
to be publicly defended  
on Wednesday 30 June 2021 at 12.45 hours

by

**Gaurav Singhai**

born on the 19<sup>th</sup> of September, 1981  
in Umaria, India

**Graduation Committee:**

Chair/Secretary:	Prof. dr. J. L. Herek	University of Twente
Supervisor:	Prof. dr. ir. J. J. L.M. Cornelissen	University of Twente
Co-supervisor:	Dr. I. Koeper	Flinders University
Members:	Prof. dr. M. A. Kostainen	Aalto University
	Prof. dr. ir. T. Vermonden	Utrecht University
	Dr. ir. J. M. J. Paulusse	University of Twente
	Prof. dr. J. Prakash	University of Twente

*This thesis is dedicated to my **father**,  
who has always been a source of  
inspiration, motivation and endurance  
to meet life's challenges and  
eventualities with passion, enthusiasm  
and commitment to work.*



## TABLE OF CONTENTS

<b>1</b>	<b>PREFACE</b>	<b>2</b>
1.1	INTRODUCTION .....	2
1.2	AIM AND OUTLINE OF THE THESIS .....	3
1.3	REFERENCES .....	5
<b>2</b>	<b>THE ASSEMBLY OF BIOHYBRID NANOCARRIERS FOR DRUG DELIVERY APPLICATIONS</b>	<b>8</b>
2.1	BIO-NANOTECHNOLOGY AT A GLANCE .....	8
2.1.1	<i>Fields of Bio-nanotechnology</i> .....	10
2.1.2	<i>Applications of Bio-nanotechnology</i> .....	11
2.2	DNA NANOTECHNOLOGY - AN OVERVIEW .....	12
2.2.1	<i>DNA origami: The art of nanoscale folding of DNA</i> .....	15
2.2.2	<i>In-silico designing of DNA nanostructures</i> .....	17
2.2.3	<i>Advances and applications of DNA Nanotechnology in biosciences</i> .....	18
2.3	DNA NANOSTRUCTURES AS DRUG CARRIERS .....	21
2.3.1	<i>Properties of an effective delivery system or a nano-vehicle</i> .....	21
2.3.2	<i>Applications for the use of DNA nanostructures as efficient drug carriers</i> .....	22
2.3.3	<i>Challenges for DNA nanostructures in drug delivery</i> .....	23
2.3.4	<i>Addressing the challenges posed by DNs in Drug delivery</i> .....	25
2.4	PLANT VIRUSES AS A TEMPLATE FOR FABRICATION .....	27
2.4.1	<i>CCMV - the natural encapsulation material</i> .....	27
2.4.2	<i>Encapsulation of different polyanionic materials using CCMV</i> .....	28
2.4.3	<i>Advantages of CCMV encapsulation of DNA over other conventional delivery carriers</i> .....	29
2.5	CONCLUSION .....	29
2.6	REFERENCES .....	31
<b>3</b>	<b>DESIGN, ASSEMBLY, PURIFICATION AND CHARACTERISATION OF MODULAR DNA ORIGAMIS</b>	<b>40</b>
3.1	INTRODUCTION .....	40
3.2	RESULTS AND DISCUSSION .....	41
3.2.1	<i>In-silico designing of modular DNA origamis</i> .....	41
3.2.2	<i>Folding DNA origami nanostructures</i> .....	43
3.2.3	<i>Purification of DNs</i> .....	46
3.2.4	<i>Characterisation of purified DNs</i> .....	48
3.3	CONCLUSIONS .....	55
3.4	ACKNOWLEDGEMENTS .....	55
3.5	MATERIALS AND METHODS .....	56



---

3.5.1	<i>3D and multilayer structure designing</i>	56
3.5.2	<i>Self-assembly of modular 3D DNs</i>	56
3.5.3	<i>Gel electrophoresis and purification of DNA origamis</i>	57
3.5.4	<i>SEM of DNs</i>	57
3.5.5	<i>AFM of DNs</i>	58
3.5.6	<i>TEM of DNs</i>	59
3.5.7	<i>Dynamic Light Scattering and Zeta potential</i>	59
3.6	REFERENCES .....	60
<b>4</b>	<b>ENCAPSULATION OF MODULAR DNA ORIGAMIS WITH VIRUS-LIKE PARTICLES (VLPS)</b>	<b>92</b>
4.1	INTRODUCTION .....	92
4.2	RESULTS AND DISCUSSION .....	94
4.2.1	<i>Fabrication of DNA origami with CPs</i>	94
4.2.2	<i>Purification of encapsulated assemblies</i>	96
4.2.3	<i>Characterisation of purified encapsulated DNs</i>	97
4.3	CONCLUSIONS.....	100
4.4	ACKNOWLEDGEMENTS.....	101
4.5	MATERIALS AND METHODS.....	101
4.5.1	<i>DNA origami preparation</i>	101
4.5.2	<i>Production of CCMV CPs</i>	101
4.5.3	<i>Encapsulation: fabrication of DNA origami with CPs</i>	102
4.5.4	<i>Electrophoretic Mobility Shift Assay (EMSA)</i>	103
4.5.5	<i>Purification of encapsulated assemblies</i>	103
4.5.6	<i>STEM/TEM of purified assemblies</i>	103
4.5.7	<i>Dynamic Light Scattering (DLS)</i>	103
4.6	REFERENCES .....	104
<b>5</b>	<b>CREATING NANOCARRIERS WITH DRUG LOADED AND VIRUS-ENCAPSULATED DNA ORIGAMIS</b>	<b>108</b>
5.1	INTRODUCTION .....	108
5.2	RESULTS AND DISCUSSION .....	109
5.2.1	<i>Daunorubicin and its absorption at varying pH</i>	109
5.2.2	<i>Drug incorporation and loading efficiency</i>	110
5.2.3	<i>Virus Capsid (CP) fabrication of drug-loaded DNs</i>	113
5.3	CONCLUSIONS.....	118
5.4	ACKNOWLEDGEMENTS.....	119
5.5	MATERIALS AND METHODS.....	119
5.5.1	<i>DNA origami preparation</i>	119

---

5.5.2	<i>Effect of pH on Daunorubicin absorption</i>	119
5.5.3	<i>DNs drug binding and quantification</i>	119
5.5.4	<i>Agarose Gel Electrophoresis</i>	120
5.5.5	<i>Confocal Microcopy</i>	120
5.5.6	<i>Creating nanocarriers: capsid fabrication of drug-loaded DNs</i>	120
5.5.7	<i>Purification of Nanocarriers</i>	120
5.5.8	<i>TEM/STEM imaging</i>	121
5.5.9	<i>Dynamic Light Scattering (DLS)</i>	121
5.6	REFERENCES .....	122
<b>6</b>	<b>MONITORING THE STABILITY AND DRUG RELEASE FROM NANOCARRIERS</b>	<b>126</b>
6.1	INTRODUCTION .....	126
6.2	RESULT AND DISCUSSION .....	128
6.2.1	<i>Assessing the stability of nanocarriers</i>	128
6.2.2	<i>Daunorubicin release profile in-vitro</i>	130
6.2.3	<i>Probing the drug leakage from nanocarriers</i>	133
6.3	CONCLUSION.....	134
6.4	ACKNOWLEDGEMENTS.....	135
6.5	MATERIALS AND METHODS.....	135
6.5.1	<i>Stability assessment of nanocarriers in the biological environment</i>	135
6.5.2	<i>Evaluating the drug release profile</i>	135
6.5.3	<i>Validating drug leakage from the nanocarriers</i>	136
6.6	REFERENCES .....	137
<b>7</b>	<b>CELLULAR VIABILITY AND UPTAKE MECHANISM OF NANOCARRIERS</b>	<b>142</b>
7.1	INTRODUCTION .....	142
7.2	RESULT AND DISCUSSION .....	144
7.2.1	<i>Cytotoxic studies for drug (dauno) and drug complexes on PANC-1 cells</i>	144
7.2.2	<i>Comparing the cytotoxicity of designed nanocarriers</i>	146
7.2.3	<i>Cellular uptake of nanocarriers by PANC-1 cells</i>	147
7.3	CONCLUSION.....	152
7.4	ACKNOWLEDGEMENTS.....	152
7.5	MATERIALS AND METHODS.....	152
7.5.1	<i>Nanocarriers design and development</i>	152
7.5.2	<i>In-vitro probing of nanocarriers</i>	153
7.5.3	<i>Statistical Analysis</i>	153
7.6	REFERENCES .....	155
<b>8</b>	<b>GENERAL DISCUSSION</b>	<b>158</b>
8.1	SUMMARY .....	158

8.2	STUDY LIMITATIONS.....	158
8.3	FUTURE DIRECTIONS.....	158
8.4	REFERENCES.....	159
	<b>ABBREVIATIONS</b>	<b>161</b>
	<b>SUMMARY</b>	<b>163</b>
	<b>SAMENVATTING</b>	<b>165</b>
	<b>ACKNOWLEDGEMENT</b>	<b>167</b>
	<b>ABOUT THE AUTHOR</b>	<b>171</b>
	<b>PUBLICATION</b>	<b>172</b>

## LIST OF FIGURES

Figure 1-1 Schematic illustration of work discussed towards attaining the aim of the thesis.....	3
Figure 2-1 Size comparison of bio-nano particles.....	8
Figure 2-2 Schematic representation of bottom-up and top-down approaches.....	9
Figure 2-3 Structure of DNA and its self-assembly patterns.....	14
Figure 2-4 Designed modular DNA origami structures.....	16
Figure 2-5 Different biological applications of DNA nanostructures.....	18
Figure 2-6 Overview of targeted drug delivery trail using DNs.....	24
Figure 2-7 Phase diagrams of CCMV capsid proteins without RNA.....	28
Figure 3-1 caDNAno designed and CanDo validated multilayer DNA origami structures.....	43
Figure 3-2 AGE analysis for assembly conditions of modular designs.....	46
Figure 3-3 AGE analyses of purified DNs with ultrafiltration (MWCO filtration) and gel excision band purification.....	47
Figure 3-4 Microscopic characterisations of purified FS.....	50
Figure 3-5 Microscopic characterisations of purified SN.....	51
Figure 3-6 Microscopic characterisations of purified HB designs.....	52
Figure 3-7 Microscopic characterisations of purified DWS designs.....	53
Figure 3-8 Average size distribution based on dynamic light scattering (DLS) of purified DNs.....	54
Figure 4-1 Schematic overview of CP fabrication of DNs to create nanoassemblies.....	94
Figure 4-2 Electrophoretic mobility shift assay (EMSA) of fabricated DNs with respective CP excess.....	96
Figure 4-3 Representative size-exclusion chromatograms for analysis.....	97
Figure 4-4 Negative stain TEM micrographs of fabricated DNs mixed with CPs.....	98
Figure 4-5 Electron microscopy characterisation of fabricated assemblies HB ( $\chi = 1$ ).....	99
Figure 4-6 Electron microscopy characterisation of fabricated assemblies DWS ( $\chi = 1$ ).....	100
Figure 4-7 Average size distribution of encapsulated nano assemblies on DLS.....	100
Figure 5-1 Effect of pH on daunorubicin absorption.....	110
Figure 5-2 Schematic overview of dauno loading into DNs.....	111
Figure 5-3 AGE to assess BPBR effect with drug-loaded supernatant.....	111
Figure 5-4 Drug loading efficiency vs BPBR.....	112
Figure 5-5 Confocal micrographs of daunorubicin bound DN (DWS).....	113
Figure 5-6 Representative SEC chromatograms.....	114
Figure 5-7 AGE analysis to determine CP fabrication on drug-DNs nanocarriers.....	116
Figure 5-8 Electron microscopy characterisation of HB+drug+CP.....	117
Figure 5-9 Electron micrographs of DWS+drug +CP.....	117
Figure 5-10 DLS analysis nanocarrier (DN+drug+CP).....	118
Figure 6-1 Drug release mechanism from polymeric nanomaterials.....	126
Figure 6-2 Virus capsids protection of nanocarriers against benzonase.....	129
Figure 6-3 Time-dependence stability against benzonase and trypsin.....	130
Figure 6-4 Dauno release profile from DN complexes.....	131
Figure 6-5 Validating drug leakage from nanocarriers.....	133
Figure 7-1 Schematic illustration of cellular internalisation of nanocarriers for daunorubicin delivery.....	144

Figure 7-2 DWS derived formulations cytotoxicity on Panc-1 represented by the half-maximal inhibitory concentration (IC50) .....	145
Figure 7-3 HB derived formulations cytotoxicity on Panc-1 cells represented by the half-maximal inhibitory concentration (IC50). .....	146
Figure 7-4 Inhibitor challenged uptake of free drug capturing fluorescence with red channel. ....	148
Figure 7-5 Inhibitor challenged uptake of DWS-drug complex capturing drug with red and blue channels overlay depicting them getting inside the cells. (Scale: 100 $\mu$ m). ....	149
Figure 7-6 Inhibitor challenged uptake of DWS nanocarriers capturing drug fluorescence with red and blue channels. (Scale: 100 $\mu$ m) .....	150
Figure 7-7 Inhibitor challenged uptake of HB-nanocarriers capturing drug fluorescence with green and blue channels (Scale: 100 $\mu$ m). ....	151
Figure 7-8 The value of the sum of fluorescence intensity obtained from microscopy in individual channels; (a) DWS based formulations (b) HB based formulations. ....	151

**Supplementary Figures**

Figure 3-S1 Microscopic analysis of M13mp18 (scaffold) at 10 nM concentration .....	88
Figure 3-S2 Microscopic analysis of ss-DNA oligonucleotides (staples) at 40 nM concentration.....	88
Figure 3-S3 SEM of negative and positive controls. ....	88
Figure 3-S4 Stability test for DNAs in Milli-Q water .....	89
Figure 5-S1 TEM micrographs of (HB+drug+CP) .....	124
Figure 5-S2 TEM micrographs of (DWS+drug+CP) .....	124
Figure 6-S1 Evaluating structural integrity of nanocarriers .....	140

---

**List of Tables**

Table 3-1 Folding temperature ramp used in a thermocycler for assembly of DN's .....	44
Table 3-2 Overview of various purification methods employed .....	46
Table 3-3 Surface charge values of the purified DN's .....	55
Table 4-1 Mass ratio comparison .....	95
Table 6-1 Content details used for the enzyme stability reactions .....	129
Table 6-2 Parameter estimation of drug released kinetics. * + 10 mM MgCl <sub>2</sub> .....	131

**Supplementary Tables**

Table 3S-1 Details about 10X6 bundle (flat-sheet) staple sequences .....	62
Table 3S-2 Details about Square nut (SN) staple sequences .....	70
Table 3S-3 Details about 24-helix bundle (HB) staple sequences .....	78
Table 3S-4 Details about Double-wall square (DWS) staple sequences .....	81
Table 3S-5 Sequence of M13mp18 scaffold DNA.....	85





# **CHAPTER 1**

---

## **Preface**

# 1 PREFACE

## 1.1 Introduction

1 In 1959, the eminent physicist Richard Feynman laid the conceptual basis for nanotechnology through his monologue entitled “There is plenty of room at the bottom” and addressed the atomic and molecular-level control of matter (1). The concept of employing changes at the nanometric scale ( $10^{-9}$  m) was seen as a significant and innovative landmark in diverse areas, including physical sciences, molecular engineering, biology, biotechnology and medicine (2). Later, Chad Mirkin’s work greatly influenced and shaped the field of bio-nanotechnology (an integration between nanotechnology and biological systems) offering new tools for controlled manipulation of biomolecules with precision and functional specificity for a variety of biological applications (3). The primary focus of the bio-nanotechnology field is to improve techniques for constructing nanostructures using biological or biologically inspired components.

Biological macromolecules like proteins, nucleic acids (DNA), polysaccharides and lipids act as building blocks for nanoscale engineering. DNA is not only the nuclear genetic material but also has inherent biocompatibility and ability to self assemble, which makes it an element of choice for the construction of novel nanoscale materials or tools for various *in vitro* as well as *in vivo* applications. Similarly, proteins are powerful macromolecules performing a variety of functions to sustain life, including molecular transport. Thus, DNA and proteins are considered promising materials in bionanotechnology due to their high and specific molecular recognition, self-assembly and various functional properties. The recent technical advances in biomolecular engineering enabled smooth designing and construction of 2D and 3D DNA nanostructures (DNs) using the DNA origami technique (4-6). Also, the progression in drug delivery system studies has enlivened the idea of utilising DNAs as nanocarriers to efficiently diagnose and cure diseases with minimal side effects (7, 8).

Despite DNAs being ideal candidates for drug delivery, these origami structures may impose some drawbacks associated with their low stability and targeted delivery efficiency for biological and medical applications (9). Moreover, DNA-based drug carriers are also known to have weak cell transfection capacity due to their polar nature. Some efforts were made towards eliminating these practical challenges, with protein coating/encapsulation or lipid modification of DNAs surfaces for efficient cellular uptake and delivery (10-12). Kostianien and coworkers demonstrated the use of a variety of materials for coating DNAs surface like different proteins (BSA and HFBI) or cationic polymers, which have been shown to improve stability and cellular transfection rates (12, 13). Further, Shih *et al.* described the encapsulation with virus inspired membrane (lipids) and PEGylated oligolysine attachment to DNAs through electrostatic interaction; protecting not only the structural

integrity but also increasing in-vivo circulation time of nanocarriers (14, 15). Alternatively, protein-DNA complexes were also developed by encapsulating DNA origamis with virus capsid protein (CP) from cowpea chlorotic mottle virus (CCMV), cowpea mosaic virus (CPMV), tobacco mosaic virus (TMV) and red clover necrotic mosaic virus (RCNMV) to achieve completely tuneable, targeted and activated drug delivery (16-18). However, a detailed study involving a drug-loaded biohybrid macromolecule is still an active area of research and bio-nanotechnology has the potential of revolutionising the development of new drug delivery systems in compliance with drug effectiveness, safety, and reduced cost of health care.

## 1.2 Aim and outline of the thesis

The research described in this thesis aimed to create 'smart' nanocarriers by designing modular (planned and customised geometries) DNs and loading them with anticancer drug (daunorubicin). Further, these drug-loaded modular DNA nanostructures are coated with capsid proteins (CP), isolated from a plant virus (CCMV). Next, these virus coated drug-loaded DNs were investigated for biological stability and efficacy on selected pancreatic cancer cell (PANC-1) (Figure 1-1). Moreover, CCMV were used as a coating material because it is a well-studied virus and considered safe for humans (19-21).

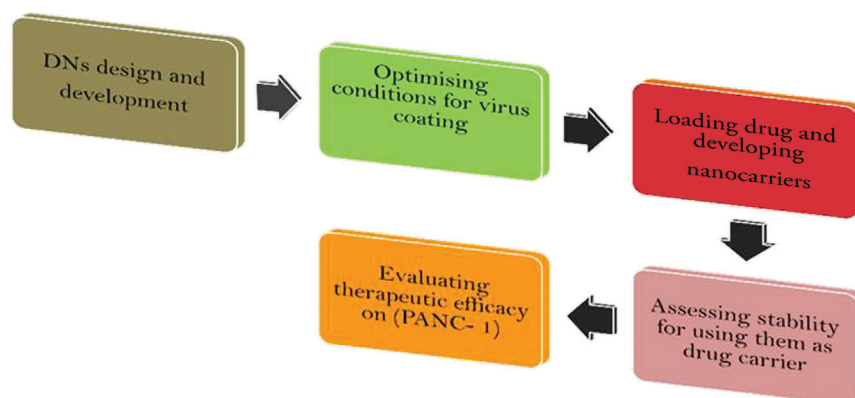


**Figure 1-1 Schematic illustration of work discussed towards attaining the aim of the thesis**

The thesis chapters are outlined as follows to gain an understanding about the conditions affecting the assembly of hybrid biomolecules together and exploring their potential as a drug carrier, particularly for carrying anticancer drugs to the target cells effectively.

**Chapter 2** of the thesis presents an overview of literature related to the research advances in the field of structural DNA nanotechnology and Virus-like particles (VLPs), and together with their usage in the various bio-nanotechnological application. It entails a brief introduction to the emergence of bionanotechnology as a research domain and its role in medical and nanotechnology. Further, in-

depth information was provided on the fabrication of DNPs with plant virus (CCMV) capsids for enhancing their functionality as drug delivery carriers.

**Chapter 3** is focussed on the discussion of protocols used to design, assemble and purify modular DNPs and to use them as drug loading templates. Different characterisation techniques were employed, including gel electrophoresis, microscopy (SEM, AFM and TEM) and biophysical (DLS and zeta potential) for confirming the details of purified nanostructures.

In **Chapter 4**, we introduce the approach for successfully creating biohybrid nano-assemblies by encapsulating the DNPs with virus capsids, verified using comprehensive analytical (AGE and FPLC) and imaging techniques. Also, we determined the excessive mass ratio of CPs required to fabricate two different DNPs.

1

**Chapter 5** describes the use of two selected DNPs explicitly to carry an anticancer drug (daunorubicin) to the target site and assessing their loading efficiency at a varying drug concentration. Finally, the drug-loaded nanocarriers (a hybrid of Drug+DNA+CP) were successfully created and were demonstrated to have high drug loading efficiency.

**Chapter 6** is directed towards performing stability studies of the developed nanocarriers under biological conditions. Two critical work elements in this area were examined: one is the drug release behaviour of the drug-loaded DNA nanostructure (Drug+DN), which was investigated *in-vitro*, mimicking the intracellular environment. Furthermore, the second element is the study of drug retaining abilities, i.e., determining the final amount of drug left within nanocarrier before they enter into the cells.

Finally, **Chapter 7** shows the results for cell viability experiments on the selected cancerous cell line, which is a crucial investigation in this thesis. The cellular uptake mechanism for the designed nanocarriers was examined with selective chemical inhibitors. Our results present the proof of concept, establishing the utility of these nanocarriers for targeted delivery, particularly in cancer theranostic applications.

Overall, the design of two multifunctional biohybrid nanocarriers was demonstrated, which are capable of delivering the drug to the target site exhibiting improved stability and stimuli-responsive drug release. So, such newly designed biologically engineered DNPs can even become critical players in the rapid progress of diverse research fields spread across from materials science to nanomedicine.

### 1.3 References

1. Gazit E, Feynman RP, World Scientific (Firm). Plenty of room for biology at the bottom : an introduction to bionanotechnology London: Imperial College Press.; 2007 [xiii, 183 p. ill. 24 cm.].
2. Goodsell DS. Bionanotechnology: Lessons from Nature: Wiley; 2004.
3. Papazoglou ES, Parthasarathy A. Bionanotechnology. Synthesis Lectures on Biomedical Engineering. 2007;2(1):1-139.
4. Zheng J, Birktoft JJ, Chen Y, Wang T, Sha R, Constantinou PE, et al. From molecular to macroscopic via the rational design of a self-assembled 3D DNA crystal. *Nature*. 2009;461(7260):74-7.
5. Nguyen N, Birktoft JJ, Sha R, Wang T, Zheng J, Constantinou PE, et al. The absence of tertiary interactions in a self-assembled DNA crystal structure. *J Mol Recognit*. 2012;25(4):234-7.
6. Seeman NC. At the crossroads of chemistry, biology, and materials: structural DNA nanotechnology. *Chem Biol*. 2003;10(12):1151-9.
7. Chhabra R, Sharma J, Liu Y, Rinker S, Yan H. DNA Self-assembly for Nanomedicine. *Advanced Drug Delivery Reviews*. 2010;62(6):617-25.
8. Nishikawa M, Rattanakiat S, Takakura Y. DNA-based nano-sized systems for pharmaceutical and biomedical applications. *Advanced Drug Delivery Reviews*. 2010;62(6):626-32.
9. Linko V, Ora A, Kostianen MA. DNA Nanostructures as Smart Drug-Delivery Vehicles and Molecular Devices. *Trends in biotechnology*. 2015;33(10):586-94.
10. Mikkilä J, Eskelinen A-P, Niemelä EH, Linko V, Frilander MJ, Törmä Pi, et al. Virus-encapsulated DNA origami nanostructures for cellular delivery. *Nano letters*. 2014;14(4):2196-200.
11. Hsu CY, Uludag H. Cellular uptake pathways of lipid-modified cationic polymers in gene delivery to primary cells. *Biomaterials*. 2012;33(31):7834-48.
12. Kiviaho JK, Linko V, Ora A, Tiainen T, Jarvihaavisto E, Mikkilä J, et al. Cationic polymers for DNA origami coating - examining their binding efficiency and tuning the enzymatic reaction rates. *Nanoscale*. 2016;8(22):11674-80.
13. Auvinen H, Zhang H, Kopilow A, Niemelä EH, Nummelin S, Correia A, et al. Protein coating of DNA nanostructures for enhanced stability and immunocompatibility. *Advanced healthcare materials*. 2017;6(18):1700692.
14. Ponnuswamy N, Bastings MMC, Nathwani B, Ryu JH, Chou LYT, Vinther M, et al. Oligolysine-based coating protects DNA nanostructures from low-salt denaturation and nuclease degradation. *Nat Commun*. 2017;8:15654.
15. Perrault SD, Shih WM. Virus-inspired membrane encapsulation of DNA nanostructures to achieve in vivo stability. *ACS Nano*. 2014;8(5):5132-40.
16. Lockney DM, Guenther RN, Loo L, Overton W, Antonelli R, Clark J, et al. The Red clover necrotic mosaic virus capsid as a multifunctional cell targeting plant viral nanoparticle. *Bioconjug Chem*. 2011;22(1):67-73.
17. Bruckman MA, Soto CM, McDowell H, Liu JL, Ratna BR, Korpany KV, et al. Role of hexahistidine in directed nanoassemblies of tobacco mosaic virus coat protein. *ACS Nano*. 2011;5(3):1606-16.
18. Douglas T, Strable E, Willits D, Aitouchen A, Libera M, Young M. Protein Engineering of a Viral Cage for Constrained Nanomaterials Synthesis. *Advanced Materials*. 2002;14(6):415-8.
19. Adolph KW, Butler P. Studies on the assembly of a spherical plant virus: III. Reassembly of infectious virus under mild conditions. *Journal of molecular biology*. 1977;109(2):345-57.
20. Liepold LO, Revis J, Allen M, Oltrogge L, Young M, Douglas T. Structural transitions in Cowpea chlorotic mottle virus (CCMV). *Phys Biol*. 2005;2(4):S166-72.
21. Lavelle L, Michel J-P, Gingery M. The disassembly, reassembly and stability of CCMV protein capsids. *Journal of virological methods*. 2007;146(1-2):311-6.





## **CHAPTER 2**

---

# **The assembly of biohybrid nanocarriers for drug delivery applications**

---

Part of this chapter will be submitted.

## 2 THE ASSEMBLY OF BIOHYBRID NANOCARRIERS FOR DRUG DELIVERY APPLICATIONS

### 2.1 Bio-nanotechnology at a glance

According to the National Nanotechnology Initiative (NNI) - “nanotechnology is the understanding and control of matter at dimensions of roughly 1 to 100 nm, enabling novel applications not feasible when working with bulk materials or even with single atoms or molecules” (1). Figure 2-1 illustrates various nanomaterials in a range of sizes (usually they are  $10^{-6}$  of a millimetre), varying from 80,000 nm in a human hair to approximately 5-10 nm in a DNA molecule. The nanoparticles used in the medical field are 100-1000 times smaller than the size of human cells ( $\sim 20\text{-}50\ \mu\text{m}$ ) and other microorganisms ( $\sim 1\text{-}5\ \mu\text{m}$ ) (2).

2

Bio-nanotechnology enables the convergence of multidisciplinary fields for therapeutic, technological and biological research (3). The term bio-nanotechnology is a subset of nanotechnology, having the ability to exploit the structure and functions of biomolecules (proteins, nucleic acids and lipids) at the nanoscale level, creating new devices, materials and systems for diverse biomedical applications (4). It also refers to “nanotechnology through biotechnology”, which involves fabrication of structures into well-defined architectures (using biological materials), having diagnostic and therapeutic applications.

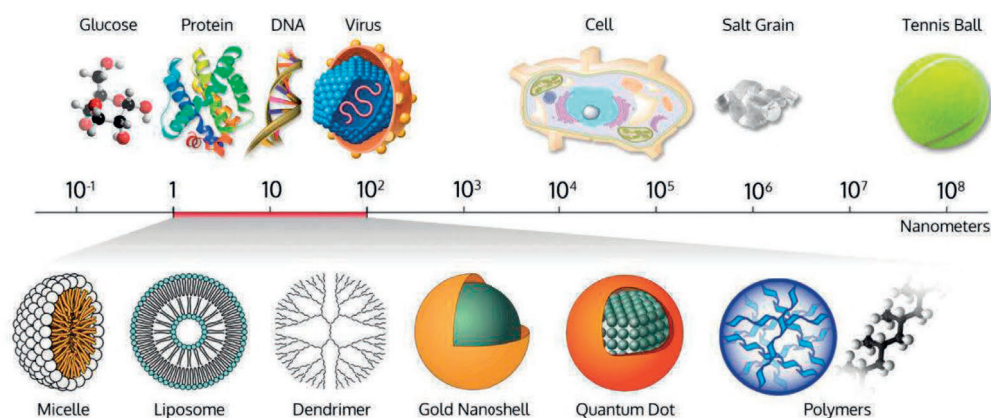


**Figure 2-1 Size comparison of bio-nano particles.**

The size of nanoscale artifacts compared with the size of cells and everyday items such as tennis ball, salt grains and other biological elements, including glucose molecule, protein and viruses (5)

The “top-down” and “bottom-up” are two well-known approaches in nanotechnology to synthesise nanomaterials (Figure 2-2). The traditional top-down process involves breaking up large size particles or materials into smaller size whereas, in the bottom-up approach, the material is

synthesised by self-assembly at the atomic level resulting into useful structural conformations (6). The top-down approach may result in imperfection or irregularities in the surface structure, affecting physical characteristics and surface chemistry of the nanomaterial. Nanolithography, anodisation and plasma etching (PE) are some of the standard top-down techniques (7). Such processes are considered time-consuming and error-prone, and therefore, are not treated suitable for large scale manufacturing of nanomaterials (8). On the other hand, the bottom-up approach involves self-assembly, entailing the random organisation of molecular building blocks into well-defined, stable and functional macroscopic structures, using non-covalent interactions (i.e., hydrogen bonding, van der Waals, electrostatic and hydrophobic interactions). While such interactions are weak, their collective synergy is known to produce very stable structures (9, 10), such as using the specificity of Watson-Crick base pairing to construct well-defined structures out of DNA and other nucleic acids. Some of the classic examples of assembled nanostructures with uniform size, shape and distribution, are motor proteins (11, 12) and DNA based nano-assemblies (13, 14).

2

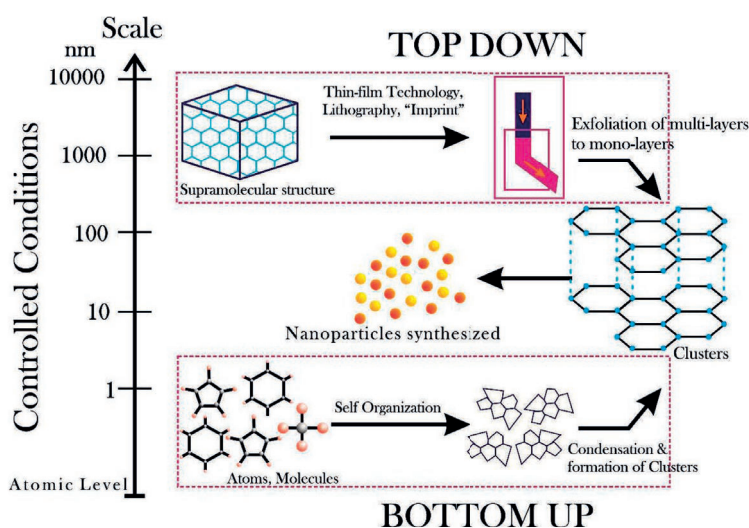


**Figure 2-2 Schematic representation of bottom-up and top-down approaches.**

Several research studies have proven that the process of self-assembly and molecular recognition (based on the bottom-up approach) is the essential technique in biomolecular engineering, having utility at various cellular and sub-cellular levels in biological and therapeutic studies (15).

Following synthesis, the 3D characterisation of newly assembled nanostructures is an essential step in verifying the structural accuracy, integrity, purity and homogeneity of the desired end-product. With the recent technical advancements, the structural and functional characterisation of nanostructures has extended to their visualisation using microscopy techniques. High-resolution electron microscopes are used to generate images of synthesised nanoparticles with the wavelength tuned by the acceleration voltage, and focusing achieved by electromagnetic lenses. Scanning

Electron Microscopy (SEM) uses secondary or reflected electrons while transmission electron microscopy (TEM) carries out imaging with transmitted electrons under vacuum conditions (16). Scanning transmission electron microscope (STEM) is a hybrid technique taking advantages of both SEM and TEM. STEM offers multiple features in the characterisation of biomolecules, including three detection modes for collection of electrons, in turn, improving the resolution of constructed nano assemblies (4).

Further, atomic force microscopy (AFM) works on the principle of scanning the tip (cantilever) across the surface structure and detects the change in the oscillation frequency of the cantilever to create high-resolution images (17). Together, all the above discussed microscopic techniques aided in the development of high ordered assemblies and establishing their structure-function relationships (18). Microscopy generates images of the artifacts with details about their structure, geometry and composition, revealing all structure's heterogeneities; this technique surely has the edge over other characterisation techniques like spectroscopy and crystallography.

## 2

### 2.1.1 Fields of Bio-nanotechnology

There are two significant research areas in the field of bio-nanotechnology: (a) biomimetics, which deals with the design of synthetic materials using natural selection; and (b) templating, which facilitates fabrication of nanomaterials with biological molecules such as microorganisms (bacteria, viruses), biomacromolecules (lipids, DNA oligonucleotides) and proteins. Fabrication of nanostructures with biological molecules is shown to improve the functionality and solubility of the resulting hybrid structures in comparison to the original synthetic materials (19). One of the interesting examples of fabrication is the presence of a regularly ordered surface layer (S layer) in bacteria (20). The S layer comprises of a single protein or glycoprotein and is a highly porous protein lattice self-assembling into a membrane, constituting the outermost cell envelope of many bacteria. The repetitive structural arrangement of S layers protein meshworks with unit cell size 3-30 nm and thickness of 5-15 nm makes them suitable for templating molecules for applied research in life and materials sciences (21). Plant viruses like mosaic viruses are considered as promising building blocks for creating new nanomaterials owing to their biological properties (22). Inclusion of negatively charged polymers in these viral capsids offers a useful way to form virus-like particles that can be potentially used for catalysis and cell-targeting applications (23).

DNA also has been extensively studied as a generic material in nanotechnology, due to its physicochemical properties (base-pairing complementarity, thermal stability) and appealing features like diameter ~ 2 nm, helical pitch 3.4 - 3.6 nm and length of 50 nm, making DNA a material of choice in nanotechnology. Nadrian Seeman and his co-workers pioneered the work of self-assembly of 2D (lattice) and 3D (cubes) architectures from synthetic DNA (24, 25) with exceptional control over their self-assembly (26).

Thus, bio-nanotechnology has proven to be a facile approach utilising biological molecules for

fabricating and creating hybrid nanoparticles (NPs) with morphologies (<100 nm), otherwise challenging to achieve with conventional top-down techniques.

### 2.1.2 Applications of Bio-nanotechnology

The tools and techniques available in the field of bio-nanotechnology led to the formation of a new class of multifunctional NPs and their applications in the areas of medical diagnostics, gene therapy, drug delivery and tissue engineering are of significant interest these days (27). Semiconductor nanoparticles like quantum dots (QDs) have been shown to play a substantial role in medical diagnostics owing to their in-built optical properties (luminescence spectra) (28). The conjugated complexes of DNA with QDs were developed and monitored for their binding to endocytic receptors and live tracking of its uptake mechanism (29). In a similar study, different metallic QDs were hybridised with DNA and used as signal tags for the early detection of HIV and TB diseases with high sensitivity (30).

The existing treatment of many genetic disorders, e.g., cystic fibrosis, cancer and Parkinson's disease, have been made possible by employing gene therapy, using viral vectors but this treatment method is known to have a side effect of inducing an immune response. Parveen *et al.* in a comprehensive study revealed the importance of a new class of functionalised nanocarriers (metal, magnetic and silicon) involved in a wide range of gene therapies and tackling the existing challenges of stability, toxicity, and immunogenicity associated with the repair and replacement of the faulty genes (31).

Bionanotechnology also aids in the development of controlled drug delivery systems (DDS) improving cell targeting and reducing drug toxicity by delivering drugs at their site of action. Nanoparticles are being widely used for the development of selective and effective DDS. A wide range of NPs, such as liposomes (32), polymeric (33-35), ceramic (36, 37), metallic (38, 39), peptides-based (40-42), nucleic acid-based (43-45), and drug-based (46-48), have been developed and used as a DDS for delivering different payloads (small molecules, peptides, proteins, nucleic acids). But as nanoparticles (NPs) are comprised of synthetic hydrophobic polymers, metals or inorganic components that are not homogenous with blood, they may sometimes be recognised as unwanted or foreign by the human body exhibiting an immunogenic response.

Surface modification or encapsulation of NPs results in extended half-lives and reduced immunogenicity in the cellular environment. Encapsulating NP's with synthetic or biological polymers such as dextran (49), polyethylene glycol (PEG) (50) and heparin (51), is known to impart stabilisation, dispersion and absorption of NPs in a biological system. Moreover, fabrication of NPs with cell-penetrating peptides (CPPs) such as transactivator of transcription (TAT) derived from (HIV-1) and polyarginine has proved to facilitate cellular internalisation (52). CPPs mostly comprise of hydrophobic or aromatic cationic residues within the amino acid chain promoting the binding of NPs



on the cell surface, enabling endosomal-escape (53). Also, the surface modification of NP's with folate (54), transferrin (55), arginine-glycine-aspartate (RGD) peptides (56) and antibodies has shown to enable their targeting, imaging and internalisation into specific target cancer cells. Therefore, fabrication of NPs is critical in targeted drug delivery, enhancing their stability, increasing the drug concentration and creating a stimuli-responsive release system (57).

2 Tissue Engineering (TE) is another research area served by the field of bionanotechnology. Herein, the lost and damaged tissues are repaired through biopolymers and biomaterials, forming a support for cellular development. Electrospinning is one of the most widely used technique in TE for constructing biomaterials nurtured with cells (27). Some of the examples using synthetic materials in TE include electrospun fibrous scaffolds, supporting cellular growth, were developed mimicking the structural and functional properties of extracellular matrix (ECM) useful in restoring and enhancing the tissue functions (58). Zhang and co-workers demonstrated the potential role of 3D fibrous scaffolds (composed of the tri-block copolymer poly ( $\epsilon$ -caprolactone) – poly (ethylene glycol) – poly ( $\epsilon$ -caprolactone) (PCL-PEG-PCL, PCEC)) and magnetic iron oxide nanoparticles ( $\text{Fe}_3\text{O}_4$  NPs) as a substitute of damaged tissues in tissue engineering (59). Tort *et al.* also showed the development of three-layered doxycycline-collagen loaded nanofibers (consisting of chitosan and sodium alginate) as an alternative for wound healing with optimised drug release (60). Several published studies manifest the use of protein-based fibres in the biomedical field with advanced applications in tissue regeneration and controlled drug delivery. Such advanced uses of these fibres are only possible because of the additional features they possess like high surface-area-to-volume ratio, porosity, tunability (60, 61), and stimuli-response wielding (62-64).

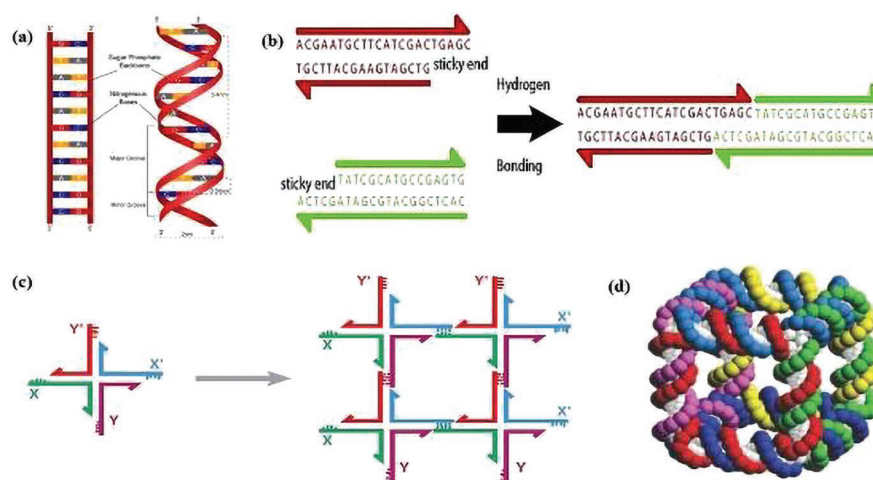
The modern challenge in bionanotechnology is to explore the possibility of engineering a novel biocompatible and multifunctional nanocarrier making use of native regenerative DNA for applications in biomedical sciences and nanomedicines. The intrinsic structural properties of DNA allows the construction of complex high ordered self-assembled nanostructures with predictable, controlled size and shape (65). The design flexibility and ease of functionalisation with DNA hold immense biomedical potential for its development as diagnostic and therapeutic systems.

## 2.2 DNA Nanotechnology - An overview

The new area of structural 'DNA nanotechnology has evolved from Nadrian Seeman's work on immobile DNA junctions and aimed towards designing robust 3D lattices to solve the 'crystal structure' of macromolecules (66). DNA is the biological building block and widely used to formulate nanomaterials owing to its exemplar functional properties like specific 3D conformations, biocompatibility, stability and complementary base pairing (67). The double-stranded (ds) helical structure of DNA consists of nitrogen-containing bases, a carbohydrate (deoxyribose) and phosphate molecule, with each strand approximately 2 nm wide (Figure 2-3a). The two DNA strands

are held together by hydrogen bonds combined along their helical axis using “sticky-ends” and  $\pi - \pi$  stacking between adjacent bases (Figure 2-3b). The ds DNA backbone shows electrostatic repulsion due to the presence of high negative charge with 1 unit of charge per phosphate group and 2 unit per base pair (68). DNA exhibits supramolecular self-assembly properties involving a bottom-up approach of building ordered structures (complexes) without external mediation (69).

Researchers have established numerous convenient methods utilising small repetitive DNA motifs and various other chemical moieties to construct 2D and 3D lattices with prescribed size, shape and functionality. Studies in structural DNA nanotechnology started with the idea of creating complex structures involving branch junctions (70) and topological structures that can be employed in various subfields of material science, biotechnology and medicine. Some of the examples where DNA molecules have been used to design various nanoscale structures and devices are as follows. Early in 1982, Seeman proposed the formation of Holliday junctions (branched DNA junction motifs containing four arms ‘tiles’ self-assembling into lattices and ordered structures) (Figure 2-3c) (66), produced via strand exchange between two juxtaposed duplexes to transfer genetic information (71). Holliday junctions exhibit sequence symmetry of homologous chromosomes during genetic recombination, and the branch point of the four arms (strands) of DNA can migrate throughout the molecule. The immobile Holliday junction-based approach of DNA nanotechnology uses the sequence complementarity of ss DNA and the ability of sticky ends to hybridise, thus, forming larger assemblies (double-crossover - DX tile, triple-crossover - TX tiles and cube-like 3D structures) with ds edges (Figure 2-3d) (72, 73).



2

**Figure 2-3 Structure of DNA and its self-assembly patterns.**

(a) DNA strands and the double helix DNA: DNA strands are complementary and antiparallel having an external skeleton and inside bases linked with hydrogen bonds. (b) Sticky-end hybridisation: Two DNA strands (red and green) with ss overhangs complementary to each other coheres in solution via hydrogen bonding. (c) Sticky end-based self-assembly of four 4-arm junctions to make a quadrilateral and (d) A stick cube having ds edges. Adapted with permission (24).

Later, these units were further developed into higher-degree crossover-based designs, extended to 5, 6, 8 or 12 arms, with self-assembly properties and shape complementarity (74, 75). The tile-based assembly process presented the basis for creating many well-defined 2D DNA-based dynamic nanomechanical devices including DNA tweezers (76), rotary devices (77), DNA scissors (77, 78) and DNA walkers for numerous biophysical applications (79). In 2009, Seeman and co-workers designed self-assembling tensegrity triangle (large 3D crystals) alternating over-and-under rigid DNA motif and a triple rotational symmetry (80). This 3D lattice is shown to diffract X-rays to 4 Å resolution, also proved useful in the conjugation with protein molecules facilitating protein crystallography (81).

Also, along with a range of motifs and short oligos, DNAs can be refined into solid support assemblies, using biotin groups and fluorescent labels, thereby having various applications in nanoelectronics (82). In one of the studies, a DNA nano assembly was designed as a molecular probe by using biotin-streptavidin interaction to label an epithelial cell-surface marker that is used to detect circulating tumour cells (83). Hence, DNA nanotechnology has transformed from basic structural design to sophisticated molecular self-assemblies, to develop nanomaterials with additional functionalities, such as determining biomolecular interactions (84), targeted drug delivery and development of smart theranostic nanodevices (85).

Smalley and colleagues work significantly contributed to the field of DNA nanotechnology by developing bucky-balls or fullerenes, an arrangement of  $C_{60}$  atoms in a spherical form laying the foundation for the development of sophisticated and practical nanodevices for future optoelectronics

and biomedical applications (86, 87). Goodman *et al.*, reported the single-step synthesis of complex DNA tetrahedron (cages) by annealing four appropriately designed ss oligonucleotides with equal edge length and different sequences suitable for drug delivery (88). Aldaye and Sleiman presented the construction of discrete modular 3D DNA assemblies such as triangular, cubic, pentameric and hexameric prisms with an application in drug delivery and protein encapsulation (89). Mao *et al.*, illustrated a strategy for controlling the chirality of DNA octahedron by mapping its stereoisomeric confirmation and using Cryo-EM imaging to determine their biomolecular structures in near-native conditions (90). Ke *et al.*, marked the role of ss tiles (SST) or 'DNA bricks' as building blocks, serving a canvas for designing arbitrary 2D and 3D objects and adaptive platform for highly-ordered assemblies (91). SST monomers are composed of floppy sticky ends and self-assemble into rectangular shape due to interaction with four neighbouring SSTs. This tile-based assembly approach serves as a canvas for designing and assembly of molecular shapes and modular components.

2

The most critical development in DNA nanotechnology was the use of 'scaffold DNA strand' for assembling highly ordered folded nanostructures. The work by Shih *et al.*, reported designing of a rigid and well-defined DNA octahedron from a long ss DNA molecule with 1669-nucleotide (nt), amplified by thermal annealing using 40-mer complementary staple strands (92). This work was considered as 'pre-origami' paving the foundation and inspiring for the discovery of DNA origami.

### 2.2.1 DNA origami: The art of nanoscale folding of DNA

From the earliest reported DNA junction motifs, an enormous library of well-defined, monodisperse and discrete DNAs and extensive DNA arrays with incredible complexity has been produced. As the designing techniques for DNAs developed rapidly, they paved the way for the birth of DNA origami. The quantum leap in the field was observed with the invention of 'DNA origami' by Rothemund in 2006 (93). DNA origami is defined as programmed self-assembly of 7-kb long M13mp18 ss genomic DNA (scaffold) with hundreds of ss-oligonucleotides (staples) complementary strands in a simple 'one-pot' reaction into desired DNA shapes like paper origami (94). The principle of DNA origami is similar to Holliday junction, i.e., multiple crossovers to connect the strands but also, the packing distances were minimised to reduce the interhelical gaps. The beauty of DNA origami designs is in its raster-like pattern forming continuous double helices providing the much-needed rigidity and stability to the final design. The DNA origami method gives an entropic edge over multistrand (tile-based) approach in the formation of nanostructure as it allows transient binding of staples to scaffolds and proof correction by strands displacement exchanges during folding (95).

The DNA origami approach was practical and prevalent as it does not necessitate any specific sequence arrangement or typical stoichiometry. DNA origami was used to produce several 2D and 3D nanostructures as shown in Figure 2-4, smiley faces, tetrahedrons (96), DNA nanotubes leading to DNA barrels and DNA "dolphins" (97), which were successfully demonstrated to be involved in

various biological applications (98). Besides planar geometric designs, there are many complex 3D shapes built, such as curved rings, spheres and hemispheres, and super twisted structures reported by Dietz and co-workers (99). The twists and bends in the designs were created using the addition or deletion of DNA base pairs within a selected array of helices. Additionally, the expansion and contraction of the helices was also made possible by inserting and deleting base pairs on the opposite sides of the design.

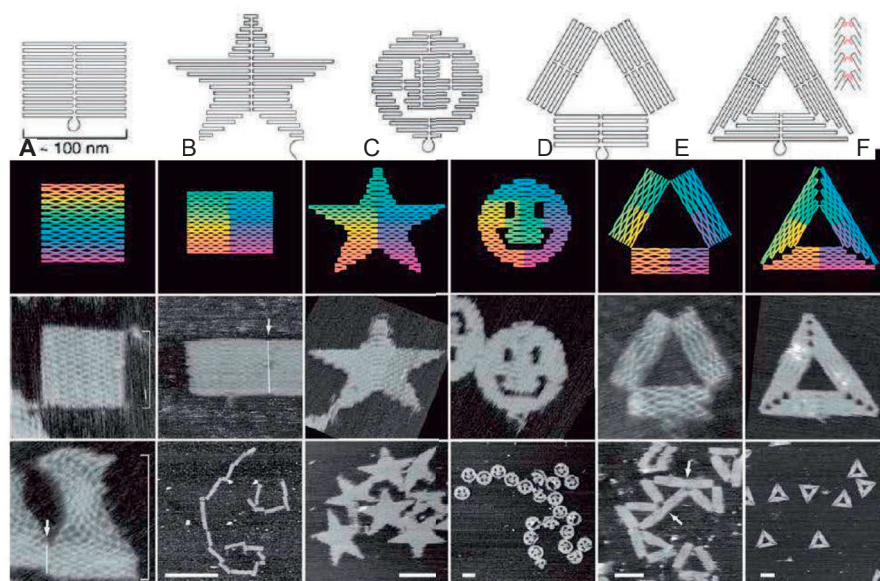


**Figure 2-4** Designed modular DNA origami structures.

The top row represents the folding paths. A) square; B) rectangle; C) star; D) smiley shapes; E) triangle with rectangular domains; F) sharp triangle with trapezoidal domains and bridges between them (shown as red lines in the inset on the right). Dangling curves and loops represent the unfolded sequence. The (middle and bottom rows) contain the resulting DNA structures as imaged by AFM. Adapted with permission from (93).

In 2011, Yan's lab developed some intricate 3D curved geometries with adjusting the particular positions and patterns of crossover points between adjacent helices in the concentric DNA rings. This technique enabled creating a variety of 2D rounded squares and 3D ellipsoidal and nano flask architectures combining both in-plane and out-of-plane curvatures (100). Yin and colleagues have synthesised a DN, based on interlocking short synthetic ss DNA to form a 3D DNA brick. They demonstrated higher versatility of DNA bricks, as each 32-nt brick was a modular component, able to interact with local neighbours and can be removed or added independently. These origami techniques enabled the engineering of different DNs from appropriate 2D/3D block canvas (with high atomic masses and larger sizes) having distinct shapes, displaying sophisticated surface features, as well as having intricate interior cavities and tunnels for fabrication (101).

In an alternative method of bottom-up assembly, Dietz and co-workers constructed a DNA-protein

hybrid macromolecule by using protein staples in place of DNA staples. Transcription activator-like (TAL) effector proteins were tailored explicitly to recognise a specifically defined DNA target sequence. These hybrid structures bind to the promoter motifs at room temperature (*in-vitro*), and are known to have excellent chances for establishing the structural-functional relation of genomic translation in living cells (102).

Han *et al.*, have formulated a new meshing origami technique, where they engineered gridiron-like DNA structures using a series of four-arm junctions as vertices of DNA network, which were further reconfigurable into multilayer and 3D structures and curved objects (103). Also, Högberg and colleagues used the graph theory to build wireframe DNA origami, where the polyhedral triangulated mesh has been transformed into the desired 3D object (a Stanford bunny) in a completely automated fashion using a routing algorithm and a relaxation simulation (104). The advantage with mesh origami scheme is the possibility of designing open conformations rather than conventional closed pack helices, conferring more stability and flexibility in biological research.

The above-discussed examples illustrate enough simplicity and robustness of DNA origami compared to the earlier variants of DNA nanotechnology. Also, the emergence of mechanical designs to synthesise DNA nanostructures, it transformed the origami from an art to a whole engineering discipline.

### 2.2.2 *In-silico* designing of DNA nanostructures

The advancements in DNA origami technique have supplemented DNA nanotechnology for the perception of intricate 3D designs and creating them in reality with the help of several freely available computational tools. Seeman and colleagues in 2006, introduced the first DNA design software GIDEON, which is still being used by the research community (105). Then, SARSE software was developed to create 3D DNA origami, which facilitated the development of the desired structure, envisioning a molecular representation framework. This software also came with an oligotracker to alter and save the list of staple strands and their sequences. Later, a GUI software caDNAo (106) was reported, which is open-source computer-aided design software used for designing scaffolded DNA origami. The software simplifies and expedites the design process of DNAs, setting up the template of parallel ds DNA strands in the cross-section and generates a list of necessary staples for folding. Another tool, CanDo analyses the flexibility and predict the shapes of designs in aqueous solution and ensure the structure's correctness based on the mechanical properties of DNA (107). CanDO is complimentary to caDNAo and used its files as input. Mark Bathe and co-workers developed DAEDALUS, a fully automated package for creating desired 3D geometries with a top-down method (108). Moreover, Tiamat (109) and vHelix (104) use an alternative wireframe strategy based on lattice-free designing approach.

The number of software packages discussed here provides sophisticated and user-friendly methods to generate staple strands for creating target DNA architecture. CaDnano is the most popular



amongst all as it has an interactive interface and design features. After the designing phase, the experimental assembly process is carried out for DNA origami (*in-vitro*), which leads to the formation of dense structures, followed by their characterisation and visualisation using various microscopic techniques.

### 2.2.3 Advances and applications of DNA Nanotechnology in biosciences

DNA nanotechnology uses DNA to synthesise nanostructures and does not interfere with the genetic information it carries. This field is now fast approaching real-world applications with great potential in nanomedicine and health sciences. The last decade marked a surge in research output describing the uses of structural DNA nanotechnology in various biological fields (110). There have been advancements in the techniques for designing, optimisation and synthesis of highly controllable, custom and accurate nanostructures of different shapes and sizes (111). These nanostructures are known to have a myriad of applications in different streams health sciences: structural biology, biocatalysis, disease diagnosis, drug delivery, gene therapy and nanomedicine (112), also shown in Figure 2-5.

2

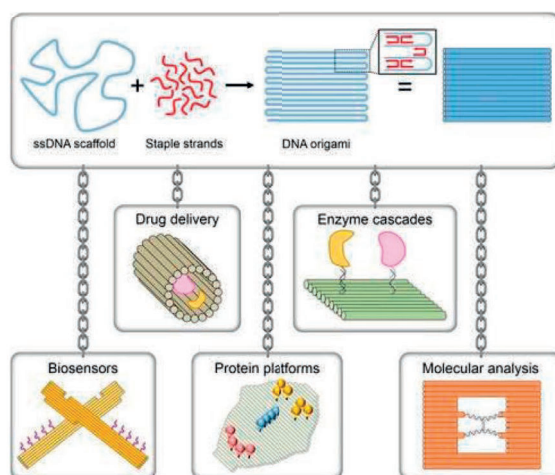


Figure 2-5 Different biological applications of DNA nanostructures.

Adapted with permission from (113)

Chemical modification of the DN's staple strands with biotin allows binding of streptavidin enabling detection of single molecular events in biological systems (114). In another study, Niemeyer group reported, the site-specific fabrication on DNA origami using a coupling system incorporating benzylguanine (BG) and chlorohexane (CH) groups to create desired protein arrangement (82). Moreover, DN's (stick-like punched DNA origami) have also shown to be capable of stepwise adding and removing functional proteins streptavidin (SVT) form a nanoarray, thus forming a totally reversible and programmable protein nanopatterning system. These nanoarrays can selectively remove the protein tetramers by using toehold-mediated strand displacement method and may

widen the scope of applications of DNA nanotechnology (115).

DNA tiles are also an example of DNA nanotechnology applications where they serve as a platform for the arrangement of two enzymes: glucose oxidase (GOx) and horseradish peroxidase (HRP) at the desired distance to monitor their enzymatic cascade activity (116). The coupling reaction between enzymes manifests a cascade in a confined space, leading to the creation of nanoscale bioreactors. In 2015, Kostianen's group designed two separate modular and tubular DNA nanoreactors conjugated with GOx and HRP using neutravidin/biotin binding (117). Then, these two tubular nanoreactors were assembled into a dimer structure to bring the two enzymes into proximity and demonstrated an efficient enzyme cascade reaction inside the tube.

The ease of modification in DNAs presents them as an ideal substrate for chemical and biological sensing. DNAs have been developed for sensing pH and enzyme activity, detecting target nucleic acids and alteration in nucleotide sequence. For detecting nucleic acids, the DNA-based 'molecular chips' were created through site-specific anchoring of DNA probes with target nucleic acid sequences, which can be easily read out in gel analysis or visualised through AFM (113). A quadruplex DNA design 'nanoplier' consisting of two levers with C-rich sequences (i-motifs) connected at junction fulcrum was developed for pH sensing (118). This nanomechanical device changes its conformation based on the pH change, i.e., the levers remain open at neutral pH with low FRET signals; meanwhile, at acidic pH, the C-rich strands bring two levers in close conformation resulting in high FRET signals.

Most of the biological processes occur discretely and randomly at the molecular level, and the bulk properties may not represent precisely the properties of each molecule. Thus, Sugiyama's group suggested the single-molecule analysis is necessary to comprehend the chemical or biochemical reaction occurring in all biological cells. One of the most salient features of the origami method that came handy for single-molecule analysis is the ability to precisely alter the structures formed: Here, each staple serve as an attachment point for different kinds of nanoobjects. Thus, the method is suitable for the positioning of various functionalities and for the single-molecule analysis of many chemical and biochemical processes (119).

Liu *et al.* provided evidence for the potential use of DNA tetrahedron in designing and making a variety of synthetic vaccines. They used DNA to assemble a model antigen with STV and CpG-oligodeoxynucleotides (ODN) adjuvant complex inducing a long-lasting and robust antibody response in the mouse models. The study showed enhanced immunogenicity of tetrahedron-STV-CpG ODN complex against the specific antigen in comparison to STV alone and STV-CpG mix, in both *in vitro* and *in vivo* conditions (120). The DNAs offers several advantages to be used as nanocarriers, including biological stability (121) and biocompatibility (122). In a study by Schuller *et al.*, DNA nanotubes are decorated with 62 unmethylated cytosine-phosphate guanine dinucleotides or 'CpG-Motifs' for immune activation in the mammalian cells. These CpG motifs are uptaken by



endosomes and elicit a higher immune response inducing an immunostimulatory cascade via Toll-like receptor (TLR9) compared to naked DNA nanotubes (123). This exhibited their potential role in the development of immunogenic vaccine and targeted drug delivery.

Ouyang *et al.*, reported the use of nanoribbons as delivery carriers for CpG motifs in macrophage-like RAW264.7 cells to acquire an immune response. Nanoribbons were said to be created using RCA (rolling circle amplification) strategy, with short periodic sequences folded with few staple strands (124). Sleiman and colleagues have described the process to construct RCA nanotubes with reducing the number of nicks in the backbone, which increases its resistant to nuclease degradation. These nanotubes were capable of penetrating in human cervical cancer (HeLa) cells, established by labelling them with dyes (Cy5 and Cy3), and imaging its cellular uptake across the membrane (125). So, RCA-based nanostructures proven to be cost-effective and rigid with the ability to efficiently penetrate the cells, making them suitable to be used as imaging agents and in biological therapeutics.

2

Hence, DNA based nanostructures are promising devices that can be readily uptaken by cells and shown enhanced stability in the cellular environment in contrast with ds-DNA (126). Moreover, being made up of natural biopolymers; they can be easily digested by cellular machinery without causing any harmful effects.

The role of DNAs has also been explicitly investigated in cancer therapeutics. Jiang *et al.*, demonstrated the non-covalent binding of the anticancer drug doxorubicin (Dox) to 2D and 3D DNA origamis and its (*in vivo*) delivery into cells. The efficacy of DN-Dox complex was shown with improved cellular uptake and increased cytotoxicity on breast cancer cells (reg- MCF 7) and dox-resistant cancer cells (res-MCF 7) (127). Further, extending studies to *in vivo* models, the DN-Dox complex exhibits higher antitumour efficacy with minimal cytotoxicity compared to bare DN (128). In similar research, Halley and his team have shown daunorubicin (Dauno) bounded to rod-shaped DNAs, form a complex. This complex achieves high drug loading efficiency with excellent stability in physiological conditions and also proved to circumvent the drug resistance in leukaemia cells (129). Hogberg *et al.*, have customised DNAs using honeycomb-lattice framework for optimal drug delivery to three different breast cancer cells (MDA-MB-231, MDA-MB-468 and MCF-7). By varying the level of relaxation in the design, they fine-tuned the drug encapsulation efficiency and the rate of drug release. Besides, higher cytotoxicity in cancer cells, lower intracellular drug elimination rate was also observed in comparison to when administering the free drug. This study suggested that regulation of drug release kinetics can be controlled by slight modifications in nanostructures exhibiting different degrees of twist (130). Thus, DNA-based nanocarriers display enhanced permeability and retention effects (EPR), causing increased accumulation of drugs in tumour cells, makes them a suitable carrier in cancer therapeutics.

The field of DNA nanotechnology witnessed exponential growth in research converging materials

sciences and biomedicine due to its engineering abilities. Further research and development in drug delivery and resolution of scalability issues of DNA nanotechnology can bring a new perspective altogether into useful clinic results.

## 2.3 DNA Nanostructures as drug carriers

In recent years, the use of DNA origami-based nanostructures in targeted drug and gene delivery has become a research hotspot. DNAs are considered as promising candidates for targeted deliveries because of their superior structural characteristics, which enhance drug solubility, minimise cytotoxicity and enable controlled drug release to achieve maximum therapeutic efficacy (131). Various natural or synthetic oligonucleotides have been used to carry drugs and build effective delivery platforms, bypassing the biological barriers for improving therapeutic results (112).

### 2.3.1 Properties of an effective delivery system or a nano-vehicle

Many drug delivery systems use commercially available artificial organic nanomaterials such as liposomes and cationic polymers for clinical use. These nanomaterials usually are of favourable nanoscale size (1-100 nm) having high surface-volume ratio and are considered suitable for cellular internalisation. However, the inherent cytotoxicity and issues related to crossing the physical cell barriers limit their application scope (132). Alternatively, the use of inorganic nanostructures emerged as another possible carrier, e.g., the use of gold nanoparticles for intracellular delivery of antisense nucleotides (133) and anticancer drugs (134). Carbon nanotubes and graphene sheets were also explored for delivering biomolecules (135). Additionally, few other inorganic materials (e.g., quantum dots, iron oxide) found uses in diagnostic imaging and *in-vivo* tracking of the delivered drugs (136). However, the inorganic nanoparticles contained toxic materials and were found difficult to degrade, raising safety concerns for their use.

Bio-nanotechnology presented the development of 'smart drug delivery systems (SDDS)' with features addressing perennial issues such as solubility and toxicity in drug delivery. Particle size and surface properties of SDSS are vital factors that affect passive or active cellular uptake of nanoparticles inside the cells. SDSS must be able to penetrate the cell membrane to deliver the drug in a controlled manner at the target site and escape from endosomes (65). In the cellular environment, delivery systems must remain stable until they enter the cells and release the payload with a trigger mechanism. Another critical attribute to be considered is their ability to release the drugs in a controlled and selective manner to recognise target cells, attain adequate circulation time and circumvent side effects (137, 138).

A suitable drug carrier retains the biological properties of medicines *in vivo*, reducing the pharmaceutical doses and minimising the possible side effects. Also, it should have an adequately controlled size (<200 nm) and high loading capacity for the cargoes (136). Therefore, an ideal drug delivery vehicle must be competent to carry payloads, resist them from chemical and enzymatic

encounters in the cellular environment, along with the escape from the early endosomes to reach the specific cellular organelles and to perform the intended task (139). DNs have some unique properties making them ideal candidates as (SDDS): (a) designed with numerous functionalities; (b) can undergo precise self-assembly; (c) low immunogenicity; (d) high flexibility for carrying a variety of drugs; (e) controlled drug release (43). DNA-based drug carriers represent characteristic functional systems with the competence to attain specific target sites and to overcome biological obstacles of targeted drug delivery. These unique systems are known to achieve their goal by selective encapsulation of recognition elements like antibodies, proteins and peptides that stimulate triggered release of cargo at the target site (140). Many studies have depicted the importance of the size and shape of the drug carrier, and the precise control of ligand placement in spatial orientation are significant determinants of the carrier's ability to deliver drugs at the target site effectively (141).

2

In the quest of developing an active and targeted SDDS, several natural (virus), biomimetic and synthetic materials based systems were developed, reported with increased blood circulation time and cellular uptake (142). However, these systems still encounter some issues related to biostability, and safety creating a scope for exploring improved delivery methods.

### 2.3.2 Applications for the use of DNA nanostructures as efficient drug carriers

DNA nanotechnology developed robust 2D and 3D nanostructures to function as artificial molecular devices controlled on a nanoscale, for multiple applications. DNs were surface modified with fluorescent dyes and were used *in-vivo* for the identification of therapeutic targets and imaging purposes (143). Numerous research studies presented the utility of DNs to simultaneously deliver different therapeutic molecules like targeting ligands, anticancer drugs and therapeutic oligonucleotides into the cells (144, 145). DNs coupled with iron transport protein (transferrin) demonstrated significantly higher cytoplasmic uptake in cancer cells compared to the planar DNA origami structure (146). A study by Ding and his team showed a controlled and slow release of doxorubicin (an anticancer drug) in acidic conditions, facilitating the delivery of small molecules and other synergistic therapies with DNs (147). Later, Xia *et al.*, observed enhanced drug uptake of glioblastoma cells when the tumour-penetrating peptide was conjugated with tetrahedral DN (148). Also, nucleolin specific aptamer-tethered DNA nanorobots containing thrombin have been constructed that act as a molecular trigger and explicitly directed to tumour-associated blood vessels, thereby activating coagulation, inducing tumour necrosis and suppressing tumour development (149). The potency of DNs is proven as a safe carrier in cancer therapeutics, showing passive accumulation and slow digestion (*in vivo* and *in vitro*); reducing non-specific drug distribution within tumour cells (128).

There are few DN geometries developed are also known to exhibit enhanced internalisation efficiency by cells. In a study, Mao *et al.*, have shown that cancer cells can effectively take up folate-labelled DNA nanotubes with zero toxicity to healthy cells (150). Other investigations by Turberfield

and co-workers have demonstrated that pure DNs can enter live-cultured mammalian cells regardless of their net charge and without the need of any transfection agent (151). As mentioned earlier, Sleiman and team constructed nuclease-resistant DNA nanotubes, which were more efficient in penetrating cells than ds DNA (125). Various DNs were adapted to carry drug cargoes as per the requirement of therapy. Hollow DNA tubes containing 62 CpG sequences were tested for immune response in spleen cells. Although they depicted a strong immune response, no toxicity was detected in splenocytes (152). DNA nanocarriers were also shown to transmit non-methylated (CpG) sequences to improve immune responses, transport monoclonal antibodies and other medications to assist the immune system in recognising and attacking cancerous cells (153). DNs have exhibited excellent biocompatibility and minimal toxicity in intracellular or *in vivo* applications. Thus, we know that DNA nanomaterials can be designed into distinct structures with an ability to optimise a range of cell delivery parameters. (136). Moreover, the modularity and predictability (planned geometries and precise 3D alterations) of designs confers DNs with tissue specificity and improved EPR beneficial in targeting cancerous cells in comparison to conventional polymeric NPs (liposomes) (154).

2

Overall, the DNs possess all the essential features required to qualify them as an efficient drug carrier (136), but the delivery of therapeutic agents using nanotechnology also poses a concern of toxicity and off-target side effects (155).

### 2.3.3 Challenges for DNA nanostructures in drug delivery

There are some practical concerns and challenges inherent to DNA-based drug delivery systems, such as improving their structural stability, cellular uptake, and payload delivery. DNs encounter degrading machinery of cells (e.g., DNases and nucleases), low physiological cation concentration and different pH levels in distinct cellular compartments after being introduced in the cellular environment (132). Together these components challenge the structural integrity of drug-carrying DNs. However, the enhanced stability of DNs was reported compared to unstructured ds-DNA under various testing conditions mimicking the intracellular environment (126, 156, 157). The structural stability of DNs is essential as it is linked to transfection efficiency and, finally, localisation inside the cells.

Biosafety is another concern as DNs trigger a strong inflammatory response is considered malicious by different cellular receptors (158). Therefore, for DN to function as a SDDS, we need methods to minimise these immune responses. One way to reduce the immune response is by surface modification of DNs, i.e., conjugating them with immune inert proteins (BSA), leading to attenuating immune activation (131). Partially degraded DNs also have a high chance of inducing an immune response, thus by tuning the stability of DNs and optimising their spatial position makes them defiant to degradation (158). In a recent study, while assessing the *in-vivo* safety profile of the DNs in a tumour cell, low cytokines levels (IL-6, TNF- $\alpha$  and IFN- $\alpha$ ) were detected, suggesting that the intact

DNs were immunologically inert (159).

The polyanionic nature of DNA and low water solubility offers a fundamental challenge in achieving a higher transfection rate or crossing the negatively charged cell membrane. The negative charges of DNs hinder their passive uptake, and so they are internalised *via* active energy-dependent transport process. However, many modular DNs reported entering cells readily without the presence of a transfection agent, possibly following the endocytotic pathway (160). In a recent study, Bastings *et al.*, emphasised the importance of the size and shape of DNs for effective cellular internalisation (161). This study provided a comparison of many variables such as morphology, aspect ratio and different cell types in affecting uptake kinetics.

2

In drug delivery, the kinetics and controllability of drug release is also an essential factor for consideration, as shown in Figure 2-6. Suppose the drug is released in a burst mechanism as opposed to a slow, tunable release. In that case, there will be a higher initial delivery leading to considerable physiological damage and a lower lifetime of the therapy, which eventually leads to the need for higher dosages (112).

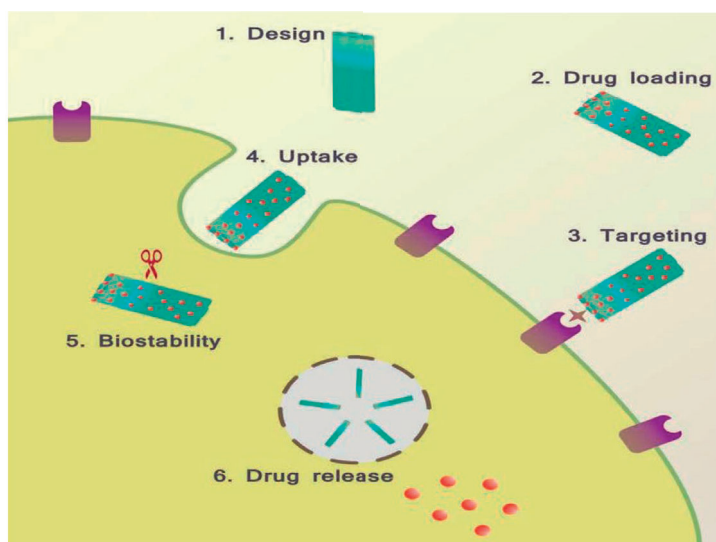


**Figure 2-6 Overview of targeted drug delivery trail using DNs.**

The design and packing of drug-loaded DNs make them stable in the cellular environment, and the drugs released in response to triggers.

Controlled release of drugs is critical and challenging for the development of SDDS. Once reaching the specific target sites, the carriers with external stimuli response should be able to trigger the release of drugs. The DNs can be designed to respond to a variety of chemical and biological cues such as a) temperature, b) pH, c) light, d) aptamer configuration, and e) enzyme activity. There are several examples reported, where several design strategies such as conjugation, encapsulation and intercalation used to modify the surface functionality of DNs responding to external cues for targeting

specific cells (162). Douglas *et al.*, designed an aptamer-encoded logic gate DNA ‘nanorobot’ to carry out controlled release of payloads, programmed to open at the target site in response to cell surface signal and release the cargo (163). In another study, logic gate-based dynamic DNA nanodevices were developed, using multiple targeting ligands that recognise cancer cell-surface markers, thereby enabling precise disease diagnosis and effective therapy (164). Many such findings point towards ideally assessing long term specificity and side effects of DNs through *in vivo* investigations.

Another essential feature is to examine the transportation mechanism of DNs into cells (*in-vivo*), including their intracellular route and pharmacokinetic properties, i.e., absorption, distribution, metabolism, elimination and toxicity (ADMET). Attention must also be focused on designing new strategies to improve the selective uptake of DNA nanocarriers by target cells. Thorough *in vitro* and *in vivo* investigations are required to understand pharmacokinetics, clearance mechanisms, and half-life circulation of various DNs (165). Future applications indicate assessing DNs in combination with other treatment strategies to attain controlled drug release. Also, obtaining purified and intact origami nanostructures in micromolar concentrations in a cost-effective way is another area where research should be focussed (142).

2

### 2.3.4 Addressing the challenges posed by DNs in Drug delivery

Several DNA architectures: tile-based DNs, origami-based DNs and supramolecular DNA assemblies have been developed using different fabrication strategies and comprising bottom-up, top-down and RCA-based approaches for a multitude of applications, including targeted drug delivery (166, 167). Further, in order to overcome the limitation of DNs (as discussed above) for their applications in cellular environments, DNs were often structurally modified through chemical modification and by the addition of an external protective coating. These methods of surface modification promote DN’s stability, extend their circulation time, enhance its functionalities, mainly enable DNs to target specific cells and precisely control drug release in a specific biological environment (136).

#### 2.3.4.1 Chemical modification of DNs

Chemical modification of DNs enhances their stability and biological functionality during cellular interaction. In 2018, Zhu *et al.*, developed nanoconjugates combining spherical nucleic acids with poly(lactic-co-glycolic acid) using click chemistry (168). This surface functionalisation was useful, mainly showcasing their immunotherapeutic potential by activating TLR9 in macrophages (168). In another study, biotin and folate modified DNA strands were attached to two differently shaped DNs, probing their intracellular pathways and fate (i.e., distribution and disintegration) in mammalian cells. The result indicated that shape, geometry and selection of target cellular receptors were pivotal in influencing the final cellular destination and affecting the circulation lifetime of the DNs (169). Ponnuswamy *et al.*, reported an alternative strategy to modify DNs surface with cationic polylysine-

PEG conjugate, preventing them from denaturing conditions, such as low salt and attack by nucleases. The study revealed a ~1000-fold increase in resistance to nuclease degradation together with modest improvement in circulation and biodistribution of DNAs *in-vivo* (170).

Moreover, forming DNA micelles complex (DOPMs) by attaching block copolymers (PEG-Plys) with DNAs, also facilitated the stabilisation and freedom to encapsulate different ligands (peptides or molecular markers) with DNAs (171). Further, in many other studies performed with chemical crosslinking (e.g. phosphorylation and enzymatic ligation) have proven successful in enhancing the stability compared to their non-crosslinked counterparts. However, their further usage was limited in DNAs as it may alter the mechanical properties affecting the loading and release of the payloads (172).

## 2

### 2.3.4.2 Biological modification of DNAs for fabrication

Biological engineering (fabrication) is a rapidly evolving technology in the biomedical field, enhancing the sensing and drug targeting capabilities of DNAs. Together with unique architectural property, DNAs offer surface modification with multivalent binding proteins to transferrin (173), cell-penetrating peptides (174) and virus capsid proteins (175) to thereby regulate enzymatic reaction and intracellular delivery of payloads.

Nevertheless, the polar nature of DNA also offers hindrance in effective transfection. As a solution, viruses are used as they are the natural transfection agents and have proved successful entrapments of drug-loaded DNA micelles and their utility as a drug delivery system (176). Viruses are biomacromolecules with a unique feature of self-assembly and encapsulation of non-native materials with highly defined structures for application in imaging and drug delivery (177, 178). Studies have established that the encapsulation of DNAs with lipid bilayers and virus capsid proteins enhances cellular uptake and increases stability and bioavailability (179). In a seminal study showcasing the packaging of DNA with viruses, Mikkilä *et al.*, allowed virus capsid proteins to self-assemble on the origami surface through electrostatic interaction, resulting in a 13-fold increase in transfection efficiency of coated DNAs compared to bare DNAs in HEK 293 cells (175). Alternatively, Perrault and Shih designed a virus mimicking structure by encapsulating DNAs with PEGylated lipid bilayer. The encapsulated nanostructure showed protection against nuclease degradation, reduced immune activation and increased pharmacokinetic bioavailability (180). In addition to virus capsid proteins, Auvinen and co-workers used bovine serum albumin (BSA) or class II hydrophobin (HFBI) conjugates attached to DNAs surface to create biohybrid materials. This study has shown that the BSA coating generates a 'shield' from immune surveillance together with improved cellular delivery (131).

Viruses are well known infectious and harmful particles, but in nanotechnology, viruses are used as templates and building blocks for fabrication. Bacteriophages and plant viruses are considered safer (non-infectious) in humans and animals.



## 2.4 Plant viruses as a template for fabrication

Plant viruses hold multiple features: stability, size and surface presentation, hierarchical assembly, response to physical and chemical stimuli and biocompatibility; these features together make viruses an attractive platform to be used in drug packing and delivery applications (181). Virus comprises of capsids proteins, which envelop the confined genetic material. On the other hand, VLPs (virus-like particles) are empty capsids (devoid of RNA) and non-infectious parts, which serve as biological container or cages with uniformity of morphology, ease of functionalisation and sizes ranging from 10 nm to few microns (182). There are various capsids used to fabricate DNs, including ones from plant viruses, animal viruses and bacteriophages, which facilitate altered surface recognition characteristics concerning specific target cell type, thereby increasing binding affinity through multi-valency effects (183).

Over the past decade, researchers have demonstrated the use of viruses and VLPs as building blocks to design complex nanostructures. Mostly, capsids from plant viruses are used as a biotemplate and fabrication tool, finding application broadly in the field of medicine and therapeutics (184). Several plant viruses such as the cowpea mosaic virus (CPMV), cowpea chlorotic mottle virus (CCMV), red clover necrotic mosaic virus (RCNMV) and rod-shaped tobacco mosaic virus (TMV) are reported to be used in vaccine development (185, 186), gene therapy (182), and in biomedical imaging (187).

2

### 2.4.1 CCMV - the natural encapsulation material

The Cowpea chlorotic mottle virus are model plant-infecting viruses obtained from *Vigna unguiculata* belonging to the family *Bromoviridae*. The CCMV is suitable for encapsulation of all kind of materials due to their distinct characteristic of being reversibly swollen and disassembled by altering the pH and ionic strength of the medium (188). Their capsid is made up of 180 identical subunits (19.8 kDa each), contributing to an icosahedral protein shell surrounding four different strands of ss RNA. The capsids have ( $T=3$  symmetry) with an external diameter of 28 nm and an internal diameter of 18 nm (Figure 2-7) (189). Being icosahedral structures, the CCMV is made from 12 pentamers and 10 ( $T-1$ ) hexamers. Each subunit of CPs comprises of 190 amino acids (AA), with the N-terminus located inside the capsids. The first 1-25 AA are basic residues with a strong affinity towards the negative phosphate group of RNA, particularly the N-terminus and the nine positively charged Arg and Lys residues (189, 190). Capsid protein (CPs) can be disassembled and purified from RNA by regulating pH along with the metal ion ( $\text{Ca}^{2+}$  or  $\text{Mg}^{2+}$  concentration) (191). Increasing pH  $\geq 6.5$  and salt concentration above 0.3M leads to the opening of 60 pores (2 nm diameter) in the capsid, thereby revealing internal protein cages to the bulk medium. However, this disassembly can be reversed back to the original  $T=3$  particle, lowering the pH to  $\leq 5$  at a high salt concentration ( $> 0.5\text{M}$ ), allowing encapsulation of cargo in the medium (192). These dynamic structural transitions in CCMV offer a distinct mechanism of molecular gating for controlling entrapment and release of organic and



inorganic materials.

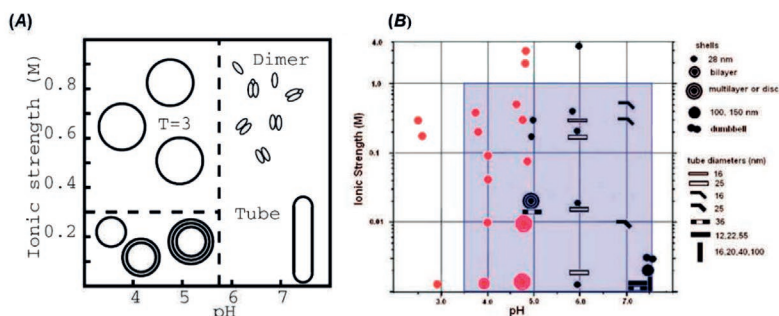


**Figure 2-7 Phase diagrams of CCMV capsid proteins without RNA.**

(A) A simple phase diagram is showing four general domains of morphologies in capsid protein assemblies (B) An extended phase diagram based on observations by Lavelle *et al.*, adapted with permission (193, 194).

2

Moreover, the assembly of CCMV CPs in and around polyanionic species like DNA or anionic polymers at neutral pH ( $\geq 7$ ) and lower ionic strength ( $< 0.3$  M) resulted in the formation of different shapes depending on the size of the cargo materials (189, 192). The assembly of the capsids was extensively studied and well defined by the two-phase diagram (Figure 2-7) covering a wide range of conditions, i.e., pH and buffer (193, 194).

#### 2.4.2 Encapsulation of different polyanionic materials using CCMV

A wide range of controlled and optimised complex systems have been developed based on the ability of virus capsids to encapsulate various components through self-assembly, chemical conjugation or genetic manipulation (184). CCMV can disassemble and remove its RNA and then self-assembles to encapsulate various negatively charged materials. The interior of the capsid is a positively charged region (N-terminus), enriched with arginine-rich motifs (ARM) interacting with anionic particles electrostatically and finally stabilising the virus (195). The negative charges of the cargoes can manifest the assembly of CPs at neutral pH and lower salt concentration to form encapsulated structures.

There are several examples of different polymer packaged inside CCMV, such as polystyrene sulfonate (PSS), and poly(2-methoxy-5-propyloxy sulfonate)-phenylene vinylene (MPS-PPV) encapsulation with CCMV CPs, forming stable and sometimes clustered VLPs (196). DNA micelles and paramagnetic micelles incorporated inside CCMV capsids, shown potential in magnetic resonance imaging (MRI) (176, 197). Additionally, metal-based gold nanoparticles (AuNPs) coupled with various, e.g., DNA, RNA or thiol based-ligands of different sizes were encapsulated, presenting the formation of biohybrid VLPs (198). Also, the semiconductor quantum dots (QDs) were encapsulated with CCMV capsids and have been explored for their function in (bio)imaging (199). Here, the CPs helped minimise the QD toxicity and enhanced their delivery inside the cells (in-vivo) compared with bare QDs. While performing Cryo-EM studies, Luque *et al.*, demonstrated the

formation of higher-order assemblies by encapsulating organic material zinc phthalocyanine (ZnPc) with CCMV, resulting in homogenous biohybrid materials. These organic filled VLPs (CCMV/ZnPc) resulted as potential vehicles for photodynamic therapy (PDT) in the treatment of cancer cells (200). Further, the cellular experiments verified the increased solubility and controlled release of ZnPc, verifying the effectiveness of CCMV encapsulation (201).

Notably, the virus capsid encapsulated systems offer biocompatibility with higher stability and can be easily modified as desired for novel functions. VLPs such as CCMV based nano-systems displayed various characteristic properties that make them a suitable vehicle for the transportation of drugs. These features include a) their stability and quality to self-assemble; b) its ability to be purified on a large scale; c) they are considered to be monodispersed nanoparticles as all the particles for every type of virus or VLPs are indistinguishable for each kind of virus (202); d) they possess suitable geometry and have the consistent structure (203). Thus, VLPs can package, deliver, and transport nucleic acids utilising viral capsids in different environmental conditions such as high or low pH, high temperature, and the host's innate immune system (204). Therefore, the mechanistic trait of VLPs drives the *in vitro* encapsulation of new cargo materials in viral capsid is an exciting area of research.

2

### 2.4.3 Advantages of CCMV encapsulation of DNA over other conventional delivery carriers

The conventional drug delivery systems (liposomal or polymeric) are a mixture of different sized molecules with difficulty controlling their shape and payload attachment. Whereas, DNA origami presents an impressive blend of physical, chemical and biological properties remains an ideal candidate for a drug delivery carrier. However, there are some challenges associated with the stability and *in-vivo* targeting of these origami structures.

The CCMV derived VLPs are not human pathogens, hence less likely to interact with specific receptor proteins and producing less toxicity to biological cells. *In-vivo* biodistribution studies carried out with CCMV showed their accumulation in a broad range of organs across the body, including the spleen and liver (205). The electrostatic binding of DNA with CCMV CPs facilitate their cellular uptake, delivery at the disease site, minimising off-target effects especially useful in tumor cells (206). Moreover, the viral protein coating serves as protective armor, increasing the stability and transfection properties of confined cargo; therefore, this nanosystem is suitable for transporting various contrast agents and drugs to the target sites.

## 2.5 Conclusion

In this chapter, we highlighted the multidirectional development of bio-nanotechnology, its components and fabrication strategies for developing programmed materials. Nucleic acids (DNA) and virus proteins are two biomaterials that serve as excellent building blocks for developing a well-

defined, stable and functional macroscopic structure. Viral capsids encapsulate genomic nucleic acids, act as molecular containers, and can be utilised for packaging and entrapment of synthetic cargo.

Improvement of existing drug delivery approaches and making them highly specific and efficient for cellular delivery are significant therapeutics challenges. The development in the area DNA nanotechnology demonstrates their unique role as drug delivery carriers, including in cancer therapies. However, in order to enhance the functionality of DNs in medical applications, new strategies need to be developed based on the principle of “the sum is always greater than the individual parts”, employing diverse methods to create functional biohybrid systems.

2

Amongst the different DNA modification approaches reported, the self-assembly of plant viruses capsids (CCMV) over RNA and DNA creating encapsulated nanostructures are of immense interest and holds great promise in their cellular process and drug delivery applications. The protein encapsulation of drug-loaded DNA origamis displays the formation of supra-biomolecular structures, i.e., protein-DNA complexes with natural transfection property and controlled drug delivery. Moreover, the complete packing of drug-loaded DNA templates ensures maximum drug delivery efficacy at the desired location.

The results presented in the following chapters in this thesis showing CP encapsulation of drug-conjugated DN expands our understanding of delivering a hydrophobic drug with functional biomaterials. Also, experiments determining the intracellular fate of these new class of nanocarriers will be crucial towards the development of smart drug delivery systems. Finally, information obtained from experimental results will be useful for encapsulating other materials and cargoes with application in medicine and nanotechnology.

## 2.6 References

1. Shapira P, Youtie J. Introduction to the symposium issue: nanotechnology innovation and policy—current strategies and future trajectories. *The Journal of Technology Transfer*. 2011;36(6):581-6.
2. Chakraborty A, Roy T, Mondal S. Development of DNA nanotechnology and uses in molecular medicine and biology. *Insights Biomed*. 2016;1(2):13.
3. Goodsell DS. *Bionanotechnology: Lessons from Nature*: Wiley; 2004.
4. Nölting B. Biophysical nanotechnology. *Methods in Modern Biophysics*. Berlin, Heidelberg: Springer Berlin Heidelberg; 2010. p. 147-63.
5. Papazoglou ES, Parthasarathy A. *Bionanotechnology*. Synthesis Lectures on Biomedical Engineering. 2007;2(1):1-139.
6. Silva GA. *Nanotechnology for biology and medicine at the building block level*. New York: Springer; 2012. 234 S. p.
7. Madou MJ. *Fundamentals of microfabrication : the science of miniaturization*. 2nd ed. Boca Raton: CRC Press; 2002. 723 p. p.
8. Rodgers P. Nanoelectronics: single file. *Nature nanotechnology*. 2006.
9. Seeman NC, Belcher AM. Emulating biology: building nanostructures from the bottom up. *Proceedings of the National Academy of Sciences*. 2002;99(suppl 2):6451-5.
10. Zhang S, Marini DM, Hwang W, Santoso S. Design of nanostructured biological materials through self-assembly of peptides and proteins. *Current opinion in chemical biology*. 2002;6(6):865-71.
11. Hess H, Bachand GD, Vogel V. Powering nanodevices with biomolecular motors. *Chemistry*. 2004;10(9):2110-6.
12. Hess H, Clemmens J, Brunner C, Doot R, Luna S, Ernst KH, et al. Molecular self-assembly of "nanowires" and "nanospools" using active transport. *Nano Lett*. 2005;5(4):629-33.
13. Seeman NC. Structural DNA nanotechnology: an overview. *Methods Mol Biol*. 2005;303:143-66.
14. Feldkamp U, Niemeyer CM. Rational design of DNA nanoarchitectures. *Angew Chem Int Ed Engl*. 2006;45(12):1856-76.
15. Thimiri Govinda Raj DB, Khan NA. Designer nanoparticle: nanobiotechnology tool for cell biology. *Nano Converg*. 2016;3(1):22.
16. Raza H. *Freshman Lectures on Nanotechnology*: Springer; 2019.
17. Demming A. Bionanotechnology: arrays in the future prospects of the field. *Nanotechnology*. 2014;25(36):360201.
18. Scheible M, Jungmann R, Simmel FC. Assembly and microscopic characterization of DNA origami structures. *Adv Exp Med Biol*. 2012;733:87-96.
19. Nagamune T. Biomolecular engineering for nanobio/bionanotechnology. *Nano Converg*. 2017;4(1):9.
20. Sleytr UB, Messner P, Pum D, Sara M. Crystalline bacterial cell surface layers (s layers): from supramolecular cell structure to biomimetics and nanotechnology. *Angew Chem Int Ed Engl*. 1999;38(8):1034-54.
21. Pum D, Toca-Herrera JL, Sleytr UB. S-layer protein self-assembly. *Int J Mol Sci*. 2013;14(2):2484-501.
22. Steinmetz NF, Evans DJ. Utilisation of plant viruses in bionanotechnology. *Org Biomol Chem*. 2007;5(18):2891-902.
23. de la Escosura A, Nolte RJ, Cornelissen JJ. Viruses and protein cages as nanocontainers and nanoreactors. *Journal of materials chemistry*. 2009;19(16):2274-8.
24. Seeman NC. DNA in a material world. *Nature*. 2003;421(6921):427-31.
25. Seeman NC. An overview of structural DNA nanotechnology. *Molecular biotechnology*. 2007;37(3):246-57.
26. Pinheiro AV, Han D, Shih WM, Yan H. Challenges and opportunities for structural DNA nanotechnology. *Nat Nanotechnol*. 2011;6(12):763-72.
27. de Morais MG, Martins VG, Steffens D, Pranke P, da Costa JA. Biological applications of nanobiotechnology. *J Nanosci Nanotechnol*. 2014;14(1):1007-17.
28. Gill R, Zayats M, Willner I. Semiconductor quantum dots for bioanalysis. *Angew Chem Int Ed Engl*. 2008;47(40):7602-25.
29. Bhatia D, Arumugam S, Nasilowski M, Joshi H, Wunder C, Chambon V, et al. Quantum dot-loaded monofunctionalized DNA icosahedra for single-particle tracking of endocytic pathways. *Nat Nanotechnol*. 2016;11(12):1112-9.
30. Yan Z, Gan N, Zhang H, Wang, Qiao L, Cao Y, et al. A sandwich-hybridization assay for simultaneous determination of HIV and tuberculosis DNA targets based on signal amplification by quantum dots-PowerVision polymer coding nanotracers. *Biosens Bioelectron*. 2015;71:207-13.
31. Parveen S, Misra R, Sahoo SK. Nanoparticles: a boon to drug delivery, therapeutics, diagnostics and imaging. *Nanomedicine*. 2012;8(2):147-66.
32. Allen TM, Cullis PR. Liposomal drug delivery systems: From concept to clinical applications. *Advanced*

- Drug Delivery Reviews. 2013;65(1):36-48.
33. Georgeta M, Marieta N, Liviu S. Dextran based Polymeric Micelles as Carriers for Delivery of Hydrophobic Drugs. *Current Drug Delivery*. 2017;14(3):406-15.
34. Drobnik J. Hyaluronan in drug delivery. *Advanced Drug Delivery Reviews*. 1991;7(2):295-308.
35. Garcia-Fuentes M, Alonso MJ. Chitosan-based drug nanocarriers: Where do we stand? *Journal of Controlled Release*. 2012;161(2):496-504.
36. Slowing II, Vivero-Escoto JL, Trewyn BG, Lin VSY. Mesoporous silica nanoparticles: structural design and applications. *Journal of Materials Chemistry*. 2010;20(37):7924-37.
37. Lu J, Choi E, Tamanoi F, Zink JI. Light-Activated Nanoimpeller-Controlled Drug Release in Cancer Cells. 2008;4(4):421-6.
38. Aryal S, Pilla S, Gong S. Multifunctional Nano-Micelles Formed by Amphiphilic Gold-Polycaprolactone-Methoxy Poly(ethylene glycol) (Au-PCL-MPEG) Nanoparticles for Potential Drug Delivery Applications. *Journal of Nanoscience and Nanotechnology*. 2009;9(10):5701-8.
39. Tkachenko AG, Xie H, Liu Y, Coleman D, Ryan J, Glomm WR, et al. Cellular Trajectories of Peptide-Modified Gold Particle Complexes: Comparison of Nuclear Localization Signals and Peptide Transduction Domains. *Bioconjugate Chemistry*. 2004;15(3):482-90.
40. Jiang T, Xu C, Liu Y, Liu Z, Wall JS, Zuo X, et al. Structurally Defined Nanoscale Sheets from Self-Assembly of Collagen-Mimetic Peptides. *Journal of the American Chemical Society*. 2014;136(11):4300-8.
41. Habibi N, Kamaly N, Memic A, Shafiee H. Self-assembled peptide-based nanostructures: Smart nanomaterials toward targeted drug delivery. *Nano Today*. 2016;11(1):41-60.
42. Soukasene S, Toft DJ, Moyer TJ, Lu H, Lee H-K, Standley SM, et al. Antitumor Activity of Peptide Amphiphile Nanofiber-Encapsulated Camptothecin. *ACS Nano*. 2011;5(11):9113-21.
43. de Vries JW, Zhang F, Herrmann A. Drug delivery systems based on nucleic acid nanostructures. *Journal of Controlled Release*. 2013;172(2):467-83.
44. Chang M, Yang C-S, Huang D-M. Aptamer-Conjugated DNA Icosahedral Nanoparticles As a Carrier of Doxorubicin for Cancer Therapy. *ACS Nano*. 2011;5(8):6156-63.
45. Jiang Q, Song C, Nangreave J, Liu X, Lin L, Qiu D, et al. DNA Origami as a Carrier for Circumvention of Drug Resistance. *Journal of the American Chemical Society*. 2012;134(32):13396-403.
46. Ma M, Xing P, Xu S, Li S, Chu X, Hao A. Reversible pH-responsive helical nanoribbons formed using camptothecin. *RSC Advances*. 2014;4(80):42372-5.
47. Wang H, Yang C, Wang L, Kong D, Zhang Y, Yang Z. Self-assembled nanospheres as a novel delivery system for taxol: a molecular hydrogel with nanosphere morphology. *Chemical Communications*. 2011;47(15):4439-41.
48. Nishiyama N, Okazaki S, Cabral H, Miyamoto M, Kato Y, Sugiyama Y, et al. Novel Cisplatin-Incorporated Polymeric Micelles Can Eradicate Solid Tumors in Mice. 2003;63(24):8977-83.
49. Alhareth K, Vauthier C, Bourasset F, Gueutin C, Ponchel G, Moussa F. Conformation of surface-decorating dextran chains affects the pharmacokinetics and biodistribution of doxorubicin-loaded nanoparticles. *European Journal of Pharmaceutics and Biopharmaceutics*. 2012;81(2):453-7.
50. Owens DE, Peppas NA. Opsonization, biodistribution, and pharmacokinetics of polymeric nanoparticles. *International Journal of Pharmaceutics*. 2006;307(1):93-102.
51. Kemp MM, Linhardt RJ. Heparin-based nanoparticles. *Wiley Interdiscip Rev Nanomed Nanobiotechnol*. 2010;2(1):77-87.
52. Kanwar JR, Gibbons J, Verma AK, Kanwar RK. Cell-penetrating properties of the transactivator of transcription and polyarginine (R9) peptides, their conjugative effect on nanoparticles and the prospect of conjugation with arsenic trioxide. *Anticancer Drugs*. 2012;23(5):471-82.
53. Bechara C, Sagan S. Cell-penetrating peptides: 20 years later, where do we stand? *FEBS Letters*. 2013;587(12):1693-702.
54. Low PS, Henne WA, Doorneweerd DD. Discovery and development of folic-acid-based receptor targeting for imaging and therapy of cancer and inflammatory diseases. *Acc Chem Res*. 2008;41(1):120-9.
55. Daniels TR, Delgado T, Helguera G, Penichet ML. The transferrin receptor part II: targeted delivery of therapeutic agents into cancer cells. *Clin Immunol*. 2006;121(2):159-76.
56. Chen K, Chen X. Integrin targeted delivery of chemotherapeutics. *Theranostics*. 2011;1:189-200.
57. Chamundeeswari M, Jeslin J, Verma ML. Nanocarriers for drug delivery applications. *Environmental Chemistry Letters*. 2019;17(2):849-65.
58. Khademhosseini A, Langer R. Drug delivery and tissue engineering. *Chem Eng Prog*. 2006;102(2):38-42.
59. Zhang H, Xia J, Pang X, Zhao M, Wang B, Yang L, et al. Magnetic nanoparticle-loaded electrospun polymeric nanofibers for tissue engineering. *Mater Sci Eng C Mater Biol Appl*. 2017;73:537-43.
60. Tort S, Acarturk F, Besikci A. Evaluation of three-layered doxycycline-collagen loaded nanofiber wound dressing. *Int J Pharm*. 2017;529(1-2):642-53.

61. Waghmare VS, Wadke PR, Dyawanapelly S, Deshpande A, Jain R, Dandekar P. Starch based nanofibrous scaffolds for wound healing applications. *Bioact Mater.* 2018;3(3):255-66.
62. Vashisth P, Raghuwanshi N, Srivastava AK, Singh H, Nagar H, Pruthi V. Ofloxacin loaded gellan/PVA nanofibers - Synthesis, characterization and evaluation of their gastroretentive/mucoadhesive drug delivery potential. *Mater Sci Eng C Mater Biol Appl.* 2017;71:611-9.
63. Lv Y, Pan Q, Bligh SW, Li H, Wu H, Sang Q, et al. Core-Sheath Nanofibers as Drug Delivery System for Thermoresponsive Controlled Release. *J Pharm Sci.* 2017;106(5):1258-65.
64. Lobmann K, Svagan AJ. Cellulose nanofibers as excipient for the delivery of poorly soluble drugs. *Int J Pharm.* 2017;533(1):285-97.
65. Tam DY, Lo PK. Multifunctional DNA Nanomaterials for Biomedical Applications. *Journal of Nanomaterials.* 2015;2015:21.
66. Seeman NC. Nucleic acid junctions and lattices. *Journal of theoretical biology.* 1982;99(2):237-47.
67. Zidegani RM, Norton ML. Structural DNA nanotechnology: from design to applications. *International journal of molecular sciences.* 2012;13(6):7149-62.
68. Watson JD. *Molecular biology of the gene*: Pearson Education India; 2004.
69. Niemeyer CM. Self-assembled nanostructures based on DNA: towards the development of nanobiotechnology. *Curr Opin Chem Biol.* 2000;4(6):609-18.
70. Kallenbach NR, Ma R-I, Seeman NC. An immobile nucleic acid junction constructed from oligonucleotides. *Nature.* 1983;305:829.
71. Seeman NC, Kallenbach NR. Design of immobile nucleic acid junctions. *Biophys J.* 1983;44(2):201-9.
72. Holliday R. A mechanism for gene conversion in fungi. *Genetical Research.* 1964;5(2):282-304.
73. Chen JH, Seeman NC. Synthesis from DNA of a molecule with the connectivity of a cube. *Nature.* 1991;350(6319):631-3.
74. Wang Y, Mueller JE, Kemper B, Seeman NC. Assembly and characterization of five-arm and six-arm DNA branched junctions. *Biochemistry.* 1991;30(23):5667-74.
75. Wang X, Seeman NC. Assembly and Characterization of 8-Arm and 12-Arm DNA Branched Junctions. *Journal of the American Chemical Society.* 2007;129(26):8169-76.
76. Yurke B, Turberfield AJ, Mills Jr AP, Simmel FC, Neumann JL. A DNA-fuelled molecular machine made of DNA. *Nature.* 2000;406(6796):605.
77. Shen W, Bruist MF, Goodman SD, Seeman NC. A protein-driven DNA device that measures the excess binding energy of proteins that distort DNA. *Angewandte Chemie International Edition.* 2004;43(36):4750-2.
78. Sherman WB, Seeman NC. A precisely controlled DNA biped walking device. *Nano Letters.* 2004;4(7):1203-7.
79. Shin J-S, Pierce NA. A synthetic DNA walker for molecular transport. *Journal of the American Chemical Society.* 2004;126(35):10834-5.
80. Zheng J, Birktoft JJ, Chen Y, Wang T, Sha R, Constantinou PE, et al. From molecular to macroscopic via the rational design of a self-assembled 3D DNA crystal. *Nature.* 2009;461(7260):74-7.
81. Seeman NC. Nanomaterials based on DNA. *Annu Rev Biochem.* 2010;79:65-87.
82. Saccà B, Niemeyer CM. DNA origami: the art of folding DNA. *Angewandte Chemie International Edition.* 2012;51(1):58-66.
83. Abu-Salah KM, Ansari AA, Alrokayan SA. DNA-based applications in nanobiotechnology. *J Biomed Biotechnol.* 2010;2010:715295.
84. Endo M, Katsuda Y, Hidaka K, Sugiyama H. Regulation of DNA methylation using different tensions of double strands constructed in a defined DNA nanostructure. *Journal of the American Chemical Society.* 2010;132(5):1592-7.
85. Amir Y, Ben-Ishay E, Levner D, Ittah S, Abu-Horowitz A, Bachelet I. Universal computing by DNA origami robots in a living animal. *Nature nanotechnology.* 2014;9(5):353-7.
86. Help from above. *Nat Nanotechnol.* 2010;5(7):473.
87. Lin CM, Lu TY. C60 fullerene derivatized nanoparticles and their application to therapeutics. *Recent Pat Nanotechnol.* 2012;6(2):105-13.
88. Goodman RP, Berry RM, Turberfield AJ. The single-step synthesis of a DNA tetrahedron. *Chem Commun (Camb).* 2004(12):1372-3.
89. Aldaye FA, Sleiman HF. Modular access to structurally switchable 3D discrete DNA assemblies. *J Am Chem Soc.* 2007;129(44):13376-7.
90. He Y, Su M, Fang PA, Zhang C, Ribbe AE, Jiang W, et al. On the chirality of self-assembled DNA octahedra. *Angew Chem Int Ed Engl.* 2010;49(4):748-51.
91. Wang P, Chatterjee G, Yan H, LaBean TH, Turberfield AJ, Castro CE, et al. Practical aspects of structural and dynamic DNA nanotechnology. *MRS Bull.* 2017;42(12):889-96.
92. Shih WM, Quispe JD, Joyce GF. A 1.7-kilobase single-stranded DNA that folds into a nanoscale octahedron. *Nature.* 2004;427:618.



93. Paul WKR. Folding DNA to create nanoscale shapes and patterns. *Nature*. 2006;440(7082):297.
94. Chandrasekaran AR, Zhuo RJAMT. A 'tile'tale: hierarchical self-assembly of DNA lattices. 2016;2:7-16.
95. Wang L, Arrabito G. Hybrid, multiplexed, functional DNA nanotechnology for bioanalysis. *Analyst*. 2015;140(17):5821-48.
96. Smith DM, Schüller V, Forthmann C, Schreiber R, Tinnefeld P, Liedl TJJona. A structurally variable hinged tetrahedron framework from DNA origami. 2011;2011.
97. Andersen ES, Dong M, Nielsen MM, Jahn K, Lind-Thomsen A, Mamdouh W, et al. DNA origami design of dolphin-shaped structures with flexible tails. 2008;2(6):1213-8.
98. Zhao Y-X, Shaw A, Zeng X, Benson E, Nystrom AM, Hogberg B. DNA origami delivery system for cancer therapy with tunable release properties. *Acs Nano*. 2012;6(10):8684-91.
99. Dietz H, Douglas SM, Shih WM. Folding DNA into twisted and curved nanoscale shapes. *Science (New York, NY)*. 2009;325(5941):725-30.
100. Han D, Pal S, Nangreave J, Deng Z, Liu Y, Yan H. DNA origami with complex curvatures in three-dimensional space. *Science*. 2011;332(6027):342-6.
101. Ke Y, Ong LL, Shih WM, Yin P. Three-dimensional structures self-assembled from DNA bricks. *Science*. 2012;338(6111):1177-83.
102. Praetorius F, Dietz H. Self-assembly of genetically encoded DNA-protein hybrid nanoscale shapes. 2017;355(6331):eaam5488.
103. Han D, Pal S, Yang Y, Jiang S, Nangreave J, Liu Y, et al. DNA Gridiron Nanostructures Based on Four-Arm Junctions. 2013;339(6126):1412-5.
104. Benson E, Mohammed A, Gardell J, Masich S, Czeizler E, Orponen P, et al. DNA rendering of polyhedral meshes at the nanoscale. *Nature*. 2015;523(7561):441-4.
105. Birac JJ, Sherman WB, Kopatsch J, Constantinou PE, Seeman NC. Architecture with GIDEON, a program for design in structural DNA nanotechnology. *J Mol Graph Model*. 2006;25(4):470-80.
106. Douglas SM, Marblestone AH, Teerapittayanon S, Vazquez A, Church GM, Shih WM. Rapid prototyping of 3D DNA-origami shapes with caDNAo. *Nucleic acids research*. 2009;37(15):5001-6.
107. Castro CE, Kilchherr F, Kim DN, Shiao EL, Wauer T, Wortmann P, et al. A primer to scaffolded DNA origami. *Nat Methods*. 2011;8(3):221-9.
108. Veneziano R, Ratanalert S, Zhang K, Zhang F, Yan H, Chiu W, et al. Designer nanoscale DNA assemblies programmed from the top down. *Science*. 2016;352(6293):1534-.
109. Williams S, Lund K, Lin C, Wonka P, Lindsay S, Yan H, editors. *Tiamat: a three-dimensional editing tool for complex DNA structures*. International Workshop on DNA-Based Computers; 2008: Springer.
110. Xavier PL, Chandrasekaran AR. DNA-based construction at the nanoscale: emerging trends and applications. *Nanotechnology*. 2018;29(6):062001.
111. Nummelin S, Kommeri J, Kostianinen MA, Linko V. Evolution of structural DNA nanotechnology. *Advanced Materials*. 2018;30(24):1703721.
112. Angell C, Xie S, Zhang L, Chen Y. DNA nanotechnology for precise control over drug delivery and gene therapy. *Small*. 2016;12(9):1117-32.
113. Chandrasekaran AR, Anderson N, Kizer M, Halvorsen K, Wang X. Beyond the Fold: Emerging Biological Applications of DNA Origami. *ChemBiochem*. 2016;17(12):1081-9.
114. Kuzyk A, Laitinen KT, Törmä P. DNA origami as a nanoscale template for protein assembly. *Nanotechnology*. 2009;20(23):235305.
115. Numajiri K, Kimura M, Kuzuya A, Komiyama M. Stepwise and reversible nanopatterning of proteins on a DNA origami scaffold. *Chem Commun (Camb)*. 2010;46(28):5127-9.
116. Fu J, Liu M, Liu Y, Woodbury NW, Yan H. Interenzyme substrate diffusion for an enzyme cascade organized on spatially addressable DNA nanostructures. *J Am Chem Soc*. 2012;134(12):5516-9.
117. Linko V, Eerikäinen M, Kostianinen MA. A modular DNA origami-based enzyme cascade nanoreactor. *Chemical Communications*. 2015;51(25):5351-4.
118. Kuzuya A, Watanabe R, Yamanaka Y, Tamaki T, Kaino M, Ohya Y. Nanomechanical DNA origami pH sensors. *Sensors (Basel)*. 2014;14(10):19329-35.
119. Rajendran A, Endo M, Sugiyama H. Single-molecule analysis using DNA origami. *Angewandte Chemie International Edition*. 2012;51(4):874-90.
120. Liu X, Xu Y, Yu T, Clifford C, Liu Y, Yan H, et al. A DNA Nanostructure Platform for Directed Assembly of Synthetic Vaccines. *Nano Letters*. 2012;12(8):4254-9.
121. Li J, Pei H, Zhu B, Liang L, Wei M, He Y, et al. Self-assembled multivalent DNA nanostructures for noninvasive intracellular delivery of immunostimulatory CpG oligonucleotides. 2011;5(11):8783-9.
122. Kocabay S, Meinh H, MacPherson IS, Cassinelli V, Manetto A, Rothenfusser S, et al. Cellular Uptake of Tile-Assembled DNA Nanotubes. *Nanomaterials (Basel)*. 2014;5(1):47-60.
123. Schuller VJ, Heidegger S, Sandholzer N, Nickels PC, Suhartha NA, Endres S, et al. Cellular immunostimulation by CpG-sequence-coated DNA origami structures. *ACS Nano*. 2011;5(12):9696-702.

124. Ouyang X, Li J, Liu H, Zhao B, Yan J, Ma Y, et al. Rolling Circle Amplification-Based DNA Origami Nanostructures for Intracellular Delivery of Immunostimulatory Drugs. 2013;9(18):3082-7.
125. Hamblin GD, Carneiro KMM, Fakhoury JF, Bujold KE, Sleiman HF. Rolling Circle Amplification-Templated DNA Nanotubes Show Increased Stability and Cell Penetration Ability. *Journal of the American Chemical Society*. 2012;134(6):2888-91.
126. Mei Q, Wei X, Su F, Liu Y, Youngbull C, Johnson R, et al. Stability of DNA origami nanoarrays in cell lysate. *Nano Lett*. 2011;11(4):1477-82.
127. Jiang Q, Song C, Nangreave J, Liu X, Lin L, Qiu D, et al. DNA origami as a carrier for circumvention of drug resistance. 2012;134(32):13396-403.
128. Zhang Q, Jiang Q, Li N, Dai L, Liu Q, Song L, et al. DNA origami as an in vivo drug delivery vehicle for cancer therapy. *ACS nano*. 2014;8(7):6633-43.
129. Halley PD, Lucas CR, McWilliams EM, Webber MJ, Patton RA, Kural C, et al. Daunorubicin-Loaded DNA Origami Nanostructures Circumvent Drug-Resistance Mechanisms in a Leukemia Model. *Small*. 2016;12(3):308-20.
130. Zhao YX, Shaw A, Zeng X, Benson E, Nystrom AM, Hogberg B. DNA origami delivery system for cancer therapy with tunable release properties. *ACS Nano*. 2012;6(10):8684-91.
131. Auvinen H, Zhang H, Kopilow A, Niemelä EH, Nummelin S, Correia A, et al. Protein Coating of DNA Nanostructures for Enhanced Stability and Immunocompatibility. *Advanced healthcare materials*. 2017.
132. Okholm AH, Kjems J. DNA nanovehicles and the biological barriers. *Advanced drug delivery reviews*. 2016;106:183-91.
133. Xu X, Rosi NL, Wang Y, Huo F, Mirkin CA. Asymmetric functionalization of gold nanoparticles with oligonucleotides. *J Am Chem Soc*. 2006;128(29):9286-7.
134. Dhar S, Daniel WL, Giljohann DA, Mirkin CA, Lippard SJ. Polyvalent oligonucleotide gold nanoparticle conjugates as delivery vehicles for platinum (IV) warheads. *Journal of the American Chemical Society*. 2009;131(41):14652-3.
135. Liu Z, Robinson JT, Tabakman SM, Yang K, Dai H. Carbon materials for drug delivery & cancer therapy. *Materials today*. 2011;14(7-8):316-23.
136. Li J, Fan C, Pei H, Shi J, Huang Q. Smart Drug Delivery Nanocarriers with Self-Assembled DNA Nanostructures. *Advanced materials*. 2013;25(32):4386-96.
137. Smith D, Schuller V, Engst C, Radler J, Liedl T. Nucleic acid nanostructures for biomedical applications. *Nanomedicine (Lond)*. 2013;8(1):105-21.
138. Nunez-Lozano R, Cano M, Pimentel B, de la Cueva-Mendez G. 'Smartening' anticancer therapeutic nanosystems using biomolecules. *Curr Opin Biotechnol*. 2015;35:135-40.
139. Tibbitt MW, Dahlman JE, Langer RJJotACS. Emerging frontiers in drug delivery. 2016;138(3):704-17.
140. Jiang Q, Liu S, Liu J, Wang ZG, Ding B. Rationally designed DNA-origami nanomaterials for drug delivery in vivo. *Advanced Materials*. 2019;31(45):1804785.
141. Kearney CJ, Lucas CR, O'Brien FJ, Castro CE. DNA Origami: Folded DNA-Nanodevices That Can Direct and Interpret Cell Behavior. *Advanced Materials*. 2016.
142. Hu Q, Li H, Wang L, Gu H, Fan C. DNA nanotechnology-enabled drug delivery systems. *Chemical reviews*. 2018;119(10):6459-506.
143. Jiang D, England CG, Cai W. DNA nanomaterials for preclinical imaging and drug delivery. *Journal of controlled release : official journal of the Controlled Release Society*. 2016;239:27-38.
144. Linko V, Ora A, Kostianen MA. DNA Nanostructures as Smart Drug-Delivery Vehicles and Molecular Devices. *Trends in biotechnology*. 2015;33(10):586-94.
145. Madhanagopal BR, Zhang S, Demirel E, Wady H, Chandrasekaran AR. DNA Nanocarriers: Programmed to Deliver. *Trends Biochem Sci*. 2018;43(12):997-1013.
146. Schaffert DH, Okholm AH, Sorensen RS, Nielsen JS, Torring T, Rosen CB, et al. Intracellular Delivery of a Planar DNA Origami Structure by the Transferrin-Receptor Internalization Pathway. *Small*. 2016;12(19):2634-40.
147. Jiang Q, Song C, Nangreave J, Liu X, Lin L, Qiu D, et al. DNA origami as a carrier for circumvention of drug resistance. *Journal of the American Chemical Society*. 2012;134(32):13396-403.
148. Xia Z, Wang P, Liu X, Liu T, Yan Y, Yan J, et al. Tumor-Penetrating Peptide-Modified DNA Tetrahedron for Targeting Drug Delivery. *Biochemistry*. 2016;55(9):1326-31.
149. Suping L, Qiao J, Shaoli L, Yinlong Z, Yanhua T, Chen S, et al. A DNA nanorobot functions as a cancer therapeutic in response to a molecular trigger in vivo. *Nature Biotechnology*. 2018;36(3).
150. Ko S, Liu H, Chen Y, Mao CJB. DNA nanotubes as combinatorial vehicles for cellular delivery. 2008;9(11):3039-43.
151. Walsh AS, Yin H, Erben CM, Wood MJ, Turberfield AJAn. DNA cage delivery to mammalian cells. 2011;5(7):5427-32.
152. Schuller VJ, Heidegger S, Sandholzer N, Nickels PC, Suhartha NA, Endres S, et al. Cellular immunostimulation by CpG-sequence-coated DNA origami structures. 2011;5(12):9696-702.



153. Lee DS, Qian H, Tay CY, Leong DTJCSR. Cellular processing and destinies of artificial DNA nanostructures. *2016*;45(15):4199-225.
154. Jahanban-Esfahlan A, Seidi K, Jaymand M, Schmidt TL, Majdi H, Javaheri T, et al. Dynamic DNA nanostructures in biomedicine: Beauty, utility and limits. *J Control Release*. 2019;315:166-85.
155. Angell C, Xie S, Zhang L, Chen Y. DNA Nanotechnology for Precise Control over Drug Delivery and Gene Therapy. Small (Weinheim an der Bergstrasse, Germany). 2016;12(9):1117-32.
156. Keum JW, Bermudez H. Enhanced resistance of DNA nanostructures to enzymatic digestion. *Chem Commun (Camb)*. 2009(45):7036-8.
157. Conway JW, McLaughlin CK, Castor KJ, Sleiman H. DNA nanostructure serum stability: greater than the sum of its parts. *Chemical Communications*. 2013;49(12):1172-4.
158. Surana S, Shenoy AR, Krishnan Y. Designing DNA nanodevices for compatibility with the immune system of higher organisms. *Nat Nanotechnol*. 2015;10(9):741-7.
159. Li S, Jiang Q, Liu S, Zhang Y, Tian Y, Song C, et al. A DNA nanorobot functions as a cancer therapeutic in response to a molecular trigger in vivo. *Nat Biotechnol*. 2018;36(3):258-64.
160. Hu Q, Wang S, Wang L, Gu H, Fan C. DNA Nanostructure-Based Systems for Intelligent Delivery of Therapeutic Oligonucleotides. *Adv Healthc Mater*. 2018;7(20):e1701153.
161. Bastings MM, Anastassacos FM, Ponnuswamy N, Leifer FG, Cuneo G, Lin C, et al. Modulation of the cellular uptake of DNA origami through control over mass and shape. *Nano letters*. 2018;18(6):3557-64.
162. Kizer ME, Linhardt RJ, Chandrasekaran AR, Wang X. A Molecular Hero Suit for In Vitro and In Vivo DNA Nanostructures. *Small*. 2019;15(26):e1805386.
163. Douglas SM, Bachelet I, Church GM. A logic-gated nanorobot for targeted transport of molecular payloads. *Science*. 2012;335(6070):831-4.
164. You M, Peng L, Shao N, Zhang L, Qiu L, Cui C, et al. DNA "Nano-Claw": Logic-based Autonomous Cancer Targeting and Therapy 2013.
165. Messaoudi S, Greschner AA, Gauthier MA. Progress Toward Absorption, Distribution, Metabolism, Elimination, and Toxicity of DNA Nanostructures. *Advanced Therapeutics*. 2019;2(12):1900144.
166. Taylor-Pashow KM, Della Rocca J, Huxford RC, Lin W. Hybrid nanomaterials for biomedical applications. *Chem Commun (Camb)*. 2010;46(32):5832-49.
167. Shao Z, Shao J, Tan B, Guan S, Liu Z, Zhao Z, et al. Targeted lung cancer therapy: preparation and optimization of transferrin-decorated nanostructured lipid carriers as novel nanomedicine for co-delivery of anticancer drugs and DNA. *International journal of nanomedicine*. 2015;10:1223-33.
168. Zhu S, Xing H, Gordiichuk P, Park J, Mirkin CA. PLGA Spherical Nucleic Acids. *Adv Mater*. 2018;30(22):e1707113.
169. Raniolo S, Vindigni G, Unida V, Ottaviani A, Romano E, Desideri A, et al. Entry, fate and degradation of DNA nanocages in mammalian cells: a matter of receptors. *Nanoscale*. 2018;10(25):12078-86.
170. Ponnuswamy N, Bastings MMC, Nathwani B, Ryu JH, Chou LYT, Vinther M, et al. Oligolysine-based coating protects DNA nanostructures from low-salt denaturation and nuclease degradation. *Nat Commun*. 2017;8:15654.
171. Agarwal NP, Matthies M, Gur FN, Osada K, Schmidt TL. Block Copolymer Micellization as a Protection Strategy for DNA Origami. *Angew Chem Int Ed Engl*. 2017;56(20):5460-4.
172. Keller A, Linko V. Challenges and Perspectives of DNA Nanostructures in Biomedicine. *Angew Chem Int Ed Engl*. 2020.
173. Schaffert DH, Okholm AH, Sørensen RS, Nielsen JS, Tørring T, Rosen CB, et al. Intracellular delivery of a planar DNA origami structure by the transferrin-receptor internalization pathway. *Small*. 2016;12(19):2634-40.
174. Ozyurt C, Ugurlu O, Evran S. Cell-penetrating peptides in nanodelivery of nucleic acids and drugs. *Nanostructures for the Engineering of Cells, Tissues and Organs: Elsevier*; 2018. p. 67-104.
175. Mikkilä J, Eskelinen A-P, Niemelä EH, Linko V, Frilander MJ, Törmä Pi, et al. Virus-encapsulated DNA origami nanostructures for cellular delivery. *Nano letters*. 2014;14(4):2196-200.
176. Kwak M, Minten IJ, Anaya DM, Musser AJ, Brasch M, Nolte RJ, et al. Virus-like particles templated by DNA micelles: a general method for loading virus nanocarriers. *J Am Chem Soc*. 2010;132(23):7834-5.
177. Yildiz I, Shukla S, Steinmetz NF. Applications of viral nanoparticles in medicine. *Curr Opin Biotechnol*. 2011;22(6):901-8.
178. Wen AM, Steinmetz NF. Design of virus-based nanomaterials for medicine, biotechnology, and energy. *Chem Soc Rev*. 2016;45(15):4074-126.
179. Wang P, Meyer TA, Pan V, Dutta PK, Ke Y. The Beauty and Utility of DNA Origami. *Chem*. 2017;2(3):359-82.
180. Perrault SD, Shih WM. Virus-inspired membrane encapsulation of DNA nanostructures to achieve in vivo stability. *ACS nano*. 2014;8(5):5132-40.
181. Ma Y, Nolte RJ, Cornelissen JJ. Virus-based nanocarriers for drug delivery. *Adv Drug Deliv Rev*.

- 2012;64(9):811-25.
182. Jeevanandam J, Pal K, Danquah MK. Virus-like nanoparticles as a novel delivery tool in gene therapy. *Biochimie*. 2019;157:38-47.
183. Rohovie MJ, Nagasawa M, Swartz JR. Virus-like particles: Next-generation nanoparticles for targeted therapeutic delivery. *Bioeng Transl Med*. 2017;2(1):43-57.
184. Zhang Y, Dong Y, Zhou J, Li X, Wang F. Application of Plant Viruses as a Biotemplate for Nanomaterial Fabrication. *Molecules*. 2018;23(9).
185. Tamborini M, Geib N, Marrero-Nodarse A, Jud M, Hauser J, Aho C, et al. A Synthetic Virus-Like Particle Streptococcal Vaccine Candidate Using B-Cell Epitopes from the Proline-Rich Region of Pneumococcal Surface Protein A. *Vaccines*. 2015;3(4):850-74.
186. Kushnir N, Streatfield SJ, Yusibov V. Virus-like particles as a highly efficient vaccine platform: diversity of targets and production systems and advances in clinical development. *Vaccine*. 2012;31(1):58-83.
187. Eiben S, Koch C, Altintoprak K, Southan A, Tovar G, Laschat S, et al. Plant virus-based materials for biomedical applications: Trends and prospects. *Adv Drug Deliv Rev*. 2019;145:96-118.
188. Wilts BD, Schaap IAT, Schmidt CF. Swelling and softening of the cowpea chlorotic mottle virus in response to pH shifts. *Biophys J*. 2015;108(10):2541-9.
189. Speir JA, Munshi S, Wang G, Baker TS, Johnson JE. Structures of the native and swollen forms of cowpea chlorotic mottle virus determined by X-ray crystallography and cryo-electron microscopy. *Structure*. 1995;3(1):63-78.
190. Johnson JM, Willits DA, Young MJ, Zlotnick A. Interaction with capsid protein alters RNA structure and the pathway for in vitro assembly of cowpea chlorotic mottle virus. *J Mol Biol*. 2004;335(2):455-64.
191. Verduin BJM. The preparation of CCMV-protein in connection with its association into a spherical particle. *FEBS Letters*. 1974;45(1):50-4.
192. Sikkema FD, Comellas-Aragones M, Fokkink RG, Verduin BJ, Cornelissen JJ, Nolte RJ. Monodisperse polymer-virus hybrid nanoparticles. *Org Biomol Chem*. 2007;5(1):54-7.
193. Lavelle L, Gingery M, Phillips M, Gelbart W, Knobler C, Cadena-Nava R, et al. Phase diagram of self-assembled viral capsid protein polymorphs. *The Journal of Physical Chemistry B*. 2009;113(12):3813-9.
194. Aragones MC. The cowpea chlorotic mottle virus as a building block in nanotechnology. 2010.
195. Garmann RF, Comas-Garcia M, Koay MS, Cornelissen JJ, Knobler CM, Gelbart WM. Role of electrostatics in the assembly pathway of a single-stranded RNA virus. *Journal of virology*. 2014;88(18):10472-9.
196. Maassen SJ, van der Ham AM, Cornelissen JJ. Combining protein cages and polymers: from understanding self-assembly to functional materials. ACS Publications; 2016.
197. Millan JG, Brasch M, Anaya-Plaza E, de la Escosura A, Velders AH, Reinhoudt DN, et al. Self-assembly triggered by self-assembly: optically active, paramagnetic micelles encapsulated in protein cage nanoparticles. *J Inorg Biochem*. 2014;136:140-6.
198. Liu A, Verwegen M, de Ruiter MV, Maassen SJ, Traulsen CH-H, Cornelissen JJ. Protein cages as containers for gold nanoparticles. *The Journal of Physical Chemistry B*. 2016;120(26):6352-7.
199. Tagit O, De Ruiter M, Brasch M, Ma Y, Cornelissen J. Quantum dot encapsulation in virus-like particles with tuneable structural properties and low toxicity. *RSC advances*. 2017;7(60):38110-8.
200. Luque D, de la Escosura A, Snijder J, Brasch M, Burnley RJ, Koay MS, et al. Self-assembly and characterization of small and monodisperse dye nanospheres in a protein cage. *Chemical science*. 2014;5(2):575-81.
201. Yang L, Liu A, de Ruiter MV, Hommersom CA, Katsonis N, Jonkheijm P, et al. Compartmentalized supramolecular hydrogels based on viral nanocages towards sophisticated cargo administration. *Nanoscale*. 2018;10(8):4123-9.
202. Lee LA, Niu Z, Wang QJNR. Viruses and virus-like protein assemblies—Chemically programmable nanoscale building blocks. 2009;2(5):349-64.
203. Zhao Q, Chen W, Chen Y, Zhang L, Zhang J, Zhang Z. Self-assembled virus-like particles from rotavirus structural protein VP6 for targeted drug delivery. *Bioconjug Chem*. 2011;22(3):346-52.
204. Uchida M, Kosuge H, Terashima M, Willits DA, Liepold LO, Young MJ, et al. Protein cage nanoparticles bearing the LyP-1 peptide for enhanced imaging of macrophage-rich vascular lesions. *ACS nano*. 2011;5(4):2493-502.
205. Kaiser CR, Flenniken ML, Gillitzer E, Harmsen AL, Harmsen AG, Jutila MA, et al. Biodistribution studies of protein cage nanoparticles demonstrate broad tissue distribution and rapid clearance in vivo. *Int J Nanomedicine*. 2007;2(4):715-33.
206. Sun X, Cui Z. Virus-Like Particles as Theranostic Platforms. *Advanced Therapeutics*. 2020;3(5):1900194.



## **CHAPTER 3**

---

# **Design, assembly, purification and characterisation of modular DNA Origami**

## 3 DESIGN, ASSEMBLY, PURIFICATION AND CHARACTERISATION OF MODULAR DNA ORIGAMIS

### 3.1 Introduction

The DNA origami technique (introduced as a one-pot method) was first presented in 2006 (1). The word 'origami' emerges from the Japanese phrase 'ori = folding' and 'kami = paper' and describes the traditional Japanese art of paper folding. Similarly, to a sheet of paper being folded into an object, DNA origami entails the folding of hundreds of staple DNA oligonucleotides on a long scaffold DNA into predecided shapes, thereby creating novel 2D/3D geometric nanostructures (2). Both arbitrary and complex origami-based DNAs were self-assembled with nanoscale precision and may range from nanometer to micrometre scale and can reach up to giga dalton weights (3). The circular viral genomic DNA from M13mp18 bacteriophage and its slight modifications are the most commonly used scaffold in numerous origami designing approaches (4). However, the length of the scaffold defines the size, shape and complexity of a DNA origami structure (5). Scaffold DNA of choice is usually a linear ss-DNA of varying lengths, with a known sequence and stable secondary structure (2).

Nevertheless, there have been several strategies reported which used both ds- and ss-DNA templates of different lengths as starting scaffolds in origami designs (4, 6). Due to the complementarity between the scaffold and the staples, staples bind specifically to the scaffold, thereby driving the exact assembly of the desired origami shape after a few trial and error steps. Here, the size of the staples is an essential factor to be considered as it determines the stability of the nanostructure, longer staples results in a more stable structure(2). Staples can also be modified in various ways which enable attachment of enzymes, metal nanoparticles, proteins onto DNA origami nanostructures (4). Moreover, the creation of larger assemblies by multimerisation of single DNA origami constructs is also reported.

Later, in 2009, 2D origami structures were extended to build 3D objects such as the famous DNA box, DNA tetrahedron molecular cages and the more complicated multi-layered 3D origamis (7-9). The honeycomb and square lattice-based strategies were used to produce a variety of 3D structures like a monolith, square nut, railed bridge, genie bottle and stacked or slotted crosses (9, 10). These methods were even extended to create close-packed combinations of hybrid DNA origami constructs (11). 3D multilayer structures offer a higher degree of freedom and robustness in independent directions and tend to minimise structural fluctuations in aqueous solutions. With controllable bends, twists and curvatures resulting from targeted insertions and deletions of base pairs between scaffold and staples, several new, functionalised, complex nanostructures (concave and convex triangles, wireframe capsules and 12-toothed gears, sphere, ellipsoid, nanoflask, 3D tensegrity prism,

tensegrity kites) were also designed (12).

The two most widely used, open-source tools – caDNAno (13) and CanDo (14, 15), together provide a user-friendly approach (with a graphical interface) to design 2D and 3D structures. caDNAno operates on square and honeycomb packaging geometries, which can be found as default lattices and sculpted into the desired target shape by predicting the curves, twist and turns of the shape in aqueous solution. Another critical factor is to estimate the right size and sequence of staples in consonance with the desired shape. caDNAno simplifies and speeds up the designing of DNAs, and CanDo, a simulation software, predicts the appearance, mechanical fluctuations and flexibility of the DN's shape.

DNA Origami methods are versatile and robust processes as with many other design principles, including different polyhedral, 2D/3D lattices and various programmable tubular shapes (4). Currently, an ever-increasing number of research groups are exploring programmable self-assembly properties of nucleic acids in devising rationally designed nano shapes for many different applications. Construction of DNA origamis becomes even more feasible through computer-aided design of DNA origami structures by selecting staple strands as well as determine their conformational flexibility.

3

The main focus of this chapter is on designing modular DNAs its microscopic characterisation. As a vital step, much effort was put into the optimisation of DN's folding conditions and purification paradigms. Here, we provide a practical step-by-step approach for designing DNA origami nanostructures and discuss the design rules followed. It is essential to purify the solutions from excess strands and misfolded structures by using methods such as electrophoretic separation, spin filtering, precipitation by poly(ethylene glycol) crowding or rate-zonal centrifugation. Also, the salt-buffer conditions were carefully optimised to establish the structural integrity of DNA objects. Later, the DNAs were characterised with different microscopy techniques-Scanning Electron Microscopy (SEM), Atomic Force Microscopy (AFM) and Transmission Electron Microscopy (TEM). So, finally, we present the work plan for design, assembly, purification and characterisation of DNA origami nanostructures.

## 3.2 Results and Discussion

### 3.2.1 *In-silico* designing of modular DNA origamis

Designing a DNA origami structure is similar to developing a prototype for a building. The long scaffold (ss-DNA) is hybridised to a set of short ss staples (small oligonucleotides) and assembled under favourable thermal and chemical conditions. So, the foremost aim of the work discussed in this chapter is to design four modular origamis having different shapes and dimensions. The designed origami nanostructures were folded from M13mp18 ss DNA (7,249 nt, Supplementary

Table 3S-5) into their respective desired shapes. 10\*6 bundle (flat-sheet), Square nut (SN) and 24-helix bundle (HB) designs were honeycomb lattice-based, whereas double-wall square (DWS) was square lattice-based, as shown in Figure 3-1. These four designs were assembled with a varying number of staple strands; detailed sequence information is given in supplementary Table 3S-1-Table 3S-4. The square lattice packing rule allowed creating densely packed objects with rectangular geometry, but it may require additional effort to eliminate potentially undesired global twist impairments. The honeycomb lattice packing rule by default create straight, albeit more porous structures (14).

3 The first step in designing DNA origamis was to define a target shape that meets individual functional requirements for the intended application and lay this out for single or multilayer DNA origami objects using a honeycomb or square lattice framework. The design was accomplished with caDNAno (13) ([www.cadnano.org](http://www.cadnano.org)), depending on the complexity of the target structure. Next, the scaffold (M13mp18) template was selected, and crossovers were introduced, followed by the generation of staples by the auto staple option in caDNAno. The sizes of the staples were adjusted at different positions restricting the staple length within the range for proper folding of DNAs. The complimentary staples were generated as csv (comma-separated values) files from caDNAno for each of the four designs and were obtained commercially to perform the assembly of the DNAs (Supplementary Table 3S-1-Table 3S-4). CanDo was then used to predict the 3D object structure, which is particularly helpful when designing shapes with curved or twisted structural architecture. Because DNA origami provides a technique for placing molecules and curbing their fluctuations in user-defined ways, DNA origami objects can not only be used to improve some existing experimental methods in the molecular biosciences, but they also open entirely new field of research (14).

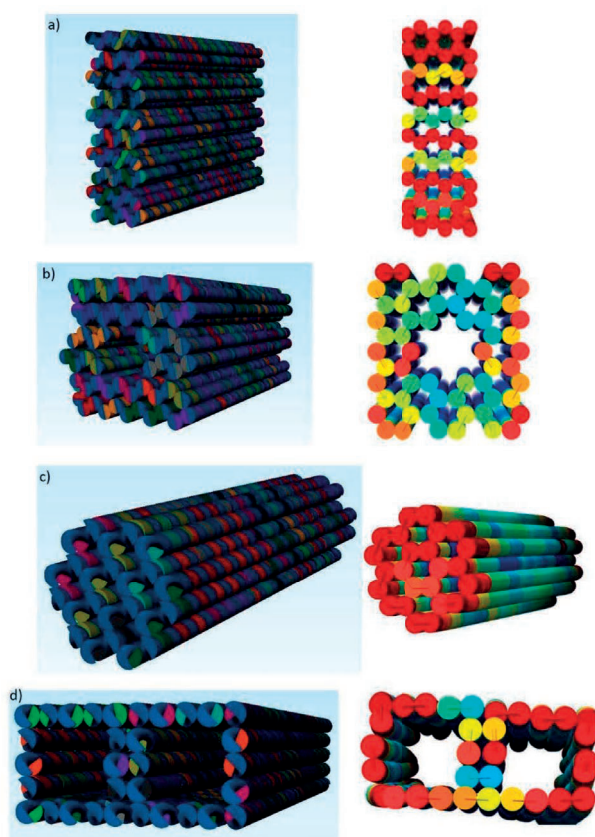


**Figure 3-1** caDNAAno designed and CanDo validated multilayer DNA origami structures.

a)  $10 \times 6$  bundle (flat-sheet)  $\sim 51 \times \sim 15 \times \sim 36$  nm, Square nut (SN)  $\sim 48 \times \sim 26 \times \sim 26$  nm, 24-helix bundle (HB)  $\sim 55 \times \sim 16 \times \sim 15$  nm and double-wall square (DWS)  $\sim 50 \times \sim 24 \times \sim 13$  nm. Left: caDNAAno images of designed nanostructures, Right: CanDo predicted images of multilayer DNA origami objects.

### 3.2.2 Folding DNA origami nanostructures

After designing, the scaffold strand and oligonucleotide staples were mixed in a 1:10 ratio and undergo thermal annealing cycles in PCR machines for a duration of minutes to days depending on the complexity to obtain the desired origami structures. The principle of assembling DNA origami structures relies on the significant staple strands access to the scaffold. Hence, the staples were in excess to the scaffold in the folding reaction leading to an increased yield of folded structures (16). The addition of divalent cations (magnesium ( $Mg^{2+}$ )) to the folding mix is vital as  $Mg^{2+}$  balances the negative charges of the DNA-backbone phosphates and reduce repulsion between the scaffold and staple strands providing desired folding of DNAs (16). Usually, concentrations of magnesium chloride ( $MgCl_2$ ) are in the 10–20 mM range, and the magnesium concentration usually needs to be optimised to find the appropriate assembly conditions in the folding reaction. For pH stabilisation, the folding reaction is generally supplemented with a folding buffer (generally prepared in 10 $\times$  working concentration) as described in methods. Some cases also describe the addition of NaCl to a final



concentration of 50 mM, as it is known to reduce the formation of undesired or lousy aggregates, but is not obligatory (9, 14).

The ultimate objective of the assembly reaction is to attain a state with minimum energy at conditions, where the minimum corresponds to the target structure (14). The scaffold-staple structural solution minimises energy through Watson-Crick base-pairing. Single-layer objects are known to self-assemble faster as compared to multilayer objects. The assembly of multilayer objects may not result in fully folded target structures, instead may also produce some partially folded dead ends (kinetic traps), in which parts of the structure need to be dissolved before assembly can proceed. Single-layer objects can be assembled by briefly heating the mixture of scaffold and staples to 80 °C, followed by annealing at room temperature during a few hours (1). Multilayer structures have been observed to require annealing over several days (9). Isothermal chemical denaturation and renaturation are reported to be as an alternative to thermal annealing (17). Folding DNA origami objects by sequential addition of staples to scaffold or by adjusting the staple length or sequence composition are alternative methods by which the user may direct the system along assembly pathways devoid of substantial kinetic folding traps.

Our folding reaction mixture contained scaffold DNA, oligonucleotides (staples), water, pH stabilising buffer and additional ions. Scaffold and staples are typically added such that each staple is present in a defined stoichiometry relative to the scaffold up to tenfold excess. Mg<sup>2+</sup> was changed for each origami in order to find the optimal conditions for folding (14 mM for flat-sheet, 16 mM for SN, 12 mM for HB and 18 mM for DWS). The folding process was carried out in a PCR tube in a thermocycler, and it involved fast heating to ~100°C and controlled hybridisation by slow and stepwise cooling to ~65°C and further to 25°C within several hours as described in Table 3-1.

	Temperature (°C)	Cycle	Time (min)
Stage 1	65	1	15
Stage 2	60	1	60
	-1	19	60
Stage 3	25	1	120
Stage 4	10	1	120
		Total	24 hrs

**Table 3-1 Folding temperature ramp used in a thermocycler for assembly of DNAs**

Each folding reaction consisted of three temperature gradients. The first stage serves denaturation; the second stage for strand annealing and folding, while stage 3 and 4 ensures cooling the reaction mixtures and incubation

The high initial temperature melts unspecific base pairs to prevent undesired secondary products. It was shown recently, by real-time PCR that the actual folding occurs with a minimum temperature

range and within only ~2 h or even a couple of minutes (18). This published report directs towards the opportunity for carrying folding at a constant temperature by tremendously minimising the folding time. The specific DNA origami structure is known to assemble at a particular temperature with ideal divalent cation concentration, so for each designed structure, the most favourable  $Mg^{2+}$  concentration was empirically identified, followed by Agarose gel electrophoresis (AGE) and AFM for quality control.

Analysis of the quality of folding of DNA origami and purification of the desired structures was worked out with AGE. Both the gels and the running buffer TBE contained 11 mM magnesium (14). The agarose gels were run in colder conditions (using an icebox) to minimise the diffusion, and it yielded a better resolution of the folded bands over an extended time. For multilayer origamis, it has been found that nanostructures with the lowest defect rate were those that advance with the highest speed through a 1.8% agarose gel. Thus, assembly reactions were optimised for the  $Mg^{2+}$  concentration to enable conditions that yield the fastest migrating groups, as shown in Figure 3-2. The desired groups were then purified from the agarose gel slabs by excising the desired bands, followed by crushing the gel slice with a pestle and centrifuging it through a microcolumn filter (see experimental section).

**3**

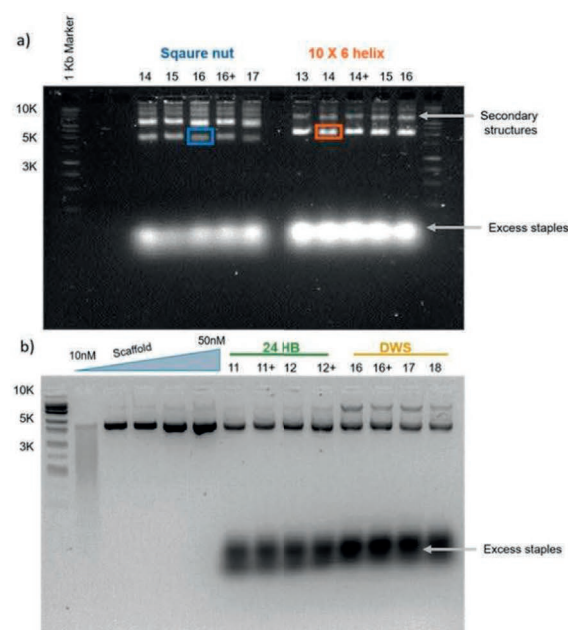


**Figure 3-2 AGE analysis for assembly conditions of modular designs.**

SYBR safe stained 1.8% agarose gel analysing the folding quality of DNA origami structure screened with different  $MgCl_2$  concentration; a) Square Nut (SN) and 10X6 helix (FS). Folded DN bands with their optimal  $Mg^{2+}$  concentration 16 mM and 14 mM, respectively (boxed). The secondary structure along with excess staples are also visible; b) 24 helix bundle (HB) and Double wall square (DWS) found with 12 mM and 18 mM  $Mg^{2+}$  for optimal folding. Different dilution scaffold (p7249) was used as reference with 1Kb DNA ladder.

### 3.2.3 Purification of DNs

The folded DNA origami nanostructures need to be extracted from the excess of staple strands, misfolded and aggregated objects before they can be used for characterisation. A number of DNA purification techniques exists (19), out of which four were tried in this thesis for purification: Gel extraction (20), PEG precipitation (21), ultrafiltration (22) and glycerol gradient-ultracentrifugation (23) but the best quality purified products along with recovered volume were obtained with ultrafiltration as shown in Table 3-2.

	Gel Filtration	PEG Precipitation	Ultrafiltration	Sedimentation
<b>Yield</b>	~25%	80-90%	60-70%	~80%
<b>Duration</b>	4-5 hrs	2 hr	1-2 hrs	4 hrs
<b>Volume recovered</b>	Best	Good	Medium	Good
<b>Dilution</b>	☑	☒	☒	☒
<b>Staple removal</b>	☑	☒	☑	☒

**Table 3-2 Overview of various purification methods employed.**

Comparison of four purification methods based on two quantitative (yield and duration) and three qualitative properties (volume recovered, dilution and staple removal). The duration is given for one sample (100  $\mu$ l).

The explicit and widely used way for purification is agarose gel electrophoresis band excision, which provides almost absolute segregation of DNA origami nanostructures from the unused staple strands and additionally helps in determining the quality of folded structures. Commonly, buffer with 11 mM MgCl<sub>2</sub> and 1.8% (wt/wt) agarose gels are used, by applying a voltage of 60–70 V for 1–3.5 h followed by extracting the DNA origami structures by using gel-extraction centrifugal filters (freeze n squeeze spin columns) (16). The quality of the gel bands provides a first conception about the nature of the folding, and it shows whether dimerisation of DNA origami nanostructures occurred, which would give rise to a gel band running slower than the monomer structures. However, the information gained from gel electrophoresis may not be sufficient and often complemented by another more explicit process, which images the DNA origami directly such as AFM. Moreover, when tested with the four designed origami structures, it showed low consistency with poor yield (~10 ng/μl) as shown in Figure 3-3b, which was not sufficient to carry out functionalisation studies.

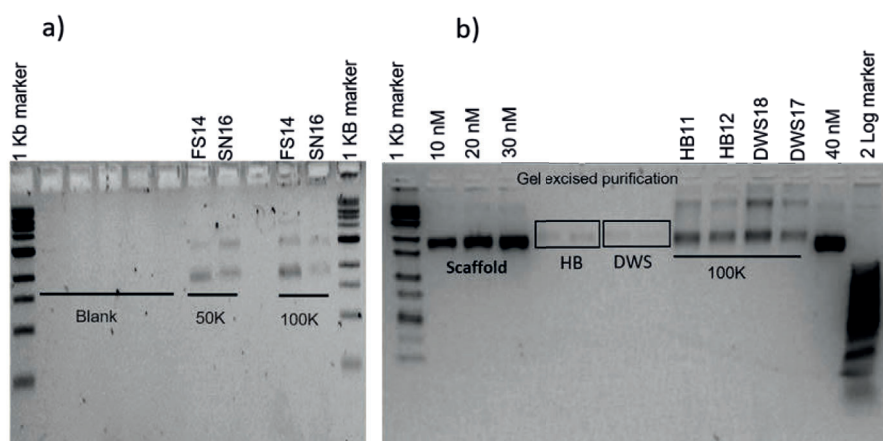


**Figure 3-3** AGE analyses of purified DNAs with ultrafiltration (MWCO filtration) and gel excision band purification.

a) FS and SN designs were purified with 50K and 100K MWCO filters; b) HB and DWS were purified with gel excision method and 100K MWCO filters. The low-intensity band (minimal yield) recovered with the gel excision method (boxed) is evident. Scaffold dilution and 1KB DNA ladder were run as a reference during the analyses.

Precipitation involving the use of crowding agents like PEG (polyethylene glycol) is reported as one of the most convenient methods for quickly separating folded objects from excess staple strands (24). PEG precipitation can be applied to a wide range of DNA shapes with up to 97% recovery yields. This method also enables the sample to be concentrated up to the solubility limit, and the buffer is known to introduce residual PEG molecules in the final recovered product (21). PEG precipitation was employed to reduce large elution volumes of the folded objects with improperly folded structures, but PEG-induced sedimentation lacked fidelity and consistency. Contamination of PEG molecules in the final product reduced the product yield considerably so, was not a preferred choice of purification in later studies.

Purification of DNA origami through sedimentation involving a glycerol gradient is reported to produce 40-80% recovery yields (23). DNA origamis conjugated with gold nanoparticles are also described to be separated through this method with an iodixanol gradient (25). Both of these methods, however, were not investigated for creating dense DNA origami solutions and therefore, Dietz *et al.*, established a slightly modified protocol without adding any residuals (24) and achieved up to 98% yield. Sedimentation is said to be a readily scalable approach utilising rate-zonal centrifugation, where DNAs remain in aqueous solution and can be easily recovered with consistent high yield without any residual contaminants (23). We found this method to be effective in removing the majority of the excess staples. Although, a caveat that limits the widespread use of sedimentation technique is the complete removal of glycerol which may affect the characterisation (26).

### 3

A fast and robust purification method is the use of centrifugal filters (ultrafiltration), which provide enough purification standard for maximum applications. Ultrafiltration needs filters with distinct pore sizes (molecular weight cut off filters) to remove unbound staple strands. However, this filtering approach is only found to be suitable for nanostructures folded with high yield because no selection of undesired objects can be made (24). To minimise the nonspecific adsorption of the DNA nanostructures with MWCO membranes, we usually prewash the columns with 0.025% (v/v) tween-20 mixed with wash buffer for 30mins. The ultrafiltration method offers residual-free separation but is less effective than PEG precipitation due to the limits posed by the pore size of the filtration membrane. 30, 50 and 100 kDa cut-off filter types were tested and 100 kDa cut-off filters efficiently separated the high-molecular-weight DNA origami structures from low-molecular-weight excess staple strands with multiple cycles of buffer exchange and filtrations. Gel mobility shifts assays of the purified assembled nanostructures show distinct bands (Figure 3-3). Purification quality was established using suitable references (10nM, 20 nM and 30 nM dilution scaffolds) which were run nearly to similar distance on the gel along with the purified DN's (8).

Ultracentrifugation is preferred method employed for the purifications of folded DNAs, considering the quality and quantity of recovered end products, together with the convenience of time and resources engaged in the entire process of purification.

#### 3.2.4 Characterisation of purified DNAs

The characterisation is the most crucial and imperative step to describe the functionality of a DNA nanosystem. Characterisation entails in-depth studies involving the yield of the end product, quantifying appropriately folded DNAs, verifying modifications of DNAs and testing the functionality of the nanostructure to be deployed correctly for its application. Characterisation techniques are known to vary with the degree of detail they provide: a rough overview of the structure or analysing the DN at the nanometre level (26).

### 3.2.4.1 Microscopy

Typically, the size of DNs are in the nanometer scales; therefore, images acquired from sophisticated microscopy techniques have become the trademark of analysis and became the facet of DNA nanotechnology in the scientific literature. DNs fall absolutely in the resolution range of AFM (5-5000 nm), and therefore AFM, along with its associated techniques, have proliferated successfully into the field of DNA nanotechnology, enabling growing acceptance of its aesthetical data (1, 27-29). Currently, this method is used to obtain high-resolution static and dynamic images with high-spatial-resolution and in near-native conditions to study the physical and mechanical properties of biological macromolecules. The AFM also allows capturing mechanical properties of the DNs in liquids using force-distance mapping, which is most suited for 3D origamis. AFM data can offer insight into the dimensional analysis of the structures, tracking the folding pathways and reaction conditions (17, 30) and can also quantify the quality of DNA substrate modifications (29, 31). In our study, AFM was primarily used to demonstrate the formation of four DNA origamis illustrating their height profiles (z-direction) and also profess the large scale organisation of individual high-ordered arrays. The substrate used to deposit DNA origami structures for AFM measurements was mica for all the four designs DNs (FS, SN, HB and DWS). Additionally, silicon wafers substrate were also used for two of the designed origamis (HB and DWS). The height profile analysis of DNs in two different substrates confirms the appropriate assembly of recovered nanostructures by comparing the theoretical and measured height as shown in the figures below (Figure 3-4 d, Figure 3-5d, Figure 3-6e and Figure 3-7e).

3

On the other hand, Scanning electron microscopy (SEM) uses an electron beam to non-destructively image and characterise conductive materials in a vacuum (32). Due to the limitations of SEM (the requirement for conductive samples, its operation under vacuum and its relatively low resolution), its advantage gets restricted in DNA nanotechnology. So, SEM imaging of biological samples requires a metal coating with such as gold (Au), platinum (Pt) (33) to mitigate the charging effects of electrons (26). SEM is a fast screening method as compared to AFM and hence, used extensively to enable a quick scan for morphology and size estimation (x-y directions) of the purified DNs. The SEM images revealed that all the DNs have a consistent size of <100 nm and demonstrate the absence of other impurities/salt in the samples, as shown in the figures below.

Transmission electron microscopy (TEM) is another well-established analytical technique, which DNA nanosystem development heavily relies on for proof of correct assembly (13, 27, 34). Like AFM, TEM data is used for doing population analysis by observing the morphology of a set of particles under the microscope. Although TEM also requires high vacuum and complicated sample treatment, it beats all other methods (SEM and AFM) in terms of resolution. For this reason, TEM has become increasingly popular in DNA nanotechnology in recent years, in particular in the context of 3D DNA nanoobjects. In contrast to SEM, TEM is performed on very thin samples, which are usually prepared

in a special way (32).

The SEM of metallic (33) coated FS, shows the presence of monodispersed structures of <100 nm in size with an ellipsoidal or cylindrical in detailed structural analysis (Figure 3-4a and b). Similar features also emerged in the AFM imaging of the structures (Figure 3-4c). Whereas, an interesting variation observed with FS design in their significant differences between the measured and theoretical height (Figure 3-4d). The factor attributed to this variation is the larger surface area ( $\sim 360\text{Å}^2$ ) and charge on the horizontal sides ( $\sim 15\text{nm}$ ) of the purified nanostructure. Hence, the height difference was envisioned, making one side more preferable for orientation during substrate deposition.

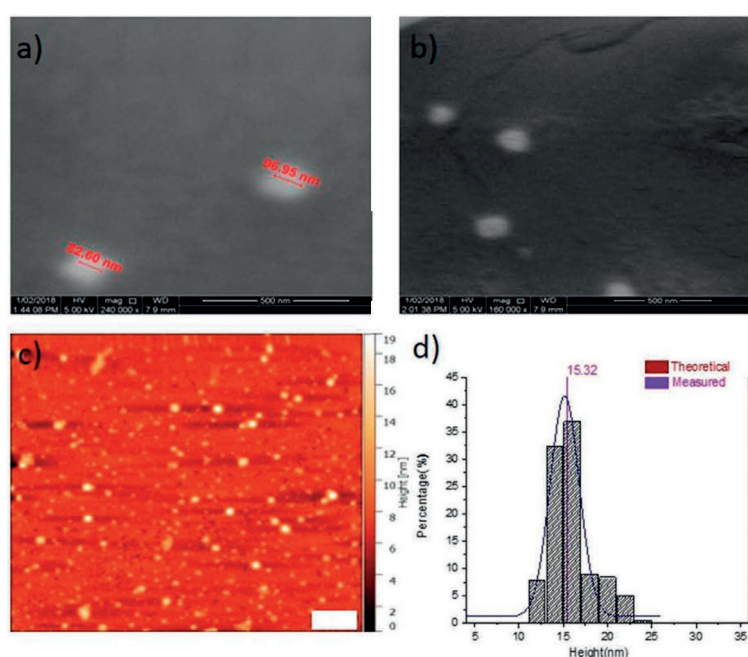


**Figure 3-4 Microscopic characterisations of purified FS.**

SEM samples were prepared and deposited on mica with 5 nm Platinum coating. a) SEM of distinctive particles with x-y dimensions <100 nm; b) SEM image displaying purified structure dispersal on the substrate; c) AFM of samples deposited on mica; d) Histogram showing the measured height distribution with Gaussian fit of the AFM images  $15.32 \pm 1.5$  nm. Scale bars in a-c: 500 nm.

The next design SN have a square-shape and appears to be ( $\sim 50$  nm) in size, homogeneously scattered detected at higher magnification SEM micrograph (Figure 3-5a and b). Multiple AFM scans of SN sample and analysis of collected images were found consistent with the SEM results in terms of size and shape (Figure 3-5c). However, aggregation of two or more structures due to adherence is also evident, but having no impact on the measured height substantiates the structures stick from sides rather than superimposed.



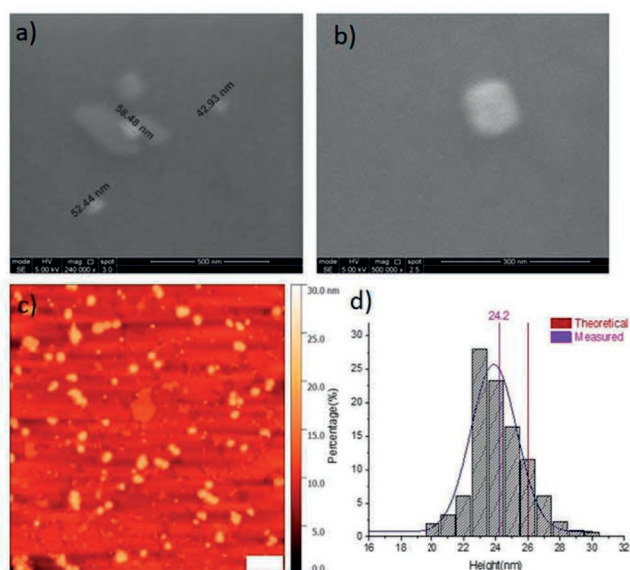


**Figure 3-5 Microscopic characterisations of purified SN.**

SEM samples were prepared and deposited on mica with 5 nm (33) coating. a) SEM of distributed particles with x-y dimensions <100 nm; b) SEM image of a single particle with clear morphology at higher resolution; c) AFM of samples deposited on mica. Few large aggregates were seen due to adhering of structures; d) Histogram showing the measured height distribution with Gaussian fit of the AFM images  $24.2 \pm 2.1$  nm. Scale bars in a: 500 nm, b: 300 nm, c: 500 nm.

Similarly, conducting SEM of HB, on a TEM grid with negative staining (1.5 % uranyl acetate) spots particles with 50 nm in dimension (Figure 3-6a). Further, the TEM verifies the assembly of HB, and the individual helices of bundles are evident in the structures (Figure 3-6b). For AFM, the samples were deposited in two different substrates to review if there is any difference in the deposition pattern (Figure 3-6c and d), but, the image analysis confirms the creation of correctly folded designs observed with a similar height profile of the scans collected from the individual substrates (Figure 3-6e).



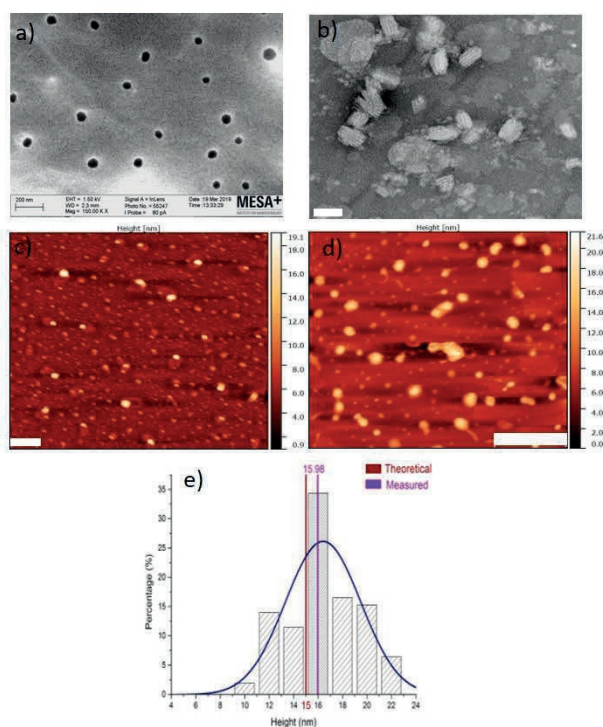


**Figure 3-6 Microscopic characterisations of purified HB designs.**

a) SEM of purified origami nanostructure adsorbed on TEM grid; b) TEM performed with negative stain 2% uranyl acetate; c) and d) AFM visualisation of HB deposited samples on two substrates silicon and mica respectively; e) Histogram showing the measured height distribution with Gaussian fit of the AFM images from both the substrates  $15.98 \pm 2.3$  nm. Scale bars in a: 200 nm, b: 50 nm, c and d: 500 nm.

Finally, for the fourth design DWS, imaging were sequentially performed with SEM and TEM validating the dimension and shape of the designs. In the TEM, the helices of design can be visualised, but the staining covers the frontal cross-section. Also, the lateral orientation of structures on the grid makes it difficult to spot the cavity of the DWS (Figure 3-7b). Besides, the AFM images revealed the inverted square boxes (Figure 3-7c), and the measured height analysis validates the structural conformation (Figure 3-7c-e). AFM imaging seems more suitable to 2D or solid internal structures but poses a limitation on 3D or structures with an internal cavity.

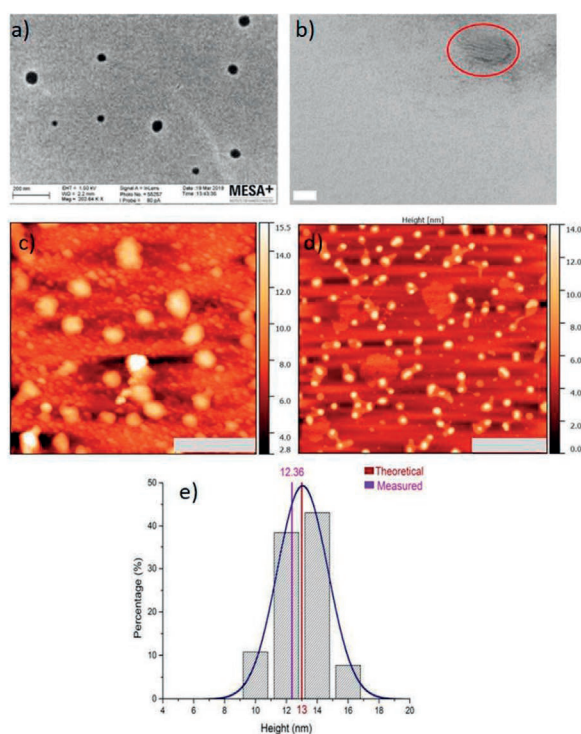


**Figure 3-7 Microscopic characterisations of purified DWS designs.**

a) SEM of purified origami nanostructure adsorbed on TEM grid; b) TEM performed with negative stain 2% uranyl acetate; c) and d) AFM visualisation of deposited samples on two substrates silicon and mica respectively; e) Histogram showing the measured height distribution with Gaussian fit of the AFM images from both the substrates  $12.36 \pm 1.4$  nm. Scale bars in a: 200 nm, b: 20 nm, c and d: 500 nm.

To make the empirical estimation for the correct folding of the four designs, we excluded other possibilities (misfolded or artefacts) by employing control experiments for all the microscopy techniques. All the imaging experiments were performed with positive and negative controls to ascertain the *in vitro* assembly of designed structures. Firstly, the microscopy images collected with different techniques for the scaffold (M13mp18 ss DNA) showing the ss-DNA are readily attached to their respective surfaces precisely appearing like string or tapeworms as seen in the supplementary Figure 3-S1. Length measurement of scaffolds also confirmed their correct length  $>1.5 \mu\text{m}$ , consistent with the size of base pairs (7.2 KB). Secondly, the staples (oligonucleotides) strands are evaluated using SEM and AFM, to mitigate the chances of visualising their random aggregation, as seen in Figure 3-S2. The formation of large aggregates, shaped as toroidal complex in the SEM (Supplementary Figure 3-S2a), may be due to the metallic coating of the samples. Finally, to omit the possibility of misconstruing any artifacts during the characterisation from the substrate, we also imaged the cleaved mica surface and divalent cations used to facilitate the binding of DNA as shown in Supplementary Figure 3-S3.

### 3.2.4.2 Biophysical Analysis

There are few other techniques considered promising to expand the scope of DNs assessment in DNA nanotechnology. We performed biophysical characterisation using Dynamic Light Scattering (DLS) experiments to estimate particle size distribution and measure the Zeta potential (surface charge). DLS works on the principle of analysing the hydrodynamic diameter of the nanostructures by measuring the intensity of the scattered light of the suspended particles in the solution (35). All the measurements were obtained in 1000  $\mu\text{l}$  solution in a 1-2 nM concentration range of purified DNs. The purified DNs have been diluted in Milli-Q water, making up the required volume for DLS measurements (36). However, the structural stability of DNs in water were pre-examined by resuspending them for 24 hrs at 4  $^{\circ}\text{C}$ , verified through AGE (Figure 3-S4).

The value of the obtained DLS measurements for all DNs fit well with the theoretical values for the size dimension of the DNA origamis <100 nm, as shown in Figure 3-8. The DLS results of the DNs are in line with the dimension of the particles sizes expected for the DNs (~50 nm), and a narrow size distribution shows a homogenous sample with monodisperse particles (37).

3

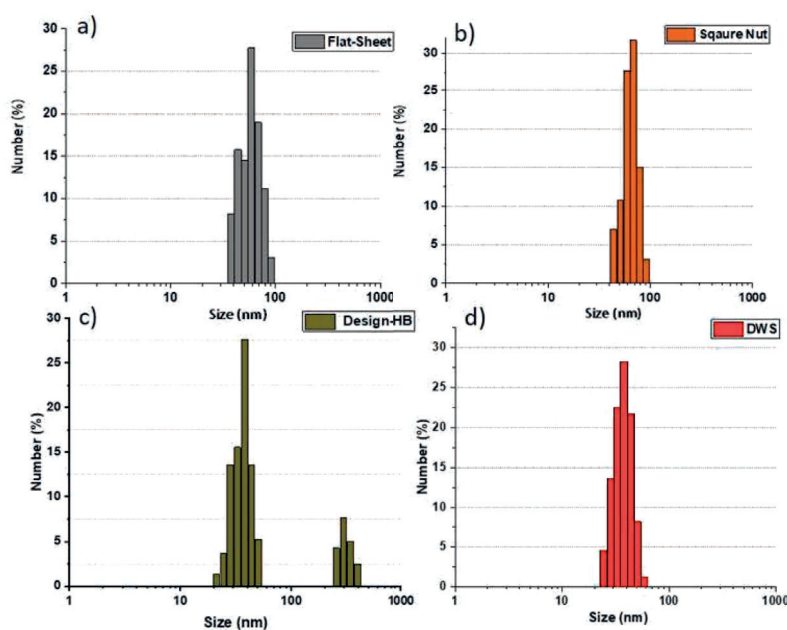


**Figure 3-8 Average size distribution based on dynamic light scattering (DLS) of purified DNs.**

a) Flat Sheet (38); b) Square Nut (SN); c) 24 helix bundle (HB); d) Double Wall Square (DWS). All purified samples were diluted to make 1 ml volume required for measurements.

The zeta potential (mV) measurements of the samples were obtained after the DLS experiments on the same instrument with different settings. The significant negative values were obtained for  $\zeta$  – potential for all the DNs (Table 3-3). The values suggest the presence of anionic particles

resuspended in the solution(39).  $\zeta$  – potential values were also compared with the negative charge of the control (scaffold ss-DNA) samples obtained.

DNA designs	$\zeta$ – potential [mV]
Flat -Sheet (FS)	-25.3
Square Nut (SN)	-32
Helix Bundle (HB)	-15.6
Double-wall square (DWS)	-17.8

**Table 3-3 Surface charge values of the purified DN's.**

### 3.3 Conclusions

In this chapter, we have successfully designed, assembled, and characterised four 3D multilayer DNA origami. The multiple control experiments explored during each stage of the workflow, verify and establishes the formation of DN assemblies with consistent size and shape. The overall work was done at two places; Flinders University, Australia (FU) and University of Twente, Netherlands (UT). The first two designs FS and SN were made during my first year at FU, with an approach towards learning the techniques and methods involved and optimising conditions to be able to use this knowledge in future studies of my research. I was able to amend the dimensions of the final designs and optimise appropriate assembly conditions leading to their characterisation. Out of the different purification methods used, ultracentrifugation (MWCO filtration) suited best for our DNs in terms of yield recovery and purification quality. Recovering a highly purified product is the utmost requirement for a wide range of applications (24).

With all analytical quantification and qualitative studies for validation, right from DNA assembly to characterisation, obtaining high concentration DNs was critical. 1-2 nM of purified samples were found to be optimum for microscopic characterisation with particles homogenously distributed over the substrate or imaging grids. Similar working concentrations of samples worked well for biophysical analysis too. After extensive characterisation of DNs with suitable controls at all stages, we conclude assembling DNs of right sizes. However, the internal cavity of SN and DWS are still not very clear on the microscopy imaging. These may be due to either the structural flaw at the assembly process or limitation of imaging, considering specific adsorption orientations on their respective substrates. The results and analysis in this chapter explicitly add to our knowledge about designing and building specific DNA nanostructures. The formation of DNs is the first important step towards various application such as electronics, biomedical and other areas. As a continuation, the DNs (HB and DWS) described in this chapter were further used for encapsulation and other functional studies.

### 3.4 Acknowledgements

I gratefully acknowledge the expertise, equipment and support provided by Australian Microscopy

and Microanalysis Research Facility (AMMRF) and the Australian National Fabrication Facility (ANFF) South Australian Node for SEM and AFM. I thank Rico Keim, Mark Smithers and Abhimanyu Rana for their assistance in TEM, SEM and AFM imaging and analysis respectively at UT. Special thanks go to Parsa Nafisi (UCLA) and Steven Perrault (Harvard University) for their valuable suggestions and advice in designing and purification of DN's.

## 3.5 Materials and Methods

### 3.5.1 3D and multilayer structure designing

Four multilayered modular origamis of different shapes and dimensions were designed. They are: i) 10\*6 bundle (flat-sheet, FS) (13), ii) square nut (SN) (9), iii) 24-helix bundle (HB) (40) and iv) double-wall square (DWS) (41) - which is an edited version of rod-like horse nanostructure. All the designs were produced with slight modifications from the ones previously reported. caDNAno was used to design origami structures, and all designs were validated with CanDo before proceeding to the self-assembly stage. FS, SN and HB designs were honey-comb lattice geometries, whereas DWS was square lattice-based shapes.

3

### 3.5.2 Self-assembly of modular 3D DNAs

After designing, the modular DNAs were folded into desired 3D shapes using the folding mix. Each origami was prepared in PCR tubes with 100  $\mu$ l of the folding mix (containing 10 nM scaffold DNA, 70 nM staple strands, variable  $Mg^{2+}$  ions optimised for individual origami designs and 1X TBE (Tris-Borate EDTA) buffer). TE buffer was used for stabilisation of pH, whereas  $Mg^{2+}$  was incorporated into folding mix to stabilise the structure of the DNA origami.  $Mg^{2+}$  ions concentration in the folding mix was optimised to ensure proper assembly of four DNA origamis (14 mM for flat-sheet, 16 mM for SN, 12 mM for HB and 18 mM for DWS). The scaffold DNA and the custom staples were ordered commercially. M13mp18 ss DNA (scaffold) was obtained from New England Biolabs (NEB, Catalog number: #N4040S). The large (>10bp) staple strands were in the format of 96-well plates at 100 nmole synthesis scale, were ordered from Integrated DNA Technologies Inc. ([www.IDTDNA.com](http://www.IDTDNA.com)). The strands were normalised to 10  $\mu$ M x 500  $\mu$ L and were used without purification.

All chemicals were purchased from Sigma Aldrich except agarose (VWR chemicals) and were used without further purification. Buffers are made in Milli-Q water obtained by ultrafiltration (Millipore Adv. A10, 18 M $\Omega$  cm at 25°C). The folding buffer 1X TE consisted of (10 mM Tris, 1 mM EDTA, pH 7.2) was used to foster the assembly. For each reaction, scaffold DNA (M13mp18 ss-DNA (7,249 nucleotides)) was mixed with staple strands in a PCR tube. 5 mM NaCl was then added to the reaction mixture to decrease the folding rate. Folding was carried out by rapid heat denaturation (100°C for 5 min) and then cooling down to 65°C, further down to 25°C to form the designed structures. The exact temperature ramps followed are as follows: 65° to 60°C for 15 minutes; 60° to

40°C for 20 hours (following a trend to decrease 1°C in every 60 minutes); 25°C forever on a thermocycler (Bio-Rad MJ mini).

### 3.5.3 Gel electrophoresis and purification of DNA origamis

The quality of the folded DNA nanostructures was determined by gel electrophoresis. 1.8% agarose gel (w/v) was prepared by mixing 1g Agarose from Sigma-Aldrich and 0.5X TBE (Tris-borate EDTA) buffer (45 mM Tris, 45 mM Boric acid, 1 mM EDTA), 11 mM MgCl<sub>2</sub>, pH 7.2 in a total volume of 50 ml. The solution was heated in the microwave until the agarose dissolved completely and 5µl of 10,000X SYBR Safe gel stain (Invitrogen) was added to make the final strength 1X SYBR Safe in the gel. 5µl of sample aliquots were mixed with 3 µl of 6X loading dye (New England Biolabs) and loaded into the gel along with 1Kb ladder. The gel was electrophoresed for 3 hours at 7 V/cm in an ice water bath to minimise the diffusion of bands and overheating. Gels were visualised on Gel-doc EZ (BioRad) using Image Lab software.

The fastest migrating bands were selected for excision and were cut from the gel. DNA was recovered by pestle crushing of excised bands, then freezing them for 5 min followed by centrifugation for 5 min at 15,000g in a tabletop centrifuge at 4°C using Freeze'N'Squeeze DNA gel extraction spin columns from Bio-Rad.

Alternatively, the DNA origami structures were also purified with centrifugal filters (Millipore 0.5 ml, 30-100K), thereby increasing the volume yield of end-products. The wash columns were pretreated with 0.025% (v/v) tween-20 mixed with wash buffer (10 mM Tris + 1 mM EDTA + 10 mM MgCl<sub>2</sub>, pH 7.2) for 30 min to reduce any non-specific absorption of the nanomaterial on the column. In this method, samples were mixed with wash buffer in a 1:4 ratio (v/v) and spun for 10 min at 15000g, 4°C. Repeated washing of the filtered sample and collection was carried out as adapted from the published protocol (16). To further determine the quality of the purified product, recovered material was put onto 1.8% agarose gel electrophoresis, and the concentration of the individual DNA origamis are determined by UV-vis absorption spectroscopy (NanoDrop 1000, Thermo Scientific). The purified samples were then stored at -20°C for further analysis.

### 3.5.4 SEM of DNAs

SEM has been used as a fast screening approach for imaging DNAs considering its limited resolving power. Purified samples were prepared using ~1 cm<sup>2</sup> mica substrate, which is then adhered onto the SEM holder. The upper layer of mica was cleaved and treated with 100 mM MgCl<sub>2</sub>, which helps to immobilise DNA origami. 5-7 µl purified DNA origami solution was added on the mica surfaces with a concentration range of ~10-15 nM and then air-dried for 10 min. The dried surface was washed three times with 50 µl of dd-H<sub>2</sub>O (double-distilled H<sub>2</sub>O) and gently dried under N<sub>2</sub> gas flow. The polymeric surface of DNA was made conductive by applying a thin 5 nm coating of platinum using

Q300T-D Dual Target sputter coater under default conditions. Prepared samples were studied with Scanning Electron Microscope (SEM) (Inspect FEI F50 SEM) for observing DN's morphology with the given settings (M:  $\times 100.000$ – $\times 200.000$ ,  $\delta = 0.5$ -1  $\mu\text{m}$ , U = 5kV).

### 3.5.5 AFM of DN's

Atomic Force Microscopy (AFM) data were collected using Multimode V2 AFM in tapping mode (Bruker AXS) with SNL-10 sharp nitride cantilevers (Bruker, MA) using resonance frequencies  $\sim 300$  kHz of the 42 N/m force constant. Mica and silicon surfaces were used for imaging. The steps followed for preparation of samples on mica surfaces are as follows:

1. Cut the mica substrates to the appropriate size (1 cm x 1 cm squares) with scissors and fix the mica sheet with epoxy resin on the round metal plate.
2. Cleave the mica surface with double-sided tape (repeat the process 3-4 times) to ensure the clean and smooth layer.
3. Pre-incubate the surface with 5-7  $\mu\text{l}$  of 100 mM  $\text{MgCl}_2$  solution for 5 min.
4. Wash the surface 2-3 times with dd- $\text{H}_2\text{O}$ .
5. Dry the surface with compressed nitrogen ( $\text{N}_2$ ) for 1 min.
6. Add the purified DNA sample (4-5  $\mu\text{l}$  of mwco (molecular weight cut-off)-centrifugal filtered samples or 7-8  $\mu\text{l}$  samples purified via agarose gel electrophoresis) and incubate for 10 min.
7. Wash the surface 2–4 times with buffer (10 mM Tris +1 mM EDTA+10 mM  $\text{MgCl}_2$ , pH-8.0) in order to remove the unbound sample.
8. Wait for at least 15 min to minimise the thermal drift and then focus the laser beam on the cantilever. Adjust the photodiode signal to the maximum.
9. Select a region of DNA origami structures to be imaged, and then take scans.

The steps followed for preparation of samples on silicon surfaces are as follows:

1. Cut silicon wafers into chips of the appropriate size to fit on a metal plate or the scan holder.
2. Clean the silicon wafer with acetone for 15 min.
3. Rinse wafer with ethanol and dry with compressed nitrogen ( $\text{N}_2$ ) flow.
4. Activate silicon surface with a benchtop oxygen plasma (SPI Plasma-Prep<sup>TM</sup> II) treatment (oxygen flow 40 sccm, plasma power 200W, temperature 30°C and time 15 min) or piranha solution for 15 min (ready for APTES deposition).
5. 3-aminopropyltriethoxysilane (APTES) vapour deposit on a silicon wafer with a vacuum dryer (desiccator).
6. Introduce the vacuum slowly in the first 5 min, and then continue vacuum for extra 10 min.
7. Leave the wafer within the vacuum dryer for 3-4 hrs.
8. Clean wafer with ethanol and dry with the  $\text{N}_2$  flow.
9. Deposit purified DN's on the wafer and incubate for 30-45 min.
10. Rinse the substrate with 100  $\mu\text{l}$  wash buffer and water and dry with  $\text{N}_2$  for 1 min.



After the engagement of the tip, the tapping amplitude set point was typically  $< 1$  mV and the scan rates ranged between 0.8–1.2 Hz. Several images were acquired from different locations of the mica surfaces to ensure reproducibility of the results. AFM images were analysed using Gwyddion analysis software.

### 3.5.6 TEM of DNAs

Transmission Electron Micrographs were obtained with a FEG-TEM (Phillips CM 30 microscope). For imaging, 3  $\mu$ l of purified structures were added onto a Formvar/carbon-coated TEM grids (Electron Microscopy Sciences) and incubated for 3 min. The solution was then blotted away using filter paper. 5–6  $\mu$ l of 2% (w/v) aqueous uranyl acetate was applied to the grid and immediately dabbed off using filter paper, followed by re-staining with 5  $\mu$ l of 2% aqueous uranyl acetate. Next is the incubation step for 40 sec before draining off the stain solution and allowing the grids to dry at least 30 min before imaging. DNAs were then imaged, TEM was operated at 200–300 kV accelerating voltage. The dimension of the imaged structures was measured with ImageJ to determine the size distribution of DNAs in the image grid.

3

### 3.5.7 Dynamic Light Scattering and Zeta potential

Measurements were made on a Nano ZS machine made by Malvern Instruments, and the data were extracted using the solution viscosity of water and refractive index of DNAs=2.1 in the standard settings of the company's software (Zetasizer).



### 3.6 References

1. Rothemund PW. Folding DNA to create nanoscale shapes and patterns. *Nature*. 2006;440(7082):297-302.
2. Joshi M, Kundapura S, Poovaiah T, Dhar PK. DNA Origami: What, How and Where. In: Singh V, Dhar PK, editors. *Systems and synthetic biology*. New York: Springer Science+Business Media; 2015. p. 357-68.
3. Schneider F, Möritz N, Dietz H. The sequence of events during folding of a DNA origami. *Science advances*. 2019;5(5):eaaw1412.
4. Nummelin S, Kommeri J, Kostianinen MA, Linko V. Evolution of structural DNA nanotechnology. *Advanced Materials*. 2018;30(24):1703721.
5. Erkelenz M, Bauer DM, Meyer R, Gatsogiannis C, Raunser S, Saccà B, et al. A Facile Method for Preparation of Tailored Scaffolds for DNA-Origami. *Small*. 2014;10(1):73-7.
6. Chandrasekaran AR, Pushpanathan M, Halvorsen K. Evolution of DNA origami scaffolds. *Materials Letters*. 2016;170:221-4.
7. Andersen ES, Dong M, Nielsen MM, Jahn K, Subramani R, Mamdouh W, et al. Self-assembly of a nanoscale DNA box with a controllable lid. *Nature*. 2009;459(7243):73.
8. Ke Y, Sharma J, Liu M, Jahn K, Liu Y, Yan H. Scaffolded DNA origami of a DNA tetrahedron molecular container. *Nano letters*. 2009;9(6):2445-7.
9. Douglas SM, Dietz H, Liedl T, Högberg B, Graf F, Shih WM. Self-assembly of DNA into nanoscale three-dimensional shapes. *Nature*. 2009;459(7245):414.
10. Ke Y, Douglas SM, Liu M, Sharma J, Cheng A, Leung A, et al. Multilayer DNA origami packed on a square lattice. *Journal of the American Chemical Society*. 2009;131(43):15903-8.
11. Ke Y, Voigt NV, Gothelf KV, Shih WM. Multilayer DNA origami packed on hexagonal and hybrid lattices. *Journal of the American Chemical Society*. 2012;134(3):1770-4.
12. Dietz H, Douglas SM, Shih WM. Folding DNA into twisted and curved nanoscale shapes. *Science (New York, NY)*. 2009;325(5941):725-30.
13. Douglas SM, Marblestone AH, Teerapittayanon S, Vazquez A, Church GM, Shih WM. Rapid prototyping of 3D DNA-origami shapes with caDNAo. *Nucleic acids research*. 2009;37(15):5001-6.
14. Castro CE, Kilchherr F, Kim DN, Shiao EL, Wauer T, Wortmann P, et al. A primer to scaffolded DNA origami. *Nat Methods*. 2011;8(3):221-9.
15. Kim D-N, Kilchherr F, Dietz H, Bathe M. Quantitative prediction of 3D solution shape and flexibility of nucleic acid nanostructures. *Nucleic acids research*. 2011;40(7):2862-8.
16. Schmied JJ, Raab M, Forthmann C, Pibiri E, Wunsch B, Dammeyer T, et al. DNA origami-based standards for quantitative fluorescence microscopy. *Nature protocols*. 2014;9(6):1367.
17. Jungmann R, Liedl T, Sobey TL, Shih W, Simmel FC. Isothermal assembly of DNA origami structures using denaturing agents. *Journal of the American Chemical Society*. 2008;130(31):10062-3.
18. Sobczak J-P, Martin TG, Gerling T, Dietz H. Rapid folding of DNA into nanoscale shapes at constant temperature. *Science*. 2012;338(6113):1458-61.
19. Tan SC, Yiap BC. DNA, RNA, and protein extraction: the past and the present. *J Biomed Biotechnol*. 2009;2009:574398.
20. Bellot G, McClintock MA, Lin C, Shih WM. Recovery of intact DNA nanostructures after agarose gel-based separation. *Nat Methods*. 2011;8(3):192-4.
21. Stahl E, Martin TG, Praetorius F, Dietz H. Facile and scalable preparation of pure and dense DNA origami solutions. *Angew Chem Int Ed Engl*. 2014;53(47):12735-40.
22. Douglas SM, Bachelet I, Church GM. A logic-gated nanorobot for targeted transport of molecular payloads. *Science*. 2012;335(6070):831-4.
23. Lin C, Perrault SD, Kwak M, Graf F, Shih WM. Purification of DNA-origami nanostructures by rate-zonal centrifugation. *Nucleic Acids Res*. 2013;41(2):e40.
24. Wagenbauer KF, Engelhardt FA, Stahl E, Hechtl VK, Stömmner P, Seebacher F, et al. How we make DNA origami. *ChemBioChem*. 2017;18(19):1873-85.
25. Ko SH, Vargas-Lara F, Patrone PN, Stavitskiy SM, Starr FW, Douglas JF, et al. High-speed, high-purity separation of gold nanoparticle–DNA origami constructs using centrifugation. *Soft Matter*. 2014;10(37):7370-8.
26. Mathur D, Medintz IL. Analyzing DNA Nanotechnology: A Call to Arms For The Analytical Chemistry Community. *Anal Chem*. 2017;89(5):2646-63.
27. Han D, Pal S, Nangreave J, Deng Z, Liu Y, Yan H. DNA origami with complex curvatures in three-dimensional space. *Science*. 2011;332(6027):342-6.
28. Winfree E, Liu F, Wenzler LA, Seeman NC. Design and self-assembly of two-dimensional DNA crystals. *Nature*. 1998;394(6693):539-44.
29. Hung AM, Micheel CM, Bozano LD, Osterbur LW, Wallraff GM, Cha JN. Large-area spatially ordered

- arrays of gold nanoparticles directed by lithographically confined DNA origami. *Nat Nanotechnol.* 2010;5(2):121-6.
30. Dunn KE, Dannenberg F, Ouldrige TE, Kwiatkowska M, Turberfield AJ, Bath J. Guiding the folding pathway of DNA origami. *Nature.* 2015;525(7567):82.
  31. Kershner RJ, Bozano LD, Micheel CM, Hung AM, Fornof AR, Cha JN, et al. Placement and orientation of individual DNA shapes on lithographically patterned surfaces. *Nature Nanotechnology.* 2009;4(9):557.
  32. Jungmann R, Scheible M, Simmel FC. Nanoscale imaging in DNA nanotechnology. *Wiley Interdisciplinary Reviews: Nanomedicine and Nanobiotechnology.* 2012;4(1):66-81.
  33. Tkachenko AG, Xie H, Liu Y, Coleman D, Ryan J, Glomm WR, et al. Cellular Trajectories of Peptide-Modified Gold Particle Complexes: Comparison of Nuclear Localization Signals and Peptide Transduction Domains. *Bioconjugate Chemistry.* 2004;15(3):482-90.
  34. Ke Y, Ong LL, Shih WM, Yin P. Three-dimensional structures self-assembled from DNA bricks. *Science.* 2012;338(6111):1177-83.
  35. Kim KR, Kim DR, Lee T, Yhee JY, Kim BS, Kwon IC, et al. Drug delivery by a self-assembled DNA tetrahedron for overcoming drug resistance in breast cancer cells. *Chem Commun (Camb).* 2013;49(20):2010-2.
  36. Kielar C, Xin Y, Shen B, Kostianen MA, Grundmeier G, Linko V, et al. On the Stability of DNA Origami Nanostructures in Low-Magnesium Buffers. *Angew Chem Int Ed Engl.* 2018;57(30):9470-4.
  37. Zhang Q, Jiang Q, Li N, Dai L, Liu Q, Song L, et al. DNA origami as an in vivo drug delivery vehicle for cancer therapy. 2014;8(7):6633-43.
  38. Ryadnov MG, Ceyhan B, Niemeyer CM, Woolfson DN. "Belt and braces": a peptide-based linker system of de novo design. *J Am Chem Soc.* 2003;125(31):9388-94.
  39. La TH, Nguyen TTT, Pham VP, Nguyen TMH, Le QH. Using DNA nanotechnology to produce a drug delivery system. *Advances in Natural Sciences: Nanoscience and Nanotechnology.* 2013;4(1):015002.
  40. Fischer S, Hartl C, Frank K, Radler JO, Liedl T, Nickel B. Shape and Interhelical Spacing of DNA Origami Nanostructures Studied by Small-Angle X-ray Scattering. *Nano Lett.* 2016;16(7):4282-7.
  41. Halley PD, Lucas CR, McWilliams EM, Webber MJ, Patton RA, Kural C, et al. Daunorubicin-Loaded DNA Origami Nanostructures Circumvent Drug-Resistance Mechanisms in a Leukemia Model. *Small.* 2016;12(3):308-20.

**Table 3S-1 Details about 10X6 bundle (flat-sheet) staple sequences**

Start	End	Sequence: left to right (5'-3')	Length
16[31]	25[30]	ATTA ACTATTA ACTTTTGTATTTTAAGTAACAACG	35
4[50]	13[53]	ACTCCAAAAGCTGGCGCCTGCAGGCAAAAGCAAC	35
38[114]	48[108]	TCTCCACCACACCACCCGCTCCCTTTTCATAAT	35
26[24]	30[32]	CGTCCGTAATGCATTATATAATAAAACGAACTTAC	35
22[80]	10[88]	TCAAGCCCTGAACTGCCCACTCACATTAATTGTA	35
27[54]	46[51]	CGAAATGTTTAAATCAAAGTACGGCTGAATCCAG	35
9[115]	0[116]	ATCGGCCTCAGACTGAGTGAAGGGGCTGGCGAAA	35
19[24]	7[16]	ATAACGGATATTCATTACTGTATCACGCGAAACCT	35
17[66]	20[81]	TTAGCCGGAACCAGGCGCGCTTGAGATGGTCCAGA	35
45[103]	42[100]	AGAATAGCCGCTCTTGCCAGTTCGAATTCGTC	35
25[10]	34[2]	ATTTGGAAGCCCGAAA	16
20[137]	19[137]	GCGGTCCACGCTTGGTGGTTCCGA	24
13[96]	22[107]	AACACCATCAGTACCAGGCGGATAAGTGCCTGCGT	35
4[141]	3[141]	GTTCCGAAATCTGGTGCC	18
25[47]	29[53]	GCATTAATGGTGTAGATGCGATCAACATTATTAC	35
51[10]	56[2]	CTGGATAGGGTTGAGT	16
59[2]	57[23]	TTATTCATTAAGGTGAATTATCACCGGAGGGAAGA	36
56[64]	52[58]	GGTGGGAACAATTTTTGTAAATGTAAACTTTGA	35
43[38]	34[39]	AGCTATCGCACATACATTGAAGTTTAACGAGAAAA	35
41[108]	51[114]	ATGGTCATAGCACCGAGCGCCAAGCATTAAATGCTG	35
51[18]	36[17]	GAGCAGCTGAAAGCGCCAAGCTTGAGAGGTCGTAC	35
58[137]	57[137]	AATCAGTAGCGATGCGGGAGAAGC	24
4[43]	7[60]	CCACCCTCAGCAGCGAAGACTTTACTGGTGCCGGA	35
40[71]	50[65]	GTATATTTATGTGCTCTCTTCGTGGTTTGCFTA	35
2[141]	1[141]	GGAAACCAGTGCGGGCCT	18
27[96]	20[107]	CTGTAGCCAACCTGTCAAACCTGCCGCTTTGGAAT	35
40[43]	43[60]	CATAAATCGGTTGTACAATGCCTAACGACAGAGT	35
30[137]	19[121]	AAGCATAAAGTGTAAAGCCGAATCGGGGCGCCATGT	36
57[2]	48[18]	GTTGTTCCAGTTTGAACAAGGTAAACCAGTCGTTG	36
54[71]	54[79]	TAAAACGGCGGATTGACCGTAAAATTTTGTAAAA	35
35[52]	25[58]	ACCGTTCCAGTAAGCGTCTTTTACCCTGACTACTT	35
19[31]	38[32]	TTGCACTGGCTGGATAGGTCCAATATTCAGAACAT	35

1[38]	11[44]	GCAAGCTATTTACCAGTTTAATGAGAAGCATAAA	35
57[73]	56[88]	CTATCAAAAGCTAAATCGTAA	21
36[50]	40[44]	AAGCAAACCTTAATTGTGTCTGTCGCAAAAGTAG	35
56[87]	57[72]	TGGGATAGGTCACGTTGTCGT	21
25[59]	21[65]	CCTGTATTTAATGTCAATCATATGTAGCTGATAAG	35
13[122]	11[137]	TATCCAGAACC GCAAGCCAATAGGAACCC	30
49[75]	58[86]	CATATGGTTACCAGTAGCACCATTACCATTAAACCG	35
12[47]	17[46]	GCTGCAGAGACGGTCCCTTATGGACTCATCTTTGAATCC	39
57[61]	47[67]	GCGCCAAAGCCAACGCGTAAAGCCTGTTTCCTGTG	35
21[2]	25[9]	GGATAAAAAATTTCCGTGGGCTC	22
22[137]	21[137]	CCGGAATAGGTGGAGTTGCAGCAA	24
44[24]	40[18]	TTTCTGATATTTCAAAAGGGTGAGATAAGCAAAGG	35
46[137]	45[137]	AACCGCCACCTCCCGTTGATAA	24
53[89]	55[95]	TTGATAATCCGTTAATTGCAA	21
21[61]	11[67]	TAAAATTAAGTATTGAAACCTGGGGTGCCTAAT	35
13[54]	25[46]	AGTGCCGGAAGTAGCAATTGTAAACGTTAAAATTC	35
25[96]	25[88]	GGTGGTTTTGGTTTTGCTCAGCCCCAAAAAATTGG	35
45[31]	59[37]	CAGGAGTGAGATGTCGTGGATTGAGGTCACCGACT	35
56[38]	37[37]	TTATCGGTCCATTTACCCTGCGCATGTAAACTT	35
48[107]	53[108]	CAAAGACTGTATAGGGTTCATTGCCCGGAGACCCC	35
29[38]	14[39]	GGAATTTAAGACCTGACGCTGTAATAAGAACGTAA	35
10[87]	6[81]	GCATCATACGAGGGCGATATTCAGGCCCTGAGAGA	35
59[94]	56[109]	AAGGCCGAAACGTCACCCCTTAGATTATGATTT	35
15[103]	0[100]	TATGGTTTTGGCATAAAAAACTACGTTTTTGTGCAA	35
55[2]	51[17]	TCCTGTAGCCAGCTTTCATGCCCGAGCCCT	30
53[17]	38[18]	AGAGTCTACAAATCAATACGGCACCTAGATTTGTT	35
30[57]	15[60]	ATGTAGAAATTGTGAAGAGTAGTTGTACCAAAGG	35
42[99]	53[88]	ACGCAAGGACGTTGTATATTTTTGAGAGCACCCGG	35
16[78]	2[72]	AAATTCGCCCCGTGCGTTATCAGATTTTCTGTATG	35
41[5]	42[2]	TAGCAAAATAAGGCCGGAGAC	21
50[141]	49[141]	TGAACGGTATCGGTCATA	18
6[115]	21[114]	CAGCGTCAAAGTCCACTATTGGTGTCCAGCACCC	35
50[64]	54[72]	TTGAAAATCCTGCCAGTAGCATGTCAATCACGCAT	35
21[17]	11[23]	GAACAAGGCTACGCCAGGGGGGAGATTCCACACAA	35

6[45]	3[30]	ATGAGGAAGTTGATCGTCATCGCCACGCATAGAA	35
48[24]	53[23]	TTAAGGAAACCCGGGCAAAGAGTTGTGAGAGATCT	35
6[137]	4[117]	TTTTACCAGTGAGACGGGGGCGAAAAATCCCTTA	35
54[137]	55[120]	GGCCGGAGACAGTCGTATAAGCAAATAGGTAAAGA	35
21[66]	17[58]	ATTCAATCGGTAAATTGGATAGGCTGGCTGACTCC	35
49[122]	47[137]	CATCTTGCCATTAGAGCCGCCACCCTCAG	30
27[130]	29[141]	TCACGTATTGCCAACGCGCGGGGAGA	26
51[115]	49[121]	AGAGTAAAAATCCCTGTAATACTTTTCAGAATCTTT	35
56[108]	52[102]	TAGAAATGTGTATTTAAATTGTAAGAAAAGGGG	35
36[16]	32[24]	CTTCGCGTTTTAATTCGCAAAAAGTAAACAGCTGC	35
35[75]	46[72]	TGAGAATGGAAGCGCTGTAGCTCAACAGTGTGG	35
47[89]	42[86]	ATTGCAAGGGCCAGCTCTGGCGAGTCACGATAAAA	35
44[137]	43[137]	TCAGAAAAGCCCCCTGCAGGTCGA	24
4[116]	2[110]	TAAATGTTCCAGTTTGGGGGCCATTGCCATTCAG	35
17[59]	20[51]	ATGTAACCGTCTATCATCCAACGTCAAAC	30
50[43]	54[51]	CTCGCTGGTGCCGGAGGATGAACGGTAATCCAGCT	35
11[115]	13[121]	GATAGCCACCCTCAGAACACGCCAATGAGTGAGC	35
52[141]	51[141]	TATTCAACCGAGAATCGA	18
16[99]	5[102]	GAACGTGGACTCCAAGTATTGCCCTTCACCCACG	35
20[106]	25[95]	GGGAAATTAAGCAATAGACAGTCGTGCCAGGCCAG	35
5[68]	3[74]	GAACGAGGGTAGCAAGAACAGCTTGATACCTATCG	35
0[31]	4[25]	CTTGCATGCCTAGCTCGAAGAAAGGTCACGTTACC	35
19[122]	14[109]	TTGAGGTTTGAGATGGGGGACGACGACAGCTGGG	35
12[141]	15[129]	TTAGTACCGCCACCCTACCGTACTTTGAGGCGCA	34
3[38]	11[30]	AAAAAGCGGAGTGAGAATATTCGTACATGGTCCGA	35
37[38]	33[44]	AGAGCCAACAGAAGCGAACCAGACCCAGAAGCATG	35
38[31]	48[25]	TCCACGGATGGCGACGGCGAGCTCGCTAACTACA	35
24[71]	35[74]	ATAAGCAAATAGGGGAGAGGGCGGCAGCTGAATACA	35
20[80]	10[74]	GCATATACAGGAATCTCTGCACACAATCCACAGACA	35
54[78]	39[81]	TTTATGTAAGTAACTTTCCCAAAGGGGGCATT	35
22[45]	18[39]	GGTATGCCTGATATGACCAGAAAACAAAGAGTAATC	35
43[61]	40[58]	TGGGTAACGTATATTTAAATGCCAAAAACATTCT	35
28[80]	38[74]	TAATTTCAACTATCTGCCCTTGCCAGCCTTCACTGT	35
40[38]	21[37]	ACATACGACGAGATAGCGTCACGTTGTGAGCGAAT	35

29[5]	30[2]	GAAGAAAAACGAGGCATAGT	21
22[106]	12[86]	TGCGCTCATGCGGTCCCGCCACCCTCAGTTGCGC	35
18[137]	28[116]	AATCGGCAAAATCCCTTATAAATCCCAAAATCCGGA	36
35[2]	36[5]	GACTTCAAATATTAATTGCTC	21
33[2]	37[9]	GAATCCCCCTCACCAATTTTT	22
25[122]	23[137]	GAAAGAGAAGGGGTTGATATAAGTATAGC	30
27[115]	25[121]	ACGTCCATCAACGTAAATTTTTGTTAAACAGTTCT	35
20[50]	35[51]	ATGTAATGTCATCAACGTCTGGCTTATAGTGGT	33
20[85]	16[79]	TCGTGGGAAAACGGTGTACAGACGAGGCGCGGCGA	35
37[24]	41[30]	TTTGTATAACAAGTTTGAATCATACTAAAGCCTCA	35
40[17]	21[16]	CAAGATCATAAATCGTCAGATTGACGGATTCTTTA	35
23[17]	19[23]	AAACAAGAGAAATCTACACCTCATAACGGGAGATGA	35
26[141]	25[141]	CGGGCAACAGTATTAAGA	18
5[103]	5[95]	CTATAGCCCGAGTGAATTTCTTATTGCAGCAAGCG	35
53[109]	44[122]	AAAAACAGGAAGATTAAGTATAATTGCATGCAAA	35
17[122]	9[114]	AGCCACAAGAGGGCGAAACCAACAAGAGTCCAGCT	35
58[85]	47[88]	TCTATCACACTATTAATACGAGCTATCCGCTCACA	35
48[101]	51[86]	CACCGGAACCACACAACAAGAACGTGTTTGGACGA	35
11[94]	8[109]	GCCACCACCCTCATTTCCAGTACGTGTAATACTA	35
17[5]	18[2]	ACGGAGATTCCAAATCAACGT	21
53[24]	56[39]	GGAGCAAACAAGGAACGCAAATGTGAGCGAGTCCC	35
42[85]	31[88]	ATTTTTAGAATACTTTTCGAGCTGAGCAGGAAGATC	35
15[61]	7[67]	GCCGAAATCGGTGACTCTAGTCTCGCTATCCAGG	35
33[101]	36[88]	CAAGTATTTCTTTTACCAGGAGTGAATAAATCC	35
15[24]	19[30]	GTCCTACCAAGTCGCTGATAAATCAAGAACGGC	35
2[71]	0[65]	GGATCCTCATAGTTAGAACGCCAGGGTTTTCCAG	35
10[137]	9[137]	ATGTACCGTAACGAAGATCGCACT	24
40[57]	21[60]	ACGCGAGAGAATAGTACATCGTACAGCTTTGTAGG	35
1[54]	12[48]	CCTACCAGAAAGCCTTCGTGCCA	24
6[80]	17[65]	CGGCTACAGAGAAGCGCCAACCGTCTATCAAATAC	35
0[64]	5[67]	TCAATTGTTATTTTGCTTAATTGGATAGTTCATCG	35
24[141]	27[129]	GGCTGAGACTCCTCAACATGAAAGCTGATTCTTT	34
15[130]	17[141]	TCGGTTTGGACGAGATAGGGTTGAGT	26
17[47]	27[53]	GCGACCTGCCTTCATCCAGAAGTACCTTATGGG	35

32[23]	28[17]	GGACCCTCGTCGCCAAAAGGAATTTCTACGTCCAG	35
23[2]	24[5]	CTGAGAGTCTGGTGTTAAATC	21
47[94]	46[109]	AGAGCCACCACCGAACCTCA	21
3[75]	24[72]	GTGGCCTCTACAATTCTTTGATGCCGCTGCCGTTCTACCCCGGATTGT	49
14[38]	0[32]	ATCATGCCAAGTCGTAATATCATGGCAGTGCCAAG	35
11[24]	6[25]	CATAATAGCTGAAAACGACGATTAACGAAAGAAAC	35
39[10]	44[2]	CGAGGCTTCTGGTGCC	16
6[24]	8[2]	GGGTAAAATACAGTTAAATATTCGGTCGCTGAGAATAATAACGCCAGGGTT	51
55[45]	43[37]	AACCTTTTTTAACCAATAGAGAATCAGGGTAGTCT	35
35[103]	31[109]	GTAATAAGTCCTGCCCGGTCCAAAATAATTCCGG	35
19[2]	27[9]	AACAAAGCTGCTGGACGTTAAC	22
25[31]	37[23]	CCATATTGCATAGCTTCAGTCAGGATTAGAGAATT	35
31[110]	19[102]	CACCTAATGAGTGAGCTGTCGTGCGAGTAACGGAT	35
36[87]	44[95]	TCATTCGGCAAATCCTGTGGCGCAACTGTTGGACG	35
53[5]	54[2]	GGTCATTGCCGCTCTGGCCT	21
30[31]	45[30]	ATAATTACCAGCCAATAACCATTAGTCCAGCCATT	35
34[137]	33[137]	CAGTGCCCGTATAAATCAGCTCAT	24
12[85]	17[88]	TCGAGAGTTAGGCGAACAAAGGCAGTCAAAGAGACG	35
43[2]	51[9]	AGTCAAATCACCAGGCTATCGC	22
36[141]	39[129]	GGAGGTTGAGGCAGGTGCCGCAATTTTGTAAT	34
22[31]	26[25]	AGAGTCGATGATTAATAATTCGCATTAATAGGAACC	35
7[2]	15[9]	CGAAGGCACCAACAAAGTATCC	22
2[109]	6[116]	GCTTCGAGTGTTCAAAAAGAGGTTTGCCCCAGCACAA	36
46[50]	50[44]	TCGTCATAGCTGGGGTGCCTAATCATTATTTTTT	35
14[108]	17[121]	GTGCGGTCACGTTAAAGACCGAACTGAAAAAGAAT	35
33[45]	29[37]	ACCATAGACTGTAAAACTCAACTAATGCAGAAAC	35
44[50]	59[53]	CTGGAAGGGAGGGTGGGAATCGGACAAAAGGGAAT	35
56[137]	55[137]	CTTTATTTCAACAAGGGTGAGAAA	24
11[68]	0[51]	GAGCAGGATCCCCGGGTGTGTGAACGACGTTGTAA	35
25[89]	29[95]	GCCTGCATTGGGGACGTCGGATTCCAGTCGGGAAA	35
38[141]	37[141]	AACGTTAATGCATTGACA	18
49[115]	59[137]	GCGTAAGTTTGAATGAAACCATCGATAGCAGCACCGT	37
38[73]	41[72]	GTTTTAAATATTTTAGCTGGCATCAATTATGACCC	35
39[82]	24[79]	GGTTGATGGCGCCTGGCGGGCAATTTGCGTCAGGA	35

57[24]	53[16]	GTCCAAGAATACAACATTCATCAAAAATAATTCTG	35
55[121]	49[114]	TTCAAGCAAGGATCTGGAGAAGTAGCATGTCAGAGC	36
26[115]	36[109]	GCAGCTATTATTAATGCCTTTAACGTTGGCCTTGA	35
51[80]	36[81]	TGGGACAAGAGCTATTACCGATTAATCCGAAATAA	35
7[68]	4[51]	CAGCTTTGAGGACTAAAAGACAGGCGCCGACAATG	35
24[115]	27[114]	AGGATTAGCGGTCCGAACTCGGGAAGCTTTCATCA	35
48[17]	44[25]	CGTTGATCCCCGGGTACCCAGTGCCATTCGCCAGC	35
5[96]	15[102]	GTCGCCTGGCTGCGCACTCCAACAAGAATTAGCAA	35
0[141]	3[129]	CTTCGCTATTACGCCACGATCGGGCAAAGCCACC	34
37[123]	35[137]	GCCCAGACGAGGGTCAGTGCCTTGAGTAA	29
44[121]	37[122]	AACAGGAAGGCGAATCATATGTACCAGAGCCCAGA	35
11[45]	6[46]	GTGTCTCGAATCTTGCATAAAGGGGCTAAAACCTC	35
54[50]	50[58]	CACGTCGGATTCTCCGTGGTTCCAGCAGGCGGGCG	35
49[10]	58[2]	CTTTTATTGACGGAAA	16
34[38]	22[46]	GCGGCAAAAATTATTTTGACGTAATCGTAAAGAG	35
14[66]	27[65]	GTTTCAATCCAATAAATCAAAGCTAAAAAGGGCGCAACGCGCACC	49
45[2]	49[9]	GGAAACCAGGCATTGCCCTCCG	22
41[31]	56[32]	GAGCTAAAGATCAACCGTCTATTTTCAGCAAGAAA	35
7[61]	1[53]	AATACGCCAGGAGCCTTAAACAACCTTCAATGTTT	35
31[115]	26[116]	CTTCTGGTGAAGGAACGGGTTTTTGCCTTCACC	35
4[24]	16[32]	GATAGGCCGCTTTTGCAGTCCATTAGGCAAAAGCG	35
32[87]	22[81]	TATCGGCCTTTAGTTTGAATGAATTGAGAAATAT	35
28[115]	31[114]	TTAAATGTGAGCCAGCTGCATTAATTGGGGTGCCG	35
16[141]	15[141]	GTTGTTCATAACCGTGC	18
37[10]	46[2]	GATACATGCCTGCAGG	16
40[141]	39[141]	CCGCTCACATAAATTGTA	18
39[130]	41[141]	ATTATCCACTGTGTGAAATTGTTAT	26
2[15]	10[2]	CTAAAGGAAATCCCCGTGTGAAATTGTT	28
51[130]	53[141]	CAAGTTCTAGATCACCATCAATATGA	26
48[141]	51[129]	GCCCCCTTATTAGCGTGGCATTATCGTAACAAA	34
38[17]	23[16]	GATTAATGCTTATTAAGATTTAACCAAATTTTAGC	35
42[137]	40[117]	CTCTAGAGGATCCCCGGTGTTCACCCGGAAA	35
59[38]	55[44]	TGAGCCATTTGGGCGACATGGACTCGCAAATAAC	35
9[18]	0[5]	TGTTTTCTGGGTACCGGCAGGTGACTCTAGA	33



28[16]	9[17]	TCACATTGAGAGCCTTTTGGAACAGATAGGGACGT	35
40[116]	38[115]	CCAGGGCGATTGTATAAGCTAAAATTGCGA	30
21[115]	24[116]	TGGCCCTGAGATAACTCACATTAATGTCGAGAATT	35
17[89]	27[95]	GTCAATCATACAGATGCAAACGGCAACCCGACTTC	35
47[68]	33[60]	TGAACGCCATGCGGGCGCAAGGCGATTATATAACCTGGCAACTAAAAAT	49
29[54]	44[51]	AGACCACATCAAATATAATAGTTGGTCAATCGGC	35
0[99]	3[88]	GGCGATTAAGTTGGGTCGTAACGTAAATGACTTGC	35
18[38]	3[37]	TTGAGTGTGCAACCCCGAGAATACAGATGTGCTCC	35
8[108]	11[93]	TTAAAGAAGTGTAGGGTTTTTCCAGACGTTAGATCTAAAAACGCCTGCA	49
33[61]	30[58]	CAGGTCTGCAGGGGGTGCTTTTGTGAGATTTAGGA	35
28[141]	27[141]	GGCGGTTTGCCAGTGAGA	18
41[89]	32[100]	GAGAAGCCTTTATTTACCATTGCGCAGCTTTCGCG	35
0[50]	4[44]	AACGACGGCTCATAGCCAGTTTCAAAGGCAACAA	35
32[99]	35[102]	TCTGGCCGAAGAGTTGGGCGAAAAATCCCTTATAACCCACAACTACTG	49
11[31]	15[23]	GCCGATCGGCCAACGCGCGTGGTTAGCCCGAAGA	35
32[137]	31[137]	TTTTTAACCAATCATACGAGCCGG	24
44[94]	48[102]	CCAGGGCGAAATGTTCCAGGACTCCAACGTTCAAT	35
56[31]	48[39]	TCAAACATTTAAAGAACGTTCAACCCAGCTGGAG	35
55[96]	45[102]	TGCCTGAGTACCCTCATATCAGGTGAGTGTGGAAA	35
13[10]	22[2]	TGGGTCAGGTCATTGC	16
31[89]	40[72]	GCCATTAATTGCGTTGCGCTCGTCAAAGAAAAAG	35
5[5]	6[2]	CTTGCAAGGGTAATGCCACTA	21
9[2]	13[9]	TTCCCAGTCACGTTGAGTGTAT	22
7[17]	2[16]	AAAAGTTGGGTAATTTTAAACAA	23
46[71]	49[74]	GTAAATTGTCGGAAGCATAAAGTGCGGGGAGAGGC	35
11[2]	12[5]	ATCCGCTCACAAGGCGGTTTG	21
0[115]	11[114]	GGGGGATGTGCCGGCGCAACTGTTGTCGTCAAGG	35
36[80]	32[88]	AGCCGCTTTTGATGATACAGTGAGACCCTGAGCAG	35
59[54]	56[65]	TAGAGCCAGCAAATCTACCAGCGAAAACTTGAT	35
29[96]	41[88]	CCTAACTCAACTCCAGCCATTGAGGCTGCGTGC	35
36[108]	41[107]	TATTACCAGAAGGTTTGCATCGGTCAAAGCGATC	35
24[78]	20[86]	AGTTGATAATCAGAAAAATATGAGGCCGGAAAGCC	35
3[130]	5[141]	GCTTCGGCAAATCCTGTTTGTGAGTGTG	26
48[38]	44[46]	TGAGAATTCGTAATCATGACGACGACTGTTGCAG	35

8[137]	7[137]	CCAGCCAGCTTTAACCGTCTATCA	24
44[45]	40[39]	GAAGGATAAATGAGTAATGTGTAGGATAAAGCTTA	35
3[31]	22[32]	AATCTGCAAGGCGGCCAGAAAGAATTTCTTTTTTG	35
47[2]	48[5]	TCGACTCTAGAGGCGCTCACT	21
27[66]	28[81]	GTGCTTAATCAGATTCATCAACTGCCCGCTTTCTT	35
52[57]	57[60]	GGGGACGATTTGCCCGAAATCGCAACGTCAAAGG	35
27[10]	32[2]	GGCGTAAATATTCATT	16
52[101]	33[100]	TAGCAAACGACCGCTATTGAAGGGCCCCAGCACAG	35
31[2]	39[9]	AAGAGCAACACTGCAAAGAGAA	22
46[108]	47[93]	GAGCCGATCGGGATGTGCTCC	21
14[141]	13[141]	ATCTGCCAGTCAGGAGGT	18
3[89]	13[95]	TTTCGAGGATTGGGAAGCCGGAACCCAGCGCAGC	35
50[57]	36[51]	CCCGATCGGGGGTTTTATAATGCAGTCTCTGAATT	35
10[73]	14[67]	GCCCGTGAGCTGCTTCCAGTCGGGCCCTTCAGTG	35
41[73]	51[79]	TGTAACCCTCACCAGGGTCGTGCATCTGGTGTAGA	35
51[87]	59[93]	TCTACAAAGGCTATATTTGTTGTACCAAAAACCGCAAAGGGCGAAAAGC	49
19[103]	16[100]	TGACCGTCGAACTTTGAAAGAGGAAGGGAAACGTG	35
15[10]	20[2]	AGTTATTTCAACGCAA	16

**Table 3S-2 Details about Square nut (SN) staple sequences**

Start	End	Sequence: left to right (5'-3')	Length
39[130]	36[115]	CCAGTGCCAAGCTTGCAACAATTCTAAAGTGTA	35
32[102]	35[87]	GCAAGCGGTCCACATTTTCTTAGGTTAGTACCAGGT	37
31[85]	28[72]	GGCGAACCAAGTCGGGAAACCCGCGCGGTACATGTCAATC	39
17[101]	23[109]	TGGGCTTGAGTCAACAGTGTATGGGTGACCCCTGACC	37
0[43]	10[44]	ATCAGATATACCGCACGCTATCTCGCTA	28
14[108]	19[108]	CAAAAACAACCTTGTCGAAGATT	22
23[25]	20[11]	TTACGGAAGCAAACCTCTATTATATCTTTACCCT	34
36[114]	43[122]	GAATGATATTACCAGAACC GCCACCCTCAGATGCCGTCCTGA	42
44[53]	51[51]	GTAATTTAGCAATCTTTTCAG	22
21[61]	24[52]	AGAACAGTTCAGAAAAATAGCGTGATG	27
58[129]	45[130]	CGGCTAATTACATTTAACTTCGCTATTACGCCACCAG	37
3[76]	0[70]	TCTTTCAACCAGACGACGACAAGCATTTTATCATAA	36
14[121]	10[115]	AAAAAAAAGGTCAGCTTGTA	21
43[123]	51[116]	TGATTTAACGGGGTCAGAAAACGAGAAAGGGTCGGT	36
48[123]	13[122]	ACTCTTGCTTCTTTCCCTTATCA	23
9[53]	5[52]	ATTATACCAGGCAGCCTTTACAGAATGTAGAACCAAGTAGAA	42
17[39]	8[32]	AAAATCAGAGAGTCAGAACATAAAAAAC	27
34[44]	38[52]	TGGACGTGGATGGAACATGTGCTGCAAGGCGCACG	35
44[66]	35[65]	CGATCCATCTTCGCCACCGGC	21
35[79]	32[86]	TCAGGCCACCCAGAGCCACCACCCTCGCTG	31
40[31]	43[38]	CCGCAAGCCTGGGGTGCCAGTCGGGTCGG	29
55[25]	49[30]	GGTAGAAACGTTTATTTTGT	20
30[42]	23[36]	AACCAATATGTTAAACCCAAAAC	24
10[106]	8[94]	GGTTAATTATTGTATAAATAAGAAAC	27
18[137]	19[137]	GATTTGTATCATAAGTACAACGGA	24
46[16]	49[17]	TCATAGAGCCGCCATTTGAAT	21
51[25]	42[25]	CAACTGATTGGGGGAGATCG	20
45[110]	38[104]	CGTTGATATCTCAGAACCACCACCAGTCACAGGTCGAC	38
10[59]	13[59]	AGAACTGGCAGTACCGAACCGAGGAATGAGCTAACT	36
35[11]	44[11]	TTCAACATACGAGCCGGAAGCATAAGCTGCAAGCGGTAGCGTCAGAC	48
1[32]	17[23]	GCCATACAAATCTTACC GCGCCCAAGCCGAGAAACACCACAAGTAC	48
32[85]	16[81]	GTTTGCCCAAATTAAGGATACATACGAGTATTG	33

55[61]	5[60]	TATCCTGTTGGTTTTCTTTCAACTTGCGTTGCGCTTTATC	42
17[24]	23[24]	CCAAATCAAGAAAAGTACAATGCTGACCT	29
46[39]	49[39]	GACGGTAGCACCTTATCACATCAA	24
52[115]	59[129]	GAATCAAGAAAACAAAATGGATTGAGTGGGAACAAA	36
27[17]	16[18]	TACTAAGGTGGTGCAACTGTA	21
48[80]	13[81]	GAAGAGGGCGACATAAAGTTTAG	23
31[25]	24[18]	TTTCATCAAAAATAATTAATTTGTTAAGCAAAGAGAGTTAG	41
16[80]	9[74]	AAAGCATAAGGGGAACAACATTATTGTTGG	30
41[63]	34[60]	TTAATAGAGCTGGCGAAAGAGGTCAAAGCTT	31
34[137]	35[137]	ATTAAGCCAGAAAATAAATCCTC	24
20[96]	22[94]	GGGTAGCTATTTTAGGTAAGATTCAACCCT	31
56[45]	49[51]	TCCGGTTTGAATAAAGGGAAAATTCAT	28
9[75]	4[78]	GATACCTTAAAGTAAGCAGATGCATCTTA	29
36[26]	39[33]	GATCGGCGCCAGCTGGCGAACAGTGTACCGA	33
27[25]	36[27]	GTAGATTGTAACGTTAATATTTGGAACGCCATCAACACAAGGGC	46
57[79]	54[87]	TTCTGGCATCGTTCAACATTAAATGTCATA	30
50[137]	49[137]	TATTAATTAATTGTAATCGTCGC	24
45[98]	48[103]	GATTAGGCTGCAAGAGTCACGAA	23
43[11]	46[17]	TGTTTAATGAATCGGCCAACGCGCCCCT	28
51[52]	55[60]	CAGGCGAAAATTCCTTATTACAAACGTCTATTCCAC	37
16[17]	14[11]	ATCTAACGCCAAATGCAGATA	21
25[68]	19[58]	ATAACAAGAGAATCCGCCA	19
59[67]	48[66]	CCAGAAAAACATCGCGCTTGA	21
2[100]	0[87]	AGGTAAAGTAGAGAATATAAATAAGAAT	28
35[66]	37[78]	GAAAGGGTTGATGGGTAACGCGTAATC	27
54[86]	47[87]	CGACATTTTATTGAGGGGCCA	21
30[94]	41[93]	CTTTAATCCTGTTATAAAGGCAGGTGCCGCCATCA	35
9[11]	50[11]	GAATTAAGCCCAATAATATGATTAAGACTCCACC	34
10[43]	25[44]	ATGCTGCTCCGCATAGTCA	19
51[46]	42[45]	CCCCACCAGTTGGGCGCGCTT	21
17[88]	23[88]	ACGACCAACTGATTTAGATTGCCTTCGGT	29
55[11]	54[11]	ATACAT	6
41[94]	44[98]	GAGCCGCCACCAAGTATAAGTAAGCAGTAACA	32
3[117]	7[122]	ACGGTAGCATTGAAATGCAAATCCCAGTTGGGTT	34

13[60]	11[59]	CACATTAAGCTTACCAGAAGGAAAGCCC	28
51[15]	55[17]	AGAGTTTTGTTCCGAGAAACCCTTTTAGCCC	31
59[106]	52[116]	CGTCGGTCCGCTCATGGTACCGAGCTCTTT	30
24[51]	28[44]	GCTATATAACGTTTAGCTATATTTCAATAAAGAAAA	36
34[24]	40[32]	AGCGGCAACTGTTGGGTATAT	21
41[88]	39[77]	CCCGCATTGATGGGTAACGGGTACCGAGCTCGAATTCCTCAAGGCGA	46
21[30]	34[33]	AAAGCACCAGACATTGCTCACAGGAAGTAGCATATGGGCGTATCGGCAA	49
34[32]	46[40]	CCAGGGGCATTTAAACCTGGGCGGTTTGCATGA	35
19[11]	26[11]	TTACATGTTTTAAATACAT	20
39[78]	42[77]	TTAAGTCACGCTATTACGCCCCACCACCGGAACCTAATCAC	41
23[110]	20[97]	CTAAAAATTTTTAGAAAAGGGTGGCCGGAGA	31
55[18]	7[23]	GAGAATCAAACAACGCGCGG	20
21[11]	28[11]	GACAACAGGTCAGGATTATA	20
16[50]	10[60]	GGATTCAAGTGAATAAGTTA	19
54[122]	55[108]	TGAAAAAATCAACCTCCGGCTTATGAGAGAGTATAG	36
52[66]	49[60]	AAAACCTGTTTCTATTATTCTGATTGGCCGGAAAATTATTTTAC	44
8[31]	6[31]	AGGGATCCCATGAACAAGAATAGCAGAAA	29
47[46]	34[45]	CCACAGTAGCTAGCCCCCTTC	21
2[54]	0[44]	GCTAATCAACATGCTGTTTAGTATC	25
33[65]	30[53]	ACCGCGATTGACGGATTCTCCAGCTGCATAAATCAG	36
13[123]	5[129]	AGATGCTGATACGCAGCGAAA	21
57[38]	51[45]	GCCTCAGGAAGAAAGAATTTTG	22
36[107]	39[114]	GCAATTGTTATCCGCTCTGCCTGCGAC	27
19[73]	26[69]	TCATTGGAGCATCTGCGATTGCAAAA	26
5[53]	56[46]	GGCCACTGCCCCAGGGTTGATGGTGGT	27
48[65]	48[81]	CGGAACGTCACCAATCCCCTGCACAGG	27
58[30]	51[24]	GTCAAAGGGCATTAAAGTTGAGTGGCAG	28
0[86]	17[87]	AAATTTTCATCTTACAAAGTCTTTCTAATCATCAGA	35
37[11]	35[18]	TTCTGCAGGTCGACTCTAGAGGATTCCACACAGGCT	36
45[116]	48[124]	TTTGCTCAGTAGCTGGCCGGCCAGCG	26
22[44]	24[30]	TTCAAAGCGAGGATTGCGACCATAAATCAAATAGTAATGAAT	43
53[82]	58[73]	TTGCACGTCAAAGGGCGCTTTCAAACC	27
24[29]	27[24]	ATGGTGTCTGGGCGGAGCTGAAAATA	27
13[82]	7[72]	CGCTTTTTCAAATAGACCA	19

7[24]	11[17]	GGAGGTCGTGCGCAGTATCCAAAAGAACTGGCAAGA	36
24[114]	27[109]	CTTATTTTGCTTTTGTCTGCTTTTCACGCC	29
2[25]	9[24]	AATAGAAATAATAAGCGCAAACA	23
49[61]	54[46]	CATGCCTAATGAGTACACAAGAGCAGGTTAAC	33
11[65]	25[67]	AAGAATGCGATTGCTTGCCATGAACGTCCCA	31
38[51]	37[59]	ACGCATGGTCATGGGATGTGCTGAGGGTTTTCCAGTATTA	42
27[61]	16[60]	GGATAACCTAGTTGATGTG	19
25[124]	21[122]	GGCAAAAAGAATACACTGGAGAAGCCTTTATTTCAACGCAGT	41
49[40]	6[38]	TATGGCAACAACGTAGCAGT	20
18[37]	17[38]	AATAGCGAGATTACGAGGACCTTCATCAACGTAAC	35
54[137]	53[137]	TAGCTGTTTCCTTAATCATGGTCA	24
45[55]	44[54]	GGTAACATGAAAGTAAGTGC GTTGCCTCGCGTTTGAGCAGCACC	45
39[34]	34[40]	GCTCGAATAAATTGTTAAAGATG	24
31[40]	25[39]	ATGGTGTAGTAACATCTCATTTGGGAAG	28
4[77]	1[86]	TCATTCCAATATTTTAGTTAACACCGGACGAGCCAGTA	39
49[52]	57[52]	ATGGTCATTAATACCAAGTAAATCAATCG	29
38[44]	31[39]	AAAACGACGGAGGGGGAAGAGTCCATTAA	29
57[53]	59[66]	CACTCCAGCCCAGTTTGCCTTCTGTAG	28
15[11]	8[11]	CATTGACAAGAACCGGATATTCATAATTGAGTTAACTGTTAGACGGGA	48
11[18]	2[12]	GCATTTTTATACAAGAAATAAGTCCT	26
47[11]	51[14]	AATCCGCCTGGCCCTGAG	18
34[59]	45[54]	TTCCGGCACCCTTATTAAGTCCCCAGGGT	31
49[31]	57[37]	CACACGTCACCGATTGCGATAGGGAACGTGGACG	35
22[93]	30[95]	CATTACCAAAGAGAGCATAAAGCGGAGAGCGGTTTGCCG	41
47[88]	43[92]	GGGTATAAACCCGTAICT	19
20[64]	19[72]	TACCCGAAAGATGAGTAATGTGTGAATCCCCCTCAAATCG	40
16[72]	9[81]	CAGCTGACGAGAAACACTGTGAATAGAAA	29
53[38]	7[37]	ATTGGATGAATTGTTCCAAAATCGGTTG	28
48[137]	47[137]	ATGCTGCAGGTTGCCAAGCTTGC	24
56[88]	58[94]	CGCTGGAAAGACGCTGAGACACACAAGAGCGAGTGGT	37
42[24]	39[24]	TGCCAAGTGATCACAATCCCC	22
44[137]	43[137]	CTGGTAATAAGTTACAGGAGTGTA	24
26[101]	26[102]	ACGTTAGTATGACCATTACAATAAAGCCTCAGTTGCACACAG	42
42[44]	38[45]	TCCTAATGAGCTGTGTGTCGTAATTTGT	28

37[60]	27[60]	AGTGTGTTGTACCCGTCCGTAATGGGCAA	29
39[103]	34[102]	CCCAGAGCCCAGACGATTT	19
42[76]	46[72]	CGGAACCTTAAGAGGCTGAGATACTATTTTCGGA	33
5[61]	3[65]	CGAAAAAGCTAATTTAGGCAGAGTAAACAACAA	33
7[123]	4[124]	ATATAACTATATGTAAATTAGTTGCTATTTTGCACCCATTTTCATGA	47
46[71]	41[87]	ACGATGGTGGTCCATTCAGGCTGAGTTGGGCTCCTCAATAGGTGGCCT	48
22[113]	33[116]	ATGTAATACCCCTCACTAGCATTTCACCAGCAATA	35
4[123]	3[116]	ACGAGCATCGCCGCTGAGGCTTGACGGGAGTGAATAATGACAACA	45
35[53]	41[62]	AACCTGTTTCTGAGCTAACTACA	24
30[122]	23[123]	ACATTTTTCTTTGATTGCTTTTG	23
25[45]	22[45]	TTCTAGAGCTTAAGAGGGAGC	22
43[108]	36[108]	ATACCTCTGAATTGGCCTATCG	22
58[53]	58[54]	GGGACGACGACAGTATCTCGAAATTGCGTAGATTTTCAGGAG	42
9[25]	18[25]	CCCTTCAACTAAAGGAAGGC	20
25[40]	14[31]	TTGCTGGCTGCATAGTTTAGGAATACC	27
7[73]	49[72]	GTGACCAGCAGCGGAAAATTAAGACCTGGGGGCGCAAAGA	42
12[107]	10[107]	ATCCTGAATCTAGCTTTGAGGACTACGAT	29
34[101]	30[108]	ACCGAGGGATAGCAAGCCTACAAACGTGGTTCGTTG	36
3[66]	16[73]	TAATGAAAATATCAGGACACAGGTAAGTACTCAGACGGTCAATAGGA	43
3[12]	56[11]	GATTTTCATCGTAGGAAATTAATGAATCGGCAGA	33
54[45]	47[45]	GTCACCTTTGAAAGGTGAAATTA	22
30[107]	24[100]	CGCTCACTGCCGATTGCCCTGAGAACATTACAGGC	36
28[71]	34[74]	ATTTAGCAAAACGGCGCACCTCTCA	26
49[73]	57[78]	CAAAGTAAATAAGAGCGCGAAATCCGGCACCGC	34
12[92]	49[102]	AACGACTTGATAGCTTAGATTAGCATTCAACCAATCAATATA	42
34[73]	44[67]	GAACTTCATAATCAAATCAGTTAATGCGAAACCAT	35
5[130]	16[129]	GACAGCATCGGAGGAAGTTTCCATGGCACCAACCT	35
31[123]	25[123]	CCTAGTTTCGCCACAGATCTAAAGTAAGA	29
16[128]	14[122]	AAAACGAAAATTGCGAACTCC	21
33[117]	45[115]	GGGCGCAGTATGGCTTGAGAGGGGGGT	27
12[44]	4[39]	CAATAATAACAGCAATATCA	20
14[30]	12[31]	ACATGAACAAAGATAACATGAAATGGAA	28
24[17]	18[11]	CTCATGCCAGAGCAAAAAGAAG	21
38[103]	32[103]	TCTAGAGTGTGAAAAATCCCTTTGATGTA	29

5[109]	2[101]	GGTACGGCTACAGAGATTATCCACAAA	28
6[30]	55[24]	CCTAGCGGTCAAAATCCCTTATAATAG	28
56[137]	55[137]	ACTACCTTTTTATAGGTCTGAGAG	24
26[137]	27[137]	TTAGCGTAACGACAGCCCTCATAG	24
1[109]	5[108]	AAGGCCGCTTACCGTGTGATAAATTAAT	28
27[54]	33[64]	CAGGATAGGACTCCAGCCAGCCAGA	25
47[25]	34[25]	AAATGCCTTTTTTCATCCAA	20
34[39]	30[43]	CCGGACTCAGGAAGATCGCTCACGTTGTGAGCGTTTTT	39
8[137]	9[137]	TAAACAGCTTGAAGGTGAATTTCT	24
54[23]	47[24]	GTAATAACGGACTTGAAGCA	21
6[100]	1[108]	CAACTAAATTAAGGCGTTAAAGTACCTA	28
49[103]	6[101]	TGCATAGCGCGGGAGGAAGA	20
53[102]	7[102]	ATAACAATTCAGAGTCATGCAGCACTTCA	29
43[39]	46[31]	TCAGACAGAATCAAGTTTCACCAGGCAA	28
35[88]	39[102]	TGATCAAAGCATAGCTGTTTCTGGATCCCCGCCAGGGTTTT	43
53[11]	54[24]	CGGAGTTTGAACAAGAGTCCACTGAAAACTGCACGTAAAACAGAACA	49
23[89]	24[81]	TGATATTTTAAATGCAATGCCCTTCGTAATACTAGAAGAG	40
51[117]	54[123]	GCGGGCCTCAATTCAGAATTCGGTG	26
16[59]	9[52]	TACACATAACCGAAAGATTCATCAGTGTC	29
36[137]	37[137]	GAGCCGGAAGCACACACAACATAC	24
24[80]	20[65]	AGTCAAATATTACTTAGCCGGAACGAGGCGCGTGCGGAATGCTT	44
58[93]	59[105]	GTAGATGGGCGTGCCGGAACCATGATGAAAGTCACGTAAACAACC	46
48[102]	53[101]	ACAGTACATAGAATTACCTGAGC	23
21[52]	27[53]	TTAATTAATTCTCATTTTATAATCATCATA	30
48[108]	43[107]	CGGGACGTTGTTGCCTTGGTC	21
35[121]	33[128]	CAAACATGGAAAAACCCATGTA	22
49[11]	48[11]	ACGGGG	6
57[110]	45[109]	ATTACCTTTAGGGCGAGGATGTGATTAG	28
58[72]	52[67]	GTGCATCTGCAGCTTTCGGC	20
1[87]	8[88]	ATAAATTCTGTACAGCCATTT	21
13[117]	57[109]	AAAGAATCCATTTATCATTGTTAATTCTCCCCGTAATGGGATAGCAAAC	49
18[114]	17[115]	TTGAAAGGAACAACCTTAAATG	21
1[5]	0[5]	CTCAACAGTAAGCCAACG	18
46[30]	53[37]	CAGGCGGTCCACGCTGGAGCCCGACTG	27



37[79]	31[84]	ATGGTAATAGCCAACCAGCA	20
28[43]	23[59]	GCATTCGCATTAAATTTTTGTTCCGGTTGTGGA	34
7[103]	12[108]	CCGCCTGGCCAATCGCTTTTGAATTTT	27
30[52]	35[52]	CTCAAGTAACATCCAGTTCTCC	22
17[116]	8[122]	CCACTACGAATAAACGGGCTTTCGTACC	28
28[137]	29[137]	ACGGGCAACAGCTTACCAGTGAG	24
6[17]	2[26]	CTGCTCATTACCAGTATAAGGGCTTAATTGAGAC	34
0[69]	11[64]	TTACTAGGTATTCTAGAACGGTT	23
8[87]	12[93]	TTGTTCTACGTAAATATCAACTTCAGAGCCTTACC	37
35[19]	31[24]	GCCCATTCGGGGGACGACGACAGCATCGTACAGC	34
2[137]	3[137]	ATATATTCCGGTCCACGCATAACCG	24
39[25]	36[18]	GGGCAAGCTTGCATGCCGCTATTATGC	27
15[87]	18[96]	CCGACCATGTTCAATTTGAGAGATCTACAAAGCATCCGCGAC	41
11[60]	2[55]	TTTGATTA AAAACCAATCATGTTCA	25
1[47]	14[45]	GCGCAGAACTACGAGCGAGAATAGGGTAATTTGA	34
18[95]	15[86]	CTGCTACAGAATAGAAAGGAGGCCTTAACGAACTAACGAA	43
0[129]	1[129]	TCACCCTCACGTTGCGGGATCG	22
24[99]	17[100]	TATCAGGTCTTAATGAATTTTCTTTTTCAGCGGAGTGTGAGTAGTAAAT	47
43[93]	45[97]	AGGCCGCCCGGAAGAGAAG	19
23[60]	21[60]	TGAACGGTAATCAAATATCGCGTTGAGGA	29
7[82]	12[82]	GCAACAGCTGAGAAAAAACCTCCCGCTAACGA	32
12[30]	58[31]	TACGTTAGCAATATAAATGAGTGTATACAGTAAATAAACAAC	42
14[44]	21[51]	GATAAGAGCAATAAAAAAGACTGGCGAGAATATCAAAAAGA	41
4[38]	1[31]	TCGACCTAATTGCGCCTGTTTATCAAATC	29
51[95]	53[81]	ACTGTTGGGATTAAGAAGAGGCAAAGCGCCATTCGTCAATTA	43
23[124]	18[115]	CGAAAACACCGAAACACGCCTGATAAA	27
8[121]	14[109]	GATAGTTGCGCCGACCCCGTTTACTC	27
36[17]	27[16]	GGGCCTGTAGCACCGTGCTTC	21
27[110]	31[122]	TGCGCCTGGGGCGCCAGGGTGGTTAATTGCCGCCTGGGGTG	41
33[129]	30[123]	CCGTAACACTGAATGAGTGAGCTAACTC	28
30[73]	35[78]	CGTGCCGTGGGCGAGATAAACCGTCTA	27
6[37]	1[46]	CGGAGCAAATATGCGTTATATTTAACAAC	29
59[5]	58[5]	AAAATTATTCGTCTATCA	18
14[137]	15[137]	CACGTTGAAAATTAATAATTTTTT	24

9[82]	3[75]	AATTAACGTCAAAAATCGGCTG	22
55[75]	7[81]	GACTCCACGGTTTGCCGACGG	21
8[93]	56[89]	GATTATTATTTGCCAGTTCTGACAGAACGCGATTGCCAGCGGTCCA	47
20[137]	21[137]	ATGATATTCAACATCACCATCAAT	24
27[11]	34[11]	CAAACTGCCAGTTTGACCA	20
44[97]	51[94]	GTGCCCGTTTTCCCGCATTACGCA	25
26[68]	30[74]	TGGTCACAAAGAAATGTACCAATGAATCGGCCAATGT	37
29[11]	36[11]	TTTCGCGTCTGGCCTTCCTC	20
10[114]	13[116]	AATAAAGACTGCTACAAGCCTT	22
23[37]	18[38]	TTTGATAATTGCAATGTTTCAA	23
19[59]	16[51]	ATACTTTACCAGACGACGACACTATGACCA	30
55[109]	48[109]	TGATTGAAAATGAGTGAATAACCTAGAGGATCCC	34
45[131]	39[129]	GCGGATAAGGCCACCACCCTCAGACGG	27
49[18]	6[18]	AAGCAAAGACTTATTACCAG	20
7[38]	12[45]	CGTATTGGGCGCGCTTCAAATACAACG	29
12[81]	55[74]	AGCCGAACAAGGAGGCGTTGTAAAGACGTG	31
18[24]	21[29]	TTTTGGGGGTAAATCAGGGTCAGAAGC	27
19[109]	22[114]	ATAAATTAATAGAAAGGCCGGAGACAAGG	29
39[115]	35[120]	GTTGTAAAACGAGCCGCCA	20
21[123]	24[115]	CAACGTTCTAGCTGATACCAAGCGTCAT	28

**Table 3S-3 Details about 24-helix bundle (HB) staple sequences**

Start	End	Sequence: left to right (5'-3')	Length
21[123]	19[143]	CCTCACTGGATAGCGTCTAAACAGTTATAGTCAGA	35
7[47]	22[44]	GTTCCAGTTCTAGCATGTCAATATCAGGTCATTGCCTTCACTATTAAAG	49
7[110]	23[114]	ACCGTCTATGAGCTGCATTAATGTTTTCTTTTC	33
12[149]	10[143]	CGCATTGGGCAATTCTACTAATTGTTCCGATCGT	35
9[53]	3[45]	GTTGTGCCTATTCGCGTGCCGGAACAGCCGTAA	35
4[128]	1[115]	AGCAATAAAATGCAGCAAAGTAAAATTGTTAGCTG	35
1[32]	14[31]	CAGGCGAACAGCCAGCTCATTTCAGCTTCGTC	35
14[135]	4[129]	AGTACGGTGTGCGGATGCAAAAACGAATCGAATTA	35
20[49]	20[50]	AGTTTGAGGATCCCCAGTTTGGAAACAAGAGTCCAATGTTCC	42
23[32]	19[38]	ACATCCAACGATCCGCTGGGTACCTGCAGGTCGAC	35
11[52]	12[67]	TAAACCTTCCTTGAACAAGAGTCCACTATTAAGA	35
17[49]	14[56]	GCACCATGCCGGAGCAGCTCATCGCCATTGTTCCA	35
14[30]	4[24]	GGATTCTCCGTCACGTTTGGTGGTTAGCCCGACAA	35
19[81]	12[80]	GTCTGATATTCCATTTCGAGCCAGGTTTGAGGGTC	35
13[74]	3[66]	ACGATAGGGTTGAGTGTTGAGGCTGCACCGCAACC	35
9[95]	12[94]	GTCCACACAACGACAGTATCGGGGCGGATTGACCG	35
5[59]	11[51]	TCACGCCTGGGTGGAACAGATAGGGTTGAGTGCAT	35
8[73]	15[72]	GAATACTATTAGCATAAATCTGCCACTTCCGGCG	35
12[93]	2[87]	TAAAAAGGGCAAATCAAAAAGAATAAAGGGCGCGCA	35
11[21]	7[27]	CATTAAAGCAAATATGATTGCCGCCAGGTAATGAA	35
7[123]	4[136]	TGGAACAAGAGTCCACTCTTCAACCCAGCTGTAGC	35
3[123]	5[129]	AGAAGGAAGAGGCGATTAAGTTGTCAGGCGAAGCG	35
16[86]	20[80]	ATTTCTACAAATCAATAAAAGGGCAAATCAAAAAGA	35
20[79]	9[80]	ATAAACCTCCTTCGCTGCTCACTGCCGGAAGA	35
22[79]	21[94]	ACTGAGTTTGCCTATTGGGCGCCAACATTATTTAA	35
8[149]	4[157]	GCCAACGTGGACTCCAAGGCGAAATAACATCCATA	35
18[149]	4[143]	CCCAAAGCGGCCCTCAAATGCTTCAATACTAAAG	35
1[67]	23[73]	GCAGTGTAATAATTCGGTAATTGGAGCAAACA	35
16[30]	20[24]	ACCGTGCATCGGAAGATTTCCAGGCATGCCGAGC	35
16[112]	16[113]	ATTGTAAATTGCCTGAGAGTAGCTTCAAATTCAAATATTTAA	42
11[11]	14[7]	TTAGCCATCATCGCGTCAAACGGC	24
23[60]	9[52]	GTCCGTAATAATGGAACAGATAGGGTTGAGTGTCCA	35

19[144]	12[143]	AGCGAAAGACTAATCGTAATCAGATATTTTCAAAT	35
7[28]	3[31]	TCGGCCATGCGCTCGTGAGCTATTCACAGAT	32
23[6]	19[12]	AGAGGGTAACCGTCTTGTTTCCAATCATGCCAGTG	35
3[32]	16[31]	AGGCAGGGTTCGCACTCCAGCCAGGGCGCATCGTA	35
3[11]	15[17]	ATCGTTGTAAACAGTATCGGCCTCATGCCAGTGGAT	35
7[144]	1[136]	AAGCGAGATAGGGTTGAGATGGTGGCCCCAGTTAG	35
12[44]	1[31]	CCAAAAATAAATTATGTACCCCGTTGATTTCCAG	35
15[73]	19[65]	CAACAATTTTTGTTAAATAGGGTAGTCTAGCTAAG	35
14[55]	16[49]	GTTTGTGAGCGAGTCGGCAAAGCGCCATTTTTTA	35
2[156]	18[150]	CCCTATAATGAGTACCTTTAATTGCTCCAACGAAG	35
9[101]	11[102]	GGGCCGAAATCGGCAAAGAACAACGGCG	30
8[119]	8[120]	GTTTGATGCGTCTATCATGTATCCTGTTGTGTTGCCAGT	42
18[53]	18[54]	GCTTTAAGTTGGAGGAACAAGAGTCCACTATTAGATAAATTA	42
11[103]	7[109]	ACGTTGTAAGTGGTTCGAAAAACGTGGTTCGAAAA	35
8[35]	8[36]	GTATTGGGCAATCAGAAAAGCCCAAGTTTAGGCGTTTGC	42
12[107]	4[115]	TCAGGGATGTTCCGCTCCCTGTCGTGCCAGTAGAT	35
0[16]	11[10]	CCTCAACAGCTTTAAATTGTAACCTTTG	28
2[86]	22[80]	CTCCATTACGGGCCTATATATTGACCCTGTAAT	35
4[93]	16[101]	GTGGGCTGCGAATCACCAGGCTATCAGGTCACGTT	35
21[150]	23[156]	GAATGAGGGGGTAATAGTTGATAGCGAGAGGCTTT	35
19[39]	15[31]	TCTGTAACGCGTTGAGTATAATCCTGTTTGAGGTG	35
13[80]	5[86]	ACTCCAACGTCTGGGATAGGGACGACATACGAGCC	35
1[25]	23[31]	GCCCACCGCCTAATGAACTGCCCTTGAGAGATCT	35
4[142]	7[143]	AATGTTAGTAGTAGCATAACCGTCTATCACCATTA	35
12[79]	8[87]	ACGCGGATTCTCCGTGGTCCCTTATGGACTCTCCC	35
17[77]	13[79]	TGAGAGACGCATTATGTTGGGGCCCGAGTGG	31
15[32]	12[45]	TAGATGGGAAAACAACCTCATCAACATTAAGTAG	35
5[130]	22[129]	GTCGCCTGGCGGCAACAGCTGATAAAATGTTTAG	35
4[23]	6[17]	CATAATTGTTCAAAGGGCGAAAAGCTATTTGCTT	35
9[81]	13[73]	ACGTAAATCAAAGAATAACCCGTTTGGTGTAAGA	35
14[112]	14[113]	GGCAAAATCTTCGCTATTACGTATAAGTTCTGGAAGTTTCAC	42
12[142]	8[150]	GGTCTGCAGGTCGACTCCTCGAATAATCGGCAATA	35
16[142]	12[150]	TTTGCTTAATTATGCAACTGCGAACGAGTAGATTT	35
18[116]	18[117]	CTGAGGCCGGAGCACAAAAATCAGGTCCTTACCTTAATTTCG	42

11[115]	11[121]	GACGGGTTTTCCATTCCATATAACAGTTGATTCTGGGTAACGCCAGGCC	49
15[18]	1[24]	AGGTGGGAACTGGCCTTCTGTAGTAACCAAGTTT	35
8[86]	4[94]	TTATGGACTCCAACGTCCAACGCGTTCCAGTATCG	35
19[13]	2[18]	CCAAGCTTTCACGACAAAAGAATCC	25
20[23]	0[17]	TCGAATTCGTTGTGTGAACGAGCCGGGGTGTGGC	35
10[142]	14[136]	AATCATGGTCTGCATGCCAATAACCCCAATTCTAA	35
22[43]	7[46]	AACGTGGACAAGGCTAATTGCGTACGCGGGGAG	35
4[135]	16[143]	AAATGAACGGTTCAAATAGACCGGAAGCAAATCC	35
5[87]	8[74]	CGCTCGGGGAGAGGCGATAAGAACGTAATCAAAA	35
22[128]	7[122]	AGAGCATAAAGTGAGACCCTGAGACATT	28
7[5]	3[10]	GTCGTGCCAAGTCGGGAAAGCCTGGAAGCAATAA	34
17[130]	21[122]	ACCATCGCGTCTGACTATTAGAAAACGAGAGTAG	35
9[66]	5[72]	GTCAGCCCGAAGAGTCCACTATTACGATGAAGCG	35
23[102]	9[94]	GGTAATCGGCAAAGGGCCGAAATCGGCAAAACAAC	35
16[48]	17[48]	ACCAATACTTTCCG	14
23[157]	19[162]	TGCATTTGCCACGTCATATTGAATCATTGCATCA	34
6[16]	0[10]	TCCGCTGCATGTGGTTTTTCTTTAGACGGGGAGA	35
21[95]	3[101]	ATGCCCTTATGAAAAACCGTCTATACAGTCACAAC	35
20[101]	9[100]	AAATCAATGCCAAGGGCGGGAAAACAATTCAAA	35
1[116]	3[122]	CAATTGCCAGCTGGCGATGGTGAGAAGAGCAAACA	35
23[74]	19[80]	AGATTTGCGGTTTTTAGGCCGAGTGGACTCCAAC	35
3[67]	23[59]	AGGCAGCTGGATAAAAAGAGAAGCCTTTATTGAGA	35
19[66]	5[58]	AACGATAGGGTTGAGTGTGCGAAGGCGAAAGGAAC	35
10[160]	14[154]	TACCGAGTAGAGGATAGATACATTTAGTCAACATG	35
0[9]	16[7]	GAGAGCGGTCTCGGCAACGTAATGTTGAGGG	31
3[46]	1[66]	GGCGATCTGGTGCCGATTCTGGTCTCGTAACCGT	35
4[114]	23[101]	TCAAAAGGGGTGAGTAACGGTTGTACCAAAGGGT	35
8[160]	2[157]	TCAAAAGAAAATCCGTGGCATGCGCGAGGTAC	32
14[153]	21[149]	TTTTAAATGCTGAAGGTTGATAAACTAGCAAGGCGCG	38
2[17]	11[20]	GAAACACGCTGTAGGAACAAATTCG	25
4[156]	17[161]	CAGGCATGTCTTAAGAGAGGTCAGG	25
4[44]	4[45]	CTGTTCCACAACTCACATTAGAGTGTGGATGTGCTG	42
10[35]	10[36]	TTGTATAATTTTTGTTAAATTTTCATCAATTAACAGGAAGA	42
12[66]	9[65]	TGGGCGCATGGTGTGAGCGAGTAACAGCCCGAAGA	35

3[102]	16[87]	TGTAACCTCAGGAAGATATCGGTGATTTTGTAAA	35
16[100]	12[108]	AATCGGGCCTCCCTTATGAAAAACCGTCTATCCAG	35
23[115]	20[102]	ACCAGCTAAATTGTGTAGATGACCATAAATCGGCA	35
5[73]	17[76]	TTGCATTACGCCAAAGCGCAACCGTCTATTTT	32
1[137]	17[129]	CTAAAAGCCCGCTTAGATGATAAGAGGTCATGCGA	35
11[122]	11[114]	AGTGCCAAGCTATAGCTGTTTCTGTTTGATGAAC	35

Table 3S-4 Details about Double-wall square (DWS) staple sequences

Start	End	Sequence: left to right (5'-3')	Length
2[101]	4[100]	TATTAACCGAGATAGGGTTGAGCAAAGGGCAGAA	34
11[82]	9[84]	GTGGACCCCTTATAAATCAAAACGTCAAAGGGCGA	35
28[85]	29[92]	AAGAGTCAAAAGAAACCGTCTATCAAGGGCGAAAA	35
17[73]	15[75]	GAACAAGGCCCGAGATAGGGTTGATTAAAGAACGT	35
5[91]	22[98]	GGGAGTCCAGTTTTCCCTTATAAATCAAATGCGTT	35
9[85]	7[87]	AAAACCGTCTAATCGGCAAAATCCCTTGAAAAACC	35
25[45]	19[47]	GGTCACCGCCTGACGGGCAGGTGGTTTCTGCCCGC	35
5[43]	7[44]	CCGGGAGACGGGCAACAGCTGGGAACAAGAGTCC	34
17[121]	25[118]	AAAGGGCTCCCTTATTGCCTAA	22
14[155]	15[155]	AGCTGATTGCCCTCACCAGTGAGA	24
26[23]	27[42]	TATAAATCAGATAGGGTTGCCACTATTAAGAACG	35
20[135]	4[116]	TCACCGGCAAAATCCCTTATAAATGTCTATCATCCA	36
14[39]	13[48]	AAAGTGTAACACAACATACGAGCCG	25
31[127]	29[129]	GTTGAGTGTGGAACAAGAGTCCACTGAAAAACCGT	35
1[71]	3[73]	TCAAAGGGCATAAATCAAAAGAATAAAAGAATAGC	35
23[33]	16[43]	CCAGTGAGGCCCTGACGGTTTGCATTTGGGTTCCA	36
15[87]	18[84]	TCAAAGGGCATAAATCAAAAGAATAAGTCCACTGTCC	37
13[79]	11[81]	CTCCAACGTGCCCGAGATAGGGTTGATTAAAGAAC	35
2[50]	31[63]	TTGATTAAAGAACGTGGACGACTCCAAGAGTGTTG	35
3[40]	5[42]	ATCGGCAACAAAGGGCTGATGGTGATTGCCCTTCA	35
29[130]	28[108]	CTATCACAAAAGAATAGCCCGAGATAGGGTT	31
9[12]	8[21]	TTGGGTAACGCCAGGGTTTTGGGGGATGTGC	31
10[109]	12[92]	CCACTATTAATAATCGGCAAAATCCAACGTCAAAGGGCATAAATCAAAAG	50
14[119]	17[120]	TGCAGCAATTGCGTATTGGGCGCCCGGGGAGAGGCGGTCAAGTC	46
14[58]	16[56]	TGTTCCAGTTTGAACAAGAGTCCACTAGTGTGT	35
24[91]	26[89]	GATAGGGTTGAGTCCAACGTCAAAGGGCATAAATC	35

13[115]	10[110]	GTCCAATCGGCAAAATCCCTTGAAAAACCGTCTATCAGAACAAGAGT	47
26[88]	28[86]	AAAAGAATACCACTATTAAGAACGAGTTTGAAC	35
2[115]	31[126]	GAACCGTCAAAGGGCGAAAAAAGAACGAGATAGG	35
27[139]	25[139]	GTGAACGAGCCGGAAGCATAATAACTCACATTA	33
27[43]	25[44]	TGGACGGTCCGAAATCGGCAATCCTGTTTGAT	34
19[11]	3[20]	TCCACTATTAAGAGCAAGCGGCCCCAGCAAGCGCCAGCTTC	42
5[56]	22[67]	CGTGCCAGACGTGGACCTGTTTGTGTTGGTCCAG	37
3[21]	1[23]	TGGTGCCGAAAGATCGCACTCCAGCCAGTATCGG	35
25[119]	26[117]	TGAGTGAGCAGTGTAAGCC	20
26[116]	27[138]	TGGGGAGGGCGAAAAACCGTCTATCA	26
8[74]	11[60]	TCAAAAGAATAGACTCCAAGAATAGCCCGAGATAGGGAAC	40
26[73]	23[75]	GATAGGGTTGATTAAGAACGTGGACTGTTGTTCAATC	38
24[157]	25[157]	CTTCCAGTCGGGACGTTGCGCTCACTG	28
22[153]	20[136]	TAATGAATCGGCCAACCGGGTGGTTATTGCCCT	34
0[104]	2[102]	AAGGGCGAAAGAACGTGGACTCCAAAAGAGTCCAC	35
21[30]	23[32]	AAATCCTGTTACGTCAAAGGGCGAGGGTTGA	31
1[89]	1[70]	TCTATCAAAACCGTCTATCATCCACTATTAAGAACGTGTCCAACG	46
19[143]	4[145]	GAGTGTTGTAACAGCTGTTTCTTTTAAAGTTG	32
4[154]	21[159]	GATCACCAGTG	11
13[12]	12[12]	TGTTATCCGCTCCTGTTTCTGTG	24
10[153]	11[131]	GAACAAGAGTCCAGTTGAGTGTTGTTCCAGTTTGAAGAATAGCCCG	46
9[134]	9[160]	TCTACTACTATTAAGAACGTGGACTC	27
15[76]	13[78]	GGACGCCGAGATAGGGTTGATTAAGAACGTGGA	35
23[11]	18[11]	AATAGGAACA	10
1[24]	0[11]	CCTCAGGATCACATCTGCCAGTTTGAAGG	29
15[105]	13[114]	TCTATCAATCGGCAAAATCCCTTGAAAAACCGTCTATCAGCG	42
25[140]	19[142]	ATTGCACATTAAGGAAACCTAGAGTCCATAGGGTT	35
28[151]	30[147]	AATCATGGTCATAGCTCGGGTACCGAGCTCGAGACTC	37
22[97]	17[101]	GCAGCAAGCGCGAGATAGGGTTGAGTAGAATAGCACGTGG	40
6[20]	21[29]	TGCGGTGCGCAACTGTTGGGAACCAGGCAAGGCGA	35
20[66]	4[51]	TGGTTTTCTTTTCAACCAGTCTATCATCAA	32
17[102]	15[104]	ACTCCAACGTATCGGCAAAATCCCTTGAAAAACCG	35
11[11]	10[11]	TGCCAAGCTTGCATGTAAAACGACGG	26
9[48]	7[52]	ACTATTAAGAACGTGGCCCGAGATAGGGTTGATTAA	37

11[61]	14[59]	AAGAGTCCACTAGTGTGTTCCAGTTTAGTCCACTAGTGT	40
22[66]	23[52]	CAGAACAGCTGCGTGGACTCCAACGTCAAAGGCAGACAGC	40
25[108]	22[113]	ATCAAAATCAAAGTTAAACCGTCTATCAGTCGGGA	35
18[83]	5[74]	ACTAGAATAGCCGTCCACGCTGGTTTGTCCGAAATTTGGGCGCATG	47
31[77]	30[99]	CAAGAGATCGGCAAAATCCCTTATAAAGAACG	32
3[11]	4[10]	GCACCTTCGCC	11
8[160]	9[133]	AAGGGCGAAAAACCGTCTATCAGGGTTGAGTGTAACCG	39
3[89]	1[88]	GTGTTGTATCGGCAAAATCCCTTGAAAAACCG	32
0[151]	1[151]	TGCATGGAACAAGAGTCCACTATTACCGTCTATCACGACGGCCAGTGC	48
16[152]	23[153]	AGCTGCATTAACCTGTCTTGAAACAGTCGTGCCAG	35
5[75]	8[75]	AATCGGGGCGCCAGGGTGGTTTCCAACGTCAAAGGGCATAAA	42
24[26]	26[24]	TTGCAGCAAGCTGCCCCAGCAGGCGAAAAATCCCT	35
14[140]	13[152]	ACCGCTGGCCCTTGCCCCAGCAGGCGAAAAATCCTGTT	38
11[31]	14[26]	AGGTCGACTGTAATCATGGTCATAGACAATCCAAGCCT	39
30[146]	31[151]	TAGAGGATCCCTGTTCCAGTTTGCCTG	27
4[115]	2[116]	ACGTTGTTGTTCCAGTTTGGTGTCCAGTTTG	32
19[95]	24[92]	GAGAGACAGCCAGTTTGGAAACAAGAATTAAGACCGA	37
6[160]	7[132]	ATTACGCCAGCTGGCGAAAGGGCTGAGAGAGTTACCGT	38
22[112]	6[108]	AACCTGTGCGAAAAACCCGCAACATCCTGTTGCTG	37
12[91]	15[86]	AATACAAAGGGCATAAATCAAAGAATATCCAACG	35
11[132]	14[120]	AGATATCCCTTATAAATCAACGCTGGTTGAGAGAGT	36
7[11]	8[11]	CTATTGGCGA	10
23[67]	25[53]	TTATACAGTGGTTCCGAAATCTGCCCTTGAACA	35
8[20]	6[21]	TGCAAACGCCAGCTGGCGAAAAGGGCGATCGG	32
31[12]	30[30]	GGCGCATCGTAACCGTGATCAAAGAATCCAACGTCAA	38
23[76]	19[82]	AAAATTAAGAAATTGCCCTTCA	23
14[25]	16[23]	GGGGTGCCTATCACATTAATTGCGTTTGTCTGTGCC	35
11[52]	11[30]	CGGGGTTGAGTGTTGTTCCAGTTTAGTCACGACGTTGCCTGC	43
16[42]	14[40]	GTCGGGAAACCGCGTCACTGCCCGTGGGAAGCAT	35
28[107]	30[108]	GAGTTCCAACGTCAAAGGGCATTAAAGAACGT	32
7[133]	7[160]	CTATCAGGAAGGGCGATCGGTGCGGGCC	28
25[54]	27[56]	AGAGTCCACTAGTGTGTTCCAGTTTTCCAACGTC	35
26[156]	27[156]	TCCACACAACATAATTGTTATCCGCT	26
16[140]	14[141]	GAATCGGCCAACGAGGGTGGTTTTTCTTTTC	32



13[49]	11[51]	GAACAAGTACCGAGCTCGAATTCCTAGAGGATCCC	35
30[29]	28[12]	AGGGCGTTAAAGAACGTGGACTTTGGAACAAGAGTAGTGTGTTCCAGTT	50
1[37]	3[39]	AAGAGTCCACTAGTGTGTTCCAGTTTGTTCGGAA	35
7[88]	5[90]	GTCTATCAAGGCGGTTTGCCTATTGCCAACGCGCG	35
7[53]	5[55]	AGAACGTGGACTTTCTTTCCACAGTGAAACCTGT	35
19[83]	3[88]	CCGCCTTTCGCTACGGCAAAGGAACAAGTAGGGTTGA	38
27[108]	25[107]	TCAAATCGGCAAAATCCCTTGAAAAACCGTCT	32
9[122]	7[123]	GGCGAATGTTCCAGTTTGGAAACCGTCAAAGGGCG	34
4[123]	18[133]	GGACTGCGTATTGGGCGCCAGCGGGGAGGCCCGAGACTA	39
30[98]	31[76]	TGGACTCCAACGTCAAGGTTGAGTGTGGAA	32
19[48]	23[66]	TTTCAGTGAGACGGGCGGAAAATGGCAAAATCCC	35
23[129]	16[141]	CCAGTCGTTGCGTTGGAAAAACCGTCTATCAAAT	34
30[107]	0[105]	GGACTCAAAGAATAGCCCGTGGACTCCAACGTCA	35
1[11]	2[11]	ACGACAGCTT	10
7[45]	9[47]	ACTAGTGTGTTCCAGTTTCCCGGAACAAGAGTCC	35
2[151]	3[151]	CGACGTTGTAAAAGGGTTGAGTGTAAACAAGAGTCCGCCAGGGTTTTCC	48
18[132]	19[109]	TTAAAGAACGTGGACAGGGCGAAGTTCTGCAT	32
4[99]	19[94]	TAGCAGGCGAAAGCGCGGGGAGAGGCGGTGGCCCT	35
27[57]	29[44]	AAAGGGCGATAGGGTTGAGTGTGTTCCAGTAGAAC	36
23[53]	20[40]	TGACACATTAATTGCGTTGGAAAAACCGTCGCCTG	35
29[93]	27[107]	ACCGTCTATCAGTTGTTCTCGACTCCAACG	31
16[22]	22[11]	AGCTGCAAACGCGCGCCAGTTTCCCGAGATAAAAACCGTCTAT	44
19[110]	23[128]	TAATGAATCAAAGAATAAGGCGGTTGCCGCTTT	35
31[48]	1[36]	ATAGGGTTCGTCAAAGGGCGAAAAACCGTCTAGGAAC	37
20[39]	18[34]	GCCCTGAGAGAGTTGCAACGTGGACTCCATTCTTT	35
6[107]	8[105]	GTTTGCCCAGCAGAACGTGGACTCCAAAAGAGTC	35
29[45]	31[47]	GTGGACTCCAAAAGAGTCCACTATTAAGCCCGAG	35
3[74]	20[67]	CCGAGAAGTCCACTATTAAGACTGCATTACAGGG	35
29[12]	30[12]	AAGAGTCCACTAAAAAACCGTCTA	24
16[55]	17[72]	TCCAGTTTCGCGCGAAAAACCGTCTATCATTG	33
8[104]	9[121]	CACTATTAATCAGAACGTGGACTCCAACGTCAAAG	35
4[144]	5[154]	GGTAACACTATTAAGAATCGCCTGGCCGGATGTGCTGCAAGGC	44
31[64]	29[65]	TTCCAGTTTGTTCAGTTTGGAAACCGTCAAAGGG	34
18[33]	24[27]	GTGTTGTTGGGAGAGGGAGAG	21

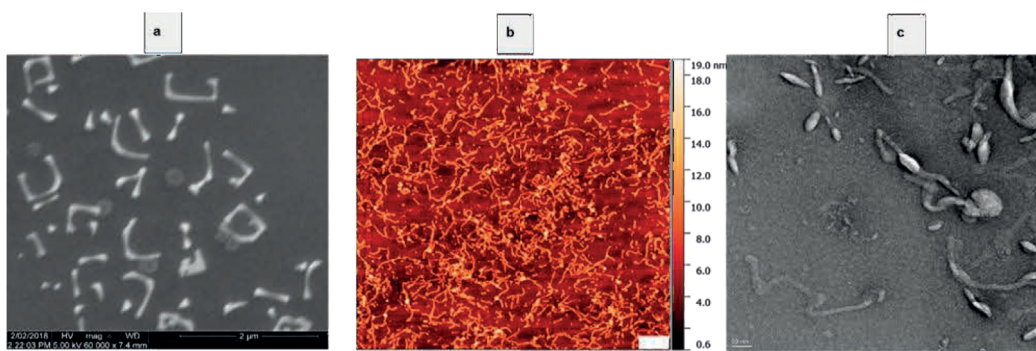
5[11]	6[11]	CAGGCGCCTC	10
12[153]	11[153]	GGTCCGAAATCGGCAAAAGGGTTGAGTGTGTCC	36
7[124]	4[124]	AAAAGCAGCAAGCGGTCCACTGATGGTGGTCCGAAACGT	40
29[66]	26[74]	CGAAAATAGCCCAGAAAAACCGTCTATCAGCCCGA	36
4[50]	2[51]	CGTAATCCCTTATAAATCAGCCCGAGATAGGG	32

Table 3S-5 Sequence of M13mp18 scaffold DNA

Numbers	Sequence (7249 bases, 5'→3')
1	AATGCTACTACTATTAGTAGAATTGATGCCACCTTTTCAGCTCGCGCCCAAAATGAAAAT
61	ATAGCTAAACAGGTTATTGACCATTTGCGAAATGTATCTAATGGTCAAACCTAAATCTACT
121	CGTTCGAGAAATGGGAATCAACTGTTATATGGAATGAAACTTCCAGACACCGTACTTTA
181	GTTGCATATTTAAAACATGTTGAGCTACAGCATTATATTCAGCAATTAAGCTCTAAGCCA
241	TCCGCAAAAATGACCTCTTATCAAAGGAGCAATTAAGGTTACTCTAATCCTGACCTG
301	TTGGAGTTTGCTCCGGTCTGGTTCGCTTTGAAGCTCGAATTAACCGCGATATTTGAAG
361	TCTTTCGGGCTTCTCTTAATCTTTTGTATGCAATCCGCTTTGCTTCTGACTATAAAGT
421	CAGGGTAAAGACCTGATTTTTGATTTATGGTCATTCTCGTTTTCTGAACCTGTTAAAGCA
481	TTTGAGGGGGATTCAATGAATATTTATGACGATCCGCAGTATTGGACGCTATCCAGTCT
541	AAACATTTTACTATTACCCCTCTGGCAAAACTCTTTTGCAAAAGCCTCTCGCTATTTT
601	GGTTTTATCGTCGCTGGTAAACGAGGGTTATGATAGTGTGCTTACTATGCCTCGT
661	AATCCCTTTGGCGTTATGTATCTGCATTAGTTGAATGTGATTCTAAATCTCAACTG
721	ATGAATCTTTCTACCTGTAATAATGTTGTTCCGTTAGTTCGTTTTATTAACGTAGATTTT
781	TCTCCCAACGCTCTGACTGGTATAATGAGCCAGTCTTAAAATCGCATAAGGTAATTCA
841	CAATGATTAAGTTGAAATTAACCATCTCAAGCCCAATTTACTACTCGTCTGGTGT
901	CTCGTCAGGGCAAGCCTTATCACTGAATGAGCAGCTTTGTACGTTGATTTGGGTAATG
961	AATATCCGGTCTTGTCAGATTACTCTTGATGAAGGTCAGCCAGCCTATGCGCCTGGTC
1021	TGTACACCGTTCATCTGTCTCTTCAAAGTTGGTCAGTTCGGTTCCTTATGATTGACC
1081	GTCTGCGCCTCGTTCGGGTAAGTAACATGGAGCAGGTCGCGGATTTGACACAAATTTAT
1141	CAGGCGATGATACAAATCTCCGTTGACTTTGTTTTCGCGCTTGGTATAATCGCTGGGGT
1201	CAAAGATGAGTGTTTTAGTGTATCTTTTGCCTTTTCGTTTTAGGTTGGTGCCTTCGTA
1261	GTGGCATTACGTATTTACCCGTTTAAATGGAAACTTCTCATGAAAAAGTCTTTAGTCT
1321	CAAAGCCTCTGTAGCCGTTGCTACCCTCGTCCGATGCTGTCTTTCGCTGCTGAGGGGA
1381	CGATCCCGCAAAAGCGGCTTTAACTCCCTGCAAGCCTCAGCGACCGAATATATCGGTTA
1441	TGCGTGGGCGATGGTTGTTGTCATTGTCGGCGCAACTATCGGTATCAAGCTGTTAAGAA
1501	ATTCACCTCGAAAGCAAGCTGATAAACCGATACAATTAAGGCTCCTTTGGAGCCTTTT
1561	TTTTGGAGATTTTCAACGTGAAAAAATTATTATTCGCAATTCCTTTAGTTGTTCTTTCT
1621	ATTCTCACTCCGCTGAAACTGTTGAAAGTTGTTAGCAAATCCCATACAGAAAATTCAT
1681	TTACTAACGTCTGAAAGACGACAAAACCTTAGATCGTTACGCTAACTATGAGGGCTGTC
1741	TGTGGAATGTACAGGCGTTGTAGTTTGTACTGGTGACGAAACTCAGTGTACGGTACAT
1801	GGGTTCTATTGGGCTTGCTATCCCTGAAAATGAGGGTGGTGGCTCTGAGGGTGGCGGTT
1861	CTGAGGGTGGCGGTTCTGAGGGTGGCGGTTAAACCTCCTGAGTACGGTGATACACCTA
1921	TCCGGGCTATACTTATATCAACCCTCTCGACGGCACTTATCCGCTGGTACTGAGCAAA
1981	ACCCCGTAATCCTAATCCTTCTCTTGAGGAGTCTCAGCCTCTAATACTTTTATGTTTC
2041	AGAATAATAGGTTCCGAAATAGGCAGGGGGCATTAACTGTTTATACGGGCACTGTTACT
2101	AAGGCACTGACCCGTTAAAACCTATTACCAGTACACTCCTGTATCATCAAAGCCATGT
2161	ATGACGCTTACTGGAACGGTAAATTCAGAGACTGCGCTTTCCATTCTGGCTTAAATGAGG
2221	ATTTATTTGTTGTGAATATCAAGGCCAATCGTCTGACCTGCCTCAACCTCCTGTCAATG
2281	CTGGCGCGGCTCTGGTGGTGGTCTGGTGGCGGCTCTGAGGGTGGTGGCTCTGAGGGT
2341	GCGGTTCTGAGGGTGGCGGCTCTGAGGGAGGCGGTTCCGGTGGTGGCTCTGGTCCGGT

2401	ATTTTGATTATGAAAAGATGGCAAACGCTAATAAGGGGGCTATGACCGAAAATGCCGATG
2461	AAAACGCGCTACAGTCTGACGCTAAAGGCCAACTTGATTCTGTCGCTACTGATTACGGTG
2521	CTGCTATCGATGGTTTCATTGGTGACGTTTCCGGCCTTGCTAATGGTAATGGTGCTACTG
2581	GTGATTTTGTGGCTCTAATCCCAAATGGCTCAAGTCGGTGACGGTGATAATTCACCTT
2641	TAATGAATAATTTCCGTC AATATTTACCTTCCCTCCCTCAATCGGTTGAATGTCGCCCTT
2701	TTGTCTTTGGCGCTGGTAAACCATATGAATTTTCTATTGATTGTGACAAAATAAACTTAT
2761	TCCGTGGTGTCTTTGCGTTTCTTTTATATGTTGCCACCTTATGTATGTATTTTCTACGT
2821	TTGCTAACATACTGCGTAATAAGGAGTCTTAATCATGCCAGTTCTTTTGGGTATTCGGTT
2881	ATTATTGCGTTTCTCGGTTTCTTCTGGTAACTTTGTTGCGCTATCTGCTTACTTTTCT
2941	TAAAAAGGGCTTCGGTAAGATAGCTATTGCTATTTTATTGTTTCTTGTCTTATTATTGG
3001	GCTTAACTCAATTCCTGTGGGTTATCTCTGATATTAGCGCTCAATTACCCTCTGACTT
3061	TGTTCAAGGTGTTCAAGTAATTCTCCCGTCTAATGCGCTTCCCTGTTTTTATGTTATTCT
3121	CTCTGTAAAGGCTGCTATTTTTCATTTTTGACGTTAAACAAAAAATCGTTTCTTATTTGGA
3181	TTGGGATAAAATAATATGGCTGTTTATTTTGTAACTGGCAAATTAGGCTCTGGAAAGACGC
3241	TCGTTAGCGTTGGTAAGATTCAGGATAAAATTGTAGCTGGGTGCAAATAGCAACTAATC
3301	TTGATTTAAGGCTTCAAACCTCCGCAAGTCGGGAGGTTTCGCTAAAACGCCCTCGCGTTC
3361	TTAGAATACCGGATAAGCCTTCTATATCTGATTGCTTGTGCTATTGGGCGCGGTAAGT
3421	CCTACGATGAAAATAAAACCGCTTGCTTGTCTCGATGAGTGCAGTACTTGGTTTAAATA
3481	CCCCTTCTTGAATGATAAGGAAAGACAGCCGATTATTGATTGGTTTCTACATGCTCGTA
3541	AATTAGGATGGGATATTATTTTCTTGTTCAGGACTTATCTATTGTTGATAAACAGGCGC
3601	GTTCTGCATTAGCTGAACATGTTGTTTATTGTCGTCGCTGGACAGAATTACTTTACCTT
3661	TTGTCGTACTTTATATTCTTATTACTGGCTCGAAAATGCCTCTGCCTAAATTACATG
3721	TTGGCGTTGTTAAATATGGCGATTCTCAATTAAGCCCTACTGTTGAGCGTTGGCTTTATA
3781	CTGGTAAGAATTTGTATAACGCATATGATACTAAACAGGCTTTTCTAGTAATTATGATT
3841	CCGGTGTTTATTTCTTATTTAACGCCTATTTATCACACGGTCGGTATTTCAAACCATTAA
3901	ATTTAGGTCAGAAGATGAAATTACTAAAATATATTTGAAAAAGTTTTCTCGCGTTCTTT
3961	GTCTTTCGATTGGATTTGCATCAGCAATTTACATATAGTTATATAACCCAACTAAGCCGG
4021	AGGTTAAAAAGGTAGTCTCTCAGACCTATGATTTTGATAAAATTCACTATTGACTCTTCTC
4081	AGCGTCTTAATCTAAGCTATCGCTATGTTTTCAAGGATTCTAAGGGAAAATTAATTAATA
4141	GCGACGATTTACAGAAGCAAGGTTATTCACCTCACATATATTGATTTATGACTGTTTCCA
4201	TTAAAAAAGGTAATTCAAATGAAATTGTTAAATGTAATTAATTTTGTCTTCTGATGTTT
4261	GTTTCATCATCTTCTTTTGTCTCAGGTAATTGAAATGAATAATTCGCCTCTGCGGATTTT
4321	GTAACCTGGTATTCAAAGCAATCAGGCGAATCCGTTATTGTTTCTCCCGATGTAAGGTT
4381	ACTGTTACTGTATATTCATCTGACGTTAAACCTGAAAATCTACGCAATTTCTTTATTTCT
4441	GTTTTACGTGCAAATAATTTTGATATGGTAGGTTCTAACCTTCCATTATTCAGAAGTAT
4501	AATCCAAACAATCAGGATTATATTGATGAATGCCATCATCTGATAATCAGGAATATGAT
4561	GATAATTCGGCTCCTTCTGGTGGTTTCTTTGTTCCGCAAATGATAATGTTACTCAAAT
4621	TTTAAAAATTAATAACGTTTCGGGCAAAGGATTTAATACGAGTTGTGCAATTGTTTGTAAAG
4681	TCTAATACTTCTAAATCCTCAAATGTATTATCTATTGACGGCTCTAATCTATTAGTTGTT
4741	AGTGCTCCTAAAGATATTTTAGATAACCTTCTCAATTCCTTCAACTGTTGATTGGCCA
4801	ACTGACCAGATATTGATTGAGGTTTGTATTTGAGGTTTCAGCAAGGTGATGCTTTAGAT
4861	TTTTCATTTGCTGCTGGCTCTCAGCGTGGCACTGTTGCAGGCGGTGTAATACTGACCGC
4921	CTCACCTCTGTTTTATCTTCTGCTGGTGGTTGTTCCGTTATTTTAAATGGCGATGTTTTA
4981	GGGCTATCAGTTTCGCGCATTAAAGACTAATAGCCATTCAAAAATATTGTCTGTGCCACGT
5041	ATTCTTACGCTTTCAGGTCAGAAGGGTTCTATCTCTGTTGGCCAGAATGTCCTTTTATT
5101	ACTGGTCGTGTGACTGGTGAATCTGCCAATGTAATAATCCATTTTCAGACGATTGAGCGT
5161	CAAAATGTAGGTATTTCCATGAGCGTTTTTCTGTTGCAATGGCTGGCGGTAATATTGTT
5221	CTGGATATTACCAGCAAGGCCGATAGTTTGGAGTTCTTCTACTCAGGCAAGTGATGTTATT
5281	ACTAATCAAAGAAGTATTGCTACAACGGTTAATTTGCGTGATGGACAGACTCTTTTACTC
5341	GGTGGCCTCACTGATTATAAAACACTTCTCAGGATTCTGGCGTACCGTTCCTGTCTAAA
5401	ATCCCTTTAATCGGCCTCCTGTTTGTAGCTCCCGCTCTGATTCTAACGAGGAAAGCACGTTA
5461	TACGTGCTCGTCAAAGCAACCATAGTACGCGCCCTGTAGCGGCGCATTAAAGCGCGCGGG
5521	TGTGGTGGTTACGCGCAGCGTGACCGCTACACTTCCAGCGCCCTAGCGCCCGCTCCTT

5581	CGCTTTCTCCCTTCTTTCTCGCCACGTTGCGCCGGCTTTCCCGTCAAGCTCTAAATCG
5641	GGGGCTCCCTTTAGGGTTCGATTAGTGCTTACGGCACCTCGACCCAAAAAACTTGA
5701	TTTGGGTGATGGTTCACGTAGTGGGCCATCGCCCTGATAGACGGTTTTTTCGCCCTTGAC
5761	GTTGGAGTCCACGTTCTTTAATAGTGGACTCTTGTTCCAAACTGGAACAACACTCAACCC
5821	TATCTCGGGCTATTCTTTGATTATAAGGGATTTGCGGATTCGGAACCACCATCAA
5881	CAGGATTTTCGCCTGCTGGGGCAAACCCAGCGTGGACCGCTTGTGCAACTCTCTCAGGGC
5941	CAGGCGGTGAAGGGCAATCAGCTGTTGCCGTCTCACTGGTGAAAAGAAAAACCACCTG
6001	GCGCCAATACGCAAACCGCTCTCCCGCGCGTTGGCCGATTCATTAATGCAGCTGGCA
6061	CGACAGGTTTCCGACTGGAAGCGGGCAGTGAGCGCAACGCAATTAATGTGAGTTAGCT
6121	CACTCATTAGGCACCCAGGCTTACACTTTATGCTTCCGGCTCGTATGTTGTGTGGAAT
6181	TGTGAGCGGATAACAATTTACACAGGAAACAGCTATGACCATGATTACGAATTCGAGCT
6241	CGGTACCCGGGGATCCTCTAGAGTCGACCTGCAGGCATGCAAGCTTGGCACTGGCCGTGC
6301	TTTTACAACGTGCTGACTGGGAAAACCTGGCGTTACCCAACTTAATCGCCTTGCAGCAC
6361	ATCCCCCTTTCGCCAGCTGGCGTAATAGCGAAGAGGCCCGCACCGATCGCCCTTCCAAC
6421	AGTTGCGCAGCCTGAATGGCGAATGGCGCTTTCCTGGTTTCCGGCACCAGAAGCGGTGC
6481	CGGAAAGCTGGCTGGAGTGCAGTCTTCTGAGGCCGATACTGTGTCGTCCTCCCTCAAAC
6541	GGCAGATGCACGGTTACGATGCGCCCATCTACACCAACGTGACCTATCCCATTACGGTCA
6601	ATCCGCCGTTTGTCCACGGAGAATCCGACGGGTTGTTACTCGCTCACATTTAATGTTG
6661	ATGAAAGCTGGCTACAGGAAGGCCAGACGCAATTAATTTTATGATGGCGTTCCTATTGGTT
6721	AAAAAATGAGCTGATTTAACAAAAATTAATGCGAATTTAACAAAAATTAACGTTTAC
6781	AATTTAAATATTTGCTTATACAATCTTCTGTTTTGGGGCTTTTCTGATTATCAACCGG
6841	GGTACATATGATTGACATGCTAGTTTTACGATTACCGTTCATCGATTCTCTTGTGCTC
6901	CAGACTCTCAGGCAATGACCTGATAGCCTTTGTAGATCTCTAAAAATAGCTACCCTCTC
6961	CGGCATTAATTTATCAGCTAGAACGGTTGAATATCATATTGATGGTGATTTGACTGTCTC
7021	CGGCCTTCTCACCTTTTGAATCTTACCTACACATACTCAGGCATTGCATTTAAAT
7081	ATATGAGGGTTCTAAAAATTTTATCCTTGCCTTGAATAAAGGCTTCTCCCGAAAAGT
7141	ATTACAGGGTCATAATGTTTTTGGTACAACCGATTAGCTTTATGCTCTGAGGCTTTATT
7201	GCTTAATTTTGCTAATCTTTGCCTTGCCTGTATGATTTATTGGATGTT



**Figure 3-S1 Microscopic analysis of M13mp18 (scaffold) at 10 nM concentration**

a) SEM with 5 nm platinum coating on the sample; b) AFM image in mica on tapping mode; c) TEM micrograph with 2% negative staining. Scale bars are 2  $\mu\text{m}$ , 500 nm and 50 nm, respectively.

3

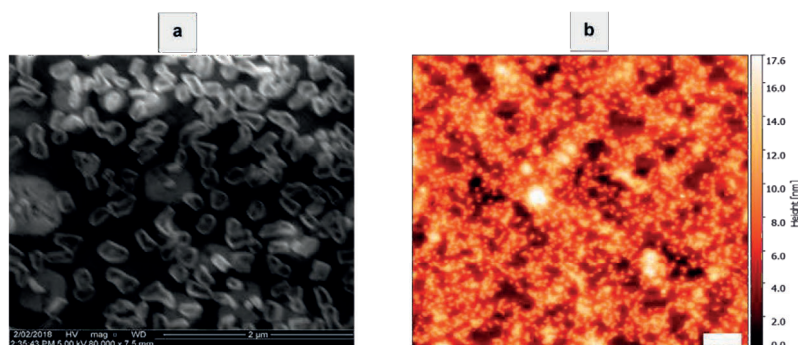


**Figure 3-S2 Microscopic analysis of ss-DNA oligonucleotides (staples) at 40 nM concentration.**

a) SEM with 5 nm coating the staples, appearing as big aggregates in closed loops (Scale-2  $\mu\text{m}$ ) b) AFM snap-on silicon substrate, capturing the aggregate formation from small oligonucleotides (Scale- 500 nm).

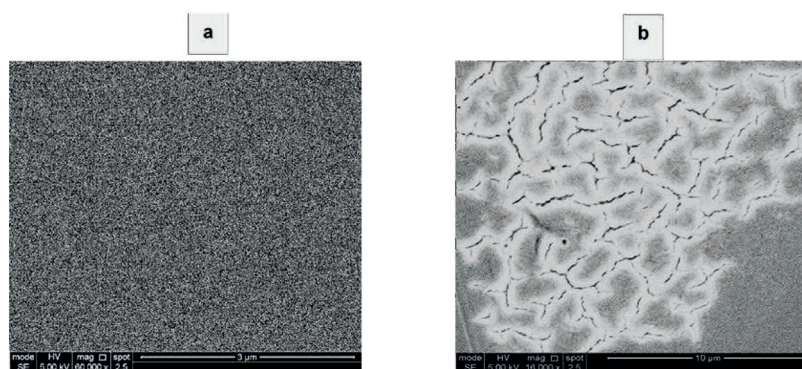


**Figure 3-S3 SEM of negative and positive controls.**

a) Mica substrates washed and dried; b) 10 mM dried magnesium salts. Scale bars are 3 and 10  $\mu\text{m}$ , respectively.

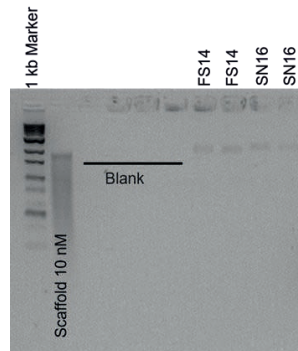


**Figure 3-S4 Stability test for DNAs in Milli-Q water**

SYBR safe stained 1.5% agarose gel analysing the DNAs after resuspending in water for 24 hrs at 4 °C



## **CHAPTER 4**

---

# **Encapsulation of Modular DNA Origami with Virus-like Particles**

---

Part of this chapter will be submitted.



## 4 ENCAPSULATION OF MODULAR DNA ORIGAMIS WITH VIRUS-LIKE PARTICLES (VLPS)

### 4.1 Introduction

Custom-designed, correctly folded, and functional DNA nanostructures (DNs) serve as versatile molecular components in numerous bio-nanotechnological applications (1). The fully addressable DNAs are impressive illustrations of precise nanoscale engineering. DNAs conjugated with functional molecules like polymers (2), peptides, proteins (3-6), lipids (7) and nucleic acids (8) have been used in various applications such as bioimaging, biosensing and nanomedicine. In recent years, the most intensely studied application of DNAs is their use as drug carriers for targeted delivery of molecular payloads inside the cells (1, 9-14).

#### 4

DNA has emerged as a highly programmable material, combined with inherent properties of biocompatibility and tunable stability in cellular environments. The invention of DNA origami provides attractive features to design different (2D and 3D) nanostructures with desirable functionality and use in various nanotechnology and biomedical applications. Chemical synthesis of tailored DNA strands offers excellent flexibility in designing DNAs with origami approach. The self-assembly properties of DNA provides an instrumental and detailed description in creating highly programmable assemblies with complex shapes for precise cellular delivery and responsive to external stimuli. These DNA-based delivery systems could either be static or dynamic and can be easily functionalised in a user-defined way. DNAs with some unique characteristics like well-defined size, geometry, surface charge, in combination with configurable and biochemically addressable components, make them a material of choice for use in drug delivery and therapeutics (1, 12). DNAs have the potential to deliver drug molecules to desired locations with improved efficiency, enhancing drug efficacy with minimal side-effects (10).

The very first application of DNA origami in drug delivery used tetrahedron (15), hollow cubes (16, 17) as molecular containers. Two DNA origami structures (rod-like and triangle-shaped) were shown to successfully deliver anticancer drugs and a DNA intercalator into cells with tunable drug release properties (18-20). This research paved the way for new possibilities for tackling various medical problems. Apart from cancer therapy, nanotubes carrying CpG sequences were examined for favourable immunostimulant delivery to immune cells (21). Successful stories have been presented involving CpG-coated origamis - DNA cages, polyrod-like structured DNA, DNA dendrimers, using DNAs as carriers for producing immuno-stimulatory effects *in vivo* (22-24). DNA-based assemblies were also used to investigate biodistribution in *in-vivo* imaging (25), inhibit protein function *in vitro* (26) and to silence target genes (27, 28). Another remarkable example of a highly sophisticated delivery model is a DNA nanorobot; the robot can selectively transport the molecular payload to the

cells (29). Apart from acting as nanocarriers, DNAs can also serve as tiny molecular devices (DNA nanodevices) in biological systems (30-32).

Although numerous exciting applications have been illustrated, there are still many unexplored opportunities and challenges that hinder translational use of DNAs into biomedical research. Challenges include the immunogenic response elicited by DNAs as they are recognised as a foreign material (12). There have been problems reported with the intrinsic bio-compatibility, biodegradability, structural integrity and off-target or non-specific gene regulation. The low success rate of nanoparticles is known and often attributed to the biological barriers in the body (33). DNAs are also said to have low transfection efficiency because of the polar nature of DNA (34). Another challenge is to improve the pharmacokinetic bio-availability of DNA-based assemblies *in vivo*; both pharmacokinetic and pharmacodynamic profiles of DNAs remain unclear *in vivo*. Moreover, large-scale production of DNAs is still a critical question, as the synthesis of starting materials remains expensive to date (1).

4

For efficient drug delivery, an ideal drug nanocarrier should preserve the biological traits of drugs *in vivo*, allowing to effectively lower the pharmaceutical dose and minimise potential side-effects (9). In order to accomplish this, a drug delivery nanocarrier should possess the following characteristics: good safety profile (water solubility and nontoxicity), ease of cargo loading, active target specificity, high cellular uptake, intracellular biostability, triggered the release of the cargo, and allowance for additional functionalities (10). The surface morphology of the DNA nanocarriers is another valuable physical property regulating the extent of payload delivery and transfection rate to different sites (35).

DNAs as delivery vehicles are used to carry a variety of therapeutic cargos like small drug molecules, proteins, nucleic acids (36). Transportation of DNAs into cells, their internalisation efficiency and biostability can be further improved to enable them to thrive in cellular environments. This advancement can be achieved by encapsulating DNAs with virus capsid proteins (CPs) (37), cationic polymers (38) or by using lactose-containing (39) or lipid-modified (40) hybrid structures. Kostianen and co-workers coated virus CPs to a DNA origami rectangle before uptake and observed a significant enhancement in cellular internalisation (37). DNAs were also reported to be layered with serum proteins for improved delivery, stability and enhanced transfection (41, 42). Such studies are still limited by the bioavailability and functionality of DNAs in living organisms.

However, cowpea chlorotic mottle virus (CCMV) CPs encapsulation has shown to enhance the effectiveness of cargo delivery to a great extent. The literature presents several examples where CCMVs have been used to encapsulate different negatively charged compounds and used for gene, siRNA, siDNA and mRNA delivery (43-45). Different polymers like polystyrene sulfonate (PSS), poly(2-methoxy-5-propyloxy sulfonate)-phenyl-ene vinylene (MPS-PPV) and polyferrocenyl silane (PFS) have also been encased inside CCMV (46, 47). Such stable CCMV-based VLPs can even be formed

into clustered VLPs. In this chapter, we have used CCMV for encapsulating designed DN (from the preceding chapter) HB and DWS. Here, we take advantage of CCMV CPs binding effectively to the negatively-charged DNA origamis and form hybrid nanoassemblies that act as a potent delivery vehicle. This would increase the *in vivo* scope of DN and will expedite the rendition of DN to the practical clinic for the development of targeted therapies.

## 4.2 Results and Discussion

Here, we coated two modular DN (HB and DWS) with virus CPs targeting enhanced cellular delivery. Our approach employs purified CCMV CPs and allows them to unite and self-assemble on the DN's external surface via electrostatic interactions which further pack the nanostructures inside the viral capsid (Figure 4-1). We took advantage of the compact geometrical structure DNA origami to allow effective encapsulation of DN molecule in a viral capsid. The discussed straightforward method could readily find applications not only in drug delivery applications but also in organising intracellular reactions by origami-based templates.

4

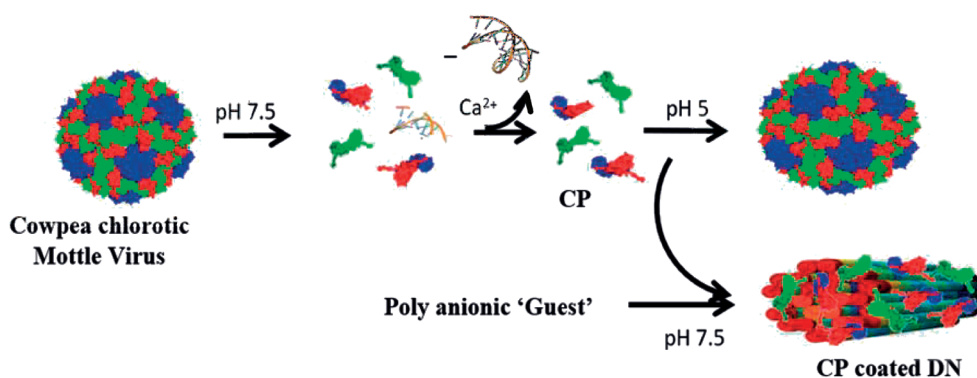


**Figure 4-1 Schematic overview of CP fabrication of DN to create nanoassemblies.**

The CCMV virus is disassembled into capsid protein (CP) dimers in calcium precipitation with the removal of viral RNA. DN were then encapsulated with CPs following incubation at neutral pH.

### 4.2.1 Fabrication of DNA origami with CPs

CCMV has become a well-studied model system widely recognised to encapsulate various synthetic and protein guest macromolecules inside the capsid (48, 49). DN and CCMV CP dimers were prepared using standard annealing and calcium chloride precipitation procedures, respectively. Surface charge density of DN and CPs, as well as other chemical and physical surface properties, are also crucial for the encapsulation of resulting nanoassemblies. The positively charged N-terminus of purified CPs enables them to bind effectively and self-assemble on the DNA (origami) nanostructures, but large excess of CPs was needed to stabilize the negative charge of the DN, leading to their complete packing. The entire assembly process is depending on the conditions i.e., pH and ionic strength. The CP-DN interactions are electrostatic in nature and lead to complete

encapsulation at high pH and comparatively low ionic strength (pH 7.5, 0.3 M NaCl) (50). At neutral pH the CP-CP attractions are weak; thus DNAs function as a template on which the CPs assemble themselves, and the resulting assembly adapt a different configuration from the native DNAs shape (37). The binding efficiency of CPs on the DNAs and the morphology of resulting complexes were studied by gel electrophoretic mobility shift assay (EMSA) and electron microscopy.

The DNA origami-CP interaction was studied over a wide CP/DNA origami ratios. In order to achieve a straightforward comparison between different samples, a ratio parameter  $\kappa$  (defined in the methods section) is noted for each sample in Table 4-1

$\kappa = \text{CP/DNA bp}$	HB	DWS
0.08	2.4	2.4
0.12	3.6	3.57
0.2	6.04	5.9
0.32	9.6	9.5
0.64	19.35	19.04
1	30.24	29.76

**Table 4-1 Mass ratio comparison.**

Different CP/DNA origami ratio ( $\kappa$ ) calculations were used in encapsulation studies for the two selected designs HB and DWS.

Electrostatic binding of positively charged N-terminus of CPs on the negatively charged surface of DNAs was analysed by EMSA (Figure 4-2). Initially, CCMV-CP was titrated at different CP/DNA ratio, i.e.  $\leq 0.2$  for both designs, without showing any noticeable or significant band shift from DNAs-CP complexes on electrophoretic mobility measurements (Figure 4-2a and b). With a low amount of CP ( $\kappa=0.08 - 0.2$ ), the migration of DNAs remains unchanged. This can primarily be attributed to the geometry (size and compactness) of the selected DNA origamis (51). However, hindrance in migration of DNAs on the gel is observed while increasing the CP ratio  $\kappa=0.32 - 1.0$ , indicating decreased mobility and pointing to an efficient binding of CPs to origamis. Furthermore, the band movement was completely prevented with high CP ratios ( $\kappa=3.2$ ) suggesting the formation of undesired aggregates. These results steadily reinforce that CPs bind to DNAs, and the EMSA follows a similar trend as reported previously with CCMV-CPs and linear ds-DNA (44).

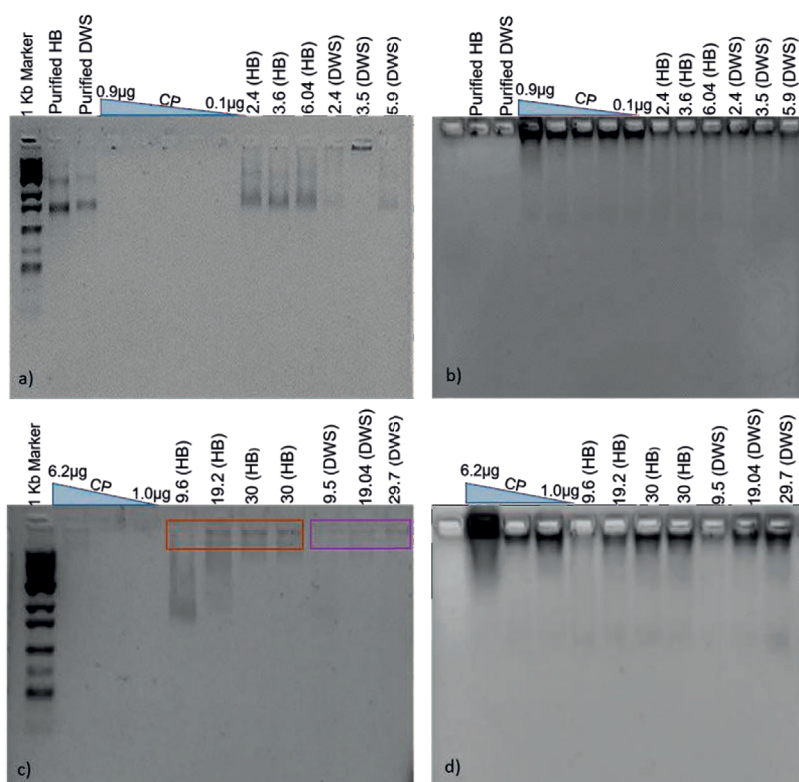


**Figure 4-2 Electrophoretic mobility shift assay (EMSA) of fabricated DNAs with respective CP excess.**

2% agarose gel EMSA of constant amounts of individually purified DNA origamis complexed with increasing amounts of CP; a) Ascending ratio  $\chi = 0.08 - 0.2$  for HB and DWS showing minimal or no upward shift in the bands, which is followed by (b) coomassie protein stain; c) Further increase of CP ratio  $\chi = 0.32 - 1$  for HB and DWS observed significant binding of CP on DNAs hindering the electrophoretic mobility of complexes (boxed) is evident, followed by (d) Coomassie protein stain. Purified DNA origamis with a different dilution of CP and 1KB marker were used as a reference.

#### 4.2.2 Purification of encapsulated assemblies

Purification and detection of any structural modification in the resulting fabricated nanoassemblies was carried out by analytical SEC. The elution of DNAs and CPs was carefully monitored at  $\lambda = 260$  nm and 280 nm, respectively and the corresponding fractions, where both peaks co-elute (Figure 4-3), were used for further microscopic characterisation. The most prominent co-elution peak of DNAs (260 nm) and CPs (280 nm) at the same volume (2.0 mL) (Figure 4-3a and b) suggests that encapsulation in the given assembly conditions resulted in fabricated stable monomeric structures. Meanwhile, comparing the peaks of CP-DNAs with FPLC chromatogram of previously investigated CP-QDs (quantum dots) (50), as we performed elution in similar conditions, we can assume the expected size of fabricated nanoassemblies is  $\geq T = 3$  particles. The shape and morphology of the fabricated assembly (pH 7.5, 0.3 M NaCl) is meant to vary as the CP dimers interaction are weak at high pH, and the CP-cargo interactions become dominant and determine the resulted assembly size

(50, 52, 53).

Meanwhile, the elution chromatogram for fabricated HB and DWS at 2 mL depicts the relative absorbance ratio (280 nm/260 nm)  $\approx 1.8$ , comparable to the study reported by Cornelissen *et al.* showing that absorbance ratio  $> 1$ , found to be the characteristic feature of CCMV capsids containing different DNA based cargo (53). Thus, we suggest that the peaks observed at 2.0 mL correspond to the assembled DN-CPs nanoassemblies. Whereas, in the control experiment (for native CCMV capsid) in similar assembly conditions, the peak at 2.0 mL resulted in higher absorbance ratio (280 nm/260 nm)  $\approx 5.2$  (Figure 4-3c) revealing the presence of capsids in the fraction and absence of any contaminants (DNA/RNA) (54). It is noteworthy that the other peak found at 1.5 mL for DWS (Figure 4-3b) is likely originating from unencapsulated or partially assembled structures.

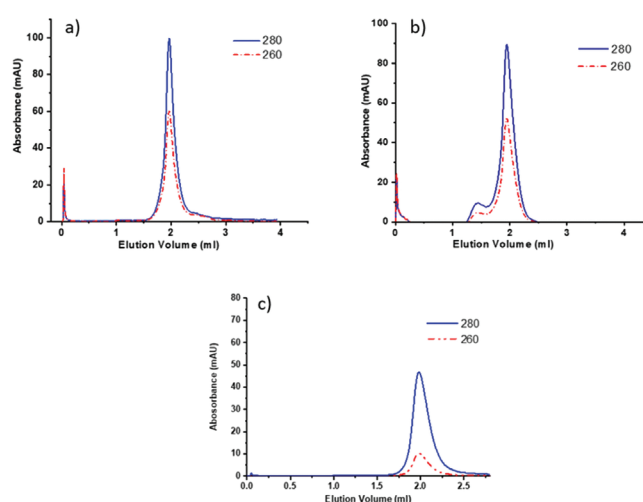


**Figure 4-3 Representative size-exclusion chromatograms for analysis.**

The purification has been carried out with encapsulation buffer (pH 7.5); a) CP fabricated HB; b) CP fabricated DWS; c) only-CP (control).

### 4.2.3 Characterisation of purified encapsulated DNAs

Microscopy techniques (TEM and STEM) and Dynamic Light Scattering (DLS) experiments were further employed to verify the encapsulation of DNAs within CPs and investigating their sizes, respectively.

#### 4.2.3.1 Microscopy (TEM/STEM)

The FPLC fraction containing the purified encapsulated assemblies eluting at the  $V=2$  mL was isolated from both HB and DWS CP mixtures. The collected samples were then examined under the microscope to detect the presence of any structural modifications resulting from the attachment of CPs to bare DNAs. First, TEM was carried out for the sample with  $\chi=0.2$  for both the designs to detect changes in the morphology of DNAs (Figure 4-4). Detailed examination of these fabricated assemblies



revealed the formation of multiple capsids (clusters) around the DNAs in CP-HB nanoassembly (Figure 4-4a). Similar clusters were also reported to be formed with >3000 nt length RNA-CP encapsulation (44). The overlong DN size can be held responsible for the formation of these clusters. Rigid confirmation of HB does not permit strict wrapping, which might have resulted in the formation of observed clusters (Figure 4-4a). However, for DWS, the presence of a thickened morphology with a discernible protein corona on the edges of nanostructures was observed (Figure 4-4b), but this is not homogenous across the sample. This difference in the framework of these two fabricated DNAs may be attributed to the difference in their distinct shapes while other conditions remained the same.

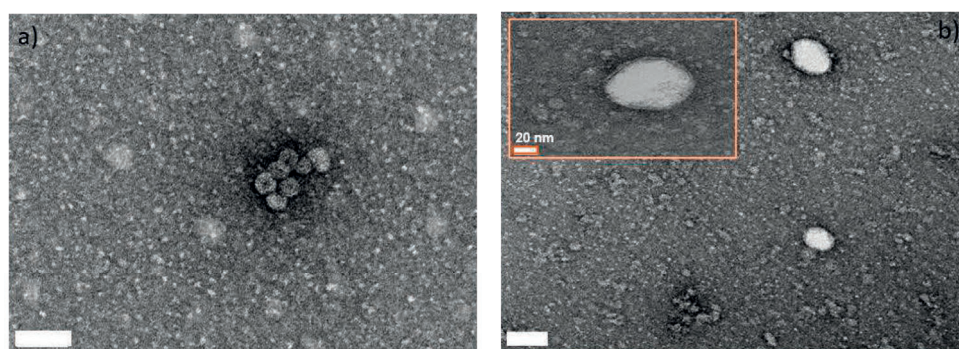


**Figure 4-4 Negative stain TEM micrographs of fabricated DNAs mixed with CPs.**

a) Images of HB samples  $\chi=0.2$  showing an arrangement of cluster capsids (multiplets); b) Images of DWS samples  $\chi=0.2$  displaying thickened layer morphology and protein corona formation on the edges (inset). Scale bar in A and B 50 nm.

The formation of nanoassemblies likely originates from electrostatic interaction between the DNAs and CP-dimers depending on the template shape. However, as the shift in EMSA was only minimal for these samples, we believe that the CP/DNA ratio was too low for the complete fabrication or high surface coverage. So, imaging was also carried out for samples with increased CP ratio ( $\chi = 1$ ), which showed substantial gel migration (Figure 4-2c). At high CP/DN ratio ( $\chi \geq 0.32$ ) the formation of CCMV-based VLPs around the DNAs resulted in particles, which are larger than the  $T=3$  structure (native CCMV) (55).

Scanning transmission electron microscopy (STEM) was also incorporated to investigate the morphology of the resulting nanoassemblies (encapsulated DNA origami-CP complexes). STEM appears to be a very similar technique to TEM in function but it can provide different information having the ability to capture the backscattered electrons or secondary electrons. The bright-field STEM of HB ( $\chi=1$ ) (Figure 4-5a) characterised the abundance of capsids attached to the nanostructures covering its surface, making them appear as swollen particles. One of the noticeable differences in STEM image is the attachment of capsids to the DNAs (inset). This resulted from the bulk adsorption of CPs into the negative template (DNAs) induced by electrostatic attractions followed by the structural organisation of capsids. The excess capsids are translocated to the exterior surface

leading to the creation of nucleocapsids, which have been reported with the use of different lengths of RNA (56). Similarly, the TEM of the same sample (Figure 4-5b) verified the formation of the nanoassemblies. The myriad of white capsids on the background with dimensions < 20 nm confirms the excess of CP dimers

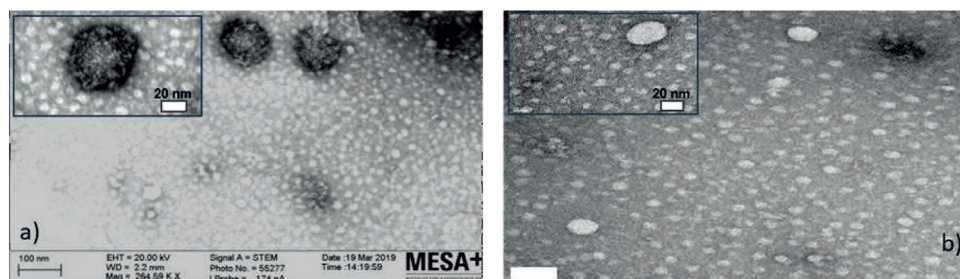


**Figure 4-5 Electron microscopy characterisation of fabricated assemblies HB ( $\chi = 1$ ).**

a) STEM (BF mode) images of the purified nanoassemblies having small white capsids in the background with large assemblies (inset); b) TEM image displaying a similar structure as in (a). Scale bar in a) is 100 nm and b) is 50 nm.

4

Further, the dark field STEM micrographs for DWS ( $\chi=1$ ) (Figure 4-6a) exhibited the bright swollen assemblies with dimension  $\sim 50$  nm having the white capsid particles adhered all over the surfaces (inset). The white capsids-like structures in the background can be explained by the excess of CPs interacting with DNAs. In the TEM, the homogeneously dispersed distinct nanoassemblies have similar dimension and morphology as those in the STEM image (Figure 4-6b). In TEM, we observe empty spherical capsids on the sample, which are approximately 18 nm in diameter and have an 8 nm cavity are likely to have a  $T=1$  confirmation. The empty capsids detected during encapsulation of negatively charged DN with  $> 0.3$  M NaCl at neutral pH could be a function of the staining agent (2% uranyl acetate) used in EM (electron microscopy) imaging. The acidic pH of uranyl acetate ( $\sim 4.5$ ) can induce the CCMV capsid formation (43). Moreover, we preclude the assumptions having the role of any free or loosely bound staples strands serving as a template for the assembly of these capsids; because electrophoretic assays monitored the structural integrity of DNAs after every step such as coating and purification (data not shown).



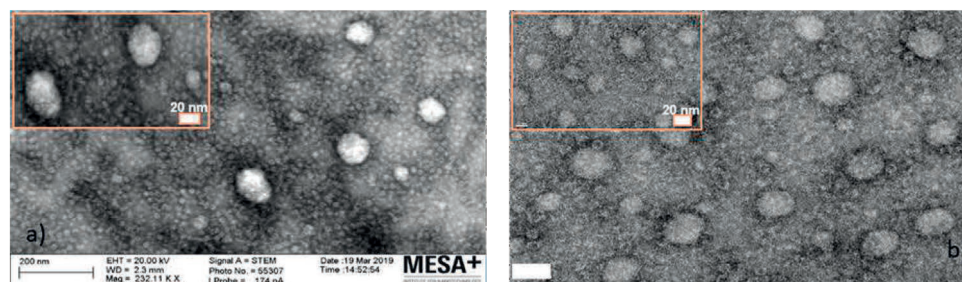


**Figure 4-6 Electron microscopy characterisation of fabricated assemblies DWS ( $\chi = 1$ ).**

a) STEM (DF mode) images of the purified nanoassemblies with small white capsid on the background and large assemblies (inset); b) TEM showing the large fabricated particles along with few spherical empty capsids. Scale bar in a) is 200 nm and in b) is 50 nm.

#### 4.2.3.2 Size estimation of the encapsulated assemblies

Dynamic Light Scattering (DLS) experiments further verified the particle size distribution of the nanoassemblies. All measurements were obtained under similar conditions, as described in Chapter 3. Three separate DLS measurements were averaged to plot the particle size distribution after the encapsulation of both designs (HB and DWS) (Figure 4-7).

4

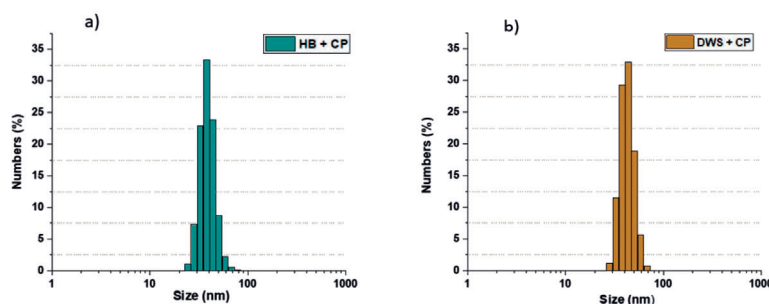


**Figure 4-7 Average size distribution of encapsulated nano assemblies on DLS.**

a) HB+CP; b) DWS+CP All purified samples were diluted to make 1 ml volume required for measurements.

DLS results indicate the existence of monodisperse particles with approximate particle sizes as HB ( $39.6 \pm 4.4$  nm) and DWS ( $44.2 \pm 3.6$  nm), respectively. It also confirms the absence of any aggregates or impurities in all the purified encapsulated fractions.

## 4.3 Conclusions

In this chapter, we studied the encapsulation of DNs in CCMV-based CPs at high mass ratios ( $\chi \Rightarrow >0.32$ ). The experimental work displayed the mass transfer of capsid protein extends all over the DN surface, leading to the formation of nanoassemblies. Hence, in conjunction with theory, we conclude that the polyanionic material (DNs) are majorly ascribed to electrostatic wonder with CPs under the applied assembly conditions (44). The modular DNA origamis used in the fabrications is

substantially rigid in the selected designs and hence, twisting and bending is not observed in the microscopic characterisation. The presence of enigmatic  $T=1$  particles observed in imaging is possibly due to the uranyl acetate induced capsid formation. However, their exact assembly principle is unclear and requires further studies under the presence of different DN templates and conditions.

The CCMV capsid proteins form a “protein corona” around DNAs, potentially enhancing cell internalisation efficiency and biostability as drug-delivery vehicles. The corona also can offer protection against nuclease digestion present in the extracellular biological environment (57). DNA nanostructures trigger an immune response, while these particular masking approaches can curtail these reactions for *in vivo* applications (36, 57). The CCMV-CP encapsulation also shows promising results in escaping the endosomal pathway, facilitating the delivery of the payloads (drugs) to the specific sites inside the cell (58).

The fabrication approach discussed here potentially improves the *in vivo* stability while curbing the cytotoxicity and addressing the challenge of cellular uptake and immunogenicity. Moreover, this approach can be adapted to encapsulate other organic nanostructures or biomaterials to obtain functional nanohybrid assemblies for *in vitro* and *in vivo* applications. This work also highlights the possibility of future studies investigating CCMV or any other model viruses encapsulation mechanistically with modular DNA origamis under varying conditions.

4

#### 4.4 Acknowledgements

I sincerely acknowledge Mark de Ruiter for introduction to the CCMV (CP) isolation and assembly studies. I want to thank Regine van der Hee for her help in FPLC set up. I also appreciate Rico Keim and Mark Smithers for their assistance in TEM and STEM imaging and analysis, respectively. Special thanks to Veikko Linko (Aalto University) for his suggestion in mass ratio calculation of CP/Origami and its encapsulation procedures.

#### 4.5 Materials and Methods

Unless specified otherwise, all compounds were purchased from Sigma-Aldrich, and all buffers were prepared with 18 M $\Omega$ ·cm MilliQ (Millipore) water.

##### 4.5.1 DNA origami preparation

24-helix bundle (HB) and double-wall square (DWS) DNA origamis were used in this chapter and were formulated/constructed/assembled using methods described in Chapter 3.

##### 4.5.2 Production of CCMV CPs

CCMV was produced in black-eyed pea plants according to the method developed by Verduin and adapted by Comellas Aragonès (59, 60). In short, ten days after planting the beans, cowpea plants

4 were infected with the virus, followed by another ten days of growth. The leaves were then harvested without the stems, crushed and mixed with a buffer containing 0.2 M sodium acetate, 10 mM ascorbic acid, 10 mM disodium EDTA, pH 4.8. The leaf-virus mixture was filtered using a cheesecloth, centrifuged and again filtered, followed by PEG-6000 precipitation. The virus was reconstituted in pH 5 acetate buffer and subjected to 16h centrifugation in 33% (w/w) CsCl at 10°C and 40 000 rpm in a Sorvall WX80 ultracentrifuge. Successful virus formation was verified using size-exclusion chromatography on a superose 6/300 column, UV-Vis absorbance and SDS-page using Mini-PROTEAN® TGX Stain-Free™ precast gels. The virus was dialysed from virus buffer (0.1 M sodium acetate, 1 mM disodium EDTA, 1 mM sodium azide, buffered at pH 5.0) to RNA isolation buffer (50 mM Tris, 0.5 M CaCl<sub>2</sub>, 1 mM DTT, buffered at pH 7.5). The viral RNA was precipitated and pelleted by overnight centrifugation at 14100 rcf (relative centrifugal force). The supernatant containing dimer of the CPs was purified using 5X clean buffer (50 mM Tris, 500 mM NaCl buffered at pH 7.5), followed by dialysis, with three times buffer replacement, against 5x assembly buffer (250 mM Tris-HCl, 250 mM NaCl, 50 mM KCl, 25 mM MgCl<sub>2</sub>, pH 7.2). Successful removal of the RNA from CPs was confirmed by a 280/260 ratio above 1.5 and the concentration of CP was determined using a 280 nm extinction coefficient of 24075 M<sup>-1</sup>cm<sup>-1</sup>.

#### 4.5.3 Encapsulation: fabrication of DNA origami with CPs

Assembly was induced by lowering the salt concentration in the presence of DNAs. The CCMV- CP in 5X assembly buffer (250 mM Tris, 250 mM NaCl, 50 mM KCl, 25 MgCl<sub>2</sub>, pH 7.2) was mixed in a 4:1(v/v) ratio with the DN in MilliQ. The solution was diluted to achieve a final mass ratio 6:1 of CP to DNAs (i.e., 0.65<sub>CP</sub>/0.11<sub>DN</sub> µg/µl), which is considered the optimum ratio for RNA encapsulation(54). This resulted in 1X clean buffer (50 mM Tris, 50 mM NaCl, 10 mM KCl, 5 mM MgCl<sub>2</sub> pH 7.2), which was determined to be optimal for capsid assembly around nucleic acids. The assembly mixtures were incubated overnight at 4°C. The resulting encapsulation was not sufficient to observe any significant modification verified through AGE and microscopy techniques.

Later, the encapsulation conditions were optimised and studied over a wide range of samples with CP/DNA origami mass ratio to achieve a direct comparison among them. The concept of ratio parameter  $\chi$  is based upon the molar mass ratio between two biomolecules in solution, which is described as the number of CPs divided by the number of DNA base pairs (bp) in the sample solution ( $n_{CP}/n_{DNA}(bp)$ ) (37, 61). The nbp taken into account for mass calculation was different for the two DNAs, i.e.,  $n_{DNA}(bp)$  HB and  $n_{DNA}(bp)$  DWS is 3600 and 4650 respectively, which resulted in varied excess of CP for same mass ratio ( $\chi$ ) in the two designs as shown in Table 4.1. The assembly was performed in the encapsulation buffer (50 mM Tris, 300 mM NaCl, 10 mM MgCl<sub>2</sub>, pH 7.5). The DN and CPs were mixed in the assembly tubes for a revolving incubation at 4°C for 48–72 hours.

#### 4.5.4 Electrophoretic Mobility Shift Assay (EMSA)

A 2% native agarose gel electrophoresis stained with SYBR-Safe DNA stain (ThermoFisher) was used to show the migration (shift) of the DNA in the gel. The gels were stained overnight with Colloidal Coomassie stain (BioRad), followed by overnight destaining in MilliQ and were subsequently analysed on gel-doc EZ imaging system (BioRad).

#### 4.5.5 Purification of encapsulated assemblies

Analysis and purification of the assembled VLPs was performed by size-exclusion chromatography (SEC) using a Superose 6 10/100 GL column on FPLC (Fast protein liquid chromatography) system (GE healthcare), eluting at 0.1 mL/min with encapsulation buffer. Absorption was mainly monitored at  $\lambda = 260$  nm and 280 nm. The collected fractions were concentrated using 50kDa MWCO filters at 4°C using 5000G for 10mins for further characterisations.

#### 4.5.6 STEM/TEM of purified assemblies

The samples were prepared using the same method as discussed earlier for TEM imaging in chapter 3. The sample grids were also imaged with Zeiss Merlin microscope in (S)TEM mode with dark and bright field options. The resulting images were analysed using ImageJ software.

4

#### 4.5.7 Dynamic Light Scattering (DLS)

Measurements were made on a Nano ZS machine by Malvern Instruments, and the data were extracted using the solution viscosity of water and refractive index of DN<sub>s</sub>=2.1 in the standard settings of the company's software (Zetasizer).

## 4.6 References

1. Linko V, Ora A, Kostianen MA. DNA Nanostructures as Smart Drug-Delivery Vehicles and Molecular Devices. *Trends in biotechnology*. 2015;33(10):586-94.
2. Knudsen JB, Liu L, Bank Kodala AL, Madsen M, Li Q, Song J, et al. Routing of individual polymers in designed patterns. *Nat Nanotechnol*. 2015;10(10):892-8.
3. Sacca B, Niemeyer CM. Functionalization of DNA nanostructures with proteins. *Chem Soc Rev*. 2011;40(12):5910-21.
4. Selmi DN, Adamson RJ, Attrill H, Goddard AD, Gilbert RJ, Watts A, et al. DNA-templated protein arrays for single-molecule imaging. *Nano Lett*. 2011;11(2):657-60.
5. Ramakrishnan S, Subramaniam S, Stewart A, Grundmeier G, Keller A. *ACS Appl. Mater. Interfaces*. 2016;8:31239.
6. Linko V, Nummelin S, Aarnos L, Tapio K, Toppari JJ, Kostianen MA. DNA-Based Enzyme Reactors and Systems. *Nanomaterials (Basel)*. 2016;6(8).
7. Perrault SD, Shih WM. Virus-inspired membrane encapsulation of DNA nanostructures to achieve in vivo stability. *ACS Nano*. 2014;8(5):5132-40.
8. Krishnan Y, Simmel FC. Nucleic acid based molecular devices. *Angewandte Chemie International Edition*. 2011;50(14):3124-56.
9. Okholm AH, Kjems J. DNA nanovehicles and the biological barriers. *Adv Drug Deliv Rev*. 2016;106(Pt A):183-91.
10. Madhanagopal BR, Zhang S, Demirel E, Wady H, Chandrasekaran AR. DNA Nanocarriers: Programmed to Deliver. *Trends Biochem Sci*. 2018;43(12):997-1013.
11. Bujold KE, Lacroix A, Sleiman HF. DNA nanostructures at the interface with biology. *Chem*. 2018;4(3):495-521.
12. Ke Y, Castro C, Choi JH. Structural DNA Nanotechnology: Artificial Nanostructures for Biomedical Research. *Annu Rev Biomed Eng*. 2018;20:375-401.
13. Smith D, Schuller V, Engst C, Radler J, Liedl T. Nucleic acid nanostructures for biomedical applications. *Nanomedicine (Lond)*. 2013;8(1):105-21.
14. Chao J, Liu H, Su S, Wang L, Huang W, Fan C. Structural DNA nanotechnology for intelligent drug delivery. *Small*. 2014;10(22):4626-35.
15. Ke Y, Sharma J, Liu M, Jahn K, Liu Y, Yan H. Scaffolded DNA origami of a DNA tetrahedron molecular container. *Nano letters*. 2009;9(6):2445-7.
16. Andersen ES, Dong M, Nielsen MM, Jahn K, Subramani R, Mamdouh W, et al. Self-assembly of a nanoscale DNA box with a controllable lid. *Nature*. 2009;459(7243):73.
17. Kuzuya A, Komiyama M. Design and construction of a box-shaped 3D-DNA origami. *Chem Commun (Camb)*. 2009(28):4182-4.
18. Jiang Q, Song C, Nangreave J, Liu X, Lin L, Qiu D, et al. DNA Origami as a Carrier for Circumvention of Drug Resistance. *Journal of the American Chemical Society*. 2012;134(32):13396-403.
19. Zhang Q, Jiang Q, Li N, Dai L, Liu Q, Song L, et al. DNA origami as an in vivo drug delivery vehicle for cancer therapy. 2014;8(7):6633-43.
20. Zhao YX, Shaw A, Zeng X, Benson E, Nystrom AM, Hogberg B. DNA origami delivery system for cancer therapy with tunable release properties. *ACS Nano*. 2012;6(10):8684-91.
21. Schuller VJ, Heidegger S, Sandholzer N, Nickels PC, Suhartha NA, Endres S, et al. Cellular immunostimulation by CpG-sequence-coated DNA origami structures. 2011;5(12):9696-702.
22. Li J, Pei H, Zhu B, Liang L, Wei M, He Y, et al. Self-assembled multivalent DNA nanostructures for noninvasive intracellular delivery of immunostimulatory CpG oligonucleotides. 2011;5(11):8783-9.
23. Mohri K, Nishikawa M, Takahashi N, Shiomi T, Matsuoka N, Ogawa K, et al. Design and development of nanosized DNA assemblies in polypod-like structures as efficient vehicles for immunostimulatory CpG motifs to immune cells. *ACS Nano*. 2012;6(7):5931-40.
24. Mohri K, Kusuki E, Ohtsuki S, Takahashi N, Endo M, Hidaka K, et al. Self-assembling DNA dendrimer for effective delivery of immunostimulatory CpG DNA to immune cells. *Biomacromolecules*. 2015;16(4):1095-101.
25. Bhatia D, Surana S, Chakraborty S, Koushika SP, Krishnan Y. A synthetic icosahedral DNA-based host-cargo complex for functional in vivo imaging. *Nat Commun*. 2011;2:339.
26. Keum JW, Ahn JH, Bermudez H. Design, assembly, and activity of antisense DNA nanostructures. *Small*. 2011;7(24):3529-35.
27. Kocabey S, Meinhart H, MacPherson IS, Cassinelli V, Manetto A, Rothenfusser S, et al. Cellular Uptake of Tile-Assembled DNA Nanotubes. *Nanomaterials (Basel)*. 2014;5(1):47-60.
28. Lee H, Lytton-Jean AK, Chen Y, Love KT, Park AI, Karagiannis ED, et al. Molecularly self-assembled nucleic acid nanoparticles for targeted in vivo siRNA delivery. *Nat Nanotechnol*. 2012;7(6):389-93.
29. Douglas SM, Bachelet I, Church GM. A logic-gated nanorobot for targeted transport of molecular

- payloads. *Science*. 2012;335(6070):831-4.
30. Simmel FC. DNA-based assembly lines and nanofactories. *Curr Opin Biotechnol*. 2012;23(4):516-21.
  31. Delebecque CJ, Lindner AB, Silver PA, Aldaye FA. Organization of intracellular reactions with rationally designed RNA assemblies. *Science*. 2011;333(6041):470-4.
  32. Wilner OI, Weizmann Y, Gill R, Lioubashevski O, Freeman R, Willner I. Enzyme cascades activated on topologically programmed DNA scaffolds. *Nat Nanotechnol*. 2009;4(4):249-54.
  33. Blanco E, Shen H, Ferrari M. Principles of nanoparticle design for overcoming biological barriers to drug delivery. *Nat Biotechnol*. 2015;33(9):941-51.
  34. Okholm AH, Nielsen JS, Vinther M, Sorensen RS, Schaffert D, Kjems J. Quantification of cellular uptake of DNA nanostructures by qPCR. *Methods*. 2014;67(2):193-7.
  35. Bastings MM, Anastassacos FM, Ponnuswamy N, Leifer FG, Cuneo G, Lin C, et al. Modulation of the cellular uptake of DNA origami through control over mass and shape. *Nano letters*. 2018;18(6):3557-64.
  36. Wang P, Meyer TA, Pan V, Dutta PK, Ke Y. The Beauty and Utility of DNA Origami. *Chem*. 2017;2(3):359-82.
  37. Mikkilä J, Eskelinen A-P, Niemelä EH, Linko V, Frilander MJ, Törmä Pi, et al. Virus-encapsulated DNA origami nanostructures for cellular delivery. *Nano letters*. 2014;14(4):2196-200.
  38. Kiviaho JK, Linko V, Ora A, Tiainen T, Jarvihaavisto E, Mikkilä J, et al. Cationic polymers for DNA origami coating - examining their binding efficiency and tuning the enzymatic reaction rates. *Nanoscale*. 2016;8(22):11674-80.
  39. Akkus Sut P, Tunc CU, Culha M. Lactose-modified DNA tile nanostructures as drug carriers. *Journal of drug targeting*. 2016;24(8):709-19.
  40. Chan MS, Tam DY, Dai Z, Liu LS, Ho JW, Chan ML, et al. Mitochondrial Delivery of Therapeutic Agents by Amphiphilic DNA Nanocarriers. *Small*. 2016;12(6):770-81.
  41. Lacroix A, Edwardson TGW, Hancock MA, Dore MD, Sleiman HF. Development of DNA Nanostructures for High-Affinity Binding to Human Serum Albumin. *J Am Chem Soc*. 2017;139(21):7355-62.
  42. Auvinen H, Zhang H, Nonappa, Kopilow A, Niemela EH, Nummelin S, et al. Protein Coating of DNA Nanostructures for Enhanced Stability and Immunocompatibility. *Adv Healthc Mater*. 2017;6(18).
  43. Garmann RF, Comas-Garcia M, Gopal A, Knobler CM, Gelbart WM. The assembly pathway of an icosahedral single-stranded RNA virus depends on the strength of inter-subunit attractions. *J Mol Biol*. 2014;426(5):1050-60.
  44. Garmann RF, Comas-Garcia M, Knobler CM, Gelbart WM. Physical Principles in the Self-Assembly of a Simple Spherical Virus. *Acc Chem Res*. 2016;49(1):48-55.
  45. Mukherjee S, Pfeifer CM, Johnson JM, Liu J, Zlotnick A. Redirecting the coat protein of a spherical virus to assemble into tubular nanostructures. *Journal of the American Chemical Society*. 2006;128(8):2538-9.
  46. Maassen SJ, van der Ham AM, Cornelissen JJ. Combining protein cages and polymers: from understanding self-assembly to functional materials. *ACS Publications*; 2016.
  47. Arnida, Malugin A, Ghandehari H. Cellular uptake and toxicity of gold nanoparticles in prostate cancer cells: a comparative study of rods and spheres. *J Appl Toxicol*. 2010;30(3):212-7.
  48. Douglas T, Young M. Host-guest encapsulation of materials by assembled virus protein cages. *Nature*. 1998;393(6681):152-5.
  49. Young M, Debbie W, Uchida M, Douglas T. Plant viruses as biotemplates for materials and their use in nanotechnology. *Annu Rev Phytopathol*. 2008;46:361-84.
  50. Tagit O, De Ruiter M, Brasch M, Ma Y, Cornelissen J. Quantum dot encapsulation in virus-like particles with tuneable structural properties and low toxicity. *RSC advances*. 2017;7(60):38110-8.
  51. Chiu YTE, Li H, Choi CHJ. Progress toward Understanding the Interactions between DNA Nanostructures and the Cell. *Small*. 2019;15(26):e1805416.
  52. Liu A, Verwegen M, de Ruiter MV, Maassen SJ, Traulsen CH-H, Cornelissen JJ. Protein cages as containers for gold nanoparticles. *The Journal of Physical Chemistry B*. 2016;120(26):6352-7.
  53. Brasch M, Putri RM, de Ruiter MV, Luque D, Koay MS, Castón JR, et al. Assembling enzymatic cascade pathways inside virus-based nanocages using dual-tasking nucleic acid tags. *Journal of the American Chemical Society*. 2017;139(4):1512-9.
  54. Cadena-Nava RD, Comas-Garcia M, Garmann RF, Rao A, Knobler CM, Gelbart WM. Self-assembly of viral capsid protein and RNA molecules of different sizes: requirement for a specific high protein/RNA mass ratio. *Journal of virology*. 2012;86(6):3318-26.
  55. Liepold LO, Revis J, Allen M, Oltrogge L, Young M, Douglas T. Structural transitions in Cowpea chlorotic mottle virus (CCMV). *Physical biology*. 2005;2(4):S166.
  56. Garmann RF, Comas-Garcia M, Koay MS, Cornelissen JJ, Knobler CM, Gelbart WM. Role of electrostatics in the assembly pathway of a single-stranded RNA virus. *Journal of virology*. 2014;88(18):10472-9.
  57. Lee DS, Qian H, Tay CY, Leong DT. Cellular processing and destinies of artificial DNA nanostructures. *Chemical Society Reviews*. 2016;45(15):4199-225.
  58. de Ruiter M, van der Hee R, Driessen A, Keurhorst E, Hamid M, Cornelissen J. Polymorphic assembly of

- virus-capsid proteins around DNA and the cellular uptake of the resulting particles. *Journal of Controlled Release*. 2019;307:342-54.
59. Verduin BJM. The preparation of CCMV-protein in connection with its association into a spherical particle. *FEBS Letters*. 1974;45(1):50-4.
60. Comellas-Aragones M, Engelkamp H, Claessen VI, Sommerdijk NAJM, Rowan AE, Christianen PCM, et al. A virus-based single-enzyme nanoreactor. *Nat Nano*. 2007;2(10):635-9.
61. Linko V, Mikkilä J, Kostianen MA. Packaging DNA Origami into Viral Protein Cages. *Virus-Derived Nanoparticles for Advanced Technologies*: Springer; 2018. p. 267-77.



## **CHAPTER 5**

---

# **Creating Nanocarriers with Drug Loaded and Virus Encapsulated DNA Origamis**

---

Part of this chapter will be submitted.



## 5 CREATING NANOCARRIERS WITH DRUG LOADED AND VIRUS-ENCAPSULATED DNA ORIGAMIS

### 5.1 Introduction

Artificial nanoparticles have long been recognised and studied for their use in smart and targeted drug delivery due to their ability to enhance therapeutics physicochemical properties (1, 2). The earliest nanocarriers were liposomes (3) and cationic dendric polymers (4), having the capacity to prolong circulation time, increase water solubility and enhance drug release. These days many organic and inorganic nanoparticles like gold nanoparticles (5), mesoporous silica nanoparticles (6), carbon nanomaterials (7), quantum dots (8), iron oxide nanoparticles (9) are in use for effective drug delivery. However, the use of inorganic nanomaterials has also posed some safety concerns and side effects (10-12).

#### 5

Meanwhile, the research developments in structural DNA nanotechnology, tethering DNA nanostructures (DNs) functionality with modifications at the nanoscale level, exhibit their great potential in drug delivery systems. The DN possess some unique features: a) predictable and well-defined structure; b) high capacity of cargo loading; c) ability to be internalised by the cells; d) structural stability in physiological conditions and e) biocompatibility (1). DN have been shown to precisely deliver fluorescent dye molecules into target cells (13, 14). In 2006, Erben *et al.* encapsulated single proteins (cytochrome c) in the cavity of a DNA tetrahedron (15), exploring how DN could be used as nanocarriers in drug delivery applications. The tightly packed nature and flexibility in cargo loading favor the direct binding of drugs (e.g., anthracyclines doxorubicin and daunorubicin) (16). Doxorubicin (Dox), an anthracycline chemotherapeutic, is a potent drug used to treat a wide range of cancers binding non-covalently (intercalating) to the DNA inhibiting the macromolecular biosynthesis. Dox is known to be delivered by numerous nanocarriers like polymer micelles nanoparticles, liposomes and inorganic materials (17). DN also offer a high number of intercalation sites to Dox, presenting a high local dose of the drug. Applications have been widely studied in different cell lines over the last decade (18). Jiang *et al.*, developed a DN-based drug delivery system, achieving high-level Dox loading efficiency into 2D origami triangles and 3D tubes compared to an unstructured ds-DNA (19).

Further, Zhao *et al.*, reported that the DN could be designed with a function of a global twist, i.e. by adding an extra base-pair after a certain distance in the structure, to vary their drug (dox) loading capabilities and release efficiency. The effect of dox-loaded with the twisted DN showed increased cytotoxicity, while a decreased elimination rate was observed compared to free dox (20). In another study, Zhang *et al.* demonstrated the effect of DN as nanocarriers in MDA-MB-231 tumour-bearing mice, where the dox-loaded DNA triangle significantly decreased the tumour size in mice without

any marked toxicity in comparison to treatment with a dox (21).

In addition to the above findings, Halley *et al.*, probed daunorubicin (dauno) efficacy as an anticancer therapeutic loaded onto rod-shaped DNAs. The results highlighted that the dauno-loaded DNAs were able to circumvent drug-resistant leukaemia cell lines (HL-60ADR) (22). The dauno-DNA complex displayed stability for more than 24 hrs in cell culture media with effective drug uptake through endocytosis. Several examples from the literature support the promising outcome of the DNA-based delivery system, but there are still concerns for *in-vivo* stability, cellular uptake, biodistribution, and potential side effects. There is no established uptake route of DNA nanocarriers and the delivery of drug molecules to cells depends upon the type of cells (such as macrophages, monocytes and dendritic cells) (23). Therefore, improving the cellular uptake efficiency by modifying the DNA nanocarriers could be a practical approach, which can be performed by involving proteins like folate (13), cell-penetrating proteins (24), and transferrin (25).

Moreover, DNA nanocarriers, when coated with virus capsid proteins (CPs), exhibited increased transfection efficiency with prolonged stability and better efficacy (26). Further studies confirmed the enhancement in DNAs cell transfection ability and bioavailability by encapsulating with virus or virus inspired materials, discussed previously in chapter 2 and 4.

5

All the studies mentioned above imply the potential of noncovalent polymer coatings in uplifting the functionality of DNA as an excellent nanocarrier. Therefore, fabricating or attaching protein to DNA enables us to create a biomolecule-based nanocarrier, allowing precise control over the relative stoichiometry of coated proteins while delivering the loaded molecules to the nucleus of the cells, which is nearly impossible to achieve with endocytosis (27).

Here, we incorporated drug molecules (daunorubicin) into two selected DNAs (HB and DWS-see chapter 3 & 4 of this thesis) and analysed their drug loading efficiencies at different drug concentrations. Drug-loaded DNAs were then fabricated with CCMV-CP (capsid protein) and devised as a functional nanocarrier (28). The resulting nanocarriers were characterised for change in surface modification using multiple techniques, including electron microscopy.

Apart from developing a dauno- DNA nanocarrier for cancer therapeutics, this study can also be used to formulate a DNA nanostructure loaded with other payloads. Future work might be undertaken to improve CP attachment to the DNA origami containing a drug load, in order to develop new carriers with applications in, for example, medicine and nanotechnology.

## 5.2 Results and Discussion

### 5.2.1 Daunorubicin and its absorption at varying pH

The anthracycline daunorubicin (dauno) is a drug of choice for binding non-covalently into the

designed DNs and fabricating the complex with CCMV-CP potentially to create smart nanocarriers for drug delivery. Dauno is a positively-charged hydrophobic drug, which acts on cancer cells by inserting itself between the planar bases of double-stranded DNA and because of its hydrophobic nature, dauno phase out all interactions with water (29). Dauno was reported to have maximum absorption spectra of  $\lambda = 480$  and  $\lambda = 490$  nm observed with two different techniques - circular dichroism and fluorescence spectroscopy, respectively (30, 31). Hence, in initial stages, the measurements were performed at both wavelengths, but no noticeable difference was observed between the two. Dauno is neutral under physiological conditions in both polar and aqueous solutions due to the presence of an anthraquinone moiety.

The UV-absorbance was measured to assess the effect of different pH (4-8) on the absorbance of dauno in PBS (Figure 5-1), considering the *in-vitro* and *in-vivo* application of nanocarriers on cancer cells. A consistent absorbance profile of drug (daunorubicin) across varying pH levels was observed. The results distinctly suggested that there is hardly any effect of pH on the absorbance spectra, discarding the variable effects while measuring *in-vitro* drug release.

5

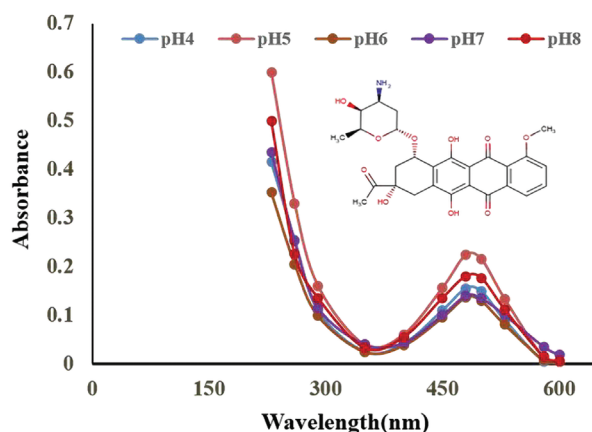
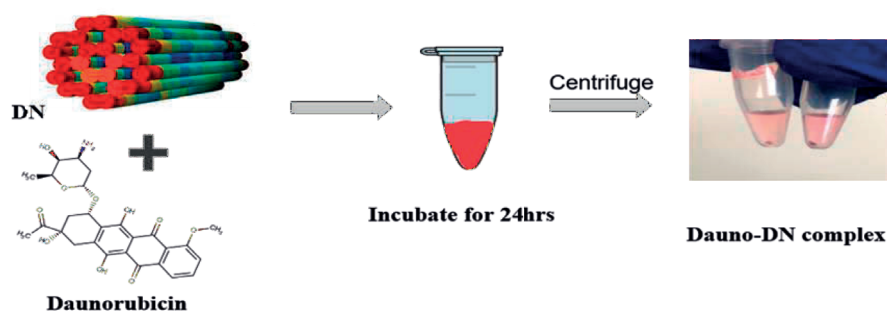


Figure 5-1 Effect of pH on daunorubicin absorption.

UV-absorption of PBS dissolved daunorubicin at different pH at  $\lambda=480$  nm wavelength

### 5.2.2 Drug incorporation and loading efficiency

While progressing towards formulating DNA-based noncarriers, the initial steps involve incorporating drug molecules into selected DNs. There has been a well-reported comprehensive approach described for dox loading and performing loading efficiency measurements for dox-loaded DNA origamis (19-21). A different method was published for dauno loading by Halley *et al.*, where they used the base pair binding ratio (BPBR); this method has been adapted in this thesis. The procedure for loading drug into DNs is illustrated in Figure 5-2.



**Figure 5-2 Schematic overview of dauno loading into DNs.**

Daunorubicin is incubated with DNs for 24 hrs at room temperature. The red DNA pellets and excess drug as supernatant were collected after centrifugation.

The drug loading capacity of DNs has been quantified in terms of base-pair binding ratio (BPBR) of drug molecules per dsDNA base pair in the DNs and the fraction of drug-loaded. One of the qualitative techniques, agarose gel electrophoresis, was used to optimise the drug loading as per BPBR for the selected DNs designs. The varying dauno concentrations (0.5-3.5 BPBR) were incubated with 30 nM DNs to check the band mobility and reverse migration of excessive (free) drug in the supernatant, collected after centrifugation of the incubated mixtures (Figure 5-3).

5

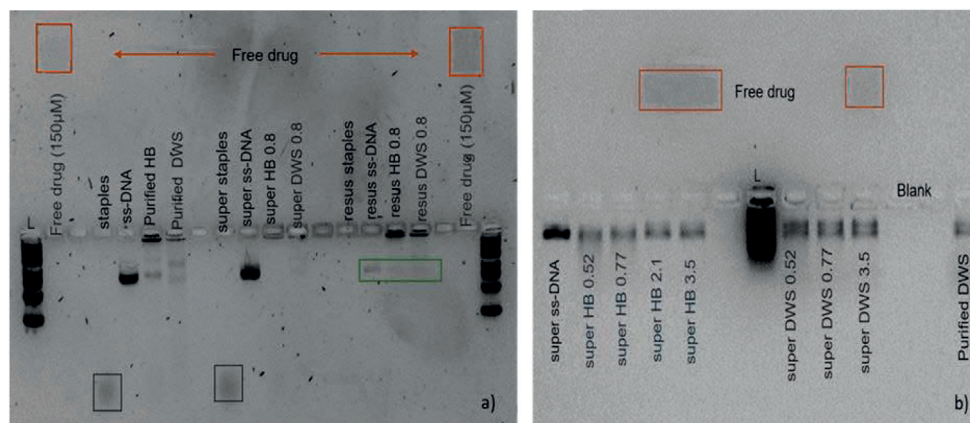


**Figure 5-3 AGE to assess BPBR effect with drug-loaded supernatant.**

The supernatant collected after centrifugation and resuspended pellets of drug complexes run on 1.8% AGE optimising the BPBR for drug loading into the DNs (HB and DWS).; a) The DNs with reduced intensity and slow migration in the resuspended bands (green-boxed), while controls (staples and scaffolds) showing no binding of the drug at same BPBR; b) For BPBR<1.0, the free drug in a supernatant fraction is hard to detect due to low concentration while increasing the BPBR>2.0 the drug loading is evident. L= DNA ladder and purified DNs used as references.

The migration of daunorubicin (free drug) in the opposite direction (towards the negative pole) in agarose gel confirmed its positive nature. The staples and scaffold (M13mp18) were ss nucleic acids and hence, not preferred for drug binding, while the selected designs for drug-loading at similar drug concentrations (0.8 BPBR) enact a quasi binder, confirmed with low-intensity bands in the

resuspended pellets (Figure 5-3a). However, the other gel presented for the supernatant with different drug concentration mixtures, by observing the free (unbounded) drug in the reverse direction, while the DNA bands were still intact at the respective positions; we can suggest that BPBR > 2.0 worked successfully for drug loading in both of our selected designs (HB and DWS) (Figure 5-3b). The results of AGE experiments corroborate that drug loading works more efficiently at higher BPBR>2.0 in both the designs (HB and DWS). However, the drug loading was also achieved with BPBR < 1.0, but due to the limited amount of free drug in the supernatant, it was hard to be detected in gel electrophoresis, though it has been confirmed later during the drug quantification calculation steps in absorbance measurements as discussed in next section.

To ascertain the effect of BPBR on drug loading efficiency within DNs, we plotted varying drug concentration (BPBR:0.5-7.1) mixed with DNs concentration  $30 \times 10^{-9}$  M, all for 24 hours. The resulting loading efficiency was linearly related to the amount of drug concentration in the reaction, which is consistent with prior studies (22). It was noted that the loading efficiency could be controlled by increasing the amount of drug in the mixture, we achieved up to ~80% of loading efficiency by this method for both DNs (Figure 5-4). Meanwhile, there are minor differences in loading efficiency observed between two DNs at the same BPBR; this could be due to one conformation (HB) serving with more intercalation sites.

5

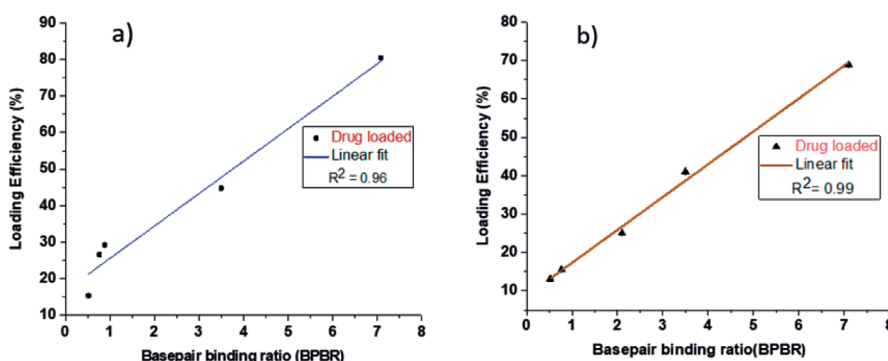


Figure 5-4 Drug loading efficiency vs BPBR

Loading efficiency (%) of the dauno in both the DNA nanostructures (HB and DWS) with linear regression. Varying concentrations of drug (BPBR) were added to nanostructures (30nM) for 24 hrs at room temperature followed by free drug removal. The amount of loaded drug was determined colourimetrically by absorbance; a) HB and b) DWS. Data presented as normalised mean relative intensity  $\pm$  SD in triplicate.

Moreover, with BPBR>2.0, we cannot rule out the possibility of drugs binding to the minor groove and physically wrapping around the poly-anionic backbone of the DNs. Nevertheless, such dauno molecules are also susceptible to detach from the surface in the course of centrifugation or CP incubation. Interestingly, a recent study by Ijas *et al.*, discusses the aggregation mechanism of doxorubicin (anthracycline drug), explaining how factors such as pH, ionic strength and incubation time affecting spectral properties of the drug, leading to overestimation of the binding efficiencies

(32). In the experimental conditions used for dauno loading studies, we didn't observe drug aggregations; however, more detailed studies are needed to exclude this entirely. The aggregation that takes place in dox is plausibly due to the intermolecular interaction between  $\text{CH}_2\text{OH}$  and  $\text{C}=\text{O}$  groups of the adjacent dox molecules; this interaction is absent in the dauno. In addition to that, our optimised drug loading environment i.e.,  $< 10 \text{ mM MgCl}_2$ ,  $\leq 750 \text{ }\mu\text{M}$  dauno and  $\text{pH } 7.5$  could be another factor of not observing any aggregation.

Additionally, the fluorescence properties of the drug enabled us to image the dauno-loaded nanostructures. The drug-loaded DNs were incubated with DAPI blue staining dyes to establish the drug binding in the nanostructures. These incubated samples were washed twice with buffer (PBS) then, imaged in solution and also fixed by 1% agarose on the well plate. The results showed the colocalisation of both the compounds appearing as twin coloured clouds of DN-drug complexes in solution, i.e., drug and DAPI on the DNs characterised with green and blue channels (Figure 5-5). Moreover, the fluorescence intensity from both the compounds are high, and their proximity binding site on DNs makes them look bigger (sub-micron). The confocal micrographs of HB design (not shown) display similar information.

5

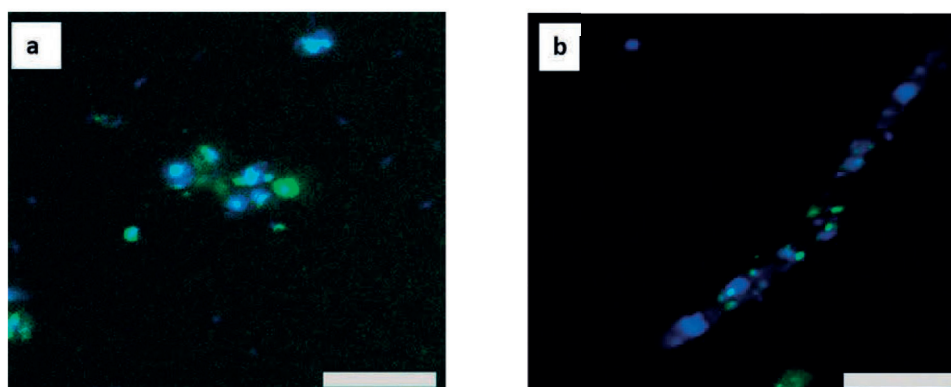


**Figure 5-5 Confocal micrographs of daunorubicin bound DN (DWS).**

The stained samples were incubated for 15 min and washed twice with wash buffer ( $\text{TE}/\text{Mg}^{2+}$ ) or PBS before imaging. The dauno-DN complex was (DAPI) stained in blue as a control, and the dauno-bound DNs were in green. a) The dauno-DN complex were imaged in buffer solution; b) the samples are fixed with 1% agarose to reduce the mobility. Scale bar in A and B is  $10 \text{ }\mu\text{M}$ .

### 5.2.3 Virus Capsid (CP) fabrication of drug-loaded DNs

The role of CCMV as a model system to encapsulate various synthetic and protein guest (13) molecules inside the capsid had been extensively discussed in chapter 4. Here, we demonstrate the fabrication of drug-loaded DNs in order to create nanocarriers for delivery applications. The protocol followed for fabrication is the same as described in section 4.5.3, while the mass ratio of CP used was always  $\geq \chi=0.64$ , to achieve thorough coverage of the DNs surface.

Following fabrication, purification is crucial to obtaining the right size particles and excluding small

particle formation by the fraction of CP (33). A small volume (<100  $\mu$ l) of purified samples was recovered and used throughout various experimental stages. Hence, to augment the purified yield, the CP fabricated drug-loaded DNs (nanocarriers) were divided into two batches for purification and subjected to two different methods: i) 100K MWCO centrifugal filters, and ii) FPLC. Next, to verify changes in newly fabricated purified nanocarriers morphology, two techniques (gel electrophoresis and FPLC) were used to detect any interaction of DNs and CPs.

To purify the capsid fabricated nanocarriers (DNA loaded with BPBR=3.5 drug concentration) size exclusion chromatography (SEC) on a superose 6 columns was used. The fabricated nanocarriers are chemically bound and expected to show co-elution profile. The isolated fractions at V=2 ml with high elution peak, correspond to larger assemblies in line with native capsids, as discussed previously in the chapter 0. Likely, these are nanocarriers (CP+DNA+dauno) as indicated by high  $\lambda$ = 280 nm (CPs) absorbance with the emergence of other peaks  $\lambda$ = 260 nm (DNs) and  $\lambda$ = 480 nm originating from DN with dauno in the complex at the same elution volume (2.0ml) (Figure 5-6a and b). Moreover, because of the small column size and high salt concentration of buffer (>0.15M), there

5

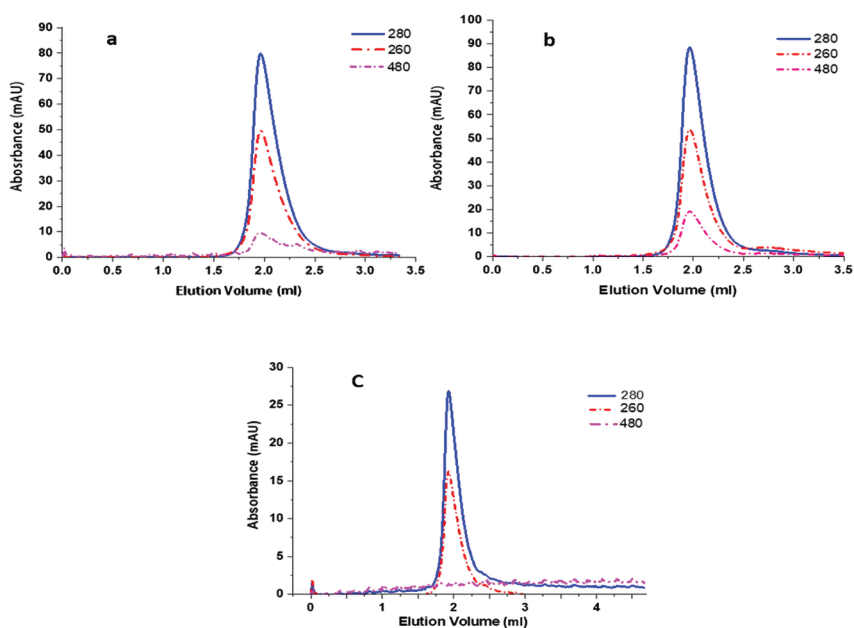


**Figure 5-6 Representative SEC chromatograms.**

The purification has been carried out with encapsulation buffer (pH 7.5); a) HB nanocarriers; b) DWS nanocarriers; c) ss-DNA scaffold with the drug (control).

is a negligible chance of having any non-specific ionic interaction making the method definite. The difference in peak pattern ( $\lambda$ = 480 ) observed with DWS (Figure 5-6b) compared to HB (Figure 5-6a) nanocarriers could be attributed to the fraying effect caused by drug incorporation. The presence of



two hollow cavities in the DWS design makes the nanostructure comparatively less rigid to HB where the tight crossover helices form a compact design. Here, a higher absorbance ratio  $\lambda = 280/260$  confirms the attachments of two biopolymers, together with the intercalated drug ( $\lambda=480$ ) within DNA. Where, >10 folds excess mass ratio of CP was mixed with the drug-DNA complex at physiological pH to induce the assembly of capsids over the surface of DNA (34).

In order to compare the difference between CP fabrication of the two drug-loaded DNAs (HB and DWS), a control experiment was also carried out with drug-loaded ss-DNA. The observed chromatogram in Figure 5-6c exhibit the possible co-assembly of ss-DNA with CP, resulting from the interaction between ss-DNA phosphate backbone and N-termini of CP at neutral pH (35). Moreover, the CP fabricated ss-DNA complex showed the absorbance ratio  $\lambda = 280/260 > 1$ , which is due to the presence of nucleic acid inside CCMV-CP. The observed flat line for dauno ( $\lambda = 480$ ) suggests the absence of any drug binding with the -ss-DNA or in the fabricated nanocarrier, as drug is an intercalator. Lastly, the negative drug binding by ss-DNA (control) exhibited in multiple experiments (AGE and FPLC) also affirms the presence of the drug inside the DNAs. Additionally, the encapsulation efficiency can also be estimated as a function of ratio between un-encapsulated and assembled CPs on elution curves for the two nanocarriers (Figure 5-6a and b), but due to experimental limitation, it is beyond the purview of current studies.

5

The purified samples with centrifugation columns (100K) and FPLC fractions were subjected to native gel electrophoresis. The gel results of the recovered samples from the respective purification methods are shown in Figure 5-7. Bands on the gel lanes 1-4 represent the controls with their respective molecular weights (Figure 5-7a). No bands have shown up in lanes 5-8 representing the purified samples. The data suggest a possible interaction between CP and drug-loaded complex were hard to visualise with SYBR safe staining.

Further, to confirm capsid proteins presence, the same gels were stained afterwards with Coomassie (Figure 5-7b). Here, we can observe intense protein bands in the lane 5-8 corresponds to higher CP concentration over the DNAs. Meanwhile, lane 7 for HB-FPLC has faint bands, possibly due to physical error during the sample loading on the well.



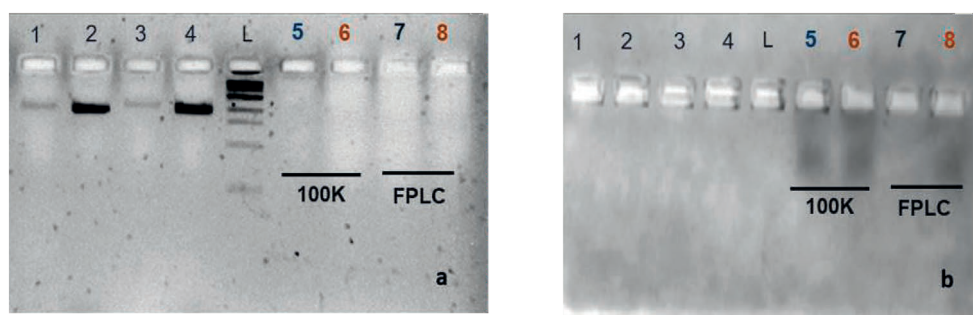


**Figure 5-7 AGE analysis to determine CP fabrication on drug-DNs nanocarriers.**

2% agarose gel for nanocarriers with 3.5 BPBR drug. The fabricated samples were divided into two tubes and each purified using FPLC and 100K MWCO. a) Syber safe stained, Lane 1 = HB (only), 2 and 4 = 7249 M13mp18 scaffold, 3 = DWS (only), 5 and 6 = 100K purified nanocarriers, 7 and 8 = FPLC collected nanocarriers; b) Coomassie-stained gel showing bands for the purified nanocarriers from both the techniques (lane 5-8). The two-colour marks for two designs Blue (HB) and brown (DWS) respectively.

The SEC and AGE data point to defined interactions between DNA- drug complex and CCMV-CP forming nanocarriers. Further, electron microscopy techniques might be used to investigate the morphology of the formed hybrid materials.

## 5

### 5.2.3.1 Microscopy (STEM/TEM)

The fraction containing the purified nanocarriers eluting at the volume  $V=2$  mL from FPLC was concentrated and filtration recovered after the spin column were pooled, to accrue the purification fraction subjecting to different microscopic techniques for structural analysis.

Firstly, scanning transmission electron microscopy (STEM) was carried out to investigate nanocarriers morphology. The dark-field STEM of HB nanocarriers with CP excess mass ( $\chi=0.64$ ) marks the presence of CP attached to discrete objects, appearing to have a sharp contrast on the edges of the particles (Figure 5-8a). The study reveals the dimension of individual HB nanocarriers with  $\geq 55$  nm and altered orthogonal morphology, which corresponds well to the previous chapter results, i.e., HB+CPs without drug-loading.

Similarly, the TEM of the same sample (Figure 5-8b) also verifies the formation of larger nanocarriers. The individual nanoparticles captured with both techniques complement each other in terms of size, shape and conformations. We observed uniformity in the distribution of these nanoparticles particles across the grids (Figure 5-S1-Figure 5-S2); thus, any ambiguity of surface or sample artefacts was avoided. The nanocarriers appearance of thickened morphology implies the drug-loaded structures are fabricated with a thick shield of capsid proteins.

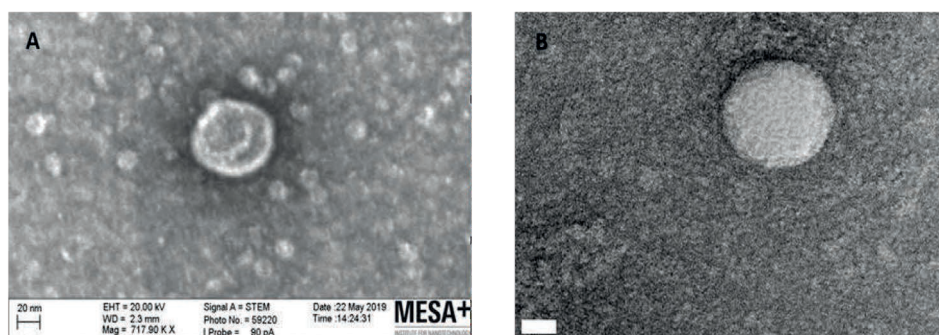


**Figure 5-8 Electron microscopy characterisation of HB+drug+CP.**

A) STEM (BF mode) image of the purified nanocarrier with sparsely dispersed small capsids; B) Negative stain TEM of nanocarrier with distinctive capsid fabrication on edges. Scale bar in A & B = 20 nm

Further, the dark field STEM micrographs for DWS nanocarriers with CP excess mass ( $\chi=0.64$ ) exhibit bright rectangular assemblies (Figure 5-9a) with dimension  $\geq 55$  nm having the white capsids adsorbed over the DNAs surfaces. The presence of white spherical particles in the backgrounds could possibly be due to uranyl acetate staining, which acidifies the solution, hence increasing the CP-CP interactions (36). Furthermore, the TEM images of the DWS nanocarriers with displaying similar dimension and morphology (Figure 5-9b) complements the STEM data. Caspar- Klug has defined the term  $T$  (triangulation) number, representing the number of distinct subunit conformations (37). The virus capsids are known to form different icosahedral geometries with  $T=1$ ,  $T=3$  and  $T=7$  under varying conditions (38, 39). The empty spherical capsids as seen in the background of Figure 5-9a, b, with  $T=1$  conformations, have an exterior diameter of  $\sim 18$  nm. Sikkema *et al.* have earlier reported a similar dimension for  $T=1$  with virus hybrid nanoparticles (40).

5

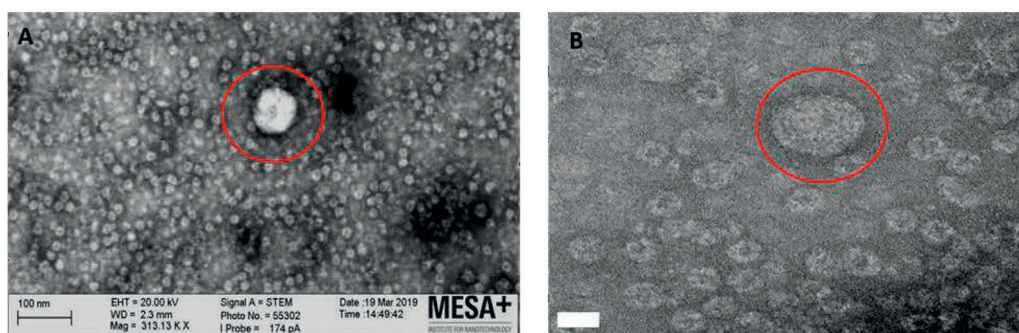


**Figure 5-9 Electron micrographs of DWS+drug +CP.**

A) STEM (DF mode) image of the purified nanocarriers(circled) with small white capsid on the background; B) Negative stain TEM of nanocarriers (circled) surrounded with spherical empty capsids. Scale bar in A = 100 nm and B = 20 nm.

Therefore, the microscopy results suggested a formation of drug-loaded protein particles under the applied assembly conditions. The homogenous distribution of particles on the samples also suggests

the optimal concentration of purified nanocarriers used for imaging, i.e.,  $\leq 5$  nM. However, the formation of unencapsulated spherical capsids on the background is an observation that needs further studies to support the hypothesis that the effect of types of salt and the shape of the anionic particles is responsible for structural change in capsid structure at pH 7.5, used in the mixture (41).

### 5.2.3.2 Size estimation of the nanocarriers

The particle size distribution of the nanocarriers was further evaluated by Dynamic Light Scattering (DLS) experiments. All measurements were obtained under similar conditions, as described in Chapter 3 and 4. Three separate DLS measurements were averaged to plot the particle size distribution after the encapsulation of both design-based nanocarriers (HB and DWS) (Figure 5-10).

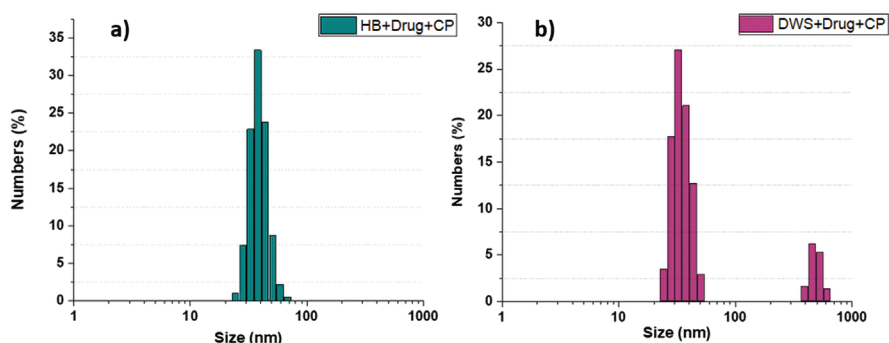


**Figure 5-10 DLS analysis nanocarrier (DN+drug+CP).**

a) HB+drug+CP; b) DWS+drug+CP. All purified samples were diluted to make 1 ml volume required for measurements.

DLS results indicate the existence of monodisperse particles for HB ( $41.4 \pm 2.9$  nm) and DWS ( $38.6 \pm 4.4$  nm) nanocarriers. This analysis also confirmed the absence of any aggregates or impurities in purified fractions of nanocarriers.

## 5.3 Conclusions

In this chapter, two different shaped DNA origami designs are employed to gain insight into their respective drug loading efficiency and create virus fabricated nanocarriers at physiological conditions for targeted drug delivery applications. These nanocarriers could be functional in anticancer therapy, subsiding the major issue of existing non-target tissue toxicity (42).

The microscopy data confirms the fabrication with the high mass transfer of capsids on the drug-DNs complex leading to create respective distinctive nanocarriers (43). These created nanocarriers resulting size is homogenous ( $\sim 55$ nm) across the surface in two imaging techniques, which has also emerged from the DLS analysis.

The cytotoxicity and *in-vivo* integrity remain two significant constraints in translating DNA-based drug

carriers into advanced stages. The results presented in this chapter serve as an alternative delivery method to improve the biological stability and minimising the off-target effects of drug-loaded DNA nanocarriers by promoting selective cellular uptake (44). Bare DNAs possess negative charge densities. With surface functionalisation, other features such as systemic circulation and bioavailability of the drug are also enhanced within the tumour cells to achieve higher efficacy (2).

This chapter's results take us one step closer to a smart, safe and targeted drug delivery system by synchronising the functionalities of two biomolecules to overcome the challenges of multiple biological barriers. Moreover, passive targeting of these nanocarriers with a size range of 25–150 nm could also improve the effects of permeability and retention (EPR) in the tumour cells (45). In the future, the detailed investigation requires these nanocarriers in both *in-vitro* and *in-vivo* conditions with parameters such as tumour targeting, uptake and intracellular fate and the drug clearance mechanism. Also, 3D structural analysis with cryo-EM of these nanocarriers will be an excellent option to resolve the actual structures of the two nanocarriers.

## 5.4 Acknowledgements

5

I acknowledge Irene Simerink Konings for her assistance and suggestions with UV-measurements and confocal imaging, including sample preparations. I thank Pramod Kunturu for his help in processing the loading quantification data. I also appreciate Rico Keim and Mark Smithers for their assistance in TEM and STEM imaging and analysis. Special thanks to Robin Klem and Melissa Goodwin for their valuable feedback during data collecting stages.

## 5.5 Materials and Methods

Unless specified otherwise, all compounds were purchased from Sigma-Aldrich, and all buffers were prepared with 18 M $\Omega$ ·cm MilliQ (Millipore) water.

### 5.5.1 DNA origami preparation

24-helix bundle (HB) and double-wall square (DWS) DNA origamis were used for drug loading studies using methods described in chapter 3 and then were fabricated with CCMV-CP obtained as described in chapter 4.

### 5.5.2 Effect of pH on Daunorubicin absorption

Five tubes with an equimolar drug (daunorubicin) concentration of 500  $\mu$ M at varying pH (4–8) were prepared. The UV absorbance of daunorubicin was recorded at both  $\lambda = 480$  nm and 490 nm on a Nanodrop1000 instrument (ThermoFisher Scientific).

### 5.5.3 DNAs drug binding and quantification

Daunorubicin HCl (Bio-Techne Ltd.) was resuspended in 1X PBS (Phosphate buffered Saline) and

filtered with 0.22  $\mu\text{m}$  filters to prepare a final stock concentration of 5 mM. Next, different dilutions of daunorubicin were made to plot a calibration curve for drug quantification. The base-pair binding ratio (BPBR) (22) was used as a drug loading parameter for both DNs (HB and DWS). After 24 hrs incubation of DNs with daunorubicin, the resulting drug-loaded DNs were centrifuged at 16,000X g for 35 min yielding a visible red-orange precipitated pellet. The drug loading efficiency of DNA origami structures was calculated as the difference between the initial concentration of daunorubicin in drug-loaded DNs and post-centrifugation concentration of daunorubicin in the supernatant (19). We report loading of the drug onto DNs as a base-pair binding ratio, described in the following equation (22):

$$\text{Base pair Binding Ratio (BPBR)} = \frac{1}{7.249} \times \frac{\text{Loaded Drug Concentration } (\mu\text{M})}{\text{Structure Concentration (nM)}}$$

#### 5.5.4 Agarose Gel Electrophoresis

The interaction of DNs with daunorubicin was validated by 1.8% native agarose gel electrophoresis stained with SYBR-Safe DNA stain (ThermoFisher). The gel was subsequently analysed on a gel-doc EZ imaging system (BioRad) to show the migration of drug-loaded DNs and the free drug. Later, for validating CP coating of drug-loaded DNs, the samples were run on the gels after staining them overnight with Colloidal Coomassie stain (BioRad), followed by overnight destaining in MilliQ and were subsequently analysed on gel-doc EZ imaging system (BioRad).

5

#### 5.5.5 Confocal Microscopy

Fluorescent confocal microscopy was performed on a Nikon confocal A1 microscope. The samples were imaged in a 96-well sensoplate (Greiner BioOne). 100  $\mu\text{l}$  of drug-loaded DNs samples were added to each well for carrying out co-localisation studies. All samples were incubated for 15 minutes with 50nM 4',6-diamidino-2-phenylindole (DAPI) (ThermoFisher scientific) to stain the DNA base-pairs of the DNs and subsequently washed with a buffer of choice (PBS/TE-Mg<sup>2+</sup>). For imaging in the static environment, the samples were fixed with 1% agarose for 45 min in the wells. The samples were then imaged using a  $\lambda=405$  and 488 nm laser, which was precalibrated using a calibration plate. The captured images were processed and analysed using ImageJ software.

#### 5.5.6 Creating nanocarriers: capsid fabrication of drug-loaded DNs

The capsid fabrication of the drug-loaded DNs (pellets recovered after the excess drug removal from centrifugation) was performed following a similar method, as discussed in section 4.5.3.

#### 5.5.7 Purification of Nanocarriers

Purification and analysis of the fabricated nanocarriers (CP-encapsulated drug-loaded DNs) was performed by size-exclusion chromatography (SEC) using a similar method described in chapter 4.5.5. Absorption was monitored at  $\lambda = 260$  nm, 280 nm and 480 nm. The collected fractions were

concentrated using 50kDa MWCO filters at 4°C using 5000G for 10 mins for further characterisations. Alternatively, the ultracentrifugation method using filter columns (100K) was also used for purification. Multiple washing of the sample was carried out with encapsulation buffer in similar conditions, as discussed in chapter 3.5.3. Ultracentrifugation is considered to be a preferable method over FPLC due to convenience and less consumption of time.

### **5.5.8 TEM/STEM imaging**

To test the effect of CP fabrication on dauno-bounded nanocarriers, we imaged them with transmission electron microscopy (TEM) on a FEG-TEM (Phillips CM 30 microscope) operated at 300KV acceleration voltage. The nanocarriers or FPLC-purified CP-fabricated nanocarrier samples were prepared on formavar Carbon 200 copper grids by incubating the samples for 1 min, followed by draining the liquid. Uranyl acetate (5  $\mu$ l, 1.5%w/v) staining was added, and the excess liquid was drained after 45 sec. The grid was dried for 30 min at room temperature. The sample grids were then imaged with a Zeiss Merlin microscope in (S)TEM mode with dark and bright field options.

### **5.5.9 Dynamic Light Scattering (DLS)**

DLS measurements were made on a Nano ZS machine by Malvern Instruments, and the data was extracted using the solution viscosity of water and refractive index of DNs=2.1 in the standard settings of the company's software (Zetasizer)



## 5.6 References

1. Li J, Fan C, Pei H, Shi J, Huang Q. Smart Drug Delivery Nanocarriers with Self-Assembled DNA Nanostructures. *Advanced materials*. 2013;25(32):4386-96.
2. Kearney CJ, Lucas CR, O'Brien FJ, Castro CE. DNA Origami: Folded DNA-Nanodevices That Can Direct and Interpret Cell Behavior. *Advanced Materials*. 2016.
3. Al-Jamal WT, Kostarelos K. Liposomes: from a clinically established drug delivery system to a nanoparticle platform for theranostic nanomedicine. *Acc Chem Res*. 2011;44(10):1094-104.
4. Pack DW, Hoffman AS, Pun S, Stayton PS. Design and development of polymers for gene delivery. *Nat Rev Drug Discov*. 2005;4(7):581-93.
5. Duncan B, Kim C, Rotello VM. Gold nanoparticle platforms as drug and biomacromolecule delivery systems. *Journal of Controlled Release*. 2010;148(1):122-7.
6. Lu J, Liong M, Li Z, Zink JI, Tamanoi F. Biocompatibility, biodistribution, and drug-delivery efficiency of mesoporous silica nanoparticles for cancer therapy in animals. *Small*. 2010;6(16):1794-805.
7. Liu Z, Robinson JT, Tabakman SM, Yang K, Dai H. Carbon materials for drug delivery & cancer therapy. *Materials today*. 2011;14(7-8):316-23.
8. Michalet X, Pinaud FF, Bentolila LA, Tsay JM, Doose S, Li JJ, et al. Quantum dots for live cells, in vivo imaging, and diagnostics. *Science*. 2005;307(5709):538-44.
9. Chertok B, Moffat BA, David AE, Yu F, Bergemann C, Ross BD, et al. Iron oxide nanoparticles as a drug delivery vehicle for MRI monitored magnetic targeting of brain tumors. *Biomaterials*. 2008;29(4):487-96.
10. De Jong WH, Hagens WI, Krystek P, Burger MC, Sips AJ, Geertsma RE. Particle size-dependent organ distribution of gold nanoparticles after intravenous administration. *Biomaterials*. 2008;29(12):1912-9.
11. Chen N, He Y, Su Y, Li X, Huang Q, Wang H, et al. The cytotoxicity of cadmium-based quantum dots. *Biomaterials*. 2012;33(5):1238-44.
12. Magrez A, Kasas S, Salicio V, Pasquier N, Seo JW, Celio M, et al. Cellular toxicity of carbon-based nanomaterials. *Nano Lett*. 2006;6(6):1121-5.
13. Ko S, Liu H, Chen Y, Mao CJB. DNA nanotubes as combinatorial vehicles for cellular delivery. 2008;9(11):3039-43.
14. Shen X, Jiang Q, Wang J, Dai L, Zou G, Wang ZG, et al. Visualization of the intracellular location and stability of DNA origami with a label-free fluorescent probe. *Chem Commun (Camb)*. 2012;48(92):11301-3.
15. Erben CM, Goodman RP, Turberfield AJ. Single-molecule protein encapsulation in a rigid DNA cage. *Angewandte Chemie International Edition*. 2006;45(44):7414-7.
16. Kearney CJ, Lucas CR, O'Brien FJ, Castro CE. DNA Origami: Folded DNA-Nanodevices That Can Direct and Interpret Cell Behavior. *Advanced Materials*. 2016;28(27):5509-24.
17. Kumar V, Palazzolo S, Bayda S, Corona G, Toffoli G, Rizzolio F. DNA nanotechnology for cancer therapy. *Theranostics*. 2016;6(5):710.
18. Madhanagopal BR, Zhang S, Demirel E, Wady H, Chandrasekaran AR. DNA Nanocarriers: Programmed to Deliver. *Trends Biochem Sci*. 2018;43(12):997-1013.
19. Jiang Q, Song C, Nangreave J, Liu X, Lin L, Qiu D, et al. DNA origami as a carrier for circumvention of drug resistance. *Journal of the American Chemical Society*. 2012;134(32):13396-403.
20. Zhao Y-X, Shaw A, Zeng X, Benson E, Nystrom AM, Hogberg B. DNA origami delivery system for cancer therapy with tunable release properties. *Acs Nano*. 2012;6(10):8684-91.
21. Zhang Q, Jiang Q, Li N, Dai L, Liu Q, Song L, et al. DNA origami as an in vivo drug delivery vehicle for cancer therapy. *ACS nano*. 2014;8(7):6633-43.
22. Halley PD, Lucas CR, McWilliams EM, Webber MJ, Patton RA, Kural C, et al. Daunorubicin-Loaded DNA Origami Nanostructures Circumvent Drug-Resistance Mechanisms in a Leukemia Model. *Small*. 2016;12(3):308-20.
23. Rejman J, Oberle V, Zuhorn IS, Hoekstra D. Size-dependent internalization of particles via the pathways of clathrin- and caveolae-mediated endocytosis. *Biochemical Journal*. 2004;377(1):159-69.
24. Yan J, Hu C, Wang P, Zhao B, Ouyang X, Zhou J, et al. Growth and Origami Folding of DNA on Nanoparticles for High-Efficiency Molecular Transport in Cellular Imaging and Drug Delivery. *Angewandte Chemie International Edition*. 2015;54(8):2431-5.
25. Schaffert DH, Okholm AH, Sørensen RS, Nielsen JS, Tørring T, Rosen CB, et al. Intracellular delivery of a planar DNA origami structure by the transferrin-receptor internalization pathway. *Small*. 2016;12(19):2634-40.
26. Mikkilä J, Eskelinen A-P, Niemelä EH, Linko V, Frilander MJ, Törmä Pi, et al. Virus-encapsulated DNA origami nanostructures for cellular delivery. *Nano letters*. 2014;14(4):2196-200.
27. Balakrishnan D, Wilkens GD, Heddle JG. Delivering DNA origami to cells. *Nanomedicine*. 2019;14(7):911-25.
28. Rother M, Nussbaumer MG, Renggli K, Bruns N. Protein cages and synthetic polymers: a fruitful

- symbiosis for drug delivery applications, bionanotechnology and materials science. *Chemical Society Reviews*. 2016;45(22):6213-49.
29. Biebricher AS, Heller I, Roijmans RF, Hoekstra TP, Peterman EJ, Wuite GJ. The impact of DNA intercalators on DNA and DNA-processing enzymes elucidated through force-dependent binding kinetics. *Nature communications*. 2015;6:7304.
  30. Htun MT. Photophysical study on daunorubicin by fluorescence spectroscopy. *Journal of Luminescence*. 2009;129(4):344-8.
  31. Gallois L, Fiallo M, Garnier-Suillerot A. Comparison of the interaction of doxorubicin, daunorubicin, idarubicin and idarubicinol with large unilamellar vesicles: circular dichroism study. *Biochimica et Biophysica Acta (BBA)-Biomembranes*. 1998;1370(1):31-40.
  32. Ijäs H, Shen B, Heuer-Jungemann A, Keller A, Kostianen MA, Liedl T, et al. Unraveling the interaction between doxorubicin and DNA origami nanostructures for customizable chemotherapeutic drug release. *Nucleic Acids Res*. 2021;49(6):3048-62.
  33. Maassen SJ, de Ruiter MV, Lindhoud S, Cornelissen JJ. Oligonucleotide Length-Dependent Formation of Virus-Like Particles. *Chemistry—A European Journal*. 2018;24(29):7456-63.
  34. Brasch M, Putri RM, de Ruiter MV, Luque D, Koay MS, Castón JR, et al. Assembling enzymatic cascade pathways inside virus-based nanocages using dual-tasking nucleic acid tags. *Journal of the American Chemical Society*. 2017;139(4):1512-9.
  35. Garmann RF, Comas-Garcia M, Knobler CM, Gelbart WM. Physical Principles in the Self-Assembly of a Simple Spherical Virus. *Acc Chem Res*. 2016;49(1):48-55.
  36. Burns K, Mukherjee S, Keef T, Johnson JM, Zlotnick A. Altering the energy landscape of virus self-assembly to generate kinetically trapped nanoparticles. *Biomacromolecules*. 2009;11(2):439-42.
  37. Caspar DL, Klug A. Physical principles in the construction of regular viruses. *Cold Spring Harb Symp Quant Biol*. 1962;27:1-24.
  38. Speir JA, Munshi S, Wang G, Baker TS, Johnson JE. Structures of the native and swollen forms of cowpea chlorotic mottle virus determined by X-ray crystallography and cryo-electron microscopy. *Structure*. 1995;3(1):63-78.
  39. Johnson JE, Speir JA. Quasi-equivalent viruses: a paradigm for protein assemblies. *J Mol Biol*. 1997;269(5):665-75.
  40. Sikkema FD, Comellas-Aragones M, Fokkink RG, Verduin BJ, Cornelissen JJ, Nolte RJ. Monodisperse polymer-virus hybrid nanoparticles. *Org Biomol Chem*. 2007;5(1):54-7.
  41. Lavelle L, Gingery M, Phillips M, Gelbart W, Knobler C, Cadena-Nava R, et al. Phase diagram of self-assembled viral capsid protein polymorphs. *The Journal of Physical Chemistry B*. 2009;113(12):3813-9.
  42. Núñez-Lozano R, Cano M, Pimentel B, de la Cueva-Méndez G. 'Smartening' anticancer therapeutic nanosystems using biomolecules. *Current opinion in biotechnology*. 2015;35:135-40.
  43. Linko V, Mikkilä J, Kostianen MA. Packaging DNA Origami into Viral Protein Cages. *Virus-Derived Nanoparticles for Advanced Technologies*: Springer; 2018. p. 267-77.
  44. Ren K, Liu Y, Wu J, Zhang Y, Zhu J, Yang M, et al. A DNA dual lock-and-key strategy for cell-subtype-specific siRNA delivery. *Nature communications*. 2016;7:13580.
  45. Jahanban-Esfahlan A, Seidi K, Jaymand M, Schmidt TL, Zare P, Javaheri T, et al. Dynamic DNA nanostructures in biomedicine: Beauty, utility and limits. *Journal of Controlled Release*. 2019.



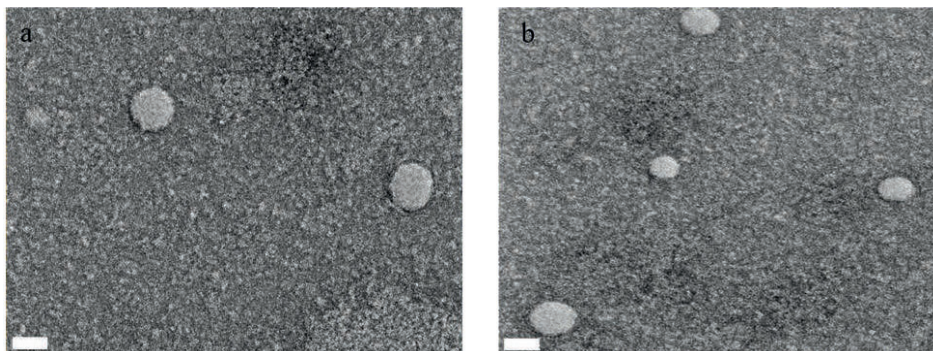


**Figure 5-S1 TEM micrographs of (HB+drug+CP)**

a) & b) Multiple imaging scans across the TEM grids show the particles consistent morphology and dimensions. *Scale bars are 50 nm*

5

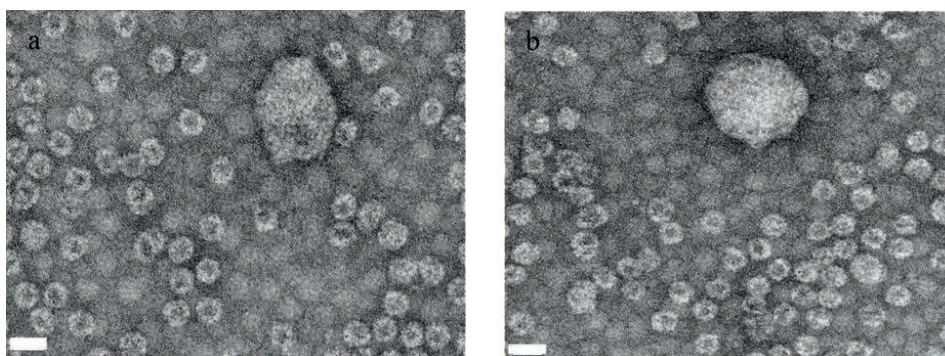


**Figure 5-S2 TEM micrographs of (DWS+drug+CP)**

a) & b) Multiple imaging scans across the TEM grids show the particles consistent morphology and dimensions. *Scale bars are 20 nm*

## **CHAPTER 6**

---

# **Monitoring the stability and drug release from nanocarriers**

---

Part of this chapter will be submitted.

## 6 MONITORING THE STABILITY AND DRUG RELEASE FROM NANOCARRIERS

### 6.1 Introduction

Cancer is one of the most severe diseases globally, and anthracyclines are the most widely used chemotherapeutic agents. DNA nanostructures (DNs) have been shown to have potential in cancer theranostics (1, 2). Modular DNs (tetrahedral, square, triangle) were tested for various drug delivery applications and have been shown to outperform ds-DNA (3-5). However, DN's anionic charge density, which is due to the phosphate-sugar backbone, makes them highly polar, resulting in difficulties for crossing biological barriers like the endosomal, epithelium and plasma membrane (6, 7). Another big hurdle in using DN as a drug carrier is that they are prone to disassembly in cellular media by *in vivo* enzymatic degradation, causing the fast and non-specific distribution of drugs (8). To overcome these problems, polymer-based nanoparticles (NPs) have been developed and used as an alternative drug carrier aiming to improve the safety and efficacy of drugs in biomedical applications (9, 10). The first generation of polymeric nanomaterial-based drug delivery systems such as Doxil (PEGylated liposomal formulation for doxorubicin) and Abraxane (paclitaxel albumin stabilised formulation) are used to deliver a spectrum of chemotherapeutics. The drugs are loaded onto NPs due to electrostatic interactions and drug release occurs through mechanisms like hydrolysis, diffusion or enzymatic degradation of NPs (Figure 6-1) (11).

6

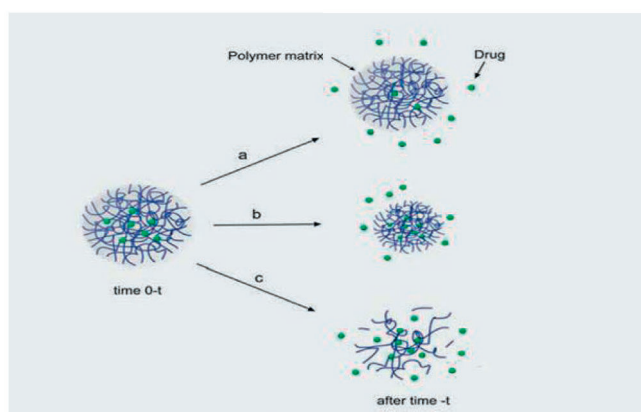


**Figure 6-1 Drug release mechanism from polymeric nanomaterials.**

a) Diffusion from the polymer complex; b) degradation of the polymeric matrix; c) biodegradation of polymeric nanomaterial due to enzymatic degradation. Adapted with permission from [11].

However, these polymeric systems lack critical features like prolonged circulation time and *in-vitro* stability, which are essential in cancer therapy (12, 13). The absence of such critical characteristics led to limited use of polymeric NPs in therapeutic applications (14, 15). Other drug delivery approaches employ inorganic nanostructures comprised of metals such as gold or non-metallic

oxides, which are sturdy and biocompatible (16). However, chronic accumulation of inorganic nanostructures in the tumorous cells (due to difficulty in their degradation) can lead to severe problems and side effects (17). In order to address these challenges, there is a need for a robust delivery system that is highly reproducible, stable under biological environments, maintains controlled drug release and does not trigger an immune response (18).

In 2009, Keum and co-workers first revealed creating relatively stable DNs, by incubating them in 10% fetal bovine serum (FBS) for 42 hours (19). The serum is known to contain a mixture of nuclease (endo- and exo-) along with some unspecific proteins. In another study, Yan's group detected the stability of DNs after incubating them for 12 hours with different cell lysates (normal and cancerous). The functionality of the DNs was found to be intact, keeping their structural integrity after exposure to cell lysate, showing their stability compared to conventional oligonucleotides (20). Further, Castro *et al.*, tested the stability of modular DNA origami designs (18-, 24-, 32-helix bundles) against different nucleases and have reported DNs to be more resistant to DNase-I as compared to regular ds-DNA (21). Hahn and co-workers, performed a comprehensive analysis to study the effect of low magnesium concentration (cation-depletion) and nuclease on three DNA origami designs (i.e. an octahedron, a 6-helix-nanotube and a 24-helix-nanorod) in a cell culture media (22). The designs were reported to be stable in low magnesium tissue culture media after 24 hours; however, the sensitivity to cation-depletion was reported as design and time-dependent. Later, Perrault and his group constructed a protective lipid coat on DNs to protect them from nuclease digestion (23). They also demonstrated a considerable reduction in *in vivo* immune activation; however, a piece of evidence was presented in the study for DNs acquiring a certain extent of immunostimulatory potential (24).

Cellular receptors may readily direct DNs to endo-lysosomal degradation while crossing the cell membrane to deliver a therapeutic cargo to the targeted location. Therefore, enhanced cellular uptake and escaping endosomal pathways are other major factors for efficient drug delivery (25, 26). Shen *et al.*, investigated the stability and distribution of DNA nanotubes in breast cancer cells and found most of the DNs were localised in the lysosomes after 12 hours of incubation and complete degradation required around 60 hours (27). In order to address the combined challenges of stability and to avoid degradation; the DN's surface was modified and bound non-covalently with other molecules. In 2014, Fan and co-workers reported different encapsulation methods for modifying the DN's surface and reported increased stability and bioavailability of DNs. Hence, these approaches suggest DNs escape the lysosomal pathways and enter into nuclei, which makes them highly appropriate to be used in targeted therapy. (28, 29). Later, In 2017, two important studies opting another strategy to modify DN's surface were published, where cationic polymers (PEG-PLys) and oligo-lysines were attached to the negatively-charged DNs. The modifications display better stability in low salt conditions with enhanced protection against serum nucleases and DNase-I digestion in

comparison to uncoated structures (30, 31). Further, the *in-vivo* results with modified (coated) DN's taken into consideration also showed a reasonable increase in pharmacokinetic bioavailability (30).

A 13-fold increase in cellular internalisation has been reported with the application of capsid proteins (from CCMV) on DN's surface using electrostatic interactions (32, 33). Similarly, other protein-related coatings - bovine serum albumin (BSA), protein-polymer and protein-dendron conjugates have also been described with multiple benefits: providing a shield against enzymes, augmenting in transfection rate and evoking a weakened immune response (34, 35). The diverse compatibility of DN's with different materials and stability in physiological conditions makes them promising for several therapeutic applications.

In this chapter, we will first discuss the stability of the designed nanocarriers (DN+ drug +CP) against enzymatic degradation using two different targeting enzymes, benzonase nuclease and protein trypsin. The literature states that by regulating the design of the DN's, the drug loading efficiency and the rate at which drug released on the tumorous sites, can be adjusted to achieve higher cytotoxicity and reduced elimination rate (36). Then, given the importance of controlled release properties of the drugs at a target site(37), *in vitro* drug release kinetic profiles of Dauno/DNA origami complexes were studied at varying pH and for up to 48 hours. Finally, important details about the amount of drug remains loaded in the drug-DN complexes was determined by quantifying total drug content in two different designed nanocarriers (HB and DWS) i.e., after the virus capsid fabrication step.

## 6

## 6.2 Result and Discussion

### 6.2.1 Assessing the stability of nanocarriers

Structural integrity is one of the essential features of DN's to be an efficient carrier along with the controlled release, widespread availability and precise targeting. Thus, it is imperative to assess the safety and stability of DN's before they can be taken to the next level of therapeutic applications. In biological environments, DN's encounter the active DNA degrading machinery involving DNAases (38). To verify the effect of the CP coating as a shielding agent over DN-Drug complex, we treated the two devised nanocarriers (HB and DWS) with Benzonase nuclease. Benzonase nucleases cause non-specific degradation of all forms of nucleic acids without any proteolytic activity (39). Similarly, the samples were also tested against trypsin digestion; the amount of the nanocarrier and enzymes are shown in Table 6-1.

Reactants	Volumes ( $\mu$ l)
Purified nanocarriers	5
Enzymes (benzonase/trypsin)	1.5
Buffer	0.5
Nuclease free water	3
Total	10

**Table 6-1** Content details used for the enzyme stability reactions.

Initially, the samples were incubated for 15 min with benzonase nuclease  $\geq 2.5$  U/ml at room temperature, which is considered an optimal enzyme concentration to achieve complete digestion of nucleic acids (40). After the enzyme treatment, the samples were validated using the AGE (Figure 6-2). The samples were run with two conditions pre (-) and post (+) benzonase enzyme-treated nanocarriers. The band mobility of the treated samples (lane 2 and 4) showed no sign of degradation in both staining gels (DNA and protein) (Figure 6-2a and b, respectively), indicating the shielding strength of the CP.

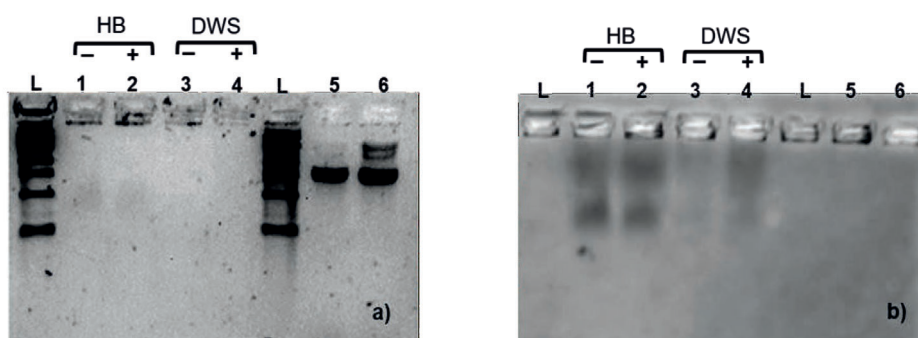


**Figure 6-2** Virus capsids protection of nanocarriers against benzonase.

a) Sybr stained, Lane 1, 2 = HB and Lane 3, 4 = DWS. The “-” and “+” denotes the absence or presence of benzonase nuclease; b) Coomassie-stained gel showing unchanged bands from the respective enzyme-treated lanes. L= DNA ladder and Lane 5, 6= purified DNAs used as a reference.

Further, to investigate the stability of nanocarriers under intense biological conditions, we extended the incubation time to 1 hour at 37 °C and also tested the samples against trypsin (proteolytic) enzyme.



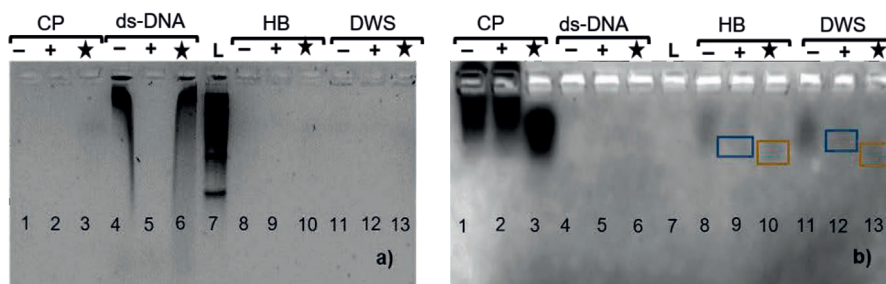


**Figure 6-3 Time-dependence stability against benzonase and trypsin.**

a) Sybr stained, the “-”, “+” and “★” in the top of the lanes denote the untreated, benzonase- and trypsin-treated samples, respectively; b) Coomassie-stained gel showing bands from the respective lanes. Top lanes from left to right showing lane1: Only CP, lane 2: CP+benzonase, lane 3: CP+trypsin, lane 4: M13mp18 ds-DNA, lane 5: M13mp18 ds-DNA+benzonase, lane 6: M13mp18 ds-DNA+trypsin, lane 7: DNA ladder, lane 8: HB nanocarrier, lane 9: HB nanocarrier+benzonase, lane10: HB nanocarrier+trypsin, lane 11: DWS nanocarrier, lane 12: DWS nanocarrier+benzonase, lane 13: DWS nanocarrier+trypsin.

## 6

The SYBR stained gel (Figure 6-3a) with controls CP and M13mp18 ds-DNA showed degradation for the enzymes trypsin and benzonase, in respective lanes 3 and 5. The bands for untreated nanocarriers (HB and DWS) were not visible as they were protein-coated (lanes 8-13). On the other hand, Figure 6-3b shows bands from nanocarriers (lane 8 and 11) after being coomassie stained. The leading bands for enzyme-treated nanocarriers (+, ★ lanes) suggest a resistance and improved stability (lanes 9, 10, 12, 13). The protective nature of coated nanocarriers has been illustrated against degrading enzymes, albeit marginal shifts in bands mobility observed in trypsin treated lanes compared to untreated samples. The possible explanation of this effect is the low CP concentration ( $\leq 450$  ng/ $\mu$ l) coated over the nanocarrier. Whereas, the high concentration of CP ( $\geq 1.5$   $\mu$ g/ $\mu$ l) used as a reference in lane 1-3 displays the limited effect of trypsin resulting in mobility shift on lane 3 compared to the only CP on lane 1. However, the migration of CP originates possibly by the net negative charge on them at a given pH ( $\geq 7$ ) as reported in previous studies (41)

### 6.2.2 Daunorubicin release profile *in-vitro*

After assessing the physiological stability of nanocarriers, their drug release capability is one of the other parameters needing validation. Most of the published reports have shown the drug release experiments of Drug/DN complex in PBS at varied pH levels or in cell lysate solution (42, 43). Largely, the drug release kinetics from DNs depends on the uptake, diffusion rate and the DN-drug complex degradation through enzymes. Thus, we evaluated the *in-vitro* release of dauno from dauno/DN complex in 1X PBS + 10 mM MgCl<sub>2</sub> solutions at pH 7.2 and pH 4.0, and in culture media (10% FBS + 10 mM MgCl<sub>2</sub>) mimicking the intercellular and physiological conditions.

The release kinetics profiles of dauno were calculated using a log plot of cumulative (%) release vs time. In all of the three selected conditions, drug release was occurred via diffusion in a time-dependent manner with slow drug release at pH 7.2 and acidic pH favoring fast release at pH 4.0

(Figure 6-4).

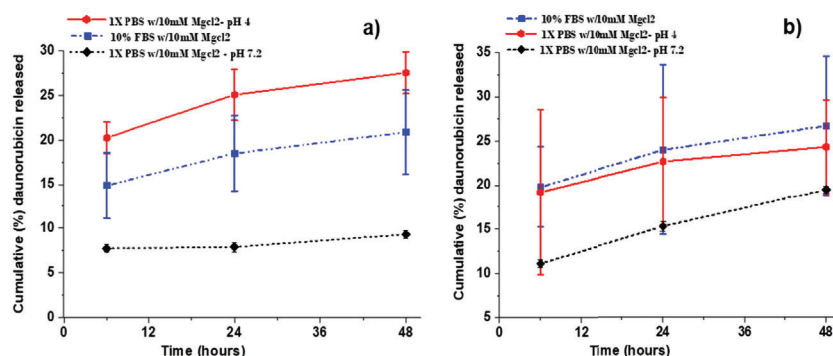


**Figure 6-4 Dauno release profile from DN complexes.**

Dauno/DN complexes (~40nM, BPBR 3.5) were incubated in three buffers (1XPBS + 10 mM MgCl<sub>2</sub>, pH 7.2, 1XPBS + 10 mM MgCl<sub>2</sub>, pH 4; 10% FBS + 10 mM MgCl<sub>2</sub>) at 37°C for 6, 24 and 48hrs; a) dauno-loaded HB and b) dauno-loaded DWS. Each data was shown as average ± SD (n=3).

We used a nonlinear least-squares approach to estimate the parameter 'b' of the Weibull model for fitting the drug release data as described in the formula (1). This model is useful in comparing drug accumulation from any given material in a solution as a function of time (44, 45). This model is useful in comparing drug accumulation from any given material in a solution as a function of time.

$$m = 1 - \exp\left[\frac{-(t-T_i)^b}{a}\right] \quad (1)$$

Where,  $m$  is the accumulated fraction of material (drug) in solution at time  $t$ ; Parameter  $a$  defines the time scale of the process;  $T_i$  represents the time lag before the onset of release;  $b$  is a shape parameter accounting for curve progression. The estimated value and the significance of parameter  $b$  are shown in Table 6-2. The estimated value of parameter  $b$  is <1, which depicts a steeper curve and slower drug release for all the experimental conditions (46).

DN design	Experiment Conditions	Parameter $a$	Parameter $b$	Standard error			
				$A$	$p$ -value ( $a$ )	$b$	$p$ -value ( $b$ )
HB	1x PBS (pH -7.2)*	14.9	0.08	1.485	2.03x10 <sup>-5</sup>	0.031	0.02
	1x PBS (pH- 4)*	5.9	0.17	0.821	0.0001	0.042	0.005
	10% FBS*	8.5	0.17	2.930	0.02	0.105	0.13
DWS	1x PBS (pH -7.2)*	11.7	0.23	1.662	0.0002	0.043	0.009
	1x PBS (pH- 4)*	6.1	0.13	3.200	0.107	0.160	0.459
	10% FBS*	7.3	0.22	3.140	0.05	0.130	0.133

**Table 6-2 Parameter estimation of drug released kinetics. \* + 10 mM MgCl<sub>2</sub>**

Comparing the individual drug/DN complex, we can observe with HBs initial two experimental conditions (pH 7.2 and pH-4 ) results in significant  $p$ -values ( $\leq 0.05$ ). In contrast, the third one (10%



FBS.) shows a lower *p-value* but not significant for parameter *b*. The next design DWS (pH 7.2) values lie in the significant range, whereas in the two remaining conditions (pH- 4 and 10% FBS), high variance was observed in the measurements leading to low parameter fitting with the model. The large deviations noticed can be attributed to limited data points ( three for each condition) or some unknown external perturbations. However, the results can be improved by extending data points in future investigations. Additionally, our experimental data follows a similar drug release pattern, further validating the effect of time and pH on drug/DN complexes shown in recent work (47).

Moreover, in our experiments, the estimated parameter *b* points to a higher slope initially (0-6 hrs), suggesting a quick drug release followed by a steady exponential growth as observed at 6-48 hrs (48). Hence, we propose that drug release mechanisms predominantly are driven by diffusion. The multilayer cross-linked helices of DNs served as a diffusion barrier. The drug release profile indicates that  $\leq 10\%$  of the drug was released from drug/DN complexes at pH 7.2 in the first 6 hrs under the examined physiological conditions, then advances gradually and reached up to  $\leq 15\%$  in 48 hours for both the complexes. On the other hand, in the other two conditions (pH 4.0 and 10% FBS), the release efficiencies reached  $\geq 20\%$  in 48 hours for both the drug/DN complexes (Figure 6-4a and b). Here, the enhanced drug release can be attributed to the effect of more than one mechanism contributing towards the release, like triggered (stimuli) response (pH difference and enzymatic degradation) in varying conditions, for biomaterials mentioned previously (49-51).

6

The percentage drug release increased by two folds at lower pH as shown in Figure 6-4, suggest an accelerated dauno release when dauno/DN complexes interact with the acidic biological environment, usually found in tumour cells. The higher glycolysis rate in tumour cells is known to lower the pH, and this is considered a substantial stimulus for triggering drug release in cancer therapy (52). The increased drug release is also observed in culture media (10% FBS), supporting the hypothesis that drug release is responsive to cellular enzymes (53). However, in all conditions mentioned above, lower drug release ( $\leq 30\%$ ) was observed for HB and DWS over 48 hrs and is likely due to the small burst effect as the drugs are intercalated. Further, the cationic strength of magnesium (10mM) stabilises the structural integrity of DNs for a longer duration.

Besides, our investigation also includes the effect of the geometric shapes of DNs on drug release. Figure 6-4b showed that DWS displays a faster release in two conditions (at pH 7.2 and 10% FBS), while it has similar release characteristics in acidic environments (at pH 4) as compared to HB. This higher release may be attributed to the designing framework of DWS, a square lattice with two internal cavities, which can increase the accessible surface area suitable for dauno release (36). Additionally, we also examined the structural integrity of the DWS nanocarriers (DN+drug+CP) after *in-vitro* drug release (Figure 6-S1), verifying the shielding effect of CP coating in the given biological

conditions.

### 6.2.3 Probing the drug leakage from nanocarriers

The formulation of nanocarriers include multiple incubations and washing steps; thus, there is a high probability of losing a certain amount of drug after every step. Therefore, to ensure a significant amount of drug remains loaded within the nanostructures at the point of cellular entry, we performed drug leakage studies.

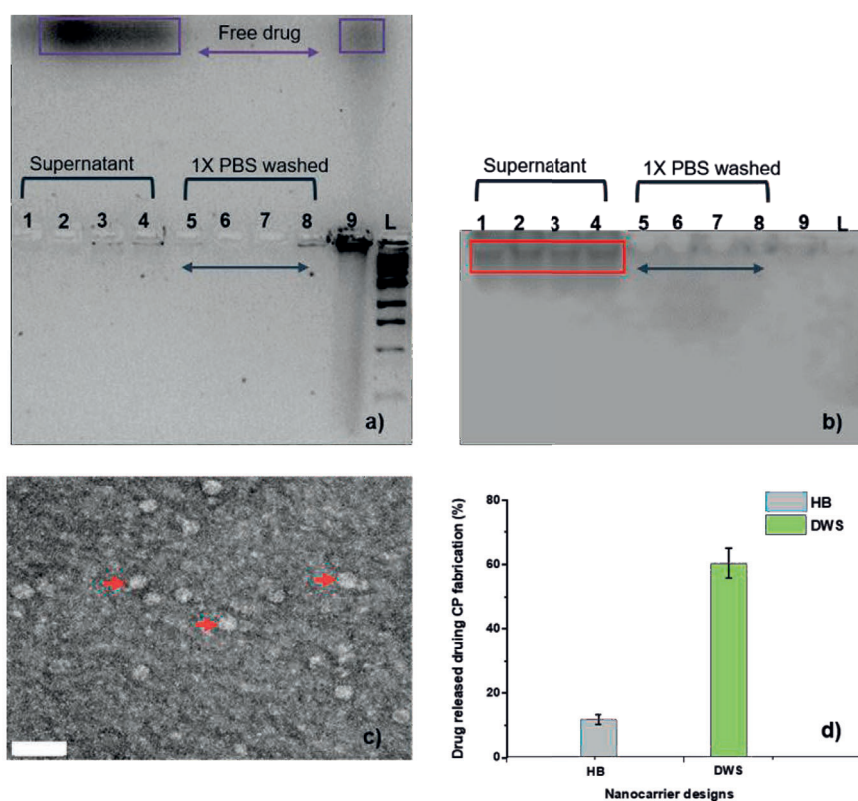


**Figure 6-5 Validating drug leakage from nanocarriers**

a) Sybr stained, 1.5% AGE having the free drug in Lane 1, 2 = HB; Lane 3, 4 = DWS after CP incubation; Lane 5-8 have PBS washed samples in the same order; b) Coomassie-stained gel; c) TEM of supernatant DWS, presenting white spherical capsids (shown with red arrows); d) Quantification of drug lost during the CP coating. Lane 9 = resuspended DWS, L = DNA marker as a reference. and scale bar for c) is 50nm.

Fabrication of dauno/DN complex with capsid proteins (CP) resulted from their incubation for ~72 hours with continuous rotation at 4°C. To calculate the amount of drug lost during the CP incubation, the free drug was removed and quantified. Moreover, drug leakage was assessed via a series of washes (i.e., centrifugation and removal of supernatant) with 1X PBS. AGE analysis Figure 6-5a showed a trace of drug lost during the CP fabrication step from the dauno/DN complex in the reverse direction (lane 1-4). However, there was no further drug leakage monitored after washing the

nanocarriers with 1X PBS buffer (lanes 5-8). The coomassie stained gel (Figure 6-5b) confirmed the presence of unbounded CPs in the supernatant fractions for both nanocarriers (marked in the box). Also, the PBS washed lanes were devoid of any material, establishing the structural integrity of the nanocarrier under physiological conditions. We further performed TEM for the same supernatant fractions collected after CP fabrications (lanes 1-4). We majorly found small spherical capsids across the grids (Figure 6-5c), in line with  $T=1$  capsids (54). The TEM micrograph of HB based nanocarriers was not presented here to avoid redundancy as it showed similar information. Lastly, the drug lost in the supernatant was quantified by determining the *in vitro* retention of drug in nanocarriers before setting up the cell-based experiments. The result in Figure 6-5d illustrates that the drug lost from DWS nanocarrier was four times higher as compared to HB. These findings are in line with previous research and reported studies about structural design affecting the drug delivery capabilities of DN based nanocarriers (42, 55).

### 6.3 Conclusion

## 6

In this chapter, we investigated the *in-vitro* stability and controlled release features of newly designed virus protein-coated nanocarriers (HB and DWS) under varying biological conditions. In comparison to ds-DNA and uncoated DNs, the nanocarriers showed increased protection against benzonase and trypsin digestion. The stability studies demonstrated the potential utility of these nanocarriers for protecting encapsulated cargo loaded DNs from biological degradation. This information enables us to understand practical limits of DNs in the field of nanomedicine and may eventually help to progress towards clinical development.

Other experiments performed in this chapter involved the time-dependent release of the drug from Dauno/DN complexes release for up to 48 hours. The results of the studies undertaken showed controlled drug delivery efficiency of the selected DNs under the given physiological conditions. Also, the study suggest that the drug delivery depends on the shape of DNs, as the densely packed HB exhibited a more sustained drug release compared to DWS containing hollow cavities. The findings in this chapter are found consistent with the published studies detailing the preference of compact design DNs in cellular internalisation and delivery (56). Furthermore, we demonstrated increased drug-release efficiency of DNs at low pH and the interaction between DNs and cellular enzymes might also trigger an additional release of daunorubicin inside the targeted cells.

Lastly, we showed the final drug retention abilities of the designed nanocarriers within the physiological environments. The proof-of-concept work presented here showed no drug leakage *in-vitro* after CP coating which gives merit to optimise the designed nanocarriers for potential drug delivery system.

The approach we discussed in this chapter not only helps in developing robust nanocarriers, but can also be used as a guide in selecting DNs for similar biomedical applications. Future work can focus

on a comprehensive study determining the impact of these nanocarriers, improving their stability in human plasma or similar conditions during clinical administration. A detailed in vitro study with more time points and with increased sample size, could give more insights into the drug release kinetics. Some experiments could also be designed for in vivo testing of these nanocarriers understanding their distribution, pharmacokinetics, and toxicity limits.

## 6.4 Acknowledgements

I acknowledge Sandra Michel Souzy for her valuable suggestions, help during stability experimental setups in the ML-1 lab and for preparing samples. I appreciate Irene Simerink Konings for her assistance during drug-releasing measurement with plate reader in the bio-nanolab. Special thanks to Dr Shailesh Tripathi for advice and support with statistical studies of in-vitro release data.

## 6.5 Materials and Methods

Unless specified otherwise, all compounds were purchased from Sigma-Aldrich, and all buffers were prepared with 18 M $\Omega$ -cm MilliQ (Millipore) water.

### 6.5.1 Stability assessment of nanocarriers in the biological environment

Stability studies were performed by treating the two nanocarriers (HB and DWS) in the reaction tube with biological enzymes (Benzonase and Trypsin). The Benzonase nuclease (>90% pure) from Merck (Millipore) and Trypsin (Promega labs) were used in the studies. The samples were prepared by mixing 3 nM DNs with enzymes to make up a final volume of 10  $\mu$ l in each reaction tube (Table 6-1). The concentration of enzymes added in the reaction tubes were 5 U/ml for benzonase and 0.1 mg/ml for trypsin as used in other studies (34, 57). M13mp18 ds-DNA was obtained from New England Biolabs (NEB, Catalog number: #N4018S). The samples were incubated for 20 min at room temperature and 1 hr at 37 °C (Eppendorf Thermomixer), creating two-time points. The structural degradation was analysed by 1.8 % agarose gel electrophoresis, using a protocol, similar to those mentioned in previous chapters. Comparing the relative intensities of the bands from treated and untreated samples, sustaining structural integrity and extending shielding effect from CP coating could be established.

### 6.5.2 Evaluating the drug release profile

The in-vitro release of daunorubicin was evaluated by resuspending Dauno/DNs complexes (see chapter 5) in 100 $\mu$ l of different phosphate-buffered saline (1X PBS + 10 x 10<sup>-3</sup> M MgCl<sub>2</sub>) solutions (pH 4.0 and 7.2 and culture media (10% FBS +10 X 10<sup>-3</sup> M MgCl<sub>2</sub>) (43). The complexes were incubated in the dark with a shaking speed of 350 rpm at 37 °C (Eppendorf Thermomixer). Data was recorded at time points (6, 24 and 48 hours), to ensure recording the maximum release of dauno. At each time point, the dauno/DNs complexes were centrifuged at 15,800g for 15 min at 4°C, and the

amount of dauno released from the DNs was determined by measuring the UV absorbance of the drug in the supernatant at  $\lambda=490$  nm for 1 sec via a plate reader (Perkin Elmer Victor X3 multiwell plate reader). The fresh buffer/media solution was refilled for the next time point collection. The release experiments were conducted in triplicates. The data were processed in the R statistical package.

### **6.5.3 Validating drug leakage from the nanocarriers**

A comprehensive analysis was performed to quantify the drug leakage from the nanocarriers during the virus capsid fabrication process. The CP coated dauno/DN complexes were centrifuged (13000g for 15 min at 4°C) after the incubation steps. Then, the amount of the dauno released from the nanocarriers was determined by measuring the UV absorbance of the drug in the supernatant at  $\lambda=490$  nm for 1 sec via a plate reader (Perkin Elmer Victor X3 multiwell plate reader). The pelleted nanocarriers after collecting the free drug were washed with 1X PBS for 20 min at room temperature. The supernatant from pre- and post-PBS washing steps were also analysed with AGE and TEM to analyse the structural integrity of the nanocarriers. The washed samples were stored at -20°C for further studies.

## 6.6 References

1. Bujold KE, Lacroix A, Sleiman HF. DNA nanostructures at the interface with biology. *Chem*. 2018;4(3):495-521.
2. Hu Q, Li H, Wang L, Gu H, Fan C. DNA nanotechnology-enabled drug delivery systems. *Chemical reviews*. 2018;119(10):6459-506.
3. Li J, Pei H, Zhu B, Liang L, Wei M, He Y, et al. Self-assembled multivalent DNA nanostructures for noninvasive intracellular delivery of immunostimulatory CpG oligonucleotides. *ACS Nano*. 2011;5(11):8783-9.
4. Walsh AS, Yin H, Erben CM, Wood MJ, Turberfield AJ. DNA cage delivery to mammalian cells. *ACS Nano*. 2011;5(7):5427-32.
5. Chao J, Liu H, Su S, Wang L, Huang W, Fan C. Structural DNA nanotechnology for intelligent drug delivery. *Small (Weinheim an der Bergstrasse, Germany)*. 2014;10(22):4626-35.
6. Okholm AH, Kjems J. DNA nanovehicles and the biological barriers. *Adv Drug Deliv Rev*. 2016;106(Pt A):183-91.
7. Pinheiro AV, Han D, Shih WM, Yan H. Challenges and opportunities for structural DNA nanotechnology. *Nat Nanotechnol*. 2011;6(12):763-72.
8. Okholm AH, Kjems J. The utility of DNA nanostructures for drug delivery in vivo. *Expert Opin Drug Deliv*. 2017;14(2):137-9.
9. Xia Y, Li W, Cobley CM, Chen J, Xia X, Zhang Q, et al. Gold nanocages: from synthesis to theranostic applications. *Acc Chem Res*. 2011;44(10):914-24.
10. Della Rocca J, Liu D, Lin W. Nanoscale metal-organic frameworks for biomedical imaging and drug delivery. *Acc Chem Res*. 2011;44(10):957-68.
11. Kamaly N, Xiao Z, Valencia PM, Radovic-Moreno AF, Farokhzad OC. Targeted polymeric therapeutic nanoparticles: design, development and clinical translation. *Chem Soc Rev*. 2012;41(7):2971-3010.
12. Nishiyama N. Nanomedicine: nanocarriers shape up for long life. *Nat Nanotechnol*. 2007;2(4):203-4.
13. Lv S, Tang Z, Li M, Lin J, Song W, Liu H, et al. Co-delivery of doxorubicin and paclitaxel by PEG-polypeptide nanovehicle for the treatment of non-small cell lung cancer. *Biomaterials*. 2014;35(23):6118-29.
14. Safra T, Muggia F, Jeffers S, Tsao-Wei D, Groshen S, Lyass O, et al. Pegylated liposomal doxorubicin (doxil): reduced clinical cardiotoxicity in patients reaching or exceeding cumulative doses of 500 mg/m<sup>2</sup>. *Annals of Oncology*. 2000;11(8):1029-33.
15. Gradishar WJ. Albumin-bound paclitaxel: a next-generation taxane. *Expert opinion on pharmacotherapy*. 2006;7(8):1041-53.
16. Minelli C, Lowe SB, Stevens MM. Engineering nanocomposite materials for cancer therapy. *Small*. 2010;6(21):2336-57.
17. Wang AZ, Langer R, Farokhzad OC. Nanoparticle delivery of cancer drugs. *Annu Rev Med*. 2012;63:185-98.
18. Jiang D, England CG, Cai W. DNA nanomaterials for preclinical imaging and drug delivery. *Journal of controlled release : official journal of the Controlled Release Society*. 2016;239:27-38.
19. Keum JW, Bermudez H. Enhanced resistance of DNA nanostructures to enzymatic digestion. *Chem Commun (Camb)*. 2009(45):7036-8.
20. Mei Q, Wei X, Su F, Liu Y, Youngbull C, Johnson R, et al. Stability of DNA origami nanoarrays in cell lysate. *Nano letters*. 2011;11(4):1477-82.
21. Castro CE, Kilchherr F, Kim DN, Shiao EL, Wauer T, Wortmann P, et al. A primer to scaffolded DNA origami. *Nat Methods*. 2011;8(3):221-9.
22. Hahn J, Wickham SF, Shih WM, Perrault SD. Addressing the instability of DNA nanostructures in tissue culture. *ACS nano*. 2014;8(9):8765-75.
23. Perrault SD, Shih WM. Virus-inspired membrane encapsulation of DNA nanostructures to achieve in vivo stability. *ACS nano*. 2014;8(5):5132-40.
24. Schuller VJ, Heidegger S, Sandholzer N, Nickels PC, Suhartha NA, Endres S, et al. Cellular immunostimulation by CpG-sequence-coated DNA origami structures. *ACS Nano*. 2011;5(12):9696-702.
25. Lee DS, Qian H, Tay CY, Leong DT. Cellular processing and destinies of artificial DNA nanostructures. *Chemical Society Reviews*. 2016;45(15):4199-225.
26. Alvisi G, Poon IK, Jans DA. Tumor-specific nuclear targeting: promises for anti-cancer therapy? *Drug Resist Updat*. 2006;9(1-2):40-50.
27. Shen X, Jiang Q, Wang J, Dai L, Zou G, Wang ZG, et al. Visualization of the intracellular location and stability of DNA origami with a label-free fluorescent probe. *Chem Commun (Camb)*. 2012;48(92):11301-3.
28. Liang L, Li J, Li Q, Huang Q, Shi J, Yan H, et al. Single-particle tracking and modulation of cell entry



- pathways of a tetrahedral DNA nanostructure in live cells. *Angew Chem Int Ed Engl.* 2014;53(30):7745-50.
29. Chao J, Liu H, Su S, Wang L, Huang W, Fan C. Structural DNA nanotechnology for intelligent drug delivery. *Small.* 2014;10(22):4626-35.
  30. Ponnuswamy N, Bastings MMC, Nathwani B, Ryu JH, Chou LYT, Vinther M, et al. Oligolysine-based coating protects DNA nanostructures from low-salt denaturation and nuclease degradation. *Nat Commun.* 2017;8:15654.
  31. Agarwal NP, Matthies M, Gur FN, Osada K, Schmidt TL. Block Copolymer Micellization as a Protection Strategy for DNA Origami. *Angew Chem Int Ed Engl.* 2017;56(20):5460-4.
  32. Mikkilä J, Eskelinen A-P, Niemelä EH, Linko V, Frilander MJ, Törmä Pi, et al. Virus-encapsulated DNA origami nanostructures for cellular delivery. *Nano letters.* 2014;14(4):2196-200.
  33. Linko V, Mikkilä J, Kostiaainen MA. Packaging DNA Origami into Viral Protein Cages. *Virus-Derived Nanoparticles for Advanced Technologies: Springer;* 2018. p. 267-77.
  34. Auvinen H, Zhang H, Kopilow A, Niemelä EH, Nummelin S, Correia A, et al. Protein Coating of DNA Nanostructures for Enhanced Stability and Immunocompatibility. *Advanced healthcare materials.* 2017.
  35. Hernandez-Garcia A, Estrich NA, Werten MW, Van Der Maarel JR, LaBean TH, de Wolf FA, et al. Precise Coating of a Wide Range of DNA Templates by a Protein Polymer with a DNA Binding Domain. *ACS Nano.* 2017;11(1):144-52.
  36. Zhao YX, Shaw A, Zeng XH, Benson E, Nystrom AM, Hogberg B. DNA Origami Delivery System for Cancer Therapy with Tunable Release Properties. *ACS nano.* 2012;6(10):8684-91.
  37. Jiang Q, Song C, Nangreave J, Liu X, Lin L, Qiu D, et al. DNA origami as a carrier for circumvention of drug resistance. *Journal of the American Chemical Society.* 2012;134(32):13396-403.
  38. Samejima K, Earnshaw WC. Trashing the genome: the role of nucleases during apoptosis. *Nat Rev Mol Cell Biol.* 2005;6(9):677-88.
  39. Meiss G, Friedhoff P, Hahn M, Gimadudinow O, Pingoud A. Sequence preferences in cleavage of dsDNA and ssDNA by the extracellular *Serratia marcescens* endonuclease. *Biochemistry.* 1995;34(37):11979-88.
  40. Sastry L, Xu Y, Cooper R, Pollok K, Cornetta K. Evaluation of plasmid DNA removal from lentiviral vectors by benzonase treatment. *Hum Gene Ther.* 2004;15(2):221-6.
  41. Maassen SJ, de Ruiter MV, Lindhoud S, Cornelissen JJ. Oligonucleotide Length-Dependent Formation of Virus-Like Particles. *Chemistry—A European Journal.* 2018;24(29):7456-63.
  42. Zhang Q, Jiang Q, Li N, Dai L, Liu Q, Song L, et al. DNA origami as an in vivo drug delivery vehicle for cancer therapy. *ACS nano.* 2014;8(7):6633-43.
  43. Halley PD, Lucas CR, McWilliams EM, Webber MJ, Patton RA, Kural C, et al. Daunorubicin-Loaded DNA Origami Nanostructures Circumvent Drug-Resistance Mechanisms in a Leukemia Model. *Small.* 2016;12(3):308-20.
  44. Langenbucher F. Linearization of dissolution rate curves by the Weibull distribution. *J Pharm Pharmacol.* 1972;24(12):979-81.
  45. Dash S, Murthy PN, Nath L, Chowdhury P. Kinetic modeling on drug release from controlled drug delivery systems. *Acta Pol Pharm.* 2010;67(3):217-23.
  46. Mircioiu C, Voicu V, Anuta V, Tudose A, Celia C, Paolino D, et al. Mathematical Modeling of Release Kinetics from Supramolecular Drug Delivery Systems. *Pharmaceutics.* 2019;11(3):140.
  47. Zeng Y, Liu J, Yang S, Liu W, Xu L, Wang R. Time-lapse live cell imaging to monitor doxorubicin release from DNA origami nanostructures. *J Mater Chem B.* 2018;6(11):1605-12.
  48. Chambers J, Hastie T. Linear models. Chapter 4 of statistical models in S. Wadsworth & Brooks/Cole. 1992.
  49. Lee JH, Yeo Y. Controlled Drug Release from Pharmaceutical Nanocarriers. *Chem Eng Sci.* 2015;125:75-84.
  50. Tan JP, Wang Q, Tam KC. Control of burst release from nanogels via layer by layer assembly. *J Control Release.* 2008;128(3):248-54.
  51. Huang Y, Huang W, Chan L, Zhou B, Chen T. A multifunctional DNA origami as carrier of metal complexes to achieve enhanced tumoral delivery and nullified systemic toxicity. *Biomaterials.* 2016;103:183-96.
  52. Stubbs M, McSheehy PM, Griffiths JR, Bashford CL. Causes and consequences of tumour acidity and implications for treatment. *Mol Med Today.* 2000;6(1):15-9.
  53. Mitra AK, Agrahari V, Mandal A, Cholkar K, Natarajan C, Shah S, et al. Novel delivery approaches for cancer therapeutics. *Journal of Controlled Release.* 2015;219:248-68.
  54. Liu A, Verwegen M, de Ruiter MV, Maassen SJ, Traulsen CH-H, Cornelissen JJ. Protein cages as containers for gold nanoparticles. *The Journal of Physical Chemistry B.* 2016;120(26):6352-7.
  55. Udomprasert A, Kangsamaksin T. DNA origami applications in cancer therapy. *Cancer Science.* 2017.
  56. Bastings MM, Anastassacos FM, Ponnuswamy N, Leifer FG, Cuneo G, Lin C, et al. Modulation of the

- cellular uptake of DNA origami through control over mass and shape. *Nano letters*. 2018;18(6):3557-64.
57. Klem R, de Ruiter MV, Cornelissen J. Protecting Encapsulin Nanoparticles with Cysteine-Knot Miniproteins. *Mol Pharm*. 2018;15(8):2991-6.



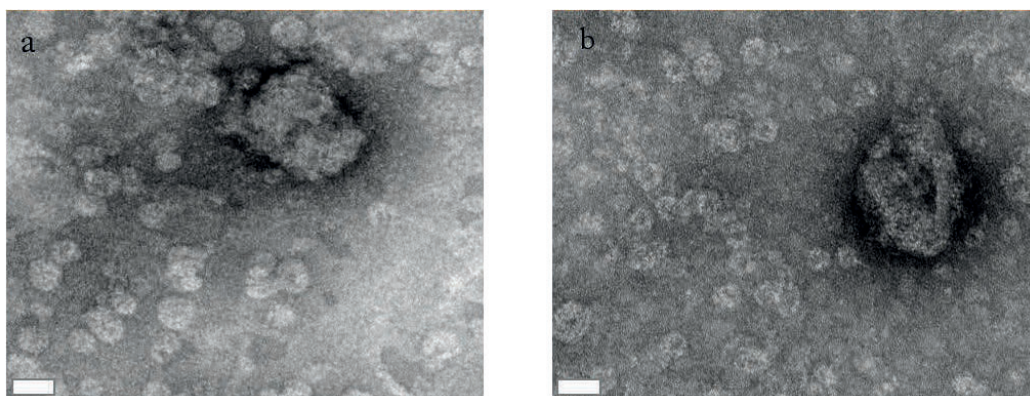


**Figure 6-S1 Evaluating structural integrity of nanocarriers**

TEM images of DWS nanocarriers after 48 hrs of *in-vitro* drug release a) 10% FBS +10 mM MgCl<sub>2</sub>, and b) 1XPBS +10 mM MgCl<sub>2</sub>, pH 4 (Scale bars are 20 nm)

## **CHAPTER 7**

---

# **Cellular viability and uptake mechanism of nanocarriers**

---

Part of this chapter will be submitted.

## 7 CELLULAR VIABILITY AND UPTAKE MECHANISM OF NANOCARRIERS

### 7.1 Introduction

The previous chapters of this thesis focused on developing two CCMV-CP coated DNA-based nanocarriers and assessing their drug-carrying capacity and release behaviour within the cellular environment. Some of the prior studies conducted on DNA nanostructures (DNs), established their utility in anticancer therapies exploiting the enhanced permeability and retention effect, leading to passive tumour-targeting and accumulation of nanostructures into the tumour cells (1, 2). Many studies found that the shape and size of a nanocarrier is an essential feature in avoiding the existing pharmacokinetic hurdles (filtration, excretion and increased cellular uptake) and developing an efficient drug delivery system (3, 4). Particle size also regulates the biological parameters like circulation half-lives and uptake of nanoparticles by macrophages (5). The effective size range for the drug carriers is usually between 15-200 nm, ensuring their integral properties such as kidney retention and intact tissue permeation (6-8). In 2018 Wang *et al.*, reported the effect of DN's morphology on their cellular uptakes within human lung cancer cells lines (9). In addition to morphologies, Bastings *et al.* further confirmed the role of mass, aspect ratio (AR) and specific cell-types in cellular uptake of DN's (10). Besides the size, surface charge, hydrophobicity, rigidity and surface chemistry are other features affecting the cellular internalisation of nanocarriers in therapeutic delivery (11). Nanoparticles (NPs) with different geometries and sizes were investigated for targeted drug delivery in various organs (12). Researchers used various NPs for mice (5-100 nm in brain; >200 nm in lungs; <100 nm in liver; and 80 nm in lymph nodes) for subcutaneous administration and found that the brain penetration efficiency of NPs decrease with an increase in size. Whereas, <200 nm particles were not trapped in lung capillaries for prolonged release of the drug and <100 nm can target the hepatocytes by crossing liver fenestrae (13-16). Therefore, size is of critical importance in designing nanocarriers for cancer targeting delivery systems.

To overcome the issues as mentioned earlier of DN's regarding their stability, the tendency to alleviate the immune response and increased intracellular concentration, researchers suggested surface modification (encapsulation) of nanostructures. Encapsulation is a surface modification technique where DN's are coated with virus-like particles (VLPs) or virus inspired materials. VLPs coating is expected to have advantages like enhanced stability, low immunogenicity and higher transfection rates for DN's, as discussed in previous chapters 4 and 6 of this thesis.

The use of the CCMV capsid protein (CP) in encapsulating, different cargoes like polymers, drugs and nucleic acids illustrates its host confining and delivery capabilities (17-19). The outside coating of CP on various cargoes helps to shield the confined materials inside, finding an increasing role in

nanomedicines and biomedical applications with added safety features for human use (20, 21).

Once administered, the nanocarriers cross plasma membranes via endocytosis to reach the target cells (22). Furthermore, the nanocarriers travel to early endosomes and finally arrive at lysosome for degradation following the "endolysosomal pathway" (23). Nanocarriers with a size  $\leq 100$  nm are considered ideal for cellular uptakes via different endocytotic vesicles (24). The cellular trafficking of nanocarriers via endocytic pathways is preferential and size-dependent, where, nanocarriers smaller than 80 nm are internalised with caveolae-mediated (CvME), and  $>100$  nm follows clathrin-mediated (CME) or multiple endocytotic mechanisms (25, 26).

The importance of size and shape of DNs in effective delivery (with reduced toxic effects and increased drug uptake) was reported (27). The results from multiple studies showed DNs drug delivery efficacy within different cancer cells (breast (MCF-7), myelocytic leukaemia (HL-60), human T-cell lymphocytic leukaemia (CEM); along with enhanced cytotoxicity and slower drug release as compared to free drug (dauno) and unfolded structures (28-30). Moreover, one of the recent works demonstrated the multifunctional utility of CCMV-CP encapsulated cargo in delivery, including enhanced cellular uptake and the inhibition of cell growth (18, 31, 32).

We evaluated the intracellular fate of our designed nanocarriers, composed of DN, CCMV-CP and daunorubicin(Dauno) and characterised with a size range of  $\leq 55$  nm (Figure 7-1). The two developed nanocarriers (based on HB and DWS) were tested for in-vitro cellular viability and uptake studies on pancreatic cancer cell lines (PANC-1). The cellular uptake routes were investigated for these nanocarriers with specific chemical inhibitors (Nystatin and Chlorpromazine) to block dominant uptake pathways (clathrin and caveolin dependent), as discussed by Donaldson *et al.*, (33). The uptake studies of nanocarriers were validated with fluorescence microscopy along with tracing the intracellular positioning. Lastly, the functional changes observed with CP-coated nanocarriers compared to the free drug and drug/DN complexes in terms of their anticancer targeted delivery was performed in collaboration with the targeted therapeutics group at TechMed Centre, UT.

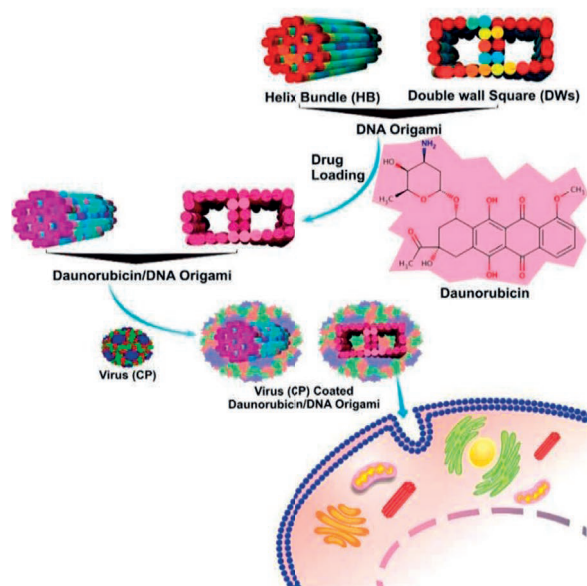


Figure 7-1 Schematic illustration of cellular internalisation of nanocarriers for daunorubicin delivery.

## 7

## 7.2 Result and Discussion

### 7.2.1 Cytotoxic studies for drug (dauno) and drug complexes on PANC-1 cells

The *in-vitro* drug release profiles from drug/DN complexes, as discussed in chapter 6, revealed release behaviour and different mechanisms depending on the cellular conditions. To determine the influence of drug-loaded DN (drug complex) on the cytotoxicity, we carried out a comparison of the cell viability profile between cell exposed to free drug and two drug-complexes (HB and DWS) for up to 72 hours. During incubation, we found that drug complexes led to a reduction in cytotoxicity levels with an improved safety profile, as compared to the free drug. The safety feature of DN as drug carriers have been verified previously, confirming that naked modular DN (2D and 3D) do not have any cytotoxic effects on the cells, having 100% viability of cancer cells even after 96 hrs of incubations (34). Cytotoxicity of the various formulations (free drug and drug complexes) for the Panc-1 cell lines was assessed after 24 hrs of cellular exposure.

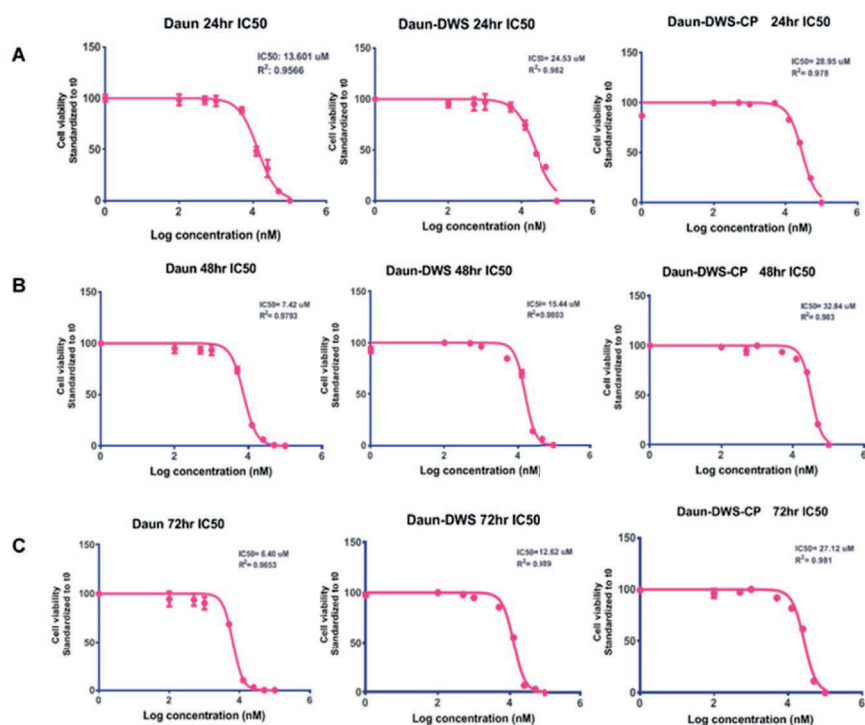
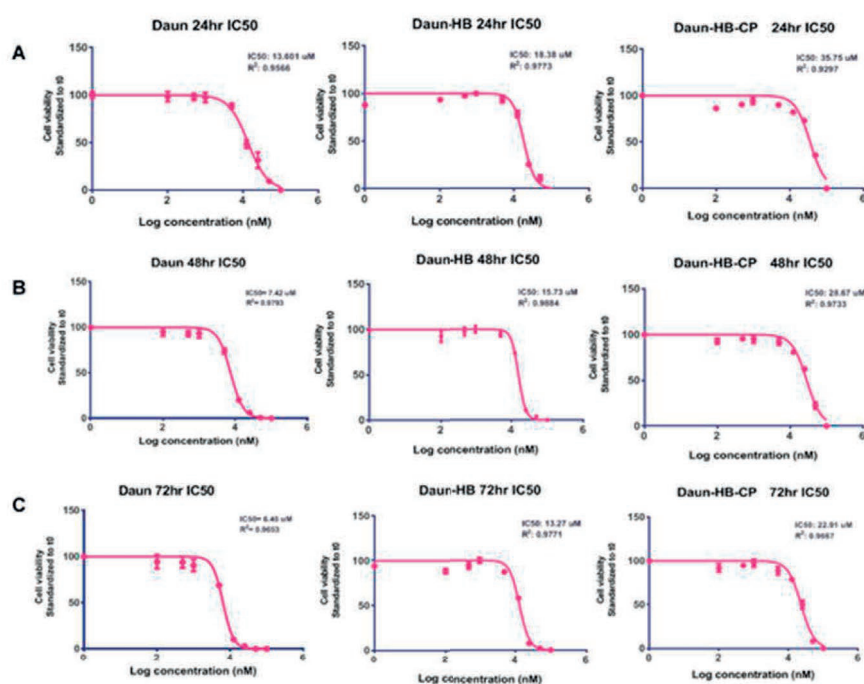


**Figure 7-2** DWS derived formulations cytotoxicity on Panc-1 represented by the half-maximal inhibitory concentration (IC<sub>50</sub>)

Alamar blue cell viability assay of Panc-1 cells after incubation with 100 μM, 50 μM, 25 μM, 12.5 μM, 5 μM, 1 μM, 0.5 μM and 0.1 μM of free drug, DWS-drug complex and the respective capsid protein (CP) coated nanocarrier for (A) 24 hours, (B) 48 hours (C) 72 hours.

We used IC<sub>50</sub> (50% inhibitory concentration to produce cell death) values as an indicator of the drug efficacy. As expected, the free drug resulted in suppression of the metabolic activity of cells at higher concentration ≈ 13.5 μM. However, the DWS-drug complex required 24.53 μM of drug for killing 50% of cell population on the first day (24 hrs), followed by 15.44 μM and 12.62 μM on the following days (48 and 72 hrs) respectively (Figure 7-2). Meanwhile, HB-drug complexes required drug concentration of 18.38 μM, 15.73 μM and 13.27 μM on the 24, 48 and 72 hours of incubation, respectively, pointing to a moderate decrease in the cytotoxic potential compared to the DWS-drug complex (Figure 7-3). This difference in cytotoxicity between the two drug complexes affirms the impact of the DNA geometry on drug delivery, which is consistent with the release pattern observed earlier in Chapter 6 of this thesis. The *in-vitro* pharmacological evaluations of both the drug complexes displayed a significant decrease in cytotoxic efficacy against Panc-1 cells (IC<sub>50</sub>) value in comparison to the free drug.



7

**Figure 7-3** HB derived formulations cytotoxicity on Panc-1 cells represented by the half-maximal inhibitory concentration (IC<sub>50</sub>).

Alamar Blue cell viability assay of Panc-1 cells after incubation with 100 μM, 50 μM, 25 μM, 12.5 μM, 5 μM, 1 μM, 0.5 μM and 0.1 μM of free drug, HB-drug complex, and their respective (CP) coated nanocarrier for (A) 24 hours, (B) 48 hours, (C) 72 hours

Furthermore, the high IC<sub>50</sub> of free drug and drug complexes against Panc-1 can be attributed to different cell uptake pathways and the controlled release of drug from DNs (35). However, the drug is slowly released inside the cells due to the retention properties of the larger DN complexes (~50 nm).

### 7.2.2 Comparing the cytotoxicity of designed nanocarriers

The effect of CP coated drug complexes (nanocarriers) on the drug cytotoxicity was assessed on the basis of the nanocarrier's stability and by checking the possibility of drug leakage from the nanocarriers before initiating cellular studies, as shown in chapter 6. Further, cell viability properties for these nanocarriers were investigated, similarly, as described in the previous section, over 72 hrs duration. The CP-drug complexes show higher IC<sub>50</sub> values (DWS-CP and HB-CP with 30 μM and 36 μM) at 24 hrs time point. This increased value indicates an improved safety profile compared to free drug and respective drug complexes (Figure 7-2 and Figure 7-3).

The order of cell cytotoxicity recorded at different selected time-points is free drug > drug complex > CP-drug complexes, which is approximately 1.5-2 fold less toxic than the free drug. This comparative higher cytotoxicity of the free drug and drug complexes is because cell membranes quickly take

them up through diffusion. However, the cellular internalisation of nanocarriers is slow likely due to the endosome-dependent mechanism (36). Further, the cytotoxic drug profile of nanocarriers is also cell-specific as reported with another DNA-protein hybrid platform used for drug delivery on two different cancer cell lines, i.e., A431 and MCF-7 (37). The research group of Wan *et al.*, developed virus-based nanoassemblies conjugating doxorubicin within cucumber mosaic virus for specific tumour-targeted delivery. The in-vitro assays of these nanoassemblies with cardiac cells finds minimal cardiotoxicity (38). On the other side, incubating similar nanoassemblies with ovarian cancer (OVCAR-3) cells depicts higher cytotoxicity in this particular cell line and tumour accumulation owing to the EPR effect. Thus, the contradictory impact of nanoassemblies on two cell lines led to strengthening the hypothesis that the efficiency of protein-coated drug carriers is size and cell-dependent.

Recently, Steinmetz and coworkers carried out some in-vitro and in-vivo studies of serum albumin (SA) coated DNs carrying doxorubicin, used as a delivery complex on cancer cells (39). The group made mouse (40) and human (HSA) serum albumin coated formulations and experimented on two different cancer cell lines (4T1 and MDA-MB-231) for their uptake and cytotoxic evaluation showing that the protein coating (SA) increases the tumour homing. Our result finding affirms the previous literature reports that the cellular uptake is dependent on specific cell types and nanoparticles design rather than tumour physiology (41). Besides, the release of drugs majorly depends on the enzymatic digestion of the complex or degradation of outer protein covering. The slow and different release kinetics of the drug from nanocarriers can be advantageous to improve the efficacy of the delivery system for *in-vivo* studies.

7

### 7.2.3 Cellular uptake of nanocarriers by PANC-1 cells

The result from the previous section examines the cytotoxicity profile of nanocarriers. However, the next step is to study the cellular uptake of these nanocarriers, along with other formulations (free drug and drug/DN complexes), using the inherent fluorescence of the drug for detection. We used blue staining (DAPI) for nuclei in all the experiments for different formulations, which on overlay detects the drugs inside the nucleus. We have quantified the uptake using fluorescence signals of drugs inside cells using Image J.

In order to determine the cellular uptake route by Panc-1 cells, we blocked specific cellular pathways using inhibitors. In particular, Nystatin was used to block caveolin-dependent endocytosis; CPZ is applied to block clathrin-dependent endocytosis; BSA for blocking unspecific cellular protein binding and inducing cell death (33).



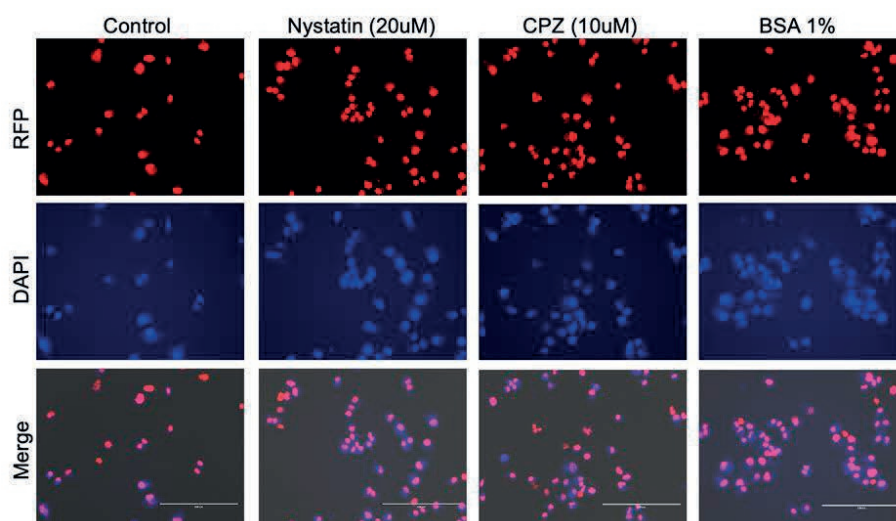


**Figure 7-4 Inhibitor challenged uptake of free drug capturing fluorescence with red channel.**

First row-micrographs of free drug (red channel) uptake with different inhibitors, after 2 hrs incubation in the cell line; Second row-the nucleus was stained with DAPI (blue channel); Third row-overlay of images confirming the co-localisation of drugs inside the cells. (Scale:100  $\mu\text{m}$ ).

## 7

Cells were incubated with free drug and drug complexes at various time points. Given the sensitivity requirements, the drug concentration was fixed at  $\geq 5 \mu\text{M}$  in all cases. The free drug can diffuse directly through the cell membranes; hence a strong drug based fluorescence was observed in the cytoplasm and nucleus of Panc-1 treated with the drug only (Figure 7-4). After 2 hrs of incubation, the free drug showed intense localisation with the nucleus pointing a rapid uptake; however, the merged images of co-localised drug/DN complex (DWS) with stained nuclei gave inferior fluorescence signals (Figure 7-5).

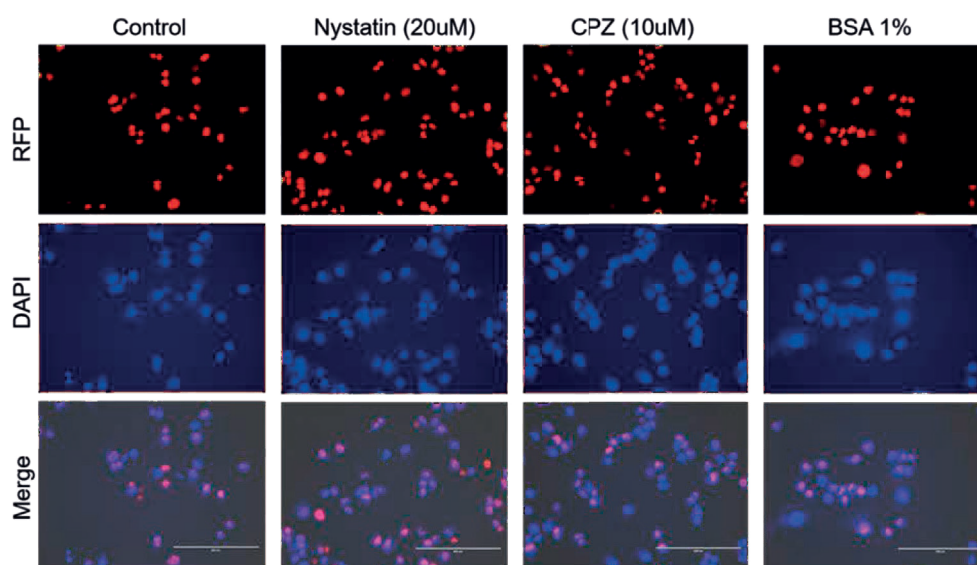


**Figure 7-5** Inhibitor challenged uptake of DWS-drug complex capturing drug with red and blue channels overlay depicting them getting inside the cells. (Scale: 100  $\mu$ m).

This uptake study with free drug and DN/drug complexes shows that through non-traditional entry routes, which are not mediated by caveolin or clathrin endocytosis pathways are followed instead, they are more shape-dependent for the drug complexes (10, 34). A similar uptake pattern has been observed with the other drug complex (HB) (image data not shown). Moreover, probing the DWS based nanocarrier, there is a significant reduction in uptake observed in the presence of CPZ compared to other pathway inhibitors, indicating clathrin-mediated as preferred endocytosis (Figure 7-6). The results are also verified with fluorescence intensity plots discussed later in this section.

7

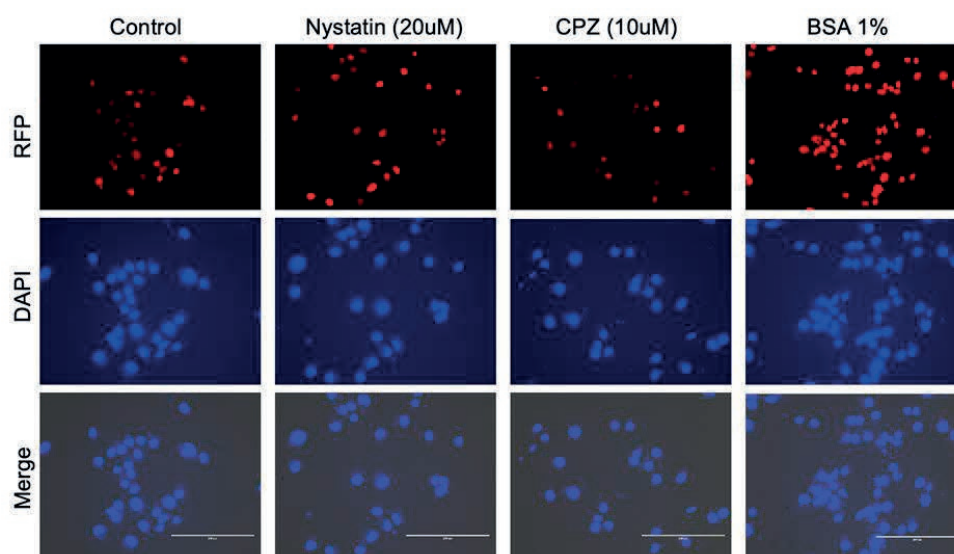


**Figure 7-6 Inhibitor challenged uptake of DWS nanocarriers capturing drug fluorescence with red and blue channels. (Scale: 100  $\mu\text{m}$ )**

7

Further, investigating the uptake of HB based nanocarriers, the cellular micrographs showed complete inhibition with CPZ (Figure 7-7). Notably, this confirms that the main uptake route for HB based nanocarriers is clathrin-mediated endocytosis. Additionally, the uptake observed is consistent with the cell viability displayed by HB nanocarriers, showing higher  $\text{IC}_{50}$  values in respect to DWS based nanocarriers. The difference in the encapsulation capacities of the nanocarriers probably results in inconsistent tendencies in premature leakage during the delivery process.

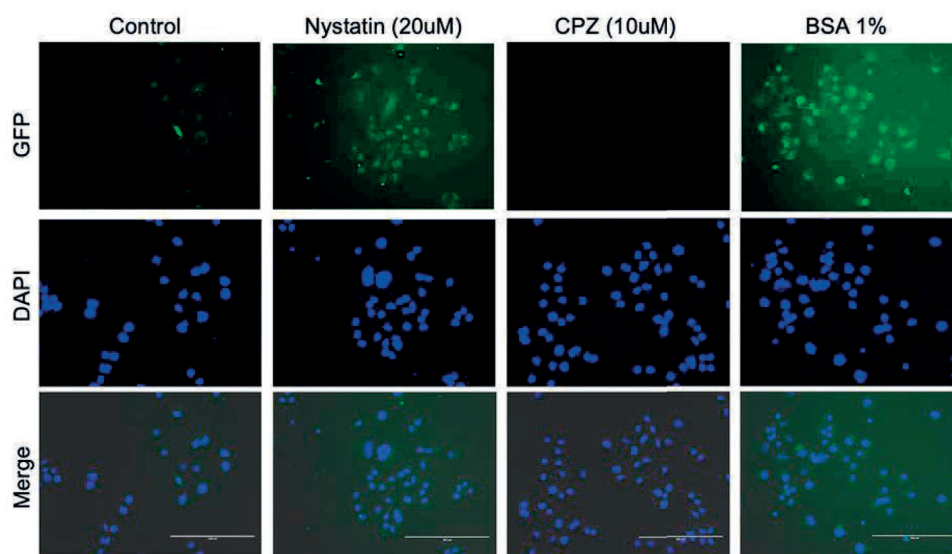


**Figure 7-7** Inhibitor challenged uptake of HB-nanocarriers capturing drug fluorescence with green and blue channels (Scale: 100  $\mu\text{m}$ ).

We also monitored the differences in fluorescence intensity in the microscopy studied between the different samples, which can be attributed to different amounts of internalised formulations. Cells incubated with the DWS based nanocarriers in the presence of inhibitors showed a much lower intensity compared to free drug and drug complexes (Figure 7-7 and Figure 7-8a). Meanwhile, the high uptake with BSA suggests that multiple pathways are possible for the uptake of virus capsids (Figure 7-8a and b)(32). Moreover, the study data also reveals that nanocarriers are readily internalised into cells, albeit at lower levels than free drug.

7

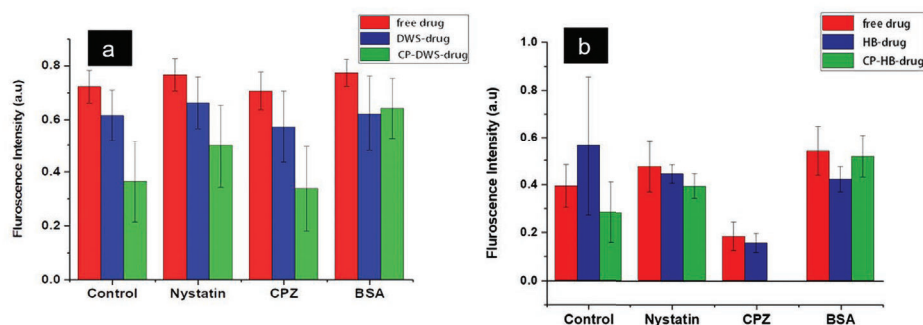


**Figure 7-8** The value of the sum of fluorescence intensity obtained from microscopy in individual channels; (a) DWS based formulations (b) HB based formulations.

Overall, the results for cell viabilities and uptake suggest that both nanocarriers can be effectively used as delivery vehicles. These developed smart drug delivery systems work the reported proof-of-

concept experiment, i.e., deliver an antineoplastic hydrophobic drug inside the cells. However, detailed investigations are necessary to reveal the exact mechanisms via which these carriers are taken up by different cell types that are relevant to potential clinical applications and practical usage.

### 7.3 Conclusion

The cell line studies in this chapter present a proof-of-principle to use biohybrid (CP/DNs) nanocarriers in anticancer drug delivery applications. The decrease in cytotoxicity observed with nanocarriers marks their biocompatibility (sustained-drug release). We have shown the drug-delivering proficiency of designed nanocarriers inside the cancer cells. The clathrin-mediated endocytosis appears as a dominant uptake route with virus encapsulated materials, which is consistent with the previous studies with HeLa cells (31, 32). Moreover, higher uptake with the BSA inhibitor suggests that depending on size-based endocytosis, there could be other possible uptake mechanisms which needs further studies (42). The study data validate the hypothesis that the cellular uptake of nanostructures is shape and cell-specific.

7 Though significant advances have been demonstrated *in-vitro*, the transition to the clinic remains challenging. Importantly, this is the, to best of our knowledge first report of plant virus coated drug-loaded DNs and probing their drug-delivering properties. For the successful *in-vivo* application in the future, improving delivery by promoting selective uptake of nanocarriers and further directing to the intended target site be an achievement. It would also be interesting to have a comprehensive immune study and pharmacokinetic evaluation for research advancement toward the clinical realisation of "smart drug delivery system". Potentially, these systems will provide promising new tools and strategies for intracellular delivery due to its size (Sub-100 nm) and their functionality in a wide range for biomedical applications.

### 7.4 Acknowledgements

I thank Ahmed Mostafa for experimental assistance, data collection, and contributions to this project and Dr Jai Prakash for his continuous guidance and support during the data analysis and writing.

### 7.5 Materials and Methods

Unless specified otherwise, all compounds were purchased from Sigma-Aldrich (Germany), and all buffers were prepared with 18 M $\Omega$ -cm MilliQ (Millipore) water.

#### 7.5.1 Nanocarriers design and development

The two modular DNs were designed and developed following the protocol, described in chapter 3. The drug (dauno) was loaded into DNs using the BPBR ratio varying from 2.1 - 3.5, adjusting the DNs concentration (nM), following the methodology outlined in section 5.2.2. Finally, the virus capsid

(CP) around the drug-loaded DNs, was created following a similar method to the one discussed in section 5.5.6. The final structures were verified for their drug retention ability by measuring the UV absorbance of the drug at  $\lambda=490$  nm via a VIKTOR™ plate reader (Perkin Elmer, Waltham, Massachusetts, USA).

## 7.5.2 *In-vitro* probing of nanocarriers

### 7.5.2.1 Cells

Panc-1 human pancreatic cancer cells were obtained from American type culture collection (ATTC, Rockville, MD) and were cultured in Dulbecco's Modified Eagles Medium (DMEM), high glucose (4.5 g/l) (Westburg, Leusden, The Netherlands), supplemented with 1% L-glutamine, 10% FBS (Lonza) and 100 µg/ml penicillin/streptomycin (Sigma-Aldrich). Cells were maintained viable at 37 °C in 5% CO<sub>2</sub> humidified climate.

### 7.5.2.2 Cell Viability Assay

Panc-1 cells were seeded at a density of 10.000 cells/well in 96 well-plates, followed by starvation with 0% FBS culture medium after 24 hours. Following 24 hours of starvation, cells were treated with daunorubicin free drug, drug/DN complexes or nanocarriers based on either HB or DWS designs. Concentrations of Daunorubicin loaded in the formulations used are 100 µM, 50 µM, 25 µM, 12.5 µM, 5 µM, 1 µM, 0.5 µM and 0.1 µM. Cell density was monitored at 24 hr, 48hr and 72 hour time points. 10% alamar blue dye (Invitrogen, Carlsbad, USA) solution in starvation culture medium was used to monitor the viability of Panc-1 cells by addition of 100 µl per well. After 4 hours of incubation, the fluorescence signal was determined using VIKTOR™ plate reader (Perkin Elmer, Waltham, Massachusetts, USA).

### 7.5.2.3 Fluorescence Microscopy

In order to evaluate the uptake of the drug/DN complexes as well as the CP-encapsulated formulations into Panc-1 cells, cells were seeded in 24 well-plate at a seeding density of  $2 \times 10^4$  cells per well. Twenty-four hours after seeding, cells were starved using 0% FBS fresh culture medium. Twenty-four hours later, cells were treated with drug complexes and nanocarriers loaded with 10 µM of Daunorubicin. Uptake was challenged with coadministration of specific inhibitors Nystatin, Chlorpromazine (CPZ) and bovine serum albumin (BSA) at concentrations of 20 µM, 10 µM and 1% respectively. After 2 hours of incubation, cells were washed with PBS and fixed with 4% formaldehyde for 20 minutes at room temperature. Next, cells were washed twice with PBS, and mounted with DAPI (Sigma-aldrich, Zwijndrecht, Netherlands) for 20 minutes and imaged for Daunorubicin (ex. 328/ em. 545 nm) and brightfield using EVOS fluorescence microscope (Life technologies).

## 7.5.3 Statistical Analysis

All graphs were made using GraphPad Prism version 5.02 (GraphPad Software Inc., San Diego,

California). All values are presented as a mean value with its standard deviation indicated (mean  $\pm$  SD, n=3).



## 7.6 References

1. Jiang Q, Song C, Nangreave J, Liu X, Lin L, Qiu D, et al. DNA origami as a carrier for circumvention of drug resistance. *Journal of the American Chemical Society*. 2012;134(32):13396-403.
2. Zhang Q, Jiang Q, Li N, Dai L, Liu Q, Song L, et al. DNA origami as an in vivo drug delivery vehicle for cancer therapy. *ACS nano*. 2014;8(7):6633-43.
3. Longmire M, Choyke PL, Kobayashi H. Clearance properties of nano-sized particles and molecules as imaging agents: considerations and caveats. *Nanomedicine (Lond)*. 2008;3(5):703-17.
4. Blanco E, Shen H, Ferrari M. Principles of nanoparticle design for overcoming biological barriers to drug delivery. *Nat Biotechnol*. 2015;33(9):941-51.
5. Nishiyama N. Nanomedicine: nanocarriers shape up for long life. *Nat Nanotechnol*. 2007;2(4):203-4.
6. Petros RA, DeSimone JM. Strategies in the design of nanoparticles for therapeutic applications. *Nat Rev Drug Discov*. 2010;9(8):615-27.
7. Rejman J, Oberle V, Zuhorn IS, Hoekstra D. Size-dependent internalization of particles via the pathways of clathrin- and caveolae-mediated endocytosis. *Biochem J*. 2004;377(Pt 1):159-69.
8. Messaoudi S, Greschner AA, Gauthier MA. Progress Toward Absorption, Distribution, Metabolism, Elimination, and Toxicity of DNA Nanostructures. *Advanced Therapeutics*. 2019;2(12):1900144.
9. Wang P, Rahman MA, Zhao Z, Weiss K, Zhang C, Chen Z, et al. Visualization of the Cellular Uptake and Trafficking of DNA Origami Nanostructures in Cancer Cells. *J Am Chem Soc*. 2018;140(7):2478-84.
10. Bastings MM, Anastassacos FM, Ponnuswamy N, Leifer FG, Cuneo G, Lin C, et al. Modulation of the cellular uptake of DNA origami through control over mass and shape. *Nano letters*. 2018;18(6):3557-64.
11. Wang J, Byrne JD, Napier ME, DeSimone JM. More effective nanomedicines through particle design. *Small*. 2011;7(14):1919-31.
12. Madhanagopal BR, Zhang S, Demirel E, Wady H, Chandrasekaran AR. DNA Nanocarriers: Programmed to Deliver. *Trends Biochem Sci*. 2018;43(12):997-1013.
13. Azarmi S, Roa WH, Lobenberg R. Targeted delivery of nanoparticles for the treatment of lung diseases. *Adv Drug Deliv Rev*. 2008;60(8):863-75.
14. Veiseh O, Sun C, Fang C, Bhattarai N, Gunn J, Kievit F, et al. Specific targeting of brain tumors with an optical/magnetic resonance imaging nanoprobe across the blood-brain barrier. *Cancer Res*. 2009;69(15):6200-7.
15. Sadauskas E, Wallin H, Stoltenberg M, Vogel U, Doering P, Larsen A, et al. Kupffer cells are central in the removal of nanoparticles from the organism. *Part Fibre Toxicol*. 2007;4:10.
16. Reddy ST, van der Vlies AJ, Simeoni E, Angeli V, Randolph GJ, O'Neil CP, et al. Exploiting lymphatic transport and complement activation in nanoparticle vaccines. *Nat Biotechnol*. 2007;25(10):1159-64.
17. Mukherjee S, Pfeifer CM, Johnson JM, Liu J, Zlotnick A. Redirecting the coat protein of a spherical virus to assemble into tubular nanostructures. *J Am Chem Soc*. 2006;128(8):2538-9.
18. Yang L, Liu A, de Ruyter MV, Hommersom CA, Katsonis N, Jonkheijm P, et al. Compartmentalized supramolecular hydrogels based on viral nanocages towards sophisticated cargo administration. *Nanoscale*. 2018;10(8):4123-9.
19. Maassen SJ, van der Ham AM, Cornelissen JJ. Combining protein cages and polymers: from understanding self-assembly to functional materials. *ACS Publications*; 2016.
20. Wen AM, Steinmetz NF. Design of virus-based nanomaterials for medicine, biotechnology, and energy. *Chem Soc Rev*. 2016;45(15):4074-126.
21. Chrastina A, Massey KA, Schnitzer JE. Overcoming in vivo barriers to targeted nanodelivery. *Wiley Interdiscip Rev Nanomed Nanobiotechnol*. 2011;3(4):421-37.
22. Schroeder A, Heller DA, Winslow MM, Dahlman JE, Pratt GW, Langer R, et al. Treating metastatic cancer with nanotechnology. *Nat Rev Cancer*. 2011;12(1):39-50.
23. Hu Q, Wang S, Wang L, Gu H, Fan C. DNA Nanostructure-Based Systems for Intelligent Delivery of Therapeutic Oligonucleotides. *Adv Healthc Mater*. 2018;7(20):e1701153.
24. Gratton SE, Ropp PA, Pohlhaus PD, Luft JC, Madden VJ, Napier ME, et al. The effect of particle design on cellular internalization pathways. *Proc Natl Acad Sci U S A*. 2008;105(33):11613-8.
25. Liang L, Li J, Li Q, Huang Q, Shi J, Yan H, et al. Single-particle tracking and modulation of cell entry pathways of a tetrahedral DNA nanostructure in live cells. *Angew Chem Int Ed Engl*. 2014;53(30):7745-50.
26. Lim KS, Lee DY, Valencia GM, Won YW, Bull DA. Nano-Self-Assembly of Nucleic Acids Capable of Transfection without a Gene Carrier. *Advanced Functional Materials*. 2015;25(34):5445-51.
27. Kearney CJ, Lucas CR, O'Brien FJ, Castro CE. DNA Origami: Folded DNA-Nanodevices That Can Direct and Interpret Cell Behavior. *Advanced Materials*. 2016.
28. Halley PD, Lucas CR, McWilliams EM, Webber MJ, Patton RA, Kural C, et al. Daunorubicin-Loaded



- DNA Origami Nanostructures Circumvent Drug-Resistance Mechanisms in a Leukemia Model. *Small*. 2016;12(3):308-20.
29. Zhao Y-X, Shaw A, Zeng X, Benson E, Nystrom AM, Hogberg B. DNA origami delivery system for cancer therapy with tunable release properties. *ACS Nano*. 2012;6(10):8684-91.
  30. Zhu G, Zheng J, Song E, Donovan M, Zhang K, Liu C, et al. Self-assembled, aptamer-tethered DNA nanostrains for targeted transport of molecular drugs in cancer theranostics. *Proc Natl Acad Sci U S A*. 2013;110(20):7998-8003.
  31. Tagit O, De Ruiter M, Brasch M, Ma Y, Cornelissen J. Quantum dot encapsulation in virus-like particles with tuneable structural properties and low toxicity. *RSC advances*. 2017;7(60):38110-8.
  32. de Ruiter M, van der Hee R, Driessen A, Keurhorst E, Hamid M, Cornelissen J. Polymorphic assembly of virus-capsid proteins around DNA and the cellular uptake of the resulting particles. *Journal of Controlled Release*. 2019;307:342-54.
  33. Dutta D, Donaldson JG. Search for inhibitors of endocytosis: Intended specificity and unintended consequences. *Cell Logist*. 2012;2(4):203-8.
  34. Zeng Y, Liu J, Yang S, Liu W, Xu L, Wang R. Time-lapse live cell imaging to monitor doxorubicin release from DNA origami nanostructures. *J Mater Chem B*. 2018;6(11):1605-12.
  35. Lv S, Tang Z, Li M, Lin J, Song W, Liu H, et al. Co-delivery of doxorubicin and paclitaxel by PEG-polypeptide nanovehicle for the treatment of non-small cell lung cancer. *Biomaterials*. 2014;35(23):6118-29.
  36. Tomuleasa C, Soritau O, Orza A, Ducea M, Petrushev B, Mosteanu O, et al. Gold nanoparticles conjugated with cisplatin/doxorubicin/capecitabine lower the chemoresistance of hepatocellular carcinoma-derived cancer cells. *J Gastrointest Liver Dis*. 2012;21(2):187-96.
  37. Ryu Y, Hong CA, Song Y, Beak J, Seo BA, Lee JJ, et al. Modular protein-DNA hybrid nanostructures as a drug delivery platform. *Nanoscale*. 2020;12(8):4975-81.
  38. Zeng Q, Wen H, Wen Q, Chen X, Wang Y, Xuan W, et al. Cucumber mosaic virus as drug delivery vehicle for doxorubicin. *Biomaterials*. 2013;34(19):4632-42.
  39. Pitek AS, Hu H, Shukla S, Steinmetz NF. Cancer Theranostic Applications of Albumin-Coated Tobacco Mosaic Virus Nanoparticles. *ACS Appl Mater Interfaces*. 2018;10(46):39468-77.
  40. Namsani S, Nair NN, Singh JK. Interaction potential models for bulk ZnS, ZnS nanoparticle, and ZnS nanoparticle-PMMA from first-principles. *J Comput Chem*. 2015;36(15):1176-86.
  41. Sokullu E, Soleymani Abyaneh H, Gauthier MA. Plant/Bacterial Virus-Based Drug Discovery, Drug Delivery, and Therapeutics. *Pharmaceutics*. 2019;11(5).
  42. Hu Q, Li H, Wang L, Gu H, Fan C. DNA nanotechnology-enabled drug delivery systems. *Chemical reviews*. 2018;119(10):6459-506.

## **CHAPTER 8**

---

### **General discussion**

## 8 GENERAL DISCUSSION

### 8.1 Summary

The co-assembly of DNA nanostructures (DNs) and proteins into functional biohybrid nanomaterials has gained increasing attention in the past few years as a versatile tool in bionanotechnology for applications in drug delivery, biosensors and biocatalysis (1-3). DNs coated with protein help to address biostability and intracellular uptake of DNs, ensuring their therapeutic functionality (4). Plant viruses also serve as a potential fabrication material, considering their size, shape and safety profile in humans (5, 6).

In the present study, we successfully designed modular DNs of similar sizes (~50 nm) but varied shapes. They could be loaded with anticancer drug 'daunorubicin' to form Drug/DN complexes. Moreover, we selected Cowpea chlorotic mottle virus (CCMV) capsid proteins (CP) as a template for coating these complexes. Due to their distinctive properties of assembly and disassembly, which the users can adjust, these proteins have proven to be ideal candidates (7-9). Here, our work reflects the bottom-up assembly approach for creating biological nanocarriers composed of nucleic acids and capsid proteins capable of carrying drug inside the cancerous cells.

8

### 8.2 Study Limitations

The research work discussed in this thesis gave us insights into the assembly of biohybrid nanomaterials and proved their efficacy as a smart drug delivery nanocarriers. Although this research was carefully designed, some of the limitations are given as follows:

- ⤴ The designing and purification steps for DNA nanostructures were time-consuming and challenging. The final optimisation of the workflow has been achieved after getting expert advise from the research group of UCLA and Harvard University.
- ⤴ The cost associated with developing DNs together with purification poses a major hurdle for their production in large quantities. However, in recent years there have been low cost, available scalable and convenient approaches reported for bulk production of DNA origami (10, 11).
- ⤴ The low yield of the purified materials (DNs) after multiple washing steps was a major hindrance in carrying out the experiments. Working with a sub-nM range of samples was challenging and led to several limitations in designing the advanced studies (*in-vitro* drug release and cell line).

### 8.3 Future directions

The work presented in this thesis has contributed to the potential application of CCMV-CP coated DNs as in cancer therapeutics. Nevertheless, few questions were left for future directions of the work, such as the unexpected presence of  $T=1$  particles during the microscope imaging of

nanocarriers, which demands further studies with altered assembly conditions and cargo to determine the formation of empty capsids. The 3D structural analysis of HB and DWS based nanocarriers with cryo-EM in the dry state can provide further insights into the morphology of the assembled nanostructures.

The CP coating act as a protective shield for nanocarriers improving their biostability and drug retention abilities in the cellular environment, which are imperative for any effective drug delivery system. The *in-vitro* drug release experiments suggest the effect of geometrical design on drug release under similar conditions. Moreover, a more thorough investigation for drug release kinetics from these nanocarriers will take one step closer towards programmable drug release at a particular site. Finally, the two developed nanocarriers mark their cytotoxic ability and cellular uptake mechanism on Pancreatic cancer cell (PANC-1), showing their sustained drug release ability and clathrin-mediated endocytosis as preferred uptake route. Future work can extend to other testing these with other cancer cell lines such as ovarian, breast or leukaemia to determine the drug delivery in a cell-specific manner. Additionally, a comprehensive pharmacological evaluation, including immunological studies, will provide advancements towards real-world applications.

## 8.4 References

8

1. Bila H, Kurisinkal EE, Bastings MMC. Engineering a stable future for DNA-origami as a biomaterial. *Biomater Sci.* 2019;7(2):532-41.
2. Auvinen H, Zhang H, Kopilow A, Niemelä EH, Nummelin S, Correia A, et al. Protein Coating of DNA Nanostructures for Enhanced Stability and Immunocompatibility. *Advanced healthcare materials.* 2017.
3. Xu Y, Jiang S, Simmons CR, Narayanan RP, Zhang F, Aziz AM, et al. Tunable Nanoscale Cages from Self-Assembling DNA and Protein Building Blocks. *ACS nano.* 2019;13(3):3545-54.
4. Xu X, Fang S, Zhuang Y, Wu S, Pan Q, Li L, et al. Cationic Albumin Encapsulated DNA Origami for Enhanced Cellular Transfection and Stability. *Materials (Basel).* 2019;12(6).
5. Liepold LO, Revis J, Allen M, Oltrogge L, Young M, Douglas T. Structural transitions in Cowpea chlorotic mottle virus (CCMV). *Phys Biol.* 2005;2(4):S166-72.
6. Ma Y, Nolte RJ, Cornelissen JJ. Virus-based nanocarriers for drug delivery. *Adv Drug Deliv Rev.* 2012;64(9):811-25.
7. Wilts BD, Schaap IAT, Schmidt CF. Swelling and softening of the cowpea chlorotic mottle virus in response to pH shifts. *Biophys J.* 2015;108(10):2541-9.
8. Tagit O, De Ruiter M, Brasch M, Ma Y, Cornelissen J. Quantum dot encapsulation in virus-like particles with tuneable structural properties and low toxicity. *RSC advances.* 2017;7(60):38110-8.
9. Kwak M, Minten IJ, Anaya DM, Musser AJ, Brasch M, Nolte RJ, et al. Virus-like particles templated by DNA micelles: a general method for loading virus nanocarriers. *J Am Chem Soc.* 2010;132(23):7834-5.
10. Halley PD, Patton RA, Chowdhury A, Byrd JC, Castro CE. Low-cost, simple, and scalable self-assembly of DNA origami nanostructures. *Nano Research.* 2019;12(5):1207-15.
11. Praetorius F, Kick B, Behler KL, Honemann MN, Weuster-Botz D, Dietz H. Biotechnological mass production of DNA origami. *Nature.* 2017;552(7683):84-7.



---

## ABBREVIATIONS

DNA	Deoxyribonucleic acid
RNA	Ribonucleic acid
CP	Capsid protein
pDNA	plasmid DNA
CCMV	Cowpea chlorotic mottle virus
TMV	Tobacco mosaic virus
RCNMV	Red clover necrotic mosaic virus
Dauno	Daunorubicin
NP	Nanoparticles
SWCNT	Single-walled carbon nanotubes
TEM	Transmission electron microscopy
AFM	Atomic force microscopy
SEM	Scanning electron microscopy
STEM	Scanning electron transmission microscopy
PEG	polyethylene glycol
CPPs	cell penetrating peptides
RGD	Arginine-glycine-aspartate
AA	Amino acids
ECM	Extracellular matrix
TAL	Transcription activator-like
STV	Streptavidin
RCA	Rolling circle amplification
CPMV	Cowpea mosaic virus
GFP	Green fluorescent protein
DNs	DNA nanostructures
PSS	Polystyrene sulfonate
PFS	Polyferrocenyl silane
HB	Helix bundle
DWS	Double wall square
SN	Square nut
AGE	Agarose Gel electrophoresis
DLS	Dynamic Light Scattering
$\zeta$	Zeta (zeta-potential)
FPLC	Fast protein liquid chromatography
SEC	Size-exclusion chromatography
EMSA	Electrophoretic mobility shift assay
Dox	Doxorubicin
HL-60 ADR	Drug resistant leukaemia cell lines
BSA	Bovine serum albumin
HFBI	Hydrophobin
BPBR	Base pair binding ratio
DAPI	4',6-diamidino-2-phenylindole
PBS	Phosphate buffer saline
TAE	Tris-acetate EDTA

TBE	Tris borate EDTA
caDNano	DNA origami designing software
CanDo	Computer-aided engineering for DNA origami
ssDNA	Single-stranded DNA
dsDNA	Double-stranded DNA
PCR	Polymerase chain reaction
MWCO	Molecular weight cutoffs
APTES	3-aminopropyltriethoxysilane
siRNAs	Small interfering RNAs
MCF 7	Human breast adenocarcinoma cancer cells
CpG	Cytosine phosphate guanosine
VLPs	Virus-like particles
PANC-1	Pancreatic cancer cell lines
PEG	Polyethylene Glycol
PLys	Polylysine block copolymer
MW	Molecular weight
MQ	Milli-Q water
rpm	Rounds per minute
EPR	Enhanced permeability and retention
FBS	Fetal bovine serum
SARSE	Semi Automated RNA Sequence Editor
DAEDALUS	DNA Origami Sequence Design Algorithm for User-defined structures
GIDEON	A Graphical Integrated Development Environment for Oligonucleotides
FRET	Förester Resonance Energy Transfer
IL	Interleukin
IFN	Interferon
TFN	Tumor Necrosis Factor
TLR	Toll-like receptor
µL	Micro-Litre
µM	Micro-moles

---

## SUMMARY

DNA and viruses are biological building blocks that in recent year have also been used to create new nanomaterials with applications in material science, nanomedicine and bio-nanotechnology. DNA nanostructures (DNs) have been used, for example, as promising drug carriers owing to their properties related to drug loading efficiency, controlled drug release mechanisms, biocompatibility and surface functionalisation. However, the literature suggests some significant challenges for the use of DN in effective and targeted drug delivery such as their stability against nuclease digestion and increasing their circulation half-life in the cellular environments. In order to tackle the challenges mentioned above, virus capsids can be often used to coat the DN's surface, facilitating their entry into cells. Such surface-modified DN exhibit also improved stability and low non-specific interactions in the cellular milieu. Thus, creating multifunctional biohybrid nanocarriers from DN and virus proteins capable of targeting specific cells and ensure stimuli-responsive drug release is of great utility in therapeutic applications.

The main objective of this research project was to create 'smart' nanocarriers by coating drug-loaded modular DN with viral capsid proteins (CP), isolated from the cowpea chlorotic mottle virus (CCMV). Four modular DN were designed and validated *in-silico* using designing and structure prediction softwares. DN were then self-assembled using a bottom-up approach and characterised using electrophoresis and imaging techniques. Next, two purified DN were coated with virus capsid proteins forming assemblies at neutral pH and tested as potential delivery vehicles. Imaging of encapsulated assemblies showed the presence of a "protein corona" around the DN, confirming the formation of encapsulated DN with CPs. One of the critical parameters in the encapsulation process is the DN-CP interaction, which was studied as a CP:DNA mass ratio and successful encapsulation of DN was only reported at only increased ratios. The resulting nano-assemblies were found to be monodisperse with an average particle size between 40-50 nm.

Following the formation of nanoassemblies, anthracycline daunorubicin, a chemotherapeutic drug was incorporated into two selected DN and evaluated for their drug-loading efficiency. DN were then, encapsulated with CPs to form a functional drug-loaded nanocarrier. The resulting nanocarriers were purified and characterised for monitoring the structural modification with analytical techniques. Next, the stability and drug-releasing properties of the nanocarriers were investigated, towards time-dependent controlled drug delivery at the target site. The formulated CP-coated nanocarriers were observed to outperform uncoated DN and unfolded ds-DNA in stability studies against enzymatic degradation. The designed nanocarriers were also evaluated for their drug retention properties and were found to be capable of transporting a large amount of drug inside cells. Additionally, the triggered drug release within the cellular environment marked the utility of the created nanocarriers in delivery, indicating its potential in biomedical applications.



Furthermore, to study the anticancer therapeutic efficacy, the intracellular fate of these nanocarriers was studied. Drug-loaded and CP-encapsulated DNs were tested in pancreatic cancer cell lines (PANC-1) for their cellular viability and drug uptake. Nanocarriers were found to prefer the clathrin-mediated endocytosis as the main uptake route, and their cellular internalisation kinetics appears to be size and cell-type dependent. Moreover, nanocarriers were identified to be endocytosed by cells after 2 hours of incubation and attain a controlled drug-release state with a protein coating on their surface, thereby facilitating drug enrichment inside cancer cells.

Overall, we successfully demonstrated the potential of using Drug/DNs-virus hybrid nanoassemblies as smart drug nanocarriers. The designed nanocarriers were reported to mimic the morphology and functionality of virus-like particles with increased stability, enhanced cellular uptake, and efficiently targeting the cancer cells. DNs provide a robust platforms for delivering chemotherapeutic agents into cancer cells. However, extending the horizon of using these designed DNs-based nanocarriers in cancer therapeutics requires more *in-vitro* and *in-vivo* studies sweeping various cancer cell lines. Hence, the results presented in this thesis form a factual basis for further research using self-assembled biohybrid materials in cancer theranostics and drug delivery. There lie different opportunities to synchronise the properties of two biomolecules and investigate their use in a wide range of other biomedical applications. Thus, on a lighter note, we can say all viruses are not dreadful, but few eventually make us better instead.

---

## SAMENVATTING

DNA en virussen zijn biologische bouwstenen die sinds een paar jaar ook worden gebruikt bij het maken van nieuwe nanomaterialen in materiaalwetenschappen, nanogeneeskunde en bionanotechnologie. Zo zijn DNA-nanostructuren (DNs) bijvoorbeeld ingezet als veelbelovende medicijndragers vanwege hun efficiëntie bij het laden van geneesmiddelen, gecontroleerde vrijgavemechanismes, biocompatibiliteit en oppervlaktefunctionalisatie. Uit vakliteratuur blijkt echter dat er enkele aanzienlijk uitdagingen zijn voor het gebruik van DN's bij het effectief en gericht toedienen van medicijnen, zoals hun stabiliteit tegen nuclease vertering en het verlengen van hun circulatiehalfwaardetijd in de cellulaire omgevingen. Bij het aangaan van bovengenoemde uitdagingen kunnen vaak viruscapsides worden gebruikt om de oppervlakte van de DN's te omhullen, waardoor ze gemakkelijker in de cellen doordringen. Dergelijke oppervlaktegemodificeerde DN's vertonen ook een betere stabiliteit en zwakke niet-specifieke interacties in de cellulaire omgeving. Het is daarom voor therapeutische toepassingen bijzonder nuttig om multifunctionele biohybride nanodragers van DN en viruseiwitten te creëren die in staat zijn specifieke cellen te targetten en te zorgen voor stimulerende geneesmiddelaflgifte.

De belangrijkste doelstelling van dit onderzoeksproject was het creëren van 'slimme' nanodragers, door met geneesmiddelen gevulde modulaire DN's te omhullen met virale capsid-eiwitten (CP's, *capsid proteins*), geïsoleerd uit het chlorotische-vlekkenvirus van koebonen (CCMV, *cowpea chlorotic mottle virus*). Er werden in silico vier modulaire DN's ontwikkeld en gevalideerd met behulp van structuurvoorspellende en ontwikkelsoftware. Vervolgens werden DN's met behulp van een bottom-up benadering zelfgeassembleerd en gekarakteriseerd met behulp van elektroforese en beeldvormingstechnieken. Daarna werden twee gezuiverde DN's omhuld met viruscapsid-eiwitten die bij neutrale pH-waarden assemblages vormen en die kunnen worden ingezet als potentiële voertuigen voor medicijnaflevering. Beelden van omhulde assemblages toonden de aanwezigheid van een 'eiwitcorona' rond de DN's, wat de vorming van met CP's omhulde DN's bevestigt. Een van de kritische parameters in het omhullingsproces is de DN-CP-interactie, die werd bestudeerd als een CP:DNA-massaverhouding. Succesvolle omhulling van DN's werd alleen gemeld bij verhoogde aandelen CP's. De resulterende nanoassemblages bleken monodispers met een gemiddelde deeltjesgrootte tussen 40 en 50 nm.

Na de vorming van nanoassemblages werd anthracycline daunorubicin, een chemotherapeutisch geneesmiddel, geïntegreerd in twee geselecteerde DN's, die vervolgens werden geëvalueerd op hun effectiviteit bij het laden van geneesmiddelen. De DN's werden daarna met CP's omhuld en vormden aldus een functionele met geneesmiddelen geladen nanodrager. De resulterende nanodragers werden gezuiverd en gekarakteriseerd om de structurele modificatie te monitoren met behulp van analytische technieken. Vervolgens werden de eigenschappen van de nanodragers op het gebied

van stabiliteit en medicijnafgifte onderzocht op tijdsafhankelijk gecontroleerde geneesmiddelfgifte in het doelgebied. In stabiliteitsstudies bleken de CP-omhulde nanodragers de niet omhulde DN's en ongevouwen ds-DNA te overtreffen bij door enzymen veroorzaakte afbraak. De ontwikkelde nanodragers werden ook geëvalueerd op hun geneesmiddelretentie-eigenschappen en ze bleken in staat grote hoeveelheden geneesmiddelen de cellen in te transporteren. Bovendien duidt de getriggerde afgifte van het geneesmiddel in de cellulaire omgeving op het nut van de gecreëerde nanodragers bij afgifte, en geeft zo een indicatie van het potentieel hiervan in biomedische toepassingen.

Met het oog op de therapeutische werking tegen kanker werd ook het intracellulaire lot van deze nanodragers onderzocht. Met geneesmiddelen gevulde en met CP omhulde DN's werden in alveolairkankercellijnen (PANC-1) getest op hun cellulaire levensvatbaarheid en geneesmiddelopname. Nanodragers bleken een voorkeur te hebben voor de clathrin-gemedieerde endocytose als voornaamste opnameroute en hun cellulaire internalisatiekinetiek lijkt afhankelijk van grootte en celtype. Verder werd vastgesteld dat nanodragers met een eiwitomhulsel op het oppervlak na twee uur incubatie worden geëndocytoseerd door cellen en een gecontroleerde staat van geneesmiddelfgifte bereiken, wat geneesmiddelverrijking binnen in kankercellen stimuleert.

Samenvattend hebben we met succes het potentieel aangetoond van het gebruik van het geneesmiddel-/DN's-virushybride nanoassemblages als slimme geneesmiddel-nanodragers. De ontwikkelde nanodragers bleken de morfologie en functionaliteit van virusachtige deeltjes na te bootsen met toenemende stabiliteit, verbeterde cellulaire opname en efficiënt gericht op de kankercellen. DN's zijn robuuste platforms die gebruikt worden voor het afleveren van chemotherapeutica in kankercellen. Voor een breder gebruik van deze ontwikkelde DN's-gebaseerde nanodragers in kankertherapeutica is meer in-vitro- en in-vivo-onderzoek nodig met verschillende kankercellijnen. De gepresenteerde resultaten in deze dissertatie vormen daarom een feitelijke basis voor verder onderzoek naar het gebruik van zelfgeassembleerde biohybride materialen in kankertheranostica en geneesmiddelfgifte. Verschillende mogelijkheden dienen zich aan om eigenschappen van twee biomoleculen te synchroniseren en onderzoek te doen naar het gebruik ervan bij diverse andere biomedische toepassingen. Om af te sluiten met een positieve noot: niet alle virussen zijn verschrikkelijk, sommige kunnen ons zelfs beter maken.

---

## ACKNOWLEDGEMENT

Finally, I am writing the most awaited part of my thesis, a distant dream a few years ago. It wasn't easy and was never a straight forward journey spanning my PhD in two continents (Australia and Europe) with having four primary supervisors during the candidature. I want to thank all of them who have contributed directly or indirectly towards accomplishing my doctorate and cherish the time spent at Flinders University (FU), Australia and University of Twente (UT), The Netherlands.

I am thankful to my first supervisor, Prof. Amanda Ellis, to offer me this opportunity and introduce me to the exciting area of nanotechnology at FU. I am also indebted to Prof. Jeroen Cornelissen for accepting me to join his research group as a *cotutelle* student at UT, providing me with much-needed guidance and promoting me further to learn and develop research skills in the field of Bionanotechnology. I express my gratitude to Dr Ingo Koeper for all he has done to support me on this path; from accepting being my primary supervisor at the beginning of my third-year candidature and putting faith in my research project. I know it wasn't easy to supervise a PhD remotely from the different time zone, I always felt like I could reach him for a chat about work or otherwise, and he has been a perfect mentor.

During my candidature, I was fortunate to interact with my other two co-supervisors Prof. Joe Shapter, and Prof. Colin Raston. I extend my thanks to them for their constructive feedback and stimulating discussions that have always helped me at various experimental designs and data analysis stages. I want to thank all of my supervisors for teaching me the importance of proper experimental planning, critical thinking and be extra careful in framing conclusion from results. Heartfelt thanks to Dr Justin Chalker for helping me with his lab access when I had a no designated laboratory during my mid-candidature at FU.

I would also like to mention a few names Renzo Fenati and Late Simon Bou for helping me in my initial days adjusting in the lab at FU. Simon, I can never forget the beautiful time and lengthy discussions we had sharing the same office. I always remember and cherish your liveliness and lighthearted jokes during our ICONN trip to Canberra (you will always be in my memories mate!). Furthermore, I also like to thank all my lab and virus lunch group members (Mark, Robin, Jenny, Stan, Aije, Aref, Rindia and Sandra) at UT for all the scientific discussions and valuable suggestions. It was a pleasure working and learning with all of you guy; a sincere token of thanks to all of them for all the help, support and friendly atmosphere they provided. I very much appreciate Mark De Ruiter for teaching me about virus extraction, encapsulation strategies and other essential techniques required to complete this research project. I also want to thank Dr Jai Prakash for providing collaborative support for the cellular studies and conceiving this final chapter of the thesis.

My thanks are also due to my lab buddies Deepak Samanta, Pramod Kunturu and Ashely Connolly, whom I always have turned up for any discussion and suggestion. Deepak and Pramod are also

closed pals in Netherlands and thanks are due for the magnificent day trips, evening drinks and light moments we shared in and around the campus. The time we spent during the workweek in Germany (excessive beers, walks and desi talks) was joyous! I am thankful to my partners in crime "Shailesh and Mukesh" for being there in all my professional and personal ups and downs and keeping all my secrets intact 😊. I always admire two of you to boost me to keep moving to reach the finishing line, when it looks distant.

Niharika has always been a fantastic partner (wife), supporting me in every possible way without fail and took the best care of home and kids while I was busy shuffling with all my PhD commitments across two continents. She believed in me (even more than myself) that eventually, I will be completing the PhD one day with all the odds!! Furthermore, my acknowledgements cannot complete without a special mention of my kids, Virag and Virahi. They both were very supportive and mindful, allowing me to finish and give my time to the thesis (which was theirs). It was a beautiful coincidence to welcome both the kids during each of the parents' PhDs.

A special thanks to Deepesh, whom I know for >20 years now, and our friendship has grown leap and bounds over this time. It was wonderful to have you around for those extra tweaks, adjustments, and insights during the thesis's final compilation. I also want to name "Vividh Bharati-देश की सुरीली धड़कन", who is not just a radio service but more like a soulmate and have always accompanied me (sometimes in dark and lonely nights) during this PhD journey, helping immensely to remain focused towards my goal.

I owe to FU and UT a deep sense of sincere thanks, providing all the facilities and friendly ambience for my research. In the form of Research Training Program and Scholarships, the Australian Government financial assistance is duly acknowledged. FU travel and field grants ensured that I could devote my entire time to scientific engagements and make a maximum of this cotutelle programme away at UT. My thanks are due to the excellent OGR staff at Flinders and the BNT office staff at UT for their assistance and continuous support for making my cotutelle journey a lifetime experience. This project would not have been possible without the professional support of staff from microscopy facilities at both the universities: Dr. Chris Gibbson and Ashley Slattery at FU for SEM and AFM; Rico Keim and Mark Smithers at MESA+ institute, UT for TEM and STEM at UT, thanks for all the help and guidance.

To my parents मम्मी- पापा यह मेरी पीएचडी आप दोनों के प्यार, त्याग और अकरणीय सहयोग को समर्पित है- पापा यह सिर्फ आप और आप ही थे जिनके साथ ने मुझे हौसला दिलाया की मुश्किलों से डर के पीछे हटने से नहीं, उनसे लड़ने से ही मंज़िल तय होती है और आपका व्यक्तित्व निखरता है। बचपन में आपके द्वारा बताई गयी यह सूक्ति इस यात्रा में मेरा जैसे मंत्र सी बन गयी:

"करत करत अभ्यास के जड़मति होत सुजान, रसरि आवत-जात ते सिल पे परत निसान"

आज आपकी बहुत याद आ रही है - काश मैं यह डिग्री आपके समक्ष लेता !!!!

गौरव सिंघई  
Gaurav Singhai



---

## ABOUT THE AUTHOR



“If curiosity can be linked to thirst, then science is a perpetual quest to quench curiosity.” The author stand up to the view that the role of curiosity and imagination for science is so important that nurturing them can be seen as an ethical obligation and suppressing them morally problematic.

Gaurav Singhai was born in the small town of Nowrozabad in central India. He completed his Bachelors in Pharmaceutical Sciences (2003) and Masters in Biotechnology from Rajiv Gandhi Technical University, India (2007). Gaurav then worked in the research sector for nearly three years and later joined an Academic National Excellence Institute as a Lecturer, focusing on pharmaco-informatics and drug development before moving to Australia in 2011.

In Australia, he worked as Research Assistant in a proteomics group at Latrobe University-Melbourne, for two years, enhancing his molecular and biochemical technology skills. In 2015, he was awarded the Australia Postgraduate Award and started his PhD with Professor Amanda V. Ellis at Flinders University in DNA Nanotechnology. Further, in 2016, he enrolled in the *cotutelle program* with Professor Cornelissen’s group at the University of Twente to extend his research project. He spent almost 18 months in the Netherlands for completing the research work presented in this dissertation.

From early childhood, the author loves travelling and learning from his surroundings. Research work for PhD carried out in two countries has fortified his original passion for travelling and his quest for learning more and more, hope this journey continues forever.



---

## PUBLICATION

De Ruiter, M. V., Overeem, N. J., Singhai, G., Cornelissen, J. J. L. M., *Induced Förster Resonance Energy Transfer by Encapsulation of DNA-Scaffold Based Probes inside a Plant Virus Based Protein Cage*, Journal of Physics Condensed Matter, 2018, 30(18), 184002.

### Manuscripts

Singhai, G., Koeper, I., Cornelissen, J. J. L. M., *Developing daunorubicin-loaded virus coated DNA nanocarriers for anticancer therapies* – in preparation.

Singhai, G., Mostafa, A., Koeper, I., Prakash, J., Cornelissen, J. J. L. M., *In -vitro activity and uptake pathway of virus coated nanocarriers on pancreatic cancer cell* – in preparation.

